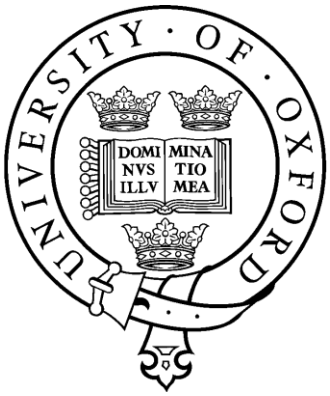
Mechanisms of Clinical Ototoxicity and Inner Ear Protection

Andrew M Breglio
Pembroke College
University of Oxford



A thesis submitted for the degree of
Doctor of Philosophy
Trinity 2017

Advisors:
Matthew JA Wood, University of Oxford, UK
Lisa L Cunningham, National Institutes of Health, USA

There was no telling what people might find out once they felt free to ask whatever questions they wanted to.

Joseph Heller, *Catch-22, 1961*

ABSTRACT

Mechanisms of Clinical Ototoxicity and Inner Ear Protection

Andrew M Breglio, Pembroke College
Submitted for the degree of *Doctor of Philosophy* in Trinity 2017

Clinical ototoxicity—permanent hearing loss caused by medications—is estimated to affect millions of patients annually. Two classes of drug are largely to blame: platinum-based chemotherapeutics, primarily cisplatin, and aminoglycoside antibiotics. Development of methods to prevent ototoxicity depends upon an understanding of its mechanisms and may benefit from an understanding of native protective pathways of the inner ear.

As the mechanisms behind cisplatin ototoxicity remain unclear, I first sought, and herein report, a refined mouse model of cisplatin ototoxicity which will allow for further *in vivo* investigation of cisplatin ototoxicity and potential methods for its prevention. This low-dose, multi-cycle model was found to accurately reproduce cisplatin ototoxicity as it has been described clinically and histopathologically.

I then used this mouse model of cisplatin ototoxicity to investigate cisplatin pharmacokinetics in the cochlea and their role in driving cisplatin ototoxicity. Cisplatin was found to be retained within the cochlea for months following its administration. This initial finding in mice was extended to cochlear tissue samples from deceased human patients. Analysis of intra-cochlear cisplatin distribution in murine and human tissue identified the stria vascularis region of the cochlea as a promising target for intervention.

With the nature of aminoglycoside ototoxicity better understood, I investigated a native inner ear protective pathway which could be leveraged to promote sensory hair cell survival. The improved hair cell survival that has previously been demonstrated as a result of heat stress was found to be mediated by cell-cell communication via extracellular vesicles. Further, hair cell protection against aminoglycosides could be reproduced through the application of exogenous, non-inner ear-derived extracellular vesicles.

In sum, these data provide new insight into mechanisms of ototoxicity and details of cellular pathways which can help protect against it.

ACKNOWLEDGEMENTS

I am deeply grateful to my mentors, Lisa Cunningham and Matthew Wood, whose contributions to my development as a scientist reach far beyond the pages of this thesis. They have supported me, challenged me, and trusted me throughout this process, and as a result, I have found this experience to be intellectually stimulating and personally satisfying.

I have been lucky to work alongside fantastic colleagues and friends in two laboratories an ocean apart. Though I appreciate the contributions of all my labmates, a few deserve special recognition. From Matthew Wood's laboratory at the University of Oxford I thank Imre Mäger, Eduard Willms, Justin Hean, and "Fiona" Yi Lee, whose thoughtful discussions and generosity with their time and resources afforded me an education in extracellular vesicles. From Lisa Cunningham's laboratory at the National Institutes of Health I thank Lindsey May, Katharine Fernandez, Aaron Rusheen, Nora Welsh, and Shimon Francis, whose contributions are so entwined in my progress that they are impossible to fully recognize. Their help ranged from intellectual input, to an extra set of hands, to personal support.

I'd also like to recognize my expert scientific collaborators, including but not limited to: Samir El Andaloussi, Lauren Amable, Matthew Hall, D. Eric Anderson, Tracy Fitzgerald, Ronald Petralia, and Ya-Xian Wang who have all been instrumental to these experiments. I'm grateful to the many administrative staff who have helped me navigate research on two continents, especially Katie Soucy of the NIH-Oxford-Cambridge Scholars program and Nicole Thompson and Vernell McKnight of the National Institute on Deafness and Other Communication Disorders. I thank the NIH-Oxford-Cambridge Scholars program and the International Biomedical Research Alliance, under the leadership of the boundlessly supportive Randi Balletta, for their financial support and the many professional development opportunities they have afforded me.

Lastly, I wish to thank my friends and family for their support and encouragement along my long pathway to becoming a physician-scientist. Thank you especially to my wife, Kimberly, who has walked this road with me and who serves as a constant reminder that there is life outside the laboratory, and that life can be truly wonderful.

DECLARATION

The experiments detailed in this thesis were conceived, conducted, and analyzed solely by me under the supervision of Matthew JA Wood, MD DPhil at the University of Oxford and Lisa L Cunningham, PhD at the National Institutes of Health, with the following exceptions:

Aaron Rusheen helped performed auditory testing of mice at intermediate time points within the cisplatin regimen and helped prepare a portion of the mouse organs for ICP-MS analysis. Lauren Amable, PhD and Eric Shide performed ICP-MS measurements on prepared samples. Katharine Fernandez, AuD PhD measured the endocochlear potentials on mice I had treated. Lindsey May helped perform utricle culture experiments represented in Figure 4.5, and to prepare utricles for transmission electron microscopy. Nora Welsh helped perform the HSP70 ELISA and to prepare utricles for immunoelectron microscopy. The entire Cunningham laboratory helped dissect utricles for proteomic analysis. Ronald Petralia, PhD and Ya-Xian Wang, MD acquired the electron microscopy images. D. Eric Anderson, PhD performed the final sample preparation and data acquisition for proteomics.

ABBREVIATIONS

a.u.	arbitrary units
AAS	atomic absorption microscopy
ABR	auditory brainstem response
AC	anterior crista
ATP	adenosine triphosphate
BC	body condition
BCS	body condition score
BOC	*tert*-butyloxycarbonyl protecting group
BODIPY	boron-dipyrromethene
CP	cuticular plate
CTR	copper transporter
dB	decibel
dB SPL	decibel sound pressure level
DMSO	dimethyl sulfoxide
DNA	deoxyribonucleic acid
DPOAE	distortion product otoacoustic emissions
DTT	dithiothreitol
dUTP	deoxyuridine triphosphate
EDTA	ethylenediaminetetraacetic
EGFP	enhanced green fluorescent protein
ELISA	enzyme-linked immunosorbent assay
EP	endocochlear potential
ESCRT	endosomal sorting complex required for transport
EV	extracellular vesicle
FBS	fetal bovine serum
FDA	United States Food and Drug Administration
g	gravity
GFI1	growth factor independent 1 transcriptional repressor
HC	hair cell
HEK	human embryonic kidney
HPLC	high-performance liquid chromatography
HS	heat shock
HSF1	heat shock factor 1
HSP27	heat shock protein 27
HSP70	heat shock protein 70

Hz	hertz
ICP-AES	inductively coupled plasma atomic emission spectrometry
ICP-MS	inductively coupled plasma mass spectrometry
IHC	inner hair cell
ILV	intraluminal vesicle
i.p.	intraperitoneal
IR	inner region
IS	interscalar septum
kHz	kilohertz
LC	lateral crista
LES	lateral extrastriolar region
LHFPL5	Lipoma HMGIC Fusion Partner-Like 5
LPR	line of polarity reversal
MES	medial extrastriolar region
MET	mechano-electrical transduction
mV	millivolt
MVB	multivesicular body
MWCO	molecular weight cut-off
NIDCD	National Institute on Deafness and Other Communication Disorders
NIH	National Institutes of Health
NINDS	National Institute of Neurological Disorders and Stroke
N-SMase II	neutral sphingomyelinase II
NTA	nanoparticle tracking analysis
N VIII	eighth cranial nerve (the vestibulocochlear nerve)
OC	organ of Corti
OCT	organic cation transporter
OHC	outer hair cell
OR	outer region
PC	posterior crista
ppb	parts per billion
PTA	pure tone audiometry
ROI	region of interest
SC	supporting cell
SEC	size-exclusion chromatography
SG	spiral ganglion
SNARE	soluble NSF attachment protein receptor
SV	stria vascularis
TEM	transmission electron microscopy

TLR4	toll-like receptor 4
TMIE	Transmembrane Inner Ear
TMC1/2	Transmembrane Channel Like 1/2
TUNEL	terminal deoxynucleotidyl transferase dUTP nick-end labeling
UC	ultracentrifugation
UV	ultraviolet
WT	wildtype

TABLE OF CONTENTS

ABSTRACT ..... **I**

ACKNOWLEDGEMENTS ..... **II**

DECLARATION ..... **III**

ABBREVIATIONS ..... **IV**

1 GENERAL INTRODUCTION **1**

1.1 Hearing **1**

1.2 The cochlea **3**

1.2.1 Cochlear mechanics 3

1.2.2 Endolymph and the stria vascularis 4

1.2.3 The organ of Corti 7

1.2.4 Innervation of cochlear hair cells 11

1.3 The utricle **14**

1.3.1 Vestibular hair cells 16

1.3.2 Innervation of vestibular hair cells 17

1.3.3 Supporting cells 18

1.4 Non-mammalian mechanosensory organs **21**

1.5 Sensorineural hearing loss **23**

1.5.1 Clinical evaluation of hearing 25

1.5.2 Ototoxicity associated with platinum-based chemotherapy 27

1.5.3 Ototoxicity associated with aminoglycoside antibiotics 29

1.5.4 Clinical consequences of ototoxicity 31

1.6 Modeling ototoxicity in the laboratory **34**

1.7 Current treatment of ototoxicity 38

1.7.1 Approaches to treating ototoxicity 38

1.7.2 Previous investigational protective strategies 39

1.8 Specific Aims 44

2 MODELING CISPLATIN OTOTOXICITY IN THE MOUSE 45

2.1 Introduction 45

2.2 Methods 50

2.2.1 Cisplatin treatment of mice 50

2.2.2 Mouse health monitoring and supportive care 51

2.2.3 Auditory testing 53

2.2.4 Hair cell counting 56

2.2.5 Statistics 58

2.3 Results 59

2.3.1 Cisplatin-treated mouse health and survival 59

2.3.2 Cisplatin-induced hearing loss 60

2.3.3 Progression of hearing loss during the cisplatin regimen 62

2.4 Discussion 65

3 THE ROLE OF CISPLATIN PHARMACOKINETICS IN CISPLATIN OTOTOXICITY 68

3.1 Introduction 68

3.2 Methods 76

3.2.1 Cisplatin treatment 76

3.2.2 Tissue collection for ICP-MS 76

3.2.3 Cochlear microdissections 76

3.2.4 Cochlear cryosections 77

3.2.5 Administration of BODIPY compounds 78
3.2.6 Human patient cochlear sections 80
3.2.7 Inductively coupled plasma mass spectrometry (ICP-MS) 81
3.2.8 Laser ablation ICP-MS 83
3.2.9 Endocochlear potential recordings 84
3.3 Results 86
3.3.1 Systemic cisplatin pharmacokinetics 86
3.3.2 Intracochlear cisplatin pharmacokinetics 89
3.3.3 Visualization of cisplatin trafficking by BODIPY FL-cisplatin 92
3.3.4 Cisplatin-induced changes in the endocochlear potential 95
3.3.5 Cisplatin retention in the human cochlea following chemotherapy 96
3.3.6 Laser ablation ICP-MS mapping of cisplatin in the cochlea 98
3.4 Discussion 100
3.5 Outlook 106
4 SENSORY HAIR CELL PROTECTION AGAINST AMINOGLYCOSIDE ANTIBIOTICS 108
4.1 Introduction 108
4.2 Methods 117
4.2.1 Mice 117
4.2.2 Utricle explant culture and aminoglycoside exposure 118
4.2.3 Utricle heat shock 119
4.2.4 Nanoparticle tracking analysis (NTA) 119
4.2.5 Pharmacologic inhibition of exosome production 121
4.2.6 Utricle co-culture 121
4.2.7 Cell culture 122
4.2.8 Extracellular vesicle isolation 123

4.2.9 Immunohistochemistry and confocal microscopy 125
4.2.10 HSP70 ELISA 126
4.2.11 Confocal imaging of vesicles released from Gfi1$^{Cre/+}$; ROSA26$^{mTmG/+}$ utricles 127
4.2.12 Transmission electron microscopy (TEM) 128
4.2.13 Quantitative tandem mass spectrometry 129
4.2.14 Cell line protection experiments 131
4.2.15 Statistics 131
4.3 Results 132
4.3.1 Release of vesicles from the utricle following heat shock 132
4.3.2 Pharmacological inhibition of vesicle release 133
4.3.3 The protective effect of heat shock requires extracellular vesicles 135
4.3.4 Association of HSP70 with vesicles 137
4.3.5 Cell type-specific production of extracellular vesicles 139
4.3.6 The fate of vesicles released from the utricle 145
4.3.7 Proteomic investigation of extracellular vesicle content 152
4.3.8 Hair cell protection in vitro using cell line-derived small EVs 157
4.4 Discussion 160
4.5 Outlook 173
5 SUMMARY OF FINDINGS 175
6 SUPPLEMENTAL DATA 176
7 REFERENCES 179

1 GENERAL INTRODUCTION

1.1 HEARING

Hearing (audition) is one of the five traditionally recognized human senses. It is central to our ability to communicate with one another and experience the world around. This sense is made possible by the collective structures of the ear, vestibulocochlear nerve, and central nervous system. The ear functions to collect sound which is transferred through surrounding medium as mechanical waves of pressure and displacement, and to convert this sound into neuronal action potentials. Neuronally encoded sound information then travels via the cochlear division of the vestibulocochlear nerve to the cochlear nuclei within the pons and medulla of the brainstem. Signals subsequently relay through the superior olivary complex, inferior colliculus, and medial geniculate body of the thalamus, before eventual projection to the primary auditory cortex within the temporal lobe of the brain (Webster and Fay, 1992). It is at the primary auditory complex where sound first becomes consciously perceived, though ascending neuronal potentials in the brainstem can be measured by modern techniques (section 2.2.3 below). Abnormalities at any stage along this pathway—the ear, vestibulocochlear nerve, or central nervous system—can all compromise hearing.

Components of the ear are anatomically categorized into those of the outer ear, middle ear, and inner ear (Figure 1.1). The outer ear includes the auricle and ear canal, which function to collect and direct sound towards the middle ear. The tympanic membrane forms the boundary between the outer ear and the middle ear, which contains the three auditory ossicles: the malleus, incus, and stapes. These reside in an otherwise air-filled space. These three small bones function to efficiently

transfer air-conducted sound energy to the fluid-filled cochlea (Flint et al., 2010). Their design is such that they provide the system with a mechanical advantage. This is achieved via leverage and a reduction in the area to which force is applied: from the larger tympanic membrane to the smaller oval window underneath the stapes footplate (Purves, 2012). Beyond the oval window, the structures of the inner ear include six separate sensory organs: the cochlea (the sensory organ of hearing), as well as the three semicircular canals, utricle, and saccule (the five sensory organs of balance and spatial orientation). Sensory information encoded by these organs is transmitted towards the central nervous system via the vestibulocochlear nerve (Flint et al., 2010).

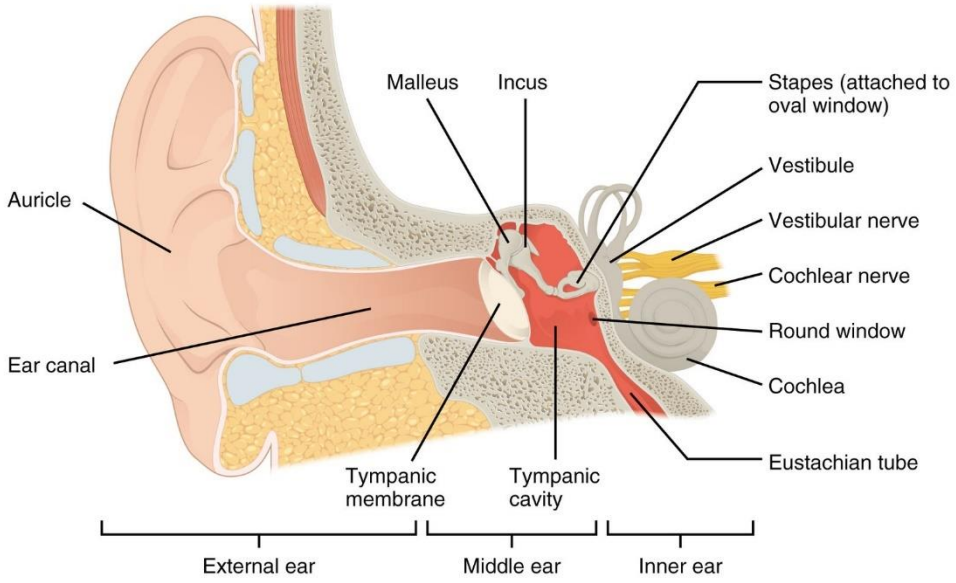


Figure 1.1: Anatomy of the human ear

The ear is divided into three anatomical regions: the outer, middle, and inner ears. Sound is collected by the outer ear. The small bones of the middle ear ossicular chain function to efficiently transfer this air-transferred sound to the fluid-filled environment of the inner ear. The sensory organs within the inner ear include the cochlea, which is responsible for sensing sound, as well as five other balance organs, which detect sensory stimuli from head orientation and movement. Figure reproduced under Creative Commons Attribution License 4.0 license from Betts et al. (2013).

1.2 THE COCHLEA

1.2.1 Cochlear mechanics

The soft tissue structures of the inner ear reside within the "bony labyrinth"; they are encapsulated and embedded within the rigid temporal bone. One inner ear organ, the spiral-shaped cochlea, is responsible for transducing sound into neuronal signals. Vibrations transmitted through the middle ear ossicles are transferred into the cochlea as the stapes vibrates against the oval window at the cochlear base. Internal to the oval window, the environment of the cochlea is fluid-filled and is divided into three separate chambers: the perilymph-filled scala vestibuli and scala tympani, which are continuous with one another at the cochlear apex, and the endolymph-filled scala media, which lies between the two other chambers. The proximal boundary of the perilymph is the oval window and its distal boundary is the round window (Dallos and Fay, 2012). As the oval window is vibrated by the stapes, pressure waves are transferred to the perilymph directly behind the membrane. These pressure waves propagate through the scala vestibuli towards the cochlear apex, and then back down towards the cochlear base in the space known as the scala tympani. The round window at the cochlear base is mobile and thus provides compliance to the system (Peterson and Bogert, 1950). The frequency of the pressure wave propagated through the perilymph matches that of the incoming sound.

The pressure wave in the scala tympani induces resonance in the basilar membrane (Lighthill, 1981, de Boer, 1991). Basilar membrane dimensions and thus mechanical properties follow a gradient along the spiral course of the cochlea (Von Békésy, 1960). At the cochlear base, the basilar membrane is at its narrowest and most stiff and as a result it resonates most efficiently in response to high frequency

sounds, while at the cochlear apex it is as its widest and least stiff and thus resonates most efficiently in response to low frequency sounds. In this way, the cochlea is tonotopically organized, with different frequency sounds perceived at distinct locations along the cochlear length. Positioned on the basilar membrane is the organ of Corti, the sensory portion of the cochlea. The apical surfaces of sensory and non-sensory cells in the organ of Corti project into the endolymph, the highly-regulated fluid which fills the scala media (reviewed in Wangemann [2006]).

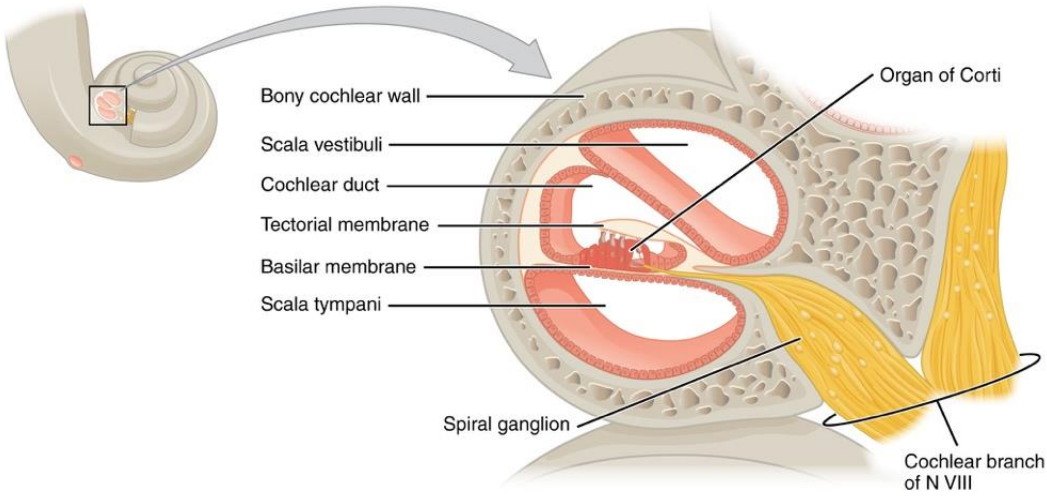


Figure 1.2: Cross sectional view of the cochlea

The spiral-shaped cochlea is divided into three major fluid-filled compartments: the scala vestibuli, the scala media (also known as the cochlear duct), and the scala tympani. These compartments track the length of the cochlear spiral and are best visualized in cross section. The scala vestibuli and scala tympani are both filled with perilymph fluid and are continuous at the cochlear apex, allowing for the unobstructed conductance of fluid pressure waves through both. The scala media is filled with specialized endolymph fluid. The sensory organ of Corti sits within this compartment and apical portions of cells within the organ of Corti are bathed in endolymph. N VII = eighth cranial nerve (the vestibulocochlear nerve). Figure reproduced under Creative Commons Attribution License 4.0 license from Betts et al. (2013).

1.2.2 Endolymph and the stria vascularis

The scala media is physically and electrochemically separated from the overlying scala vestibuli by the epithelial cells of Reissner's membrane and from the

underlying scala tympani by the cells of the organ of Corti and the adjacent epithelial cells of the inner and outer sulcus (Dallos and Fay, 2012). Tight junctions between neighboring cells allow these structures to function as diffusion barriers, preventing the passive movement of ions out of the scala media (Nadol, 1978, Gulley and Reese, 1976). This architecture is critical because the endolymph fluid which fills the scala media is unique in its composition. A positive voltage of ~80 mV referred to as the endocochlear potential (EP) is maintained in the endolymph, and is necessary for proper function of the organ of Corti—specifically for driving depolarization of hair cells (Von Békésy, 1951, Davis, 1953, Wangemann, 2002). Endolymph is uniquely high in potassium ions, which are present at a concentration of ~150 mM, and low in sodium ions, which are present at a concentration of ~1 mM (Wangemann, 2006). The endocochlear potential and endolymph composition overall are understood to be generated and maintained by a highly vascular tissue in the lateral wall of the cochlea, known as the stria vascularis (Tasaki and Spyropoulos, 1959).

Within the stria vascularis exist layers of three predominant cell types (Figure 1.3). A single layer of marginal cells contacts the endolymphatic space, and those cells are highly interdigitated with a deeper layer of intermediate cells. Deep to the intermediate cells lie multiple layers of flat, interleaved basal cells (Echandia and Burgos, 1965). The space between the marginal cell layer and the intermediate cell layer is referred to as the intrastrial space and has been demonstrated to be electrically isolated from neighboring extracellular fluids via tight junctions of the marginal cells and tight junctions of the basal cells (Jahnke, 1975, Reale et al., 1975). Intrastrial fluid has a low K^+ concentration, but a similar positive potential to the endocochlear potential (Salt et al., 1987, Ikeda and Morizono, 1989). This "intrastrial potential" together with Na^+,K^+-ATPases and $Na^+,K^+,2Cl^-$ cotransporters on the basolateral membrane of the marginal cell facilitates K^+ movement into the marginal

cell (Nakazawa et al., 1995, Crouch et al., 1997, Nin et al., 2008). Subsequent movement of K^+ into the endolymph is then facilitated by KCNQ1/KCNE1 channels on the luminal (endolymph-facing) cell surface (Casimiro et al., 2001, Vetter et al., 1996). During the process of hearing, K^+ flows from endolymph to perilymph by transiting through the sensory hair cells (section 1.2.3 below). This K^+ is recycled back to the endolymph through a pathway comprised of perilymph, supporting cells, fibrocytes in the spiral ligament, and intermediate cells in the stria vascularis (Kikuchi et al., 2000, Spicer and Schulte, 1998, Wangemann, 2002). This recycling process helps maintain the high K^+ concentration of the endolymph.

The stria vascularis is also home to a dense capillary network which runs in the intrastrial space. Strial capillary endothelial cells are connected by tight junctions and lack the typical fenestrations (Juhn, 1988, Sakagami et al., 1999). Endothelial cells are further surrounded by a thick basement membrane and pericytes (Shi et al., 2008). Together these structures comprise the "cochlear-vascular unit", a barrier against movement of substances out of these capillaries and into the intrastrial compartment. Collectively, this specialized capillary system is termed the "blood-labyrinth barrier" as it is understood to act as a selective barrier between the systemic circulation and the cochlea. Disruption of this barrier is understood to be associated with a number of pathological conditions including autoimmune inner ear disease, Meniere's disease, drug-induced hearing loss, noise-induced hearing loss, sudden deafness, and genetically-linked hearing dysfunction (Shi, 2016). Overall, the cells of the stria vascularis maintain the endocochlear environment, form the blood-labyrinth barrier, and are thus central to proper cochlear function.

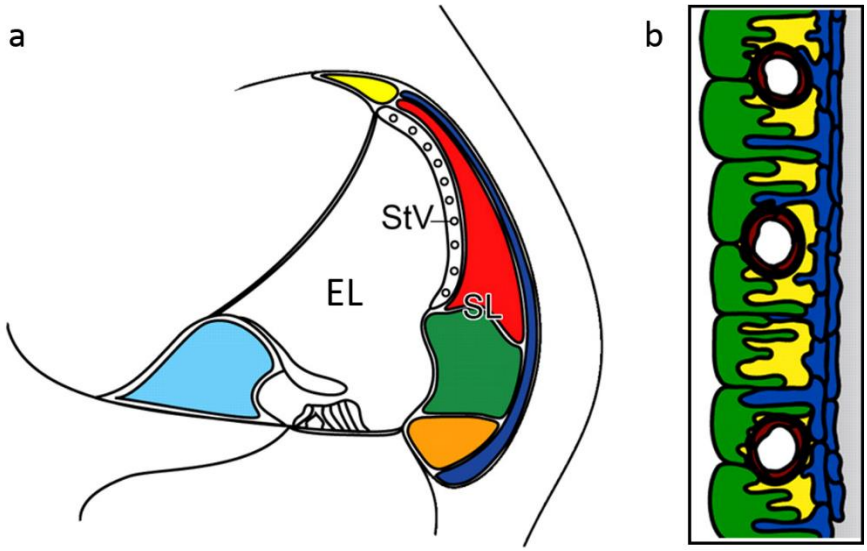


Figure 1.3: Anatomy of the stria vascularis

The stria vascularis is a highly vascular region of tissue located in the cochlear lateral wall and responsible for generating the endocochlear potential, among other functions. (a) Cross sectional view of the cochlea. StV = stria vascularis, SL = spiral ligament, EL = endolymph. (b) Higher magnification view of the tissue architecture of the stria vascularis. The luminal (endolymph-facing) surface is to the left. Three unique cell types form three tissue layers. Marginal cells are shown in green, intermediate cells in yellow, and basal cells in blue. The space between the marginal cell layer and the intermediate cell layer is referred to as the intrastrial space. Capillaries run in the intrastrial space and are drawn in red. Marginal and intermediate cells are highly interdigitated. Figure adapted with permission from Trowe et al. (2008).

1.2.3 The organ of Corti

The organ of Corti is the sensory domain within the cochlea (Corti, 1851). This highly-organized sensory epithelium is positioned on the basilar membrane such that it travels with basilar membrane displacement. The organ of Corti contains the sensory cells of hearing—mechanosensitive hair cells (Figure 1.4). Three adjacent rows of outer hair cells lie lateral (closer to the cochlear lateral wall), and a single row of inner hair cells lies more medial. Hair cells are named for the "hairy" appearance of the bundles of stereocilia ("hair bundles") which project from their apical surfaces. The apical surfaces of cells in the organ of Corti are in direct contact with endolymph fluid, and thus the hair cell stereocilia project into and are bathed

by endolymph. Hair bundles extend to the overlying tectorial membrane, a gel-like, acellular structure composed of extracellular matrix secreted by cells of the spiral limbus (Iurato, 1960, Kimura, 1966). As the basilar membrane moves in response to pressure waves in the cochlea, hair cells in the organ of Corti are brought closer to the tectorial membrane and their stereocilia are deflected.

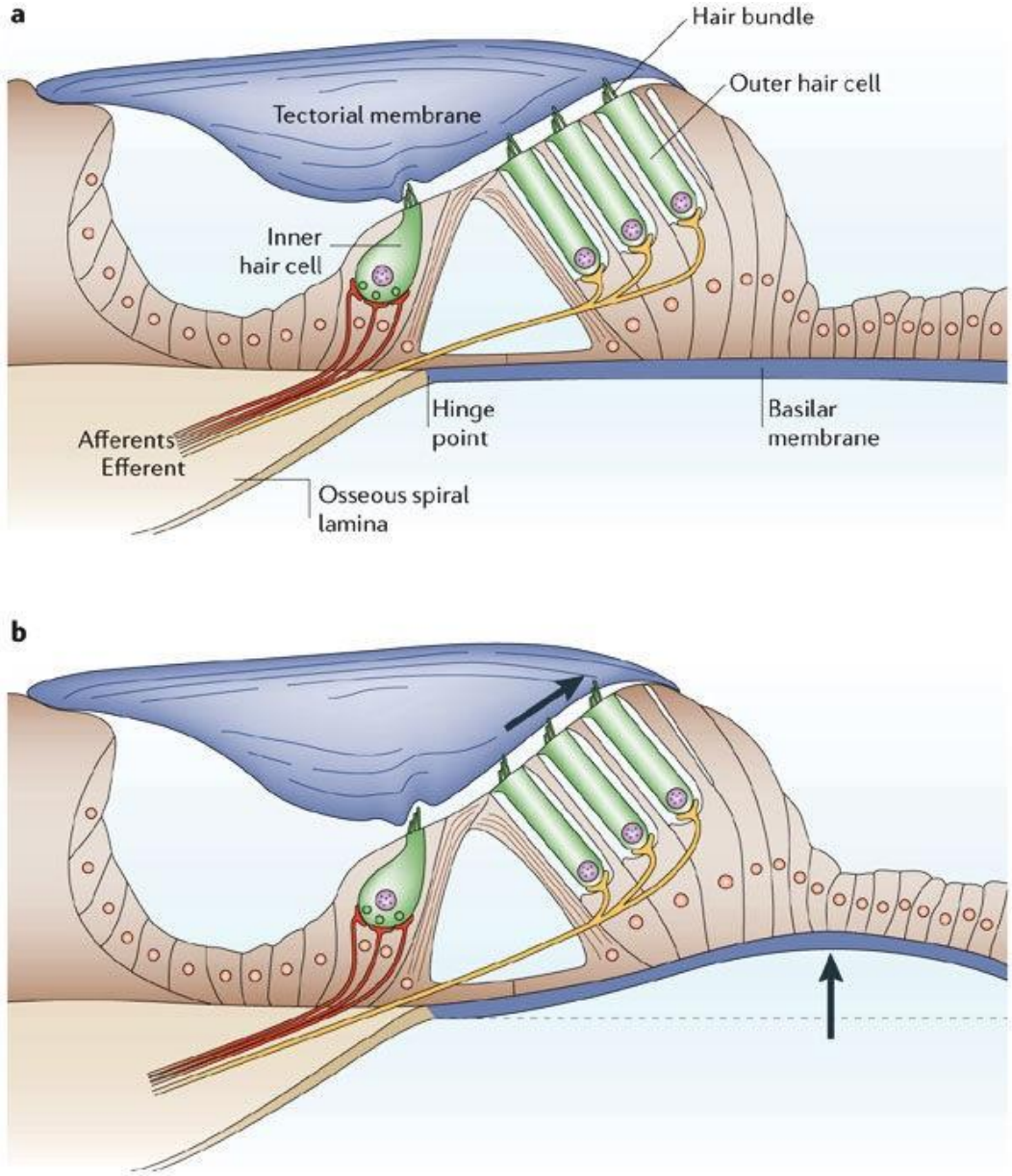


Figure 1.4: Structure and function of the organ of Corti

Cross-sectional view of the organ of Corti. (a) Two distinct populations of sensory hair cells occupy unique positions within the organ, with outer hair cells more lateral and inner hair cells more medial (to the central axis of the cochlea). Both types of hair cells have slanted bundles of stereocilia ("hair bundles") which project into (in the case of outer hair cells) or close to (in the case of inner hair cells) the overlying tectorial membrane. Inner hair cells are more richly innervated with afferent nerve fibers (shown in red), while outer hair cells are more richly innervated with efferent nerve fibers (shown in yellow). However, both hair cell types receive both types of fibers. (b) Upward movement of the basilar membrane (lower arrow) caused by sound pressure waves in the scala tympani creates a shearing force between hair cell stereocilia bundles and the tectorial membrane (upper arrow). This shearing force deflects the hair bundle, a mechanical input

which ultimately results in depolarization of the hair cell. Figure reproduced with permission from Fettiplace and Hackney (2006).

Hair cell stereocilia contain molecular structures central to the process of mechanotransduction—the conversion of mechanical stimuli in the form of sound into cellular electrochemical activity. The stereocilia bundle has a staircase orientation. This arrangement gives the bundle directional polarity (Hudspeth and Corey, 1977, Shotwell et al., 1981). In the cochlea, these bundles are oriented such that the tallest stereocilia lie most lateral and the shortest most medial. Stereocilia tips are tethered to the side of adjacent taller stereocilia via a structure known as the tip link (Pickles et al., 1984, Kachar et al., 2000). Additional side links connect the sides of adjacent stereocilia. Tip links are understood to be composed of the proteins protocadherin 15 (the lower third of the tip link) and cadherin 23 (the upper two thirds of the tip link). These two proteins are associated through a calcium-dependent molecular interaction (Sotomayor et al., 2012, Kazmierczak et al., 2007, Furness et al., 2008). Positive deflection of the hair cell bundle (deflection towards the tallest stereocilia) applies tension to the tip links. Tip links in turn transfer this tension via an elastic gating spring to the mechano-electrical transduction (MET) channel embedded in the membrane of the stereocilium (Araya-Secchi et al., 2016). This tension is understood to pull open the transduction channel, allowing potassium from the endolymph to flow down its electrochemical gradient into the hair cell, resulting in cellular depolarization (Assad et al., 1991, Corey and Hudspeth, 1979). Positive deflection of the hair bundle results in a graded hair cell depolarization. Negative deflection of the hair bundle (deflection towards the shortest stereocilia) conversely results in hair cell hyperpolarization (Hudspeth and Corey, 1977, Shotwell et al., 1981). The mechanoelectrical transduction apparatus is exquisitely sensitive to stereocilium displacement, with minimum auditory stimuli

corresponding to a bundle displacement of only ~1 nm (Rhode and Geisler, 1967, Corey and Hudspeth, 1983). Identification of the molecular components of the MET channel itself remains an area of active research, with four different proteins, TMHS/LHFPL5, TMIE, TMC1, and TMC2, implicated to be involved at this time (Xiong et al., 2012, Zhao et al., 2014, Pan et al., 2013, Kurima et al., 2015).

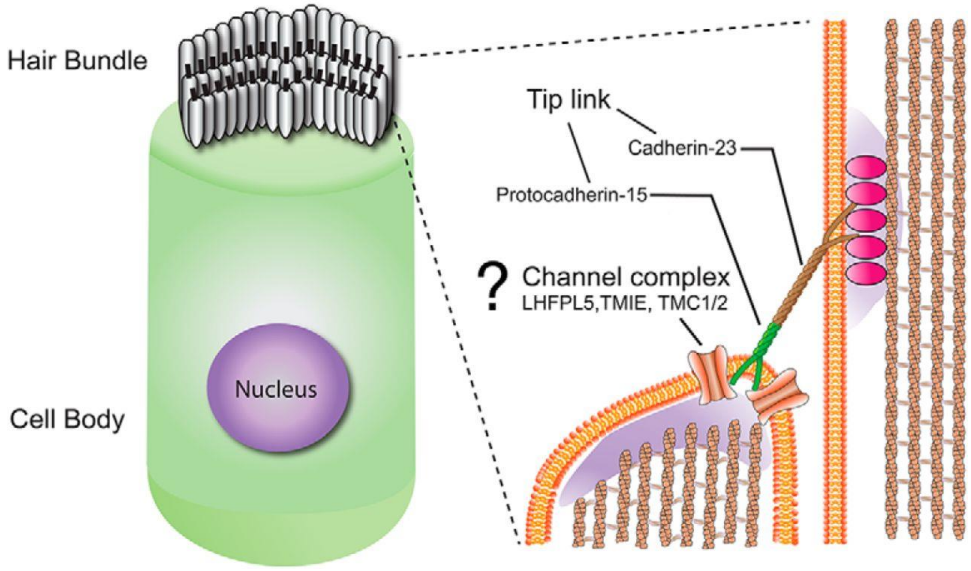


Figure 1.5: Mechanotransduction

The stereocilia bundle of hair cells mediates mechanotransduction. A cochlear outer hair cell is schematized. Hair cell apical stereocilia are arranged in a "W" shape with rows of stereocilia arranged in order of increasing height. Tips of stereocilium are tethered to the lateral insertion density on neighboring, taller stereocilium via tip links composed of protocadherin-15 and cadherin-23. Positive deflection of the hair bundle applies tension to the tip links and this tension is transferred to the MET channel complex. In response, the channel complex increases its permeability to cations, allowing potassium present in the endolymph to enter and depolarize the hair cell. The molecular composition of the channel complex is still being fully elucidated, but has been proposed to include the following proteins: LHFPL5 = Lipoma HMGIC Fusion Partner-Like 5, TMIE = Transmembrane Inner Ear, and TMC1/2 = Transmembrane Channel Like 1/2. Figure reproduced with permission from Wu and Muller (2016).

1.2.4 Innervation of cochlear hair cells

Though both inner and outer hair cells are stimulated in response to sound, the two populations play a different role in facilitating hearing, and their respective

innervations reflect this (Purves, 2012). Inner hair cells receive the majority (~95%) of afferent nerve fibers, which carry sensory information towards the cochlear nuclei for higher order processing. This afferent innervation comes in the form of large diameter, myelinated type I afferents which each contact a single inner hair cell. 10-30 individual afferent fibers may form single bouton-like endings on an individual inner hair cell (Dannhof and Bruns, 1993, Spoendlin, 1969, Spoendlin and Tachtensteiger, 1967). In contrast, outer hair cells receive afferent innervation in the form of far fewer small, unmyelinated type II afferents, which each contact numerous outer hair cells (Perkins and Morest, 1975, Ginzberg and Merest, 1983, Ginzberg and Morest, 1984, Berglund and Ryugo, 1987, Echteler, 1992). The rich afferent innervation of inner hair cells is fitting with the understanding of these hair cells as the "true" receptors.

Opening of the inner hair cell MET channel drives a graded depolarization of the membrane potential. This depolarization induces the opening of basally-located voltage gated calcium channels ($Ca_V1.3$), and the ensuing influx of calcium triggers glutamate release from the basal hair cell membrane (Fuchs et al., 1990, Moser and Beutner, 2000). Glutamate vesicle release occurs via a specialized structure known as a ribbon. This electron-dense ribbon is anchored to the presynaptic plasma membrane and tethers synaptic vesicles (Smith and Sjöstrand, 1961). The ribbon synapse helps mediate the challenging neurotransmitter release requirements of the hair cell synapse. It is understood to permit sustained neurotransmitter release in response to long-lasting stimuli. It is also essential for the temporally precise synaptic transmission required for the encoding of sub-millisecond interaural time differences which are used to localize sound (Safieddine et al., 2012). Glutamate released from the hair cell ribbon stimulates an action potential in the closely-associated bouton process of an afferent nerve of the cochlear spiral ganglion. The

hair cell stimulation is encoded as a series of action potentials from that point forward in the auditory pathway.

In contrast, the primary function of outer hair cells is to act as the "cochlear amplifier", and their innervation reflects this. While inner hair cells are more richly innervated by afferent fibers, outer hair cells are more richly innervated by efferent fibers, which act as a feedback pathway to the hair cells. Efferent fibers from the olivocochlear system synapse upon multiple outer hair cells and mediate hyperpolarization of the hair cell, with acetylcholine acting as the primary neurotransmitter (Warr and Guinan Jr, 1979, Sziklai and Dallos, 1993, Dallos and Fay, 2012). In this way, hair cells can receive higher-order feedback which modulates their potential.

This feedback helps modulate a mechanical response unique to the outer hair cell. In a phenomenon termed somatic electromotility, outer hair cells oscillate their length in response to membrane potential (Brownell et al., 1985, Kachar et al., 1986, Zenner, 1986, Ashmore, 1987). As the outer hair cells shorten or lengthen they can influence the movement of the organ of Corti relative to the tectorial membrane. This modulation is understood to allow for non-linear amplification of sounds of different frequencies and to improve frequency discrimination (Hudspeth, 2014). Outer hair cell movement can increase displacement caused by quieter sounds, and in that way act as a "cochlear amplifier" (Hudspeth, 2008). Therefore, while inner and outer hair cells both perform mechanotransduction, their downstream roles in hearing are quite distinct.

1.3 THE UTRICLE

The cochlea represents only one of the six sensory organs of the inner ear, the other five being organs of the vestibular system: the utricle, saccule, and the three semicircular canals. Sensory perception in these organs is too mediated by the hair cell, however, while hair cells in the cochlea depolarize in response to sound stimuli, hair cells in the vestibular organs are responsive to mechanical stimuli in the form of head movement and positional orientation (Purves, 2012). Only the utricle will be discussed in detail here, as it is most relevant to this thesis and its anatomy and physiology is very analogous to the saccule and somewhat analogous to the sensory ampullae of the semicircular canals. The utricle is a roughly oval-shaped, planar organ oriented horizontally, and thus capable of sensing horizontal linear acceleration (Figure 1.6). Utricular hair cells in the sensory epithelium extend their hair bundle—which includes a kinocilium—into an overlying gelatinous matrix known as the otolith (or otoconial) membrane (Johnsson and Hawkins, 1967, Lindeman, 1973). Embedded in this membrane are calcium carbonate crystals known as otoconia, which contribute mass. The greater relative mass of the otolithic membrane gives it greater inertia and thus causes it to lag behind the utricle sensory epithelium temporarily when the head is displaced. This lag causes the otolith membrane to translate across the sensory epithelium, producing a shearing force (Purves, 2012). This shearing force deflects hair cell stereocilia bundles, causing a change in the cation permeability of MET channels (Géléoc et al., 1997).

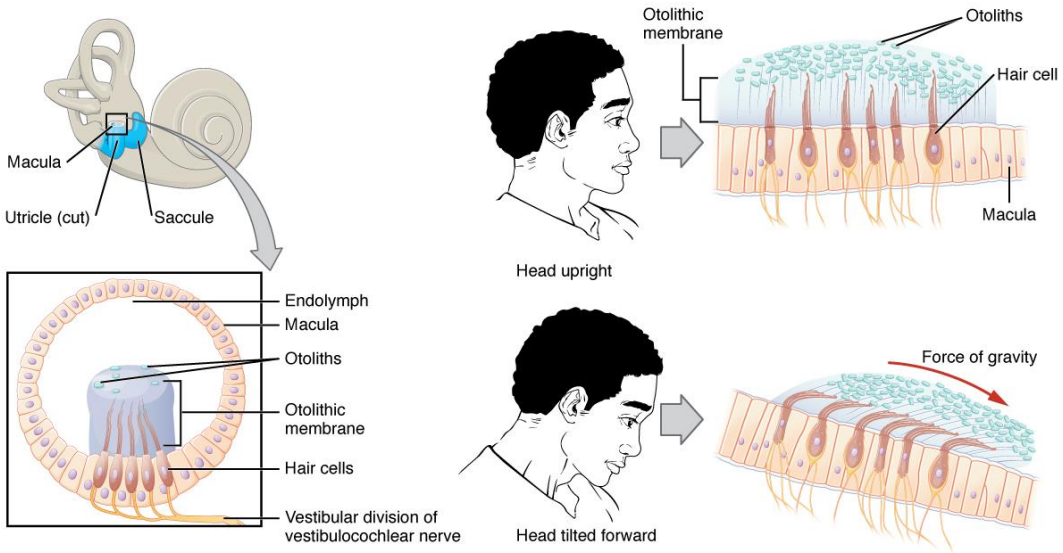


Figure 1.6: Structure and function of the utricle

The utricle is a vestibular organ specialized for detection of linear acceleration in the horizontal plane. The organ is filled with specialized vestibular endolymph. Hair cells in the sensory epithelium are overlain by the dense otolith membrane. The difference in inertia between the sensory epithelium and the overlying otolith membrane generates a shearing force on the hair cell stereocilia bundles as the head undergoes linear acceleration or head tilt. Figure reproduced under Creative Commons Attribution License 4.0 license from Betts et al. (2013).

In the utricle, hair cell bundles face one of two directions, depending upon whether the hair cell is medial or lateral to the line of polarity reversal, which runs roughly down the midline of the utricle (Denman-Johnson and Forge, 1999, Li et al., 2008, Spoendlin, 1964). Hair bundles on either side of the line of polarity reversal are oriented toward each other in the utricle and away from each other in the saccule. Therefore, the same stimulus depolarizes hair cells on one side of the line of polarity reversal while hyperpolarizing hair cells on the opposite side (Hudspeth and Corey, 1977, Shotwell et al., 1981).

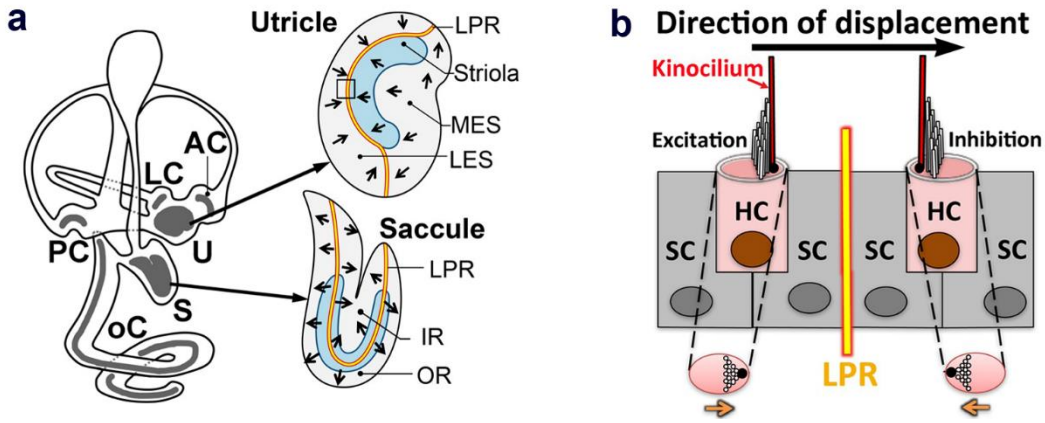


Figure 1.7: Organization of the sensory epithelium of otolith organs

Hair cell organization of the mammalian otolith organs. (a) The mammalian inner ear (mouse is shown) includes six sensory organs, which are shaded in grey. AC = anterior crista, LC = lateral crista, PC = posterior crista, U = utricle, S = saccule, oC = organ of Corti. The two otolith organs, the utricle and saccule detect linear acceleration and gravity and are shown enlarged at right. The central striola is shaded in blue. The line of polarity reversal (LPR) divides the lateral extrastriola (LES) from the striola and medial extrastriola (MES) regions. Similarly, in the saccule the LPR divides the inner region (IR) from the outer region (OR). (b) The line of polarity reversal divides populations of hair cells with opposite hair bundle polarities. The same displacement results in excitation of hair cells on one side of the LPR and inhibition of hair cells on the other. SC = supporting cell, HC = hair cell. Image adapted under Creative Commons Attribution License 4.0 license from Jiang et al. (2017).

1.3.1 Vestibular hair cells

Vestibular hair cells are analogous to their auditory counterparts in fundamental ways, though important differences do exist (Eatock et al., 2006). Both hair cell types utilize the mechanotransduction apparatus described above to alter their cation permeability in response to hair bundle displacement. Both cochlear and vestibular hair cells release glutamate containing synaptic vesicles onto the dendrites of afferent neurons by way of the ribbon synapse, and both hair cell types receive cholinergic fibers from the brainstem. As two populations of hair cells exist in the cochlea, similarly two distinct populations of hair cells exist in the vestibular organs, where they are termed “type I” and “type II” hair cells (section 1.3.2 below). However, unlike cochlear outer and inner hair cells, type I and type II hair cells do

not have unique anatomical positions within the sensory epithelium, but are rather both distributed throughout (Lindeman, 1969, Li et al., 2008).

Fundamental characteristics of mechanotransduction also differ between cochlear and supporting cells. Vestibular hair cells respond to stimuli of a lower frequency, typically in the range of a few Hz up to ~20 Hz (Grossman et al., 1988, Minor et al., 1999). In contrast, hair cells in the cochlea allow for the perception of sounds ranging from ~20 Hz to ~20 kHz (Pumphrey, 1950, Purves, 2012). Hair bundles from both cochlear and vestibular hair cells project into specialized endolymph fluid, and it is the cations present in this endolymph—most notably potassium cations—which drive depolarization of the hair cell. However, while cochlear endolymph has a potential of ~80 mV, endolymph in the utricle has a potential of ~3 mV. This vestibular endolymph is produced by the dark cell epithelium, which lines the endolymphatic space and is analogous to the stria vascularis in the cochlea (Wangemann, 1995, Marcus and Shen, 1994).

1.3.2 Innervation of vestibular hair cells

Type I and Type II hair cells are distinguished primarily by the type of post-synaptic contact made by their afferent nerve fibers. Type I hair cells receive a cup-shaped calyx, whereas type II hair cells receive multiple small bouton endings (Desai et al., 2005). Both hair cell types populate both the striolar and extrastriolar regions of the utricle, though the manner of innervation differs in these two regions. Afferent nerves which exclusively end in calyxes only innervate striolar, type I hair cells. Afferent nerves which exclusively end in boutons only innervate extrastriolar type II hair cells. Dimorphic afferents—those with both calyx and bouton endings—innervate both hair cell types in both regions (Fernandez et al., 1990).

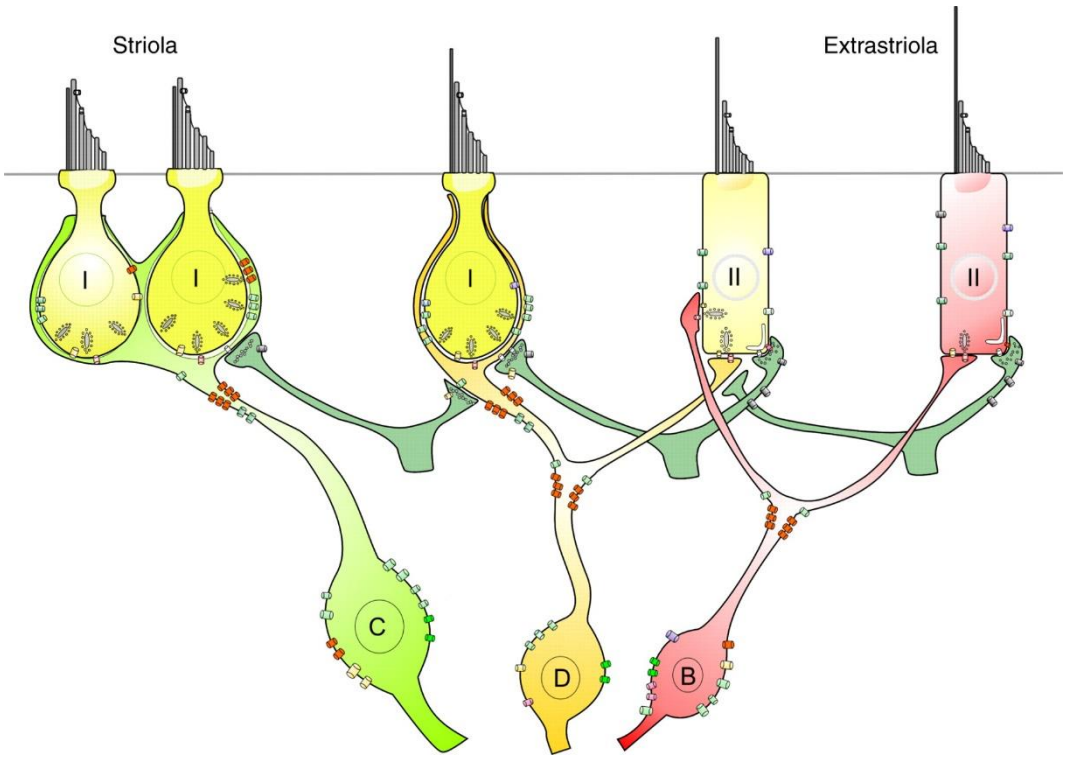


Figure 1.8: Hair cell innervation in the utricle

Innervation of vestibular hair cells. Vestibular afferent neurons have one of three terminal morphologies: calyx-only (C), bouton-only (B), or dimorphic (D). Calyx-only afferents exclusively innervate type I hair cells in the striola, sometimes forming complex calyces which envelope multiple type I hair cells (labeled with I). Bouton-only afferents exclusively innervate type II hair cells (labeled with II) in the extrastriola, and can innervate tens of cells. Afferent neurons with dimorphic terminations can innervate either hair cell type in either region. Efferent fibers arising from the brainstem are shaded in green. Figure adapted with permission from Eatock et al. (2008).

1.3.3 Supporting cells

In both the cochlea and vestibular organs, hair cells are immediately surrounded by supporting cells. In the cochlea, supporting cells actually outnumber hair cells. Supporting cells are responsible for both physically and physiologically "supporting" hair cells (Wan et al., 2013). Within the cochlea, supporting cells are divided into several distinct populations with distinct morphologies and locations. Cochlear supporting cell types include (from medial to lateral) border cells, inner phalangeal cells, pillar cells, Deiters' cells, and Hensen's cells. These populations

express both some shared and some unique molecular markers (Burns et al., 2015). Inner hair cells are cupped and surrounded by border cells and inner phalangeal cells, while outer hair cells are seated on Deiters' cells. In the vestibular organs, multiple populations of supporting cells haven't been clearly defined. Vestibular supporting cells are morphologically more uniform, though functionally distinct subpopulations seem to exist (Wang et al., 2015). Like cochlear hair cells, vestibular hair cells are cupped and surrounded by supporting cells.

Supporting cells are understood to play a growing number of roles in cochlear and vestibular development, structure, homeostasis, and response to damage (Wan et al., 2013). The structural contributions of supporting cells have long been recognized. It is the supporting cells and not the hair cells which are directly anchored to the basilar membrane. Supporting cells are rich in cytoskeletal proteins and can provide a rigid structural framework for the organ (Slepecky et al., 1995), the most striking example of which is arguably the triangular tunnel of Corti formed by the inner and outer pillar cells.

At their apical surface, supporting cells and hair cells are joined together by tight junctions and adherens junctions to form the reticular lamina, a physical barrier for endolymph which allows for preservation of the endolymph's unique ion concentrations, namely high potassium and low sodium (Gulley and Reese, 1976). Not only do they help form this barrier, but supporting cells also function to actively regulate homeostasis of the endolymph by absorbing sodium and helping to recycle potassium (Wangemann, 2002). Supporting cells are biochemically linked via gap junctions while hair cells appear to share gap junctions neither with each other nor with their surrounding supporting cells.

Though hair cells are highly sensitive to several types of stress, including loud noise, ototoxic drugs, and aging, supporting cells seem more robust. The

notable exception to this being cisplatin ototoxicity, which appears to affect both cell types (Slattery and Warchol, 2010, Monzack et al., 2015, Ramírez-Camacho et al., 2004). As hair cells die by apoptosis, the surviving neighboring supporting cells can surround and phagocytose the hair cell body and apoptotic bodies, converging to maintain the integrity of the reticular lamina (Hawkins, 1973, Bohne and Rabbitt, 1983, Forge, 1985, Leonova and Raphael, 1997, Bird et al., 2010, Monzack et al., 2015).

Beyond cleanup of dying hair cells, supporting cells can also be central to hair cell regeneration. In mammals, the adult cochlea does not possess a native capacity to regenerate lost hair cells. However, spontaneous hair cell regeneration has been described in the adult utricle (Forge et al., 1993, Li and Forge, 1997, Forge et al., 1998, Warchol et al., 1993, Rubel et al., 1995) and in neonatal cochleae (White et al., 2006, Cox et al., 2014). In both organs, hair cell regeneration is understood to occur via transdifferentiation of supporting cells, either directly or following a cellular division. The finding that hair cell regeneration can occur in mammals under specific conditions suggests that therapeutic, induced hair cell regeneration may be possible if one can reproduce the necessary conditions. Efforts to induce supporting cell-mediated replacement of hair cells are underway, including in clinical trial (ClinicalTrials.gov, Identifier: NCT02132130). With such a diverse set of critical roles in the inner ear, the importance of supporting cells to hearing and balance cannot be overstated.

1.4 NON-MAMMALIAN MECHANOSENSORY ORGANS

The anatomy and physiology of the inner ear as described above holds true for mammals, however, differences exist in non-mammalian vertebrates. The chick, frog, and zebrafish have been the most utilized experimentally. In the chick, there are a total of eight inner ear organs, all of which utilize sensory hair cells. The single auditory sensory organ is known as the basilar papilla. The seven vestibular organs include a utricle, saccule, and three crista ampullae as well as two additional organs: the lagena and the macula neglecta (Knowlton, 1967, Wu and Oh, 1996). The organization of the basilar papilla is distinct from that of the mammalian cochlea. Unlike the tight spiral shape of the mammalian cochlea, the chick basilar papilla has only a slight curvature. The basilar papilla is populated with two distinct types of hair cells, tall hair cells (THCs) and short hair cells (SHCs), generally considered analogous to the mammalian inner and outer hair cells, respectively (Tanaka and Smith, 1978, Fischer, 1992). These hair cell types coexist in a single sensory epithelium, with the proportion of SHCs to THCs increasing towards the high-frequency end of the papilla (Hirokawa, 1978), and the basilar papilla is overlain by a tectorial membrane which deflects hair cell bundles. Unlike their mammalian counterparts, these auditory hair cells can regenerate *in vivo* and *in vitro* and are thus of significant scientific interest (Tucci and Rubel, 1990, Oesterle et al., 1993).

Historically, there has been similar interest in the inner ear sensory organs of the frog which is also known to regenerate hair cells (Baird et al., 1996). In addition to otolith organs analogous to their mammalian counterparts, the frog possesses two auditory receptors organs, the amphibian papilla and basilar papilla (Wever, 1973). These auditory organs have a more convoluted shape, with the amphibian papilla being roughly “S” shaped and basilar papilla roughly “C” shaped(Lewis et al., 1982a). Tonotopic organization has been characterized for the

amphibian papilla only (Lewis et al., 1982b, Van Dijk et al., 2011). Hair cells in both auditory organs project stereocilia into overlying tectorial membranes. Both the frog and chick lack the selective amplification of sound made possible by outer hair cell somatic electromotility. Additionally, they lack the compact spiral shape of the mammalian cochlea which is believed to have allowed for the evolutionary development of a longer auditory organ and thus a wider frequency range of hearing.

Though the zebrafish possesses inner ear auditory and vestibular sensory organs which utilize mechanosensitive hair cells, scientific interest in this species has largely focused on its lateral line system. The lateral line is a collection of sensory units on the surface of the fish which functions to detect movement, vibration, and pressure gradients in the surrounding water (Dijkgraaf, 1963). Individual sensory units are known as neuromasts. Each neuromast is populated with 5–20 mechanosensitive hair cells, supporting cells, and an outer ring of mantle cells and is considered somewhat analogous to auditory and vestibular sensory organs (Metcalfe et al., 1985). The lateral line provides a model system especially useful for the study of hair cells as surface neuromasts can be exposed to dyes, drugs, or other soluble treatments simply by submerging the fish. As they are on the surface of the fish, neuromasts are also very amenable to imaging. In this way, the response of *in vivo* hair cells and supporting cells to a wide variety of treatments can be studied using the zebrafish model (Whitfield, 2002).

1.5 SENSORINEURAL HEARING LOSS

Hearing loss is the world's most common sensory deficit, affecting an estimated 554 million people in 2013 (Stevens et al., 2013). This hearing loss is broadly classified into three etiologies: conductive, sensorineural, or mixed (involving both conductive and sensorineural causes). These designations are anatomically based. Conductive etiologies are those which affect structures upstream of the cochlea (the outer or middle ear) and thus impair the *conduction* of sound waves to the cochlea, while sensorineural etiologies are those which directly affect the cochlea or vestibulocochlear nerve and thus impair one's ability to convert sound into neuronal action potentials or to transmit those action potentials to the central nervous system. Rarely, sensorineural deafness may be a result of cortical or "central" deafness in which a brain lesion results in the patient's inability to perceive sound. This pathology can be seen with bilateral temporal lobe lesions, and the patient's ability to perceive sound and process language may vary depending upon the exact location and extent of the cortical lesion(s) (Graham et al., 1980, Setzen et al., 1999).

Sensorineural hearing loss is vastly more common than conductive hearing loss, and is unfortunately more likely to be irreversible. The major cochlear causes of sensorineural hearing loss include genetic or other congenital abnormalities, aging ("presbycusis"), noise exposure, infection, and exposure to "ototoxic" drugs—drugs toxic to the inner ear. Several drugs are known to cause sensorineural hearing loss. High-dose aspirin and other salicylates (Curhan et al., 2010) as well as antimalarials such as quinine (Roche et al., 1990) have been shown to cause reversible hearing loss. Phosphodiesterase type 5 inhibitors such as sildenafil and loop diuretics such as furosemide have limited potential to cause permanent hearing loss (Cianfrone et al., 2011, McGwin, 2010, Maddox et al., 2009). However, two classes of clinical drugs

are responsible for the vast majority of permanent drug-related hearing loss—aminoglycoside antibiotics and platinum chemotherapy. Together these drugs cause permanent hearing loss for an estimated 500,000 Americans annually, with global data lacking (Rybak et al., 2007). Despite long-established knowledge of their potential ototoxicity, both classes of drug remain in very high use due to their high efficacy and lack of suitable alternatives.

1.5.1 Clinical evaluation of hearing

In the clinical setting, hearing can be evaluated using several different techniques. These testing methods can either be subjective—requiring the full cooperation of the patient—or objective and they can be qualitative—reporting results as simply normal or abnormal—or quantitative. Quantitative methods for assessing sensorineural hearing loss are most relevant to this thesis. A standard and common method of audiometry in applicable patients is pure tone audiometry (PTA). In this type of testing, the patient is placed in a quiet environment and played pure or warbled tones and asked to indicate whether they heard the tone. In this way, the patient's ability to detect soft sounds across a range of different frequencies can be evaluated. The hearing threshold at a frequency is determined as the intensity (measured in decibels) level at which the patient can detect the tone at least half the time (Walker et al., 2013). Results are plotted on an audiogram (Figure 1.9). Though humans are generally understood to be able to perceive frequencies ranging from 20 Hz to 20,000 Hz, pure tone audiometry is typically only performed between 250 Hz and 8,000 Hz (at specific frequencies of 250, 500, 1000, 2000, 4000, 6000, and 8000 Hz). Testing beyond this range is more time-intensive and priority is given to testing those frequencies closer to the normal range of human speech (Furman and Lempert, 2016). Of course, testing of limited frequencies can result in a

failure to detect any high (or especially low) frequency hearing loss, and thus a failure to diagnose and properly treat those patients.

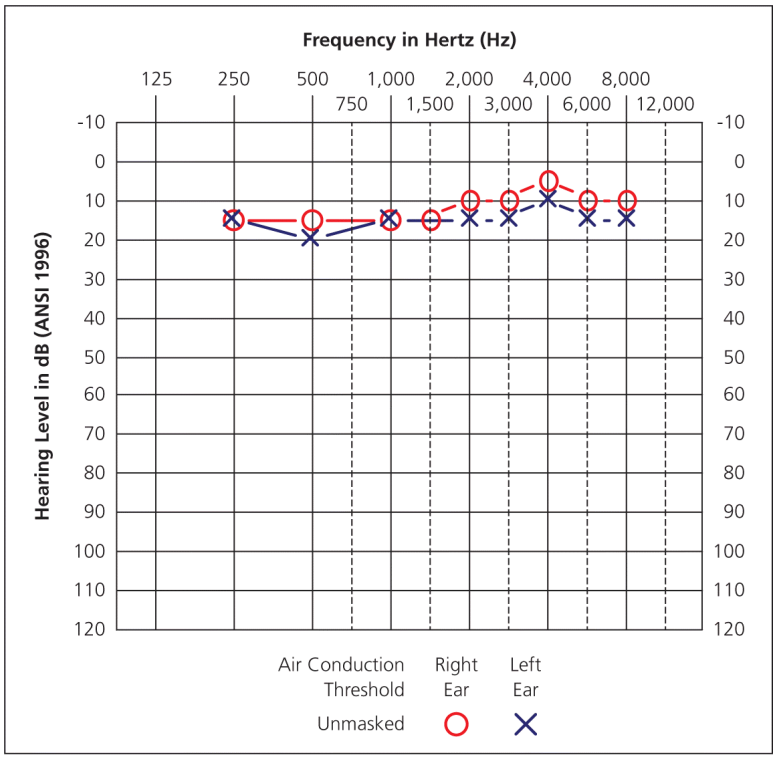


Figure 1.9: A representative audiogram obtained from a hearing individual

Pure tone audiometry is typically performed at frequencies between 250 Hz and 8,000 Hz, with the results plotted on an audiogram. Sound frequency is plotted along the horizontal axis and the hearing threshold at each tested frequency is plotted along the vertical axis, with higher (louder) hearing thresholds plotted towards the bottom of the chart. The hearing threshold at a frequency represents the decibel level at which the patient can detect the tone at least half the time. Thresholds for each ear are determined individually and plotted on the same audiogram, with right ear thresholds recorded as a (red) circle and left ear thresholds recorded as a (blue) X. Figure reproduced from Walker et al. (2013).

Pure tone audiometry is of course a subjective method, requiring the cooperation of the patient. Two commonly employed objective testing methods, which may be used as an alternative or in addition to PTA are auditory brainstem response (ABR) audiometry and distortion product otoacoustic emissions (DPOAE) audiometry. ABR audiometry evaluates the response to sound on the neurological level, while DPOAE audiometry evaluates the collective function of cochlear outer

hair cells (the so-called “cochlear amplifier”). Both techniques are quantitative and do not require active patient participation, making them especially useful for testing young children in the clinical setting. Further, they can be directly adopted to audiometric testing of laboratory animals in the research setting. Both these techniques are described in greater detail in section 2.2.3 below.

1.5.2 Ototoxicity associated with platinum-based chemotherapy

Platinum-based chemotherapeutics are a widely-used class of drugs, the only FDA-approved members of which are cisplatin, carboplatin, and oxaliplatin. Cisplatin was FDA approved in 1978 and became the first drug in the class. Currently, it is used in adults as monotherapy or in combination therapy to treat bladder, ovarian, testicular, breast, cervical, endometrial, gastric, head and neck, lung, and penile cancers, Hodgkin lymphoma, pleural mesothelioma, multiple myeloma, and osteosarcoma. In children, it is used to treat high-risk neuroblastoma, medulloblastoma, osteosarcoma, hepatoblastoma, and germ cell tumors (Lexicomp Online). Platinum chemotherapeutics are given intravenously, and their anti-cancer mechanism of action has been understood to primarily be interference with DNA replication by the formation of intra- and inter-strand crosslinks. Their use is associated with a number of side effects, the most common of which include nausea and vomiting, peripheral neurotoxicity, nephrotoxicity, and ototoxicity.

The platinum-based chemotherapeutics differ in their propensity to cause ototoxicity, with hearing loss common after cisplatin treatment, uncommon after carboplatin treatment (Qaddoumi et al., 2012), and rare after oxaliplatin treatment (Oh et al., 2013). Because cisplatin was the first approved, subsequent drugs in the class need to prove equivalence or non-inferiority. For many cancer types, there is insufficient data to this effect. For other cancers, such as testicular, cisplatin has been shown to be more effective (Bajorin et al., 1993, Bokemeyer et al., 1996). For

these reasons, cisplatin remains the preferred drug in this class for most regimens, despite its greater toxicity, both to the inner ear and other organs. As such, it is responsible for the bulk of ototoxicity associated with platinum-based chemotherapy.

Cisplatin chemotherapy causes permanent hearing loss in approximately 40-80% of adults and at least 51% of children (Stohr et al., 2005, Frisina et al., 2016, Knight et al., 2005, Knight et al., 2017). Individual studies have reported rates of ototoxicity as high as 90 to 100% (Benedetti Panici et al., 1993). Young children are more susceptible than adults (Li et al., 2004). It must be noted that reported rates of hearing loss caused by cisplatin chemotherapy have been highly variable (van As et al., 2016). Factors affecting the occurrence or severity of hearing loss include the cumulative dose administered, the age of the patient and previous noise exposure (Bokemeyer et al., 1998, Li et al., 2004), patient nutritional state (Kopelman et al., 1988), and concomitant cranial irradiation (Hitchcock et al., 2009, Huang et al., 2002). Compounding this true variability is the additional variability introduced by unstandardized methods for monitoring and classifying hearing loss (van As et al., 2016).

Cisplatin ototoxicity presents as bilateral (but not necessarily symmetric), high frequency, sensorineural hearing loss. This can be accompanied by tinnitus, but is not typically accompanied by balance dysfunction. Hearing loss progresses from high frequencies towards low frequencies as the basal cochlear region exhibits cell damage and loss before more apical regions (discussed in detail in section 3.1 below). Progression of hearing loss typically occurs in the days to weeks immediately following administration of successive rounds of cisplatin, but in some cases can progress weeks-to-months after completion of therapy (Sprauten et al., 2012); this may be particularly common in pediatric patients (Al-Khatib et al., 2010,

Bertolini et al., 2004, Knight et al., 2005, Stohr et al., 2005). Despite the high ototoxic potential, no standard audiometric monitoring for adults is in place in most clinical settings (Schmitt and Page, 2017).

Owing to improved cancer detection and treatment, as well as a growing and aging population, the number of cancer survivors continues to increase (DeSantis et al., 2014). As this population grows, so does the importance of addressing the long-term sequelae of cancer treatment. At this time, no treatments for preventing or reversing cisplatin ototoxicity have been approved for clinical use; current progress is discussed in section 1.7.2 below.

1.5.3 Ototoxicity associated with aminoglycoside antibiotics

The aminoglycosides are a large, widely-used class of antibiotics, which includes the first-in-class streptomycin, as well as gentamicin, tobramycin, amikacin, neomycin, and paromomycin. They are understood to act via inhibition of bacterial protein synthesis by binding to the cytosolic bacterial ribosome and are effective against aerobic gram-negative bacterial infections. In developed countries, due to their nephrotoxic and ototoxic potential, aminoglycoside use is largely restricted to serious infections and empiric treatment before the specific infectious agent is identified. They are commonly administered intravenously in the treatment of sepsis, endocarditis, nosocomial respiratory infections, osteomyelitis, and complicated infections of the abdomen and urinary tract, are used to treat some mycobacterial infections such as drug-resistant tuberculosis, and are used extensively as prophylaxis against pneumonia often caused by *Pseudomonas aeruginosa* in patients with cystic fibrosis. In developing countries, aminoglycoside use is even more widespread as the drugs are often available without a prescription (Morgan et al., 2011, Ocan et al., 2015). The low cost of these drugs combined with a high prevalence of tuberculosis has led to the aminoglycosides being some of the

most widely used drugs in the world. As with the platinum-based chemotherapeutics, aminoglycosides carry the potential side effects of nephrotoxicity and ototoxicity, which can be dose-limiting.

The different aminoglycosides vary in their ototoxic potential and their propensity to cause hearing loss ("cochleotoxicity") versus balance disturbances ("vestibulotoxicity"). Neomycin is thought to be the most ototoxic (Xie et al., 2011). Neomycin, amikacin, and kanamycin are more cochleotoxic than vestibulotoxic, while gentamicin and streptomycin seem to be preferentially vestibulotoxic. The well-established vestibulotoxicity of gentamicin has led to its adoption as a vestibular ablation-based method for treating Menière's disease (Perez et al., 2003).

In the setting of short-term aminoglycoside treatment for an acute infection, the overall rate of hearing loss is about 20%, and vestibular toxicity occurs at a rate of about 15% (Lanvers-Kaminsky et al., 2017). When high frequency hearing testing has been performed, the observed rate of hearing loss has been 47% (Fausti et al., 1992). Amongst cystic fibrosis patients receiving aminoglycoside treatment as pneumonia prophylaxis, the rates of reported hearing loss have ranged from 17% to 21% (Fee, 1980, Lerner et al., 1986, Cardinaal et al., 2000).

Patient factors affecting rates of aminoglycoside ototoxicity are not well-established. In animal studies, rates of ototoxicity vary expectedly with the specific drug used and the dose and timing of its administration (Wu et al., 2001). However, in clinical studies this association with dose and timing has not been established (Gatell et al., 1987). The best-established patient risk factors for aminoglycoside ototoxicity are certain genetic mutations. Point mutations in the small 12S ribosomal RNA gene increase the affinity of aminoglycosides for the human ribosome (which is typically extremely low) and have been associated with high-susceptibility to

aminoglycoside ototoxicity in families carrying these mutations (Casano et al., 1999, Hamasaki and Rando, 1997, Prezant et al., 1993).

Aminoglycoside cochleotoxicity presents as progressive, high-frequency sensorineural hearing loss with or without tinnitus, while vestibulotoxicity can present as vertigo, disequilibrium, lightheadedness, nausea, vomiting, and ataxia (Lanvers-Kaminsky et al., 2017). Current recommendations from the American Academy of Audiology for monitoring hearing loss in these patients are pure-tone audiograms in the standard range of 125 Hz to 8 kHz and the additional high frequency range of 8 kHz up to 16 or 20 kHz (Durrant et al., 2009). Diagnosis of vestibulotoxicity is performed through rotary chair testing, vestibular autorotation, or testing of the vestibular-ocular reflex.

The number of patients treated with aminoglycoside antibiotics continues to rise with population growth and the propagation of drug-resistant bacteria. There are currently no approved therapies for the prevention of aminoglycoside ototoxicity. However, one currently promising approach is the recent development of a designer aminoglycoside intended to be less ototoxic. An initial study in mice has demonstrated significantly reduced ototoxicity while retaining similar efficacy against *E. coli* urinary tract infections as the FDA-approved aminoglycoside sisomicin (Huth et al., 2015).

1.5.4 Clinical consequences of ototoxicity

As cisplatin and the aminoglycoside antibiotics both cause a high-frequency, progressive, permanent, sensorineural hearing loss, their impacts upon patient quality of life are similar. In both patient populations, initial hearing deficits may develop at frequencies above the range of normal speech (>4kHz), which although affecting the perception of music and environmental noises, can go largely

undetected. With further progression, the ability to perceive phonemes—units of sound within speech—is lost in a frequency-dependent manner. The perceived result is both a decrease in the volume of and a distortion of speech, leading to difficulty in speech recognition and comprehension (Stelmachowicz et al., 2004).

The effects of hearing loss upon a pediatric or adult patient's life are complex and multifactorial. Acutely, hearing loss can impact safety as the impacted individual loses situational awareness and can miss the warning sounds of an impending accident. Indeed, hearing loss has been associated with an increased risk of workplace accidents (Girard et al., 2009). In children, impaired hearing is associated with an increase in required effort at school as well as poor overall academic performance (Grewal et al., 2010, Gurney et al., 2007). More fundamentally, hearing is required for proper speech development, and so young hearing-impaired children are likely to experience delayed or impaired cognitive and social development (Tharpe, 2008, Yancey et al., 2012).

More deeply, hearing loss can have profound effects upon a patient's social engagement. Difficulty recognizing others' spoken words can be frustrating, tiring, and embarrassing, and has been shown to lead to withdrawal from social life (Arlinger, 2003). As much as the hearing-impaired individual may withdraw from social life, those around them may also become more reluctant to engage them as they find communication to take more effort, requiring them to speak louder, slower, and with more distinct articulation, move closer to the individual, and/or face the individual as they speak. The patient is likely unaware of the full social impact of their impairment as they can't recognize attempted social interactions never heard. With social disengagement comes reduced intellectual engagement and mood alterations in the form of feelings of isolation, paranoia, and symptoms of depression (Arlinger, 2003).

In addition to its social consequences—and the secondary consequences thereof—hearing loss seems to have other direct consequences on cognition. Impaired hearing requires the patient to engage in "effortful listening". Hearing is both a sensory and cognitive process, and when extra cognitive effort is required to recognize the words spoken, one can have difficulty committing conversation to memory or even following rapid and complex speech (Wingfield et al., 2005, Wingfield et al., 2006). In the elderly population, hearing loss is associated with developing dementia (Davies et al., 2017, Gates et al., 2011, Lin et al., 2011), but the nature of this association is not yet understood. Increased hearing perceptual effort may monopolize cognitive reserves, cognitive decline may be a result of social isolation and mood depression, or hearing loss may cause dissociation and disorientation from the outside world (Wingfield and Peelle, 2012).

1.6 MODELING OTOTOXICITY IN THE LABORATORY

Development of treatments for ototoxicity requires the ability to model ototoxicity in the laboratory, however this task remains challenging. Ototoxicity can be successfully modeled *in vivo* through systemic administration of cisplatin (Chapter 2) or aminoglycosides, however, the cochleae of mammalian models are directly encased in bone making them inaccessible to many *in vivo* imaging modalities, as well as difficult to access for *in vivo* treatments. Most treatments requiring local application to the inner ear are currently administered into the middle ear (transtympanic), by injection directly into the perilymph (by first passing through the round window), or via injection into the posterior semicircular canal (El Kechai et al., 2015). These techniques are invasive and require technical skill, but can be effective.

In vitro systems for modeling ototoxicity in the mature cochlea remain restrictive. Multiple cell lines have been developed to model hair cells. These lines: UB/OC-1, UB/OC-2, and HEI-OC1, have been derived from the H-2Kb-*ts*A58 transgenic mouse, which ubiquitously expresses the immortalizing oncogene simian virus 40 (SV40) thermolabile large tumor (T) antigen (TAg) (Jat et al., 1991, Holley et al., 1997, Holley and Lawlor, 1997, Kalinec et al., 2016). Though these cell lines express some hair cell markers, including math 1, prestin, and myosin VIIa, their overall phenotype is closer to that of hair cell progenitors (Germiller et al., 2004, Holley and Lawlor, 1997, Kalinec et al., 2016, Rivolta et al., 1998). These cell lines do not display the characteristic hair cell stereocilia bundles and their electrophysiology is more similar to that of developing hair cells (Jagger et al., 1999). Their utility in studying ototoxicity is further brought into question by the observation that they are not sensitive to aminoglycoside antibiotics (Cederroth, 2012, Chen et al., 2012).

More recently, a new inner ear *in vitro* model has been developed. Three-dimensional culture has been used to differentiate inner ear sensory epithelia initially from mouse embryonic stem cells and more recently from human pluripotent stem cells (Koehler et al., 2017, Koehler et al., 2013). This differentiation process generates otic-vesicle-like "organoids" with luminal-facing sensory epithelia. These sensory epithelia contain both hair cells and supporting cells and some appear to be innervated by sensory neurons. The hair cells have stereocilia bundles and electrophysiological properties similar to native hair cells. This system seems very promising for certain *in vitro* studies, though its immediate utility in studying ototoxicity is limited. This method produces a complex culture containing many different cell types arranged in irregular clusters and organoids. It lacks the simplicity, yield, and high-throughput adaptability of a cell line, while at the same time lacking the level of physiological relevance afforded by inner ear organ explant culture. Improvements in yield, development of culture methods for driving the production of certain cell types, or development of methods to sort and subculture specific cell types may all expand the utility of this approach for future work.

One of the most popular *in vitro* approaches to inner ear research remains explant culture of mouse inner ear organs. Culture of embryonic and neonatal mouse cochleae is straightforward and cultures can be maintained for up to two weeks (Munnamalai and Fekete, 2016). Unfortunately, the developing mouse cochlea is not an ideal model for studying ototoxicity—which exclusively affects the mature cochlea—as cochlear cells, particularly hair cells, have not yet fully differentiated and taken on their final adult function and expression profiles. Additionally, cochleae from neonatal mice regenerate lost hair cells both *in vitro* and *in vivo*, suggesting a different capability to respond to damage (Cox et al., 2014). Though the

adult mouse cochlea would of course make a more appropriate model, attempts to maintain it in culture have so far been unsuccessful.

Unlike the cochlea, the adult mouse utricle can be kept alive in culture for over a week, and thus it can be used to study mature, mammalian hair cells *in vitro*. Hair cell regeneration is not entirely absent in the adult mouse utricle, but is very limited and appears to generate morphologically distinct replacement hair cells through direct (non-mitotic) transdifferentiation of supporting cells (Golub et al., 2012). Adult mouse utricles can be cultured free-floating using commercially available culture media. Their use as a model system allows not only for the *in vitro* study of mature hair cells, but also the study of supporting cells and examination of the biological interactions between the two cell types (Cunningham, 2006, Brandon et al., 2012). The major disadvantages of the utricle culture system are largely related to yield. A single mouse yields two utricles, each of which contains only ~3,800 hair cells and ~2,200 supporting cells each (Burns et al., 2012, Kirkegaard and Nyengaard, 2005). Therefore, the dissection of several mice still yields only a small amount of biological material. The throughput of this system is further limited by the technical skill and time required to isolate the utricle and place it into culture.

Of course, while the vestibular hair cells of the utricle may be analogous to those of the cochlea, they are not identical and this represents a limitation of using the utricle to model physiologic and pathologic conditions of the cochlea. Some of the fundamental differences between these two populations of hair cells are detailed in section 1.3.1 above. Notably, cochlear and vestibular hair cells differ significantly in the manner in which they are stimulated. Vestibular hair cells respond to stimuli of much lower frequencies and are depolarized by endolymph fluid of much lower positive potential. These differences in mechanotransduction, among other differences, may be pertinent to the transfer of findings from the utricle to the

cochlea. An additional limitation of the utricle culture system is the tissue complexity. Because multiple cell types are present, biological processes observed *in vitro* are not easily assigned to a particular cell type, as they would be for a cell line for example. Therefore, teasing apart biological mechanisms also requires the ability to determine the cell type responsible for changes in transcript expression, protein expression, protein secretion, etc. first observed at the whole-utricle level. Nonetheless, utricle culture likely represents the most physiologically relevant *in vitro* method for studying ototoxicity in mature hair cells and supporting cells currently available.

1.7 CURRENT TREATMENT OF OTOTOXICITY

No approved medical interventions currently exist for primary prevention of either cisplatin or aminoglycoside ototoxicity, or for the reversal of ototoxic inner ear damage. Current treatment is limited to the prescription of hearing devices to those patients experiencing hearing loss. For many patients, hearing aids are clinically indicated and can be beneficial. Recent advancements in hearing aid technology, including extended bandwidth and frequency lowering devices may increase the extent of their benefit (Yorgason et al., 2006). For patients who are profoundly and bilaterally deafened by ototoxic drugs, cochlear implants have been shown to be helpful, specifically for improving speech recognition (Nichani et al., 2013). The effectiveness of implants for a particular patient may depend upon the level of preservation of the spiral ganglion neurons and cochlear nerve. Unfortunately, owing to inconsistent monitoring of ototoxicity, many patients who could benefit from hearing aids are not promptly identified (Fausti et al., 1992).

1.7.1 Approaches to treating ototoxicity

Current experimental strategies to treat ototoxicity can be broadly categorized as either regenerative or protective. Regenerative strategies are those designed to replace lost hair cells. This may be approached by either cell therapy, in which cells are generated *ex vivo* and then delivered to the inner ear, or by inducing surviving cochlear cells (supporting cells) to proliferate and transdifferentiate into hair cells. Development of these methods would hold a great deal of promise for treating not only ototoxicity, but many pathologies selectively affecting hair cells. However, the challenge is significant and successful application of these approaches is likely many years away (Groves, 2010). For replacement hair cells to function properly requires developing not only the ability to generate mature hair cells, but

the ability to ensure they are positioned correctly in the cochlear architecture, and that they receive proper innervation.

Protective strategies are those designed to prevent hair cell death under otherwise toxic conditions. This approach will likely require some knowledge of the timing of the potentially toxic insult, so that the protective therapy may be delivered at an appropriate time. While this makes these approaches more limited in potential scope, the timing of the toxic insult is of course known in cases of ototoxicity. The pathway to successful implementation of these approaches seems shorter than that to regeneration as it is conceivable that a single drug may prevent uptake of ototoxic drugs into sensitive inner ear cells or may act in an inhibitory fashion on a key pathway mediating drug-induced cell death across multiple cell types. A protective strategy has another particular advantage in the case of cisplatin ototoxicity specifically. As cisplatin is known to damage multiple cell types in the cochlea (not solely hair cells), regeneration of lost hair cells would be a partially effective treatment for cisplatin ototoxicity at best, while a protective approach may address the problem more globally within the inner ear.

1.7.2 Previous investigational protective strategies

Over the years, many investigational protective drugs have been reported, but at this time none is approved for clinical use, and very few clinical trials have been completed. For those not directly involved in the studies it is of course difficult to know the specific reasons why many of these positive results at the laboratory bench have not made it to clinical trial. In reviewing the existing data on otoprotective drugs, it is important to note that the activities of these drugs have been tested in a diverse set of models. *In vitro* models have ranged from cell lines to auditory organ explants, and *in vivo* models vary in the species used, the ototoxic drug given, and the quantity and timing of its dosing, among other aspects.

A common class of drugs investigated for prevention of either cisplatin or aminoglycoside ototoxicity is antioxidants. The antioxidant N-acetylcysteine has been investigated as a protectant against both aminoglycosides and cisplatin. Multiple clinical studies have demonstrated its utility against aminoglycoside ototoxicity (Feldman et al., 2007, Tokgoz et al., 2011, Kocyigit et al., 2015), though its utility in preventing cisplatin ototoxicity is unproven. It has been suggested to blunt ototoxicity in an animal model, but a clinical trial has yet to be successfully performed (Choe et al., 2004). Many more antioxidants have been proposed as specifically protective against cisplatin ototoxicity. Recently, promising results have been observed for the antioxidant sodium thiosulfate. Following successful animal trials, systemic administration of sodium thiosulfate hours after cisplatin administration has been shown to decrease the overall incidence of hearing loss in a group of pediatric patients receiving cisplatin chemotherapy for several cancer types (Freyer et al., 2017). Amifostine, a cytoprotective adjuvant for chemotherapy, and a free-radical scavenger, has been studied fairly extensively in the context of cisplatin ototoxicity. Several clinical studies have been performed with conflicting results (Rubin et al., 1995, Ekborn et al., 2004, Fisher et al., 2004, Marina et al., 2005, Fouladi et al., 2008). D-methionine has also been reported to protect against cisplatin ototoxicity in animal models via a proposed effect on cochlear oxidative state (Korver et al., 2002, Campbell et al., 2003). Yet another antioxidant, alpha lipoic acid, has been shown to protect against cisplatin ototoxicity in rats (Rybak et al., 1999), but was ineffective in clinical trial (ClinicalTrials.gov, Identifier: NCT00477607).

The stated scientific rationale behind use of antioxidants has been their ability to counteract the increase in intracochlear reactive oxygen species (ROS) proposed by some to underlie ototoxicity. However, in the case of cisplatin

ototoxicity, they may instead be acting via direct binding and inactivation of cisplatin. Notably, with the exception of N-acetylcysteine, all the above-mentioned drugs have only been reported to protect against cisplatin ototoxicity, and not aminoglycoside ototoxicity. Sodium thiosulfate has been directly demonstrated to bind and inactivate cisplatin (Shea et al., 1984, Elferink et al., 1986) and cisplatin is well known to avidly bind methionine as well (Arnesano et al., 2007, Crider et al., 2010). Alpha lipoic acid, N-acetylcysteine, and the active metabolite of amifostine, 2-((aminopropyl)amino)ethanethiol, are all thiols and cisplatin has a well-documented affinity for binding thiols (Ishikawa and Ali-Osman, 1993, Karasawa et al., 2013). Any compound capable of directly binding cisplatin holds a strong possibility for decreasing the effectiveness of cisplatin chemotherapy if administered systemically. Local delivery of such drugs thus presents the most realistic path forward to clinical implementation.

Yet another therapy that has been investigated for protection against cisplatin ototoxicity is transtympanically administered Ringer's lactate solution. Animal studies have shown conflicting results (Choe et al., 2004, Munguia et al., 2010) and clinical trials have not been completed. Aspirin (salicylate) has also been investigated as an otoprotectant against both cisplatin and aminoglycosides. Its ability to blunt cisplatin ototoxicity has been reported in animal models (Li et al., 2002, Hyppolito et al., 2006) though no clinical studies have been reported. A clinical study has demonstrated effectiveness against aminoglycoside ototoxicity (Sha et al., 2006), but gastric symptoms, including gastric bleeding (a well-known side effect of salicylate) were more common in the treated group and may likely prevent its clinical adoption.

Other explored otoprotectants include those designed to decrease inflammation associated with intracochlear ototoxic damage. Most notably, the

corticosteroid dexamethasone has been taken to clinical trial, where it was shown to have a modest effect on cisplatin ototoxicity when given transtympanically (Marshak et al., 2014). Apoptosis inhibitors, which presumably act at the final common endpoint of cellular toxicity, have also been investigated and suggested to protect against cisplatin (Wang et al., 2004) or aminoglycoside (Ylikoski et al., 2002, Pfannenstiel et al., 2009) ototoxicity *in vivo.*

The above-mentioned drugs do not represent an exhaustive, but rather an illustrative list of some of the more promising drugs investigated to-date. As the mechanisms of cisplatin ototoxicity are yet to be fully elucidated, rational design of preventive therapies has been lacking. The difficulty of producing consistent cisplatin ototoxicity in mice has led to the use of a diverse set of animal models. The low rate of transfer of *in vitro* and *in vivo* successes to successful clinical treatments suggests that the models of ototoxicity employed may not be accurately recapitulating clinical conditions.

In this thesis, a novel mouse model of cisplatin ototoxicity is presented (Chapter 2), which has already been adopted by other groups and with further adoption may help standardize modeling of cisplatin in the laboratory. Amongst the wide variety of drugs previously investigated for preventing cisplatin ototoxicity, the majority of positive results have come from drugs which are able to directly bind cisplatin (whether or not that is their intended mechanism of action). Pharmacokinetic studies performed using the mouse model reported here illustrate why prevention of initial cisplatin accumulation in the cochlea may be the most promising approach to preventing ototoxicity moving forward (Chapter 3), and these studies highlight methods of identifying such drugs. As compared to cisplatin, there have been fewer promising drugs for preventing aminoglycoside ototoxicity. One approach to rational design of these therapies is through first understanding

and subsequently leveraging innate inner ear stress response and pro-survival mechanisms. A previously undescribed inner ear stress response mechanism is described here (Chapter 4). Further improved understanding of pro-survival pathways in the inner ear may ultimately prove useful in protecting hearing against ototoxic drugs as well as a broader range of stresses including loud noise and aging.

1.8 SPECIFIC AIMS

The work presented in this thesis aims to advance the ability to address ototoxicity experienced both by patients receiving cisplatin chemotherapy as well as those receiving aminoglycoside antibiotics. As the mechanisms of cisplatin ototoxicity remain poorly understood, focus is upon improving this understanding to better position the field to rationally develop protective therapies. With aminoglycoside ototoxicity understood to preferentially damage hair cells, focus on that front is upon understanding innate protective mechanisms of the inner ear and leveraging that understanding to test a method of protecting hair cells. The specific aims of each chapter are as follows:

Chapter 2:

- Refine a mouse model of cisplatin ototoxicity
- Physiologically and histopathologically characterize cisplatin-induced hearing loss in this model

Chapter 3:

- Describe the pharmacokinetics of cisplatin in the mouse cochlea
- Map the distribution of cisplatin in the murine and human cochlea

Chapter 4:

- Determine the role of extracellular vesicles in mediating inner ear protection against aminoglycoside ototoxicity
- Test the capacity of exogenous vesicles to protect against hair cell death

2 MODELING CISPLATIN OTOTOXICITY IN THE MOUSE

2.1 INTRODUCTION

An appropriate animal model of cisplatin ototoxicity is central to our ability to study cisplatin ototoxicity and to develop successful interventions for preventing it. An ideal model would first be accurate to the clinical characteristics of cisplatin ototoxicity. Detailed understanding of these characteristics has been limited by a current lack of standardized clinical studies. Clinical cohorts and methodologies have varied so significantly that a proper meta-analysis has not been feasible (van As et al., 2016). Despite this, a few characteristics of cisplatin ototoxicity have been established. As discussed above (section 1.5.2), cisplatin-induced hearing loss is known to be high-frequency, bilateral, and progressive, affecting children more severely than adults. In studies of cochlear morphology, the most commonly noted change is degeneration of outer hair cells in the organ of Corti. A gradient of hair cell loss has been well described, with hair cells near the cochlear base (high frequencies) dying before more apical hair cells (low frequencies), and outer hair cells lost before inner hair cells (Rybak et al., 2009, Rybak et al., 2007). Additionally, cisplatin ototoxicity is also understood to be dose-dependent (Frisina et al., 2016, Langer et al., 2013), and to progress both shortly after drug administration, as well as weeks-to-months later (Sprauten et al., 2012, Al-Khatib et al., 2010, Bertolini et al., 2004, Knight et al., 2005, Stohr et al., 2005). An appropriate animal model of ototoxicity would demonstrate these clinical characteristics. The data presented in this chapter demonstrate recapitulation of these clinical characteristics of cisplatin

ototoxicity (with the exception of age-related differences in severity) in a mouse model.

A clinically relevant model of cisplatin ototoxicity would also be accurate to the nature of cisplatin administration in the clinic. Though cisplatin ototoxicity is being studied in both mammalian and non-mammalian vertebrates, the pathway to clinical trials of preventive therapies passes through mammalian models. Historically, any method of cisplatin administration resulting in significant hearing loss has been considered a sufficient model. However, this view rests upon the assumption that similar endpoints between these models and human patients (i.e. hearing loss) equate to similar mechanistic pathways to that endpoint. The validity of this assumption, or lack thereof, underlies the validity of any results derived from these models. In the clinic, cisplatin is administered as a spaced (by several days) series of slow, systemic infusions with intervening recovery days, and yet previous mouse models (and some currently in use) have administered cisplatin as a single, high dose. Beyond their inconsistency with clinical cisplatin regimens, these models have at least two major limitations. First, they often result in high systemic toxicity, with mice surviving only a few days after drug administration, and second, the hearing loss they produce is highly variable (Qureshy et al., 2011, Poirrier et al., 2010, More et al., 2010, Hill et al., 2008). Such variance inherent to the model decreases the statistical power of analyses and thus requires the use of additional animals to achieve statistical power.

Given the high systemic toxicity and variable lesion produced in single-dose mouse models, it has previously been concluded that "the mouse is not a good model for ototoxicity" (Poirrier et al., 2010). Some groups have sidestepped these challenges by administering cisplatin locally to the inner ear or by co-administering cisplatin with the loop diuretic furosemide to potentiate ototoxic effects, however,

these approaches have limitations regarding their clinical relevance (He et al., 2009, Li et al., 2011). Several other rodent models have also been used, largely because they are more susceptible to cisplatin ototoxicity and so hearing loss can be observed at doses causing less systemic toxicity than in the mouse. The guinea pig has been a popular model for studying mechanisms of ototoxicity as well as testing protective strategies (Estrem et al., 1981, Hamers et al., 2003, Hellberg et al., 2009, Mohan et al., 2014, Sepmeijer and Klis, 2009, van Ruijven et al., 2005). It has the additional advantage of possessing a larger inner ear, thus making micro-surgical or micro-dissection based techniques easier to execute and providing more biological material for study. The rat and gerbil have also been used extensively (Alam et al., 2000, Harrison et al., 2016, Minami et al., 2004, Sie and Norton, 1997, Thomas Dickey et al., 2004).

Despite the challenges, a mouse model of cisplatin ototoxicity remains particularly attractive for the same reasons the mouse is an attractive animal model for many studies; these include the well-characterized nature of the mouse genome and the availability of tools to manipulate that genome. Other rodent models, including the guinea pig and gerbil, are outbred and genetically heterozygous, which may hamper the reproducibility of data and the study of specific genes. An additional advantage of studying cisplatin ototoxicity in the mouse is the pre-existing scientific body of knowledge derived in the mouse which may be drawn from. From a practical perspective, mice have a short generation time, are relatively inexpensive to maintain in a colony, and are a familiar species to animal care personnel.

Our laboratory developed a suitable mouse model for cisplatin ototoxicity shortly before the start of this dissertation (Roy et al., 2013). This model was similar to one previously reported in rats (Minami et al., 2004). CBA/CaJ mice at 12 weeks

of age were given three cycles of cisplatin, with each cycle consisting of four days of once-daily intraperitoneal injections of cisplatin at a dose of 4mg/kg. The choice of CBA/CaJ mice was based upon the published long-term stability of hearing in CBA strains, as compared to others (Henry and Chole, 1980, Henry, 2004) as well as the decreased incidence of otitis media in CBA/CaJ versus CBA/J mice (McGinn et al., 1992). Resistance to age-related hearing loss removed presbycusis as a confounder over the course of the six-week experiment, as confirmed by longitudinal audiology on control mice. In that experiment, mice were used at 12 weeks of age in order to parallel similar experiments on protection against hearing loss performed in a separate laboratory (Yoshida and Liberman, 2000). Notably, CBA/CaJ mice at this age have fully mature hearing but are still months away from developing age-related hearing changes (Ohlemiller et al., 2010). For these reasons, and for continuity with our previous study, CBA/CaJ mice predominantly at ~12 weeks of age were used for the studies reported in this chapter and the one that follows.

Our previously reported mouse model involved three cycles of four, once-daily cisplatin injections at a dose of 4mg/kg. This dosing regimen was reached after an audiometric analysis of the ototoxicity produced by several different regimens of varying dose size and number (Matt Ryals, unpublished). Though this model achieved a significant hearing loss on average, the specific hearing loss in some mice was so severe it was beyond the range of the auditory testing equipment and thus couldn't be accurately quantified. Additionally, the mice in our laboratory's original study and a similar study I conducted using the same regimen had a mortality rate of 20-25% (data not shown). These mice were typically lost during or after the final cycle of cisplatin, prior to completion of auditory testing (the experimental endpoint), and so they provided minimal useful data. Therefore, the model had significant remaining room for improvement both in the resulting hearing loss and

the mouse survival rate. This chapter presents a modified model with an improved severity of hearing loss and an improved rate of mouse survival. After experimentation with the total number of cisplatin doses, a decrease in the size of each dose was instead settled upon. This change along with improved supportive care helped address both the major limitations of the previous model—excessive hearing loss and poor survival. The nature and progression of ototoxicity in this model were characterized by multiple physiologic measures of cochlear function as well as immunohistochemistry of surviving cochlear hair cells.

2.2 METHODS

2.2.1 Cisplatin treatment of mice

Mice were systemically administered cisplatin in order to induce ototoxicity. Equal numbers CBA/CaJ male and female mice (The Jackson Laboratory), age 6-16 weeks, were used for all work presented in Chapters 2 & 3. All animal procedures were performed at the United States National Institutes of Health and were approved by the NIDCD/NINDS Animal Care and Use Committee (protocol #1327). Mice were assigned numbers sequentially and a random number generator was then used to partition them into either the cisplatin-treated experimental group or saline-treated control group, as well as into specific time point sub-groups. Male and female mice were randomized independently to ensure even sex distribution throughout experimental groups (n = 10 males and n = 10 females per group). Cisplatin-treated (APP Pharmaceuticals) mice received 3 cycles of once-daily i.p. injections (3.5 mg/kg) for four days followed by ten days of recovery (for a total of 42 days of treatment), as schematized below. Control mice received 3 rounds of once-daily i.p. injections of saline dosed at the equivalent volume to cisplatin doses. All mice were individually housed throughout the entirety of the protocol.

In order to examine the progression of hearing loss throughout the cisplatin regimen, sub-groups of mice underwent physiologic testing and were euthanized at time points throughout the regimen (n = 3-4 mice at each time point, except for day 42, where n = 7). These time points were as follows (days are as shown in Figure 2.1 below): on day 4—"Cycle 1" group, day 14—"Recovery 1", day 18—"Cycle 2" group, day 28—"Recovery 2", day 32—"Cycle 3", day 42—"Recovery 3" or "complete regimen". Following euthanization, several mouse organs were dissected and analyzed for cisplatin content as detailed in Chapter 3. Left cochleae were removed

and analyzed for total cisplatin content. Right cochleae were removed, further microdissected into specific cochlear regions, and those microdissected cochlear portions were similarly analyzed for total cisplatin content (Chapter 3). Amongst the seven mice which completed the entire cisplatin regimen, four had their tissues processed as described above, while cochleae from the remaining three were used for immunohistochemistry in order to quantify hair cell loss caused by cisplatin treatment.

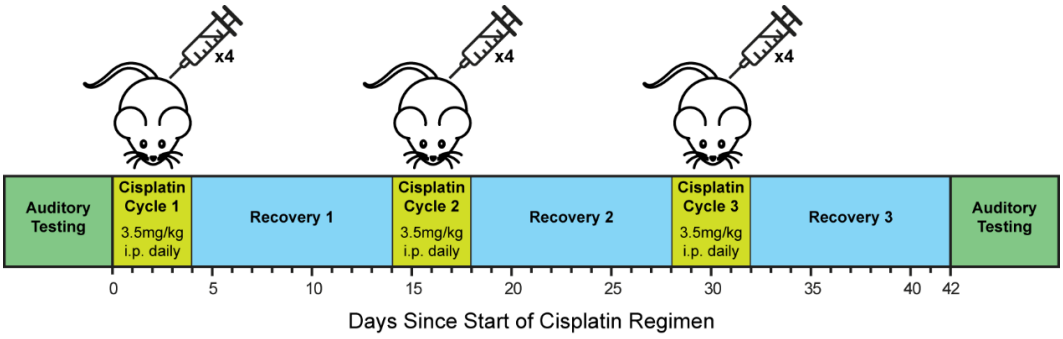


Figure 2.1: Cisplatin regimen administered to experimental mice

In the complete cisplatin regimen, mice received three cycles of cisplatin and three intervening recovery cycles. Cisplatin cycles were each composed of four days of once-daily intraperitoneal injections at a dose of 3.5 mg/kg of mouse body weight. Groups of experimental and control mice (n = 3-4 each) were removed from the cisplatin regimen following each cisplatin cycle and each recovery cycle in order to assess intermediate time points.

2.2.2 Mouse health monitoring and supportive care

All mice were observed at least twice daily to assess activity and any abnormal behavior. Body weights were recorded each morning prior to the administration of any injections. Overall health was evaluated daily through body condition scoring (Ullman-Cullere and Foltz, 1999). The vertebral column and dorsal pelvic bones were palpated and each mouse was assigned a score between 1 and 5 according to the criteria described in

Figure 2.2. Incremental scoring (2+, 3-, etc.) was used, and it was predetermined that any mouse assessed to have a body condition score of 2 or below would be promptly removed from the study and euthanized.

To minimize cisplatin nephrotoxicity and to ensure sufficient hydration, daily subcutaneous injections of 1mL of each 0.9% NaCl and the multiple electrolyte solution Plasma-LYTE (Abbott Laboratories) were administered to all mice. Supplemental nutrition in the form of soft pellet chow and fresh fruit was available throughout. Mice with a body condition score below 3- or progressively decreasing body weight were hand fed a high calorie liquid supplement (STAT®, PRN Pharmacal) to help maintain acceptable body weight.

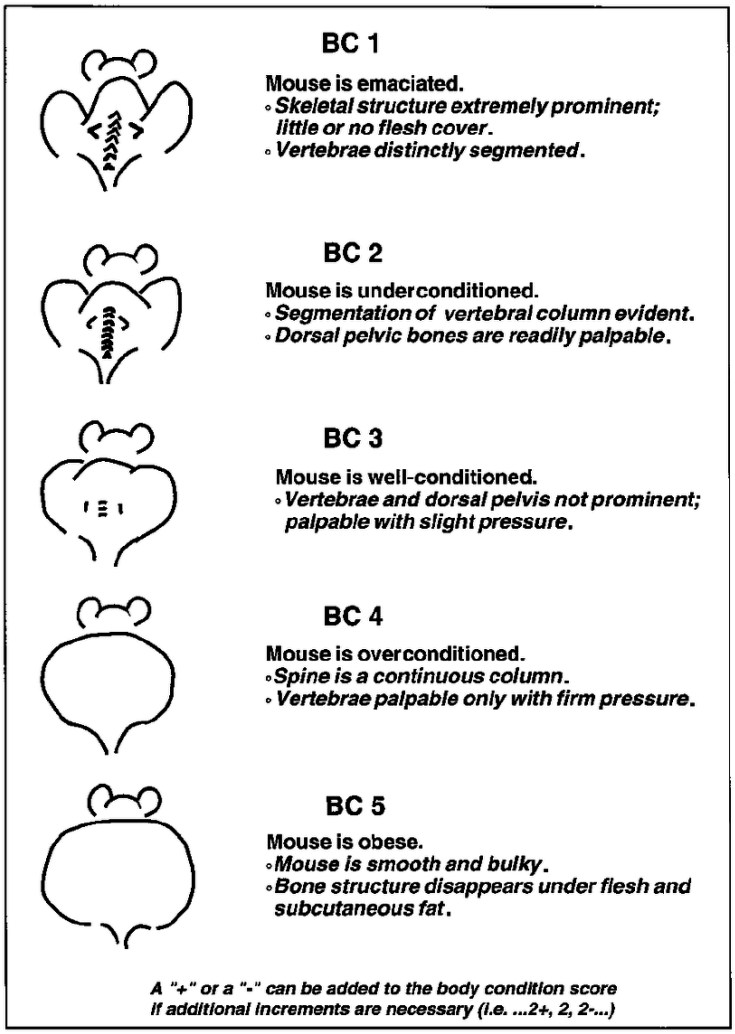


Figure 2.2: Body condition scoring criteria

Body condition scores were assessed and recorded daily according to this classification scheme. Figure reproduced from Ullman-Cullere and Foltz (1999).

2.2.3 Auditory testing

All mice underwent auditory testing prior to and following their respective course of treatment in order to measure cisplatin-induced hearing loss. Mice were anesthetized with ketamine (Putney Inc., Portland, ME; 100mg/kg i.p.) and xylazine (Akorn Inc., Lake Forest, IL; 10mg/kg i.p.). Supplemental injections at 1/3 to 1/2 of the original dose were administered if the anesthetic depth was not sufficient (as

determined by animal movement or response to painful stimulus). Animals were placed on a temperature-controlled (37°C) heating pad (World Precision Instruments T-2000, Sarasota, FL, USA) inside a sound-attenuated booth (Acoustic Systems, Austin, TX, USA). Auditory brainstem responses (ABRs) and distortion-product otoacoustic emissions (DPOAEs) were recorded from right ears only using Tucker-Davis Technologies (Alachua, FL, USA) hardware (RZ6 Processor) and software (BioSigRZ).

Auditory brainstem responses were used as a measure of overall auditory function. ABR testing is an established and widely-used method for testing hearing in newborns and children otherwise too young to cooperate with the pure tone audiometry procedure. In mice, the ABR can be performed under general anesthesia. The ABR is an electroencephalographic response measured via scalp electrodes. An auditory stimulus is played into the ear and voltage changes (neuronal activity) starting at the auditory nerve and travelling centrally to the auditory cortex are recorded. Background neural activity is eliminated by time-locking the recordings to immediately follow the presentation of the auditory stimulus and by performing a high number of repeated recordings. When the repeated recordings are averaged, the background activity is largely cancelled-out and the evoked response (if present) can be visualized. The hearing threshold is determined by progressively lowering the sound intensity of the stimulus until a reproducible response is no longer observed. By presenting pure tone stimuli, the hearing sensitivity at specific frequencies can be tested independently.

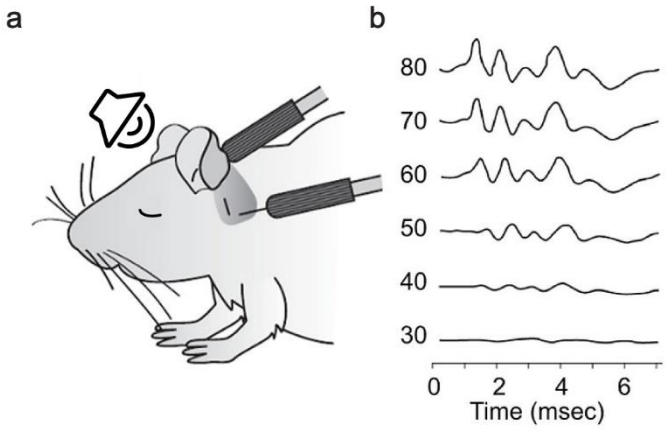


Figure 2.3: Mouse auditory brainstem response testing

Auditory brainstem response testing allows for the assessment of hearing in anesthetized laboratory mice. (a) Auditory stimuli of a specific frequency are presented to an anesthetized mouse (through a speaker inserted into the external auditory canal). Evoked electroencephalographic activity is recording via electrodes inserted in the scalp. (b) At each frequency tested, the intensity of the presented auditory stimulus is progressively decreased until an evoked response is no longer observable. The lowest sound intensity level at which a response is observable is determined to be the hearing threshold. In the test illustrated, 40 decibels would be considered the threshold. Figure modified from International Mouse Phenotyping Resource of Standardised Screens.

ABRs were generated using tone burst stimuli (3 msec, 29.9/sec, alternating polarity) at 8, 11.2, 16, 22.4, 32, and 40 kHz via a closed-field Tucker-Davis Technologies MF-1 speaker. Subdermal recording electrodes (Rhythmlink, Columbia, SC, USA) were placed at the vertex, under the test ear, and at the base of the tail (ground). Average waveforms from 1024 presentations were generated, amplified (20x), filtered (.3-3 kHz), digitized (25 kHz) and stored for offline analysis. For each test frequency, recording began at 80 dB SPL and decreased until the ABR waveform was no longer evident. If no response was obtained at 80 dB SPL, testing was performed at a maximum level of 90 dB SPL. ABR thresholds were determined by visual inspection of stacked waveforms for the lowest stimulus level that yielded repeatable waves. Whenever possible, testing was performed under blinded conditions.

Distortion product otoacoustic emissions were used as a measure of outer hair cell function. DPOAE testing is another clinically-utilized method for non-invasive auditory testing. Otoacoustic emissions are sounds produced by the cochlea which are reverse propagated through the middle ear and can be recorded in the ear canal (Kemp, 1978). These emissions can be spontaneous or evoked by an auditory stimulus. In DPOAE testing, otoacoustic emissions are evoked by presenting a simultaneous pair of primary tones at frequencies f1 and f2. The resulting most prominent (and most commonly measured) emission is of a third frequency, specifically 2f1-f2, and is thus a "distortion product" (Goldstein, 1967). The amplitude of this emission is dependent upon the activity of cochlear outer hair cells—the "cochlear amplifier"—which elongate or contract longitudinally in response to sound stimuli (Brownell et al., 1985). This outer hair cell activity generates otoacoustic emissions measurable by a sensitive microphone placed in the ear canal.

The DPOAE at 2f1-f2 was recorded in the mouse ear canal using an ER-10B+ microphone (Etymotic, Elk Grove Village, IL, USA) covered with a modified pipette tip. The DPOAE primary tones were presented at constant levels of f1 = 65 dB SPL and f2 = 55 dB SPL at 14 f2 frequencies between 8000-40000 Hz (f2/f1 = 1.25) via two Tucker-Davis Technologies MF-1 speakers. Mean noise floors were calculated from six spectra surrounding the DPOAE frequency (+/- 150 Hz).

2.2.4 Hair cell counting

Mouse cochleae were imaged in order to assess numbers of surviving hair cells following *in vivo* cisplatin treatment. Cisplatin-treated and saline-treated control mice were euthanized by CO_2 inhalation followed by rapid decapitation. Complete bony labyrinths (the cochlea and all vestibular organs) were removed by hand and were placed into 4% paraformaldehyde (PFA) solution. Using micro

forceps, the round window and oval window membranes were punctured and a hole was made near the cochlear apex to allow penetration of the fixative throughout the cochlea. Bony labyrinths were kept in fixative overnight at 4°C. The following day, they were rinsed in PBS and then placed into 0.5M ethylenediaminetetraacetic acid (EDTA) solution of pH 8.0 and incubated at room temperature for 48 hours to fully decalcify the tissue. Decalcified cochleae were rinsed in PBS and then microdissected using ophthalmic straight knives (Accutome) under a dissecting microscope (Carl Zeiss Microscopy, Stemi) to isolate the organ of Corti. In the process, the organ of Corti was divided into three approximately equal pieces—the apical, middle, and basal turns.

Organ of Corti tissue pieces were then incubated for 2 hours at room temperature in blocking solution composed of 0.5% triton X-100 (Sigma-Aldrich), 2% BSA (Sigma-Aldrich), and 0.8% normal goat serum in PBS. Tissues were stained overnight at 4° C with a primary antibody against Myosin VIIa (Developmental Studies Hybridoma Bank, MYO7A 138-1, supernatant) diluted 1:100 in blocking solution, followed by Alexa Fluor 546 conjugated goat anti-mouse IgG (Invitrogen) diluted 1:500 in blocking solution for 4 hours at room temperature. F-actin was stained with Alexa Fluor 647 Phalloidin (Molecular Probes, 200 units/mL) diluted 1:60 in blocking solution for 45 minutes at room temperature, and nuclei were stained with Hoechst 33342 (Molecular Probes) diluted 1:500 in blocking solution for 5 minutes. Tissues were mounted in Fluoromount-G (Southern Biotech) and imaged on an LSM 780 laser scanning confocal microscope (Carl Zeiss Microscopy). To quantify hair cell survival, Myosin VIIa positive cells in 135μm-long regions from the center of each cochlear turn (apical, medial, and basal) were manually counted. Inner and outer hair cell populations were counted separately and counts from cisplatin-treated mice were compared to those from saline-treated mice.

2.2.5 Statistics

Data are presented as mean ± s.e.m. throughout. Each replicate was derived from an individual animal. Data graphing and all statistical analyses were performed using GraphPad Prism 6 software. Statistical significance was determined by one- or two-way ANOVA followed by the Holm-Šidák multiple comparisons test or by unpaired two-tailed t-tests with or without correction for multiple comparisons by the Holm-Šidák method. No multiple comparisons correction was performed when only a small number (≤ 3) of predetermined statistical comparisons were made. Specific statistical tests are noted in respective figure legends. Alpha was set at 0.05 in all cases.

2.3 RESULTS

2.3.1 Cisplatin-treated mouse health and survival

In total, twenty mice received at least one cycle of cisplatin, with subsets of mice removed at the end of each cisplatin cycle and each recovery cycle. Of the seven mice pre-assigned to undergo the complete regimen, all seven survived and were in sufficient health to undergo auditory testing under general anesthesia. Body weights of all mice remaining in the study were taken each day. The average weights of cisplatin-treated mice were normalized to those of saline-treated controls, and are plotted in Figure 2.4. Weight loss closely coincided with the cisplatin cycles, with some weight regain during the recovery periods. At the end of the regimen, cisplatin-treated mice (who began at 93% the body weight of their controls) showed a significant net-loss of weight, with final body weights at 61% of controls. The disparity in body weights between cisplatin-treated mice and controls was a product both of net weight loss in cisplatin-treated mice (from 25.6gm to 18.8gm) and net weight gain in saline-treated mice (from 27.5gm to 30.8gm). The net weight gain in saline-treated mice was likely a result of the enriched diet made available to all mice in combination with expected weight gain associated with aging. These results demonstrate that although this cisplatin regimen is physically demanding of the mice and work-intensive for the experimenter, it can be completed with a high rate of animal survival.

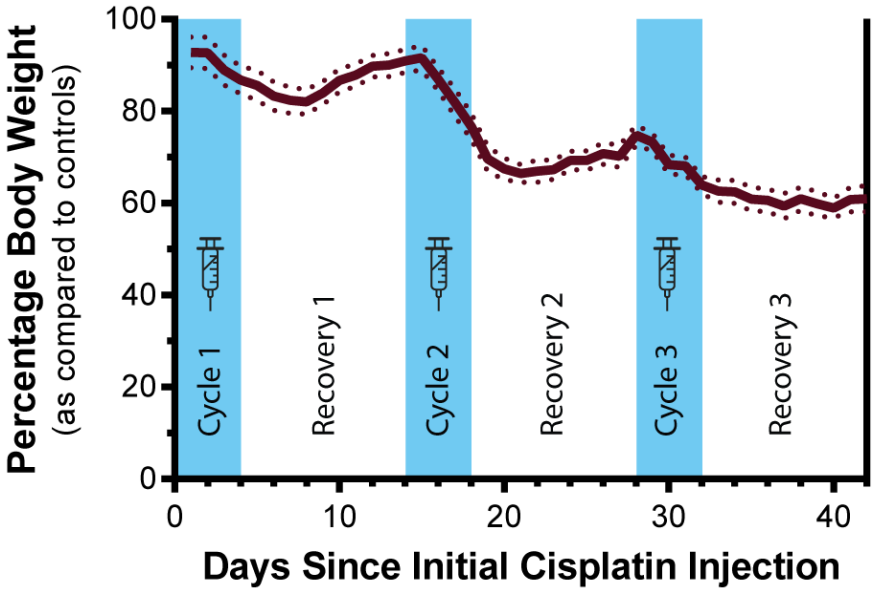


Figure 2.4: Mouse body weight changes throughout the cisplatin regimen

Daily normalized body weights of cisplatin-treated mice. Mice were randomly assigned to receive either cisplatin or saline with imposed equal allocation of males and females to each group. All mice were individually housed and were provided with an enriched diet *ad libitum*. Cisplatin-treated mice started the regimen at 92.8% the body weight of saline controls and finished the regimen at 61.0% the weight of controls. Dotted lines denote the standard error. All mice remaining in the study are plotted at each timepoint: n = 20 through Cycle 1, n = 16 through Recovery 1, n = 13 through Cycle 2, n = 10 through Recovery 2, n = 7 through Cycle 3, n = 4 through Recovery 3.

2.3.2 Cisplatin-induced hearing loss

Following the complete cisplatin regimen, mice demonstrated significant hearing loss across all tested frequencies (Figure 2.5). However, hearing thresholds remained testable for all mice. Saline-treated mice experienced no change in hearing sensitivity. Hearing loss was most severe at the highest frequencies, ranging from an average threshold shift of 34 decibels at 8 kHz to 51 decibels at 40 kHz ($P < 0.0001$, two-tailed t-test). This high frequency hearing loss is fitting for clinical ototoxicity and suggesting this to be an appropriate mouse model.

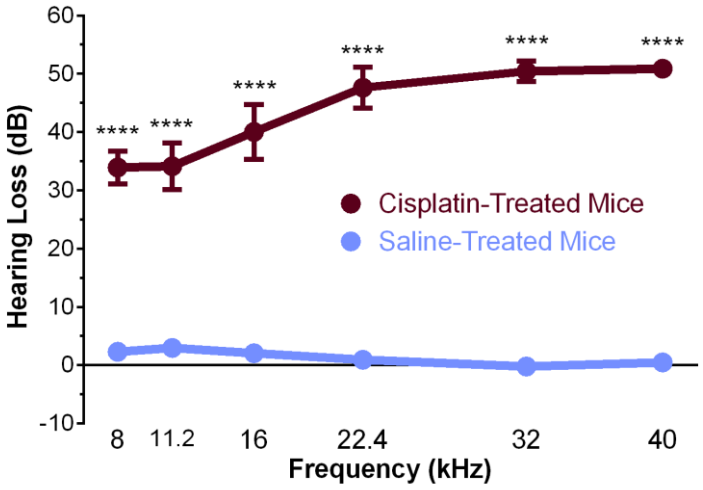


Figure 2.5: Cisplatin-induced hearing loss as measured by auditory brainstem responses

Hearing loss following the complete cisplatin regimen was measured by closed-field auditory brainstem response recordings from right ears only. ABR results are presented as threshold shifts, the calculated difference in hearing thresholds determined pre-treatment and post-treatment. Three cycles of cisplatin caused a moderate to severe hearing loss across all tested frequencies. n = 7 mixed-gender mice (n = 4 females, n = 3 males) in each group. Two-way ANOVA followed by the Holm-Šidák multiple comparisons test was used to determine significance. **** $P < 0.0001$.

Cisplatin ototoxicity is known to be associated with outer hair cell loss, and indeed cisplatin-treated mice had fewer surviving outer hair cells than their controls (Figure 2.6). This hair cell loss was most severe at the cochlear base, and was restricted to outer hair cells only, as inner hair cells were almost entirely preserved. This finding is fitting both with previous reports (Rybak et al., 2007) as well as with the ABR results above demonstrating hearing loss to be most severe at high frequencies.

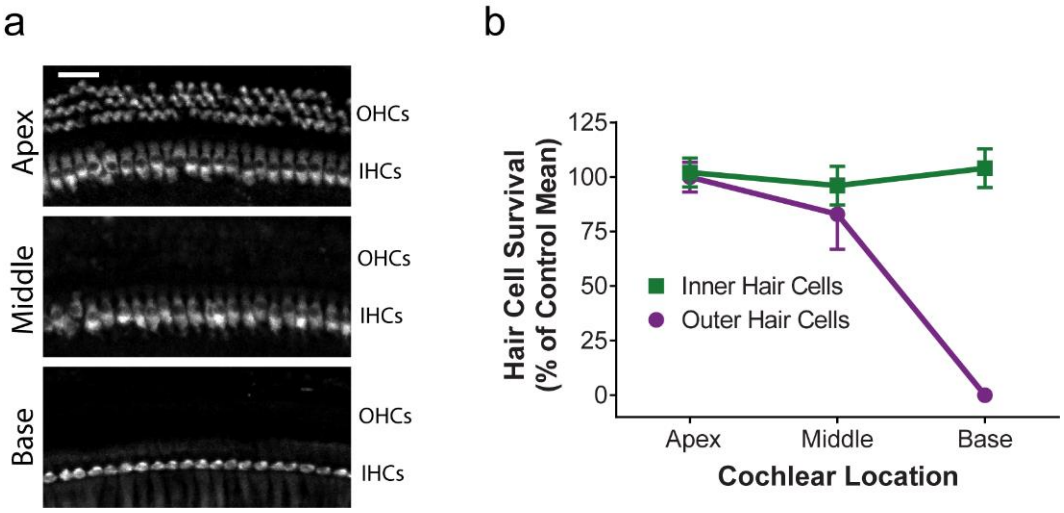


Figure 2.6: Loss of basal cochlear outer hair cells

Surviving inner and outer cochlear hair cells were imaged and quantified following cisplatin or saline treatment. (a) Representative confocal maximum intensity projections from the three cochlear turns—apex, middle, and base. Immunoreactivity to myosin VIIa, a hair cell specific maker, is shown. "IHCs" marks the region of the inner hair cells, "OHCs" marks the region of the outer hair cells. Scale bar = 25μm. (b) Percentages of surviving inner and outer hair cells (as compared to control averages) at the end of the cisplatin regimen (day 42). Right cochleae were microdissected and stained for the hair cell marker myosin VIIa. Remaining myosin VIIa positive hair cells were counted in central, 135μm-long regions of each of the three cochlear turns (apex, middle, and base). Predominantly outer hair cells in the basal portion of the cochlea were lost, with minimal loss of outer hair cells observed in the middle turn, and no perceivable loss of either outer hair cells in the apex or of inner hair cells in any cochlear turn. n = 3 mice in each group.

2.3.3 Progression of hearing loss during the cisplatin regimen

Auditory testing was performed at the end of each cisplatin cycle and recovery period to clarify the temporal relationship between cisplatin administration and resulting hearing loss, as well as to assess whether cisplatin ototoxicity could be appropriately modeled with a truncated regimen. An shorter regimen would have the benefits of less significant impact upon the health of the mice and a quicker experimental turnaround time. Successive ABR testing demonstrated progressive hearing loss which significantly progressed with each subsequent cisplatin cycle as well as during recoveries 1 and 3 (Figure 2.7). By the

end of Recovery 2, mice had severe hearing loss only at the highest frequency tested (40kHz), with mild hearing loss present at 32kHz. This demonstrated the necessity of 3 cycles of cisplatin for modeling significant hearing loss across multiple frequencies. The progression of hearing loss within recovery periods (during which mice received no cisplatin) demonstrated that cisplatin ototoxicity could progress for at least days-to-weeks following cessation of drug administration.

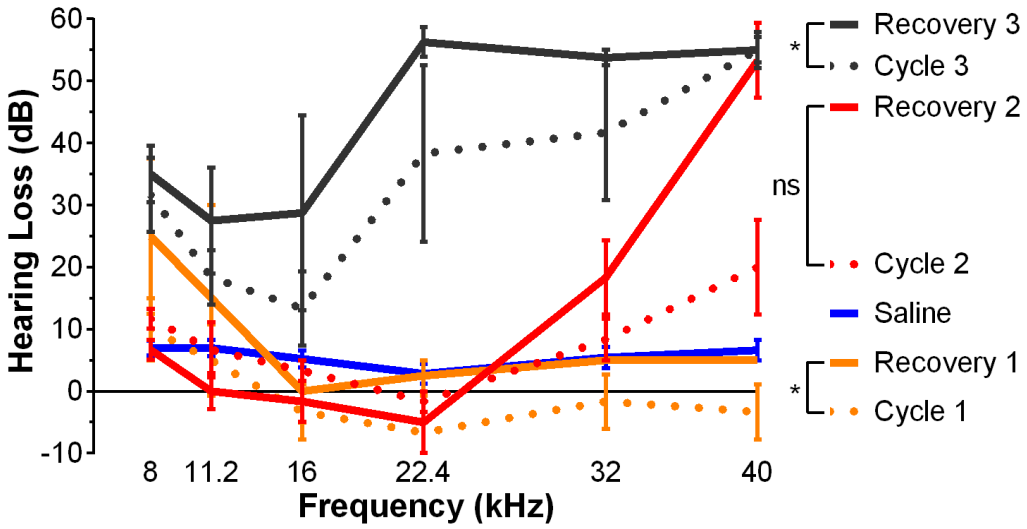


Figure 2.7: Progression of hearing loss during the cisplatin regimen

Sub-groups of cisplatin-treated mice underwent physiological testing at several intermediate time points throughout the complete cisplatin regimen. Hearing loss measured by ABR after each cycle of cisplatin and subsequent recovery is shown. High-frequency hearing loss became evident after Recovery 2. Robust hearing loss across all frequencies was only evident after three cycles. n = 3-5 mice at each time point. Two-way ANOVA followed by the Holm-Šidák multiple comparisons test was used to determine significance. ns = not significant, * $P < 0.05$.

The more targeted auditory examination provided by DPOAE testing revealed a similar progression of dysfunction. Significant, progressive loss of DPOAE amplitude was observed with successive cycles of cisplatin (Figure 2.8). By the end of the complete regimen, only amplitudes in the lower frequency regions were

distinguishable above background. These results suggest that outer hair cell loss and/or dysfunction is progressive throughout the cisplatin regimen and parallels the loss of hearing measured by ABR testing.

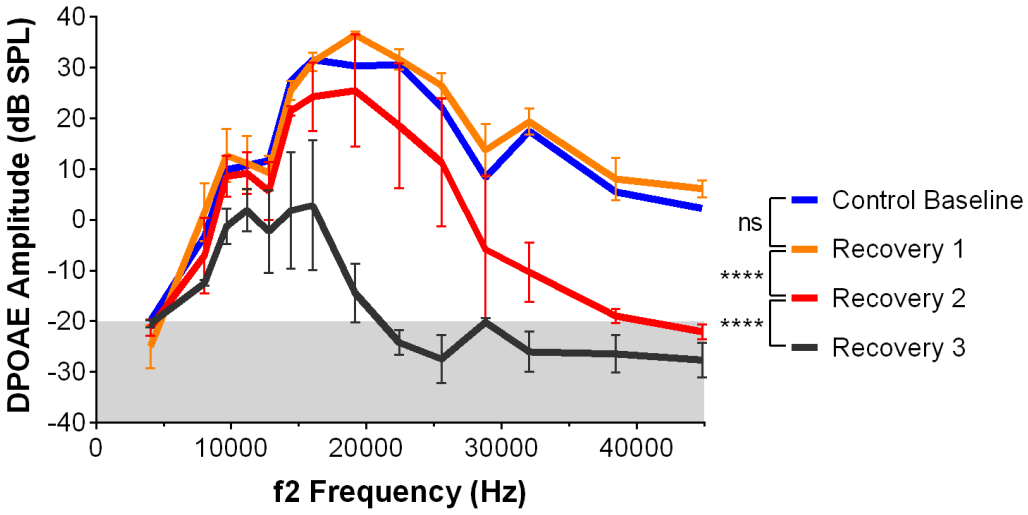


Figure 2.8: Progressive decline in distortion product otoacoustic emission amplitudes during the cisplatin regimen

Sub-groups of cisplatin-treated mice underwent physiological testing at several intermediate time points throughout the complete cisplatin regimen. DPOAE amplitudes after each cisplatin cycle and recovery period are shown. Loss of outer hair cell function occurred on a time-course similar to hearing loss (as measured by ABR testing). Grey shaded area depicts the approximate testing noise floor (the underlying background noise detected by the system microphone). n = 3-5 mice at each time point. Two-way ANOVA followed by the Holm-Šidák multiple comparisons test was used to determine significance. ns = not significant, **** $P < 0.0001$.

2.4 DISCUSSION

The primary aim of this chapter was to refine and characterize a mouse model of cisplatin ototoxicity. The timing structure of our previously-reported model was kept, thus maintaining its similarity to a clinical cisplatin regimen. Improved mouse survival was achieved by decreasing the daily cisplatin dose from 4mg/kg to 3.5mg/kg and providing more advanced supportive care, including the substitution of a multiple electrolyte solution for normal saline and hand-feeding of a high calorie diet supplement. Though cisplatin-treated mice lost significant body weight and were observably frail, the survival rate amongst mice receiving three full cycles of cisplatin was 100% (7/7), demonstrating that mice can be successfully taken through the entire regimen.

At the end of the regimen, mice had moderate-to-severe hearing loss across across the range of tested frequencies and most severe at higher frequencies. The severity of observed hearing loss, ranging from approximately 34 decibels to 51 decibels, should make this model well optimized for future studies. The severity of hearing loss is high enough to be statistically significantly different from control mice at all testable frequencies, while still remaining within the detectable range of the auditory testing equipment. The variability of hearing loss is also less than that seen in previous mouse models.

Cisplatin treatment resulted in a loss of outer hair cells, the severity of which was dependent upon the position along the cochlea, with total outer hair cell loss occurring at the cochlear base. Outer hair cell loss following exposure to cisplatin has previously been described in animal models and posthumously collected human cochleae, and has been presumed to be the central etiology of cisplatin-induced hearing loss (Rybak et al., 2009, Rybak et al., 2007), as discussed in detail in section 3.1 below. Given the thoroughness of these preexisting studies a detailed frequency-

mapped analysis of outer hair cell survival was not performed. The entire cochlear length was simply divided into three approximately equal turns (apex, middle, and base) and hair cell survival was assessed in each of these turns. The hair cell counts presented here further validate the association of cisplatin ototoxicity with outer hair cells, though they do not rule out cisplatin-induced pathology elsewhere in the cochlea and do not prove hair cell loss to be a direct result of exposure of those cells to cisplatin.

Auditory testing performed at intermediate time points in the cisplatin regimen revealed a few salient points regarding the model. First, this analysis demonstrated cisplatin ototoxicity to be high frequency and progressive in nature, demonstrating the similarity of the model to the clinical scenario. Second, this analysis demonstrated the necessity of three cycles of cisplatin for achieving significant hearing loss across multiple frequencies. There is understandable interest in the field to identify a shorter and less labor-intensive protocol for modeling cisplatin ototoxicity in the mouse, however, a truncated version of this protocol does not seem like a viable approach. Our laboratory has previously tested a variety of shorter cisplatin protocols which made use of higher individual doses of cisplatin and found those protocols to cause high mortality rates while achieving inconsistent hearing loss. Third, cisplatin ototoxicity progressed in the days-to-weeks following cessation of cisplatin administration (i.e. during the recovery periods). This recapitulates the delayed hearing loss reported in patients and provides additional insight into the mechanisms of cisplatin ototoxicity, suggesting that ototoxicity may be more related to a cumulative exposure than an initial acute exposure. Overall, this chapter presents and validates a refined version of our laboratory's mouse model of cisplatin ototoxicity. This model has permitted examination of the mechanisms underlying cisplatin ototoxicity (presented in the

following chapter) and is also allowing for the testing of interventions intended to prevent cisplatin ototoxicity. In addition, the model has now been adopted by several other laboratories.

3 THE ROLE OF CISPLATIN PHARMACOKINETICS IN CISPLATIN OTOTOXICITY

3.1 INTRODUCTION

Current understanding of cisplatin ototoxicity is largely a result of two types of investigation: studies of cochlear morphological changes following cisplatin exposure and targeted studies examining the activation of certain cellular pathways in response to cisplatin. In studies of cochlear morphology, the most commonly noted change is degeneration of outer hair cells in the organ of Corti. A gradient of hair cell loss has been well described, with hair cells near the cochlear base dying before more apical cells, and outer hair cells lost before inner hair cells (Rybak et al., 2009, Rybak et al., 2007). The mechanism underlying this gradient of damage from base to apex is unclear. Though hair cell specific mechanisms have been proposed, they fail to explain the similar gradient of damage observed in other areas of the cochlea. A simpler explanation may be a gradient of drug exposure. These lost hair cells are later replaced by a layer of non-specialized scar tissue (Estrem et al., 1981, Laurell and Bagger-Sjoback, 1991, Monzack et al., 2015).

In vivo studies in the guinea pig have also demonstrated damage to spiral ganglion cells, including detachment from their encircling myelin sheaths. The fact that this damage occurred at the same time as (and not following) hair cell loss suggests that this spiral ganglion damage is directly mediated by cisplatin (van Ruijven et al., 2005). This conclusion is further supported by a clinical case report describing loss of benefit from a cochlear implant in a child who received cisplatin chemotherapy. The cochlear implant bypasses the need for hair cells, but is reliant upon proper functioning of the auditory nerve, and so for the implant to lose its

benefit in a patient with preexisting hair cell loss suggests direct damage to the spiral ganglion (Harris et al., 2011).

Cisplatin ototoxicity has also been associated with damage to the stria vascularis. Studies in rats have described strial edema and a variety of morphological changes specifically in strial marginal cells days after cisplatin administration (Meech et al., 1998). In guinea pigs, strial shrinkage driven primarily by intermediate cell shrinkage and secondarily by marginal cell shrinkage was described weeks after cisplatin administration (Sluyter et al., 2003). The findings from both these studies were limited to the basal turn of the cochlea. Multiple studies have utilized terminal deoxynucleotidyl transferase dUTP nick-end labeling (TUNEL) staining, to identify and quantify apoptotic cells in the cochlea following cisplatin. TUNEL staining is a marker of DNA fragmentation, which often is, but does not have to be, associated with cellular apoptosis (Gavrieli et al., 1992). Interestingly, studies using this technique have suggested more apoptosis in the stria than other cochlear regions. In one study of gerbils treated with cisplatin, TUNEL positive hair cells and spiral ganglion cells were limited to the cochlear base while TUNEL positive cells in the stria vascularis extended from the base to apex (Alam et al., 2000). In another case, a cisplatin dose in guinea pigs which was insufficient to cause TUNEL-positive hair cells resulted in TUNEL-positive marginal cells in the stria vascularis (Watanabe et al., 2003). These studies suggest that the stria vascularis experiences DNA damage—and potentially apoptosis—at doses of cisplatin insufficient to damage other cochlear cell types.

Studies of human cochlear morphology following cisplatin chemotherapy have been limited. However, their conclusions tend to agree with those derived from animal models. A histopathological study of human temporal bone samples after cisplatin chemotherapy noted loss of inner and outer hair cells, decreased spiral

ganglion cells, and atrophy of the stria vascularis in agreement with many of the above-mentioned animal studies (Hoistad et al., 1998).

Investigations into the cellular mechanisms of cisplatin ototoxicity have implicated several pathways with the final common endpoint understood to be cellular apoptosis. Though the anti-cancer effects of cisplatin have traditionally been understood to be mediated through covalent crosslinking of the DNA backbone and interference with DNA replication, more recent work has highlighted the importance of other cytotoxic mechanisms. It is now understood that a small fraction of intracellular cisplatin may be bound to nuclear DNA (Gonzalez et al., 2001), and that cisplatin has robust cytotoxic effects even in enucleated cells (Yang et al., 2006). Though it appears that cisplatin interacts with a great number of cellular proteins and biomolecules, aquated cisplatin (traditionally considered the intracellular activated form) appears particularly reactive with thiol-containing molecules such as glutathione (Fuertes et al., 2003).

The most commonly proposed cytoplasmic mechanism for cisplatin ototoxicity is via accumulation of reactive oxygen species. Diverse cochlear cell types including outer hair cells, spiral ganglion cells, and cells of the stria vascularis and spiral ligament have been demonstrated to generate significant reactive oxygen species following exposure to cisplatin (Mukherjea et al., 2011, Rybak et al., 2009, Rybak et al., 2007). The depletion or inhibition of cochlear anti-oxidant enzymes has also been reported (Khynriam and Prasad, 2002, Rybak et al., 2000). This depletion may be a result of direct cisplatin binding and interference with enzyme function, depletion of glutathione and NADPH, or inactivation of these enzymes by already-formed ROS. Reactive oxygen species formed in cochlear cells can have many deleterious downstream effects including, but not limited to, nitrosylation and inactivation of proteins, reaction with fatty acids to form the toxic aldehyde 4-

hydroxynonenal (Lee et al., 2004a, Lee et al., 2004b) and caspase activation via a Bax-dependent pathway (Watanabe et al., 2003). The tumor suppressor p53 is also understood to be involved in cisplatin ototoxicity, but its activation may be triggered by DNA damage (Devarajan et al., 2002, Zhang et al., 2003).

A few studies have described specific ototoxic mechanisms in the spiral ganglion and stria vascularis. In the spiral ganglion, current evidence points towards DNA damage-dependent apoptosis. Upregulation of the DNA-binding high mobility group protein (HMG1) (Li et al., 2006) has been implicated, as has translocation of nucleotide excision repair factors from the cytoplasm to nucleus (Guthrie et al., 2008). For the stria vascularis and lateral wall, cisplatin ototoxicity has been associated with increased NF-κB expression leading to induction of nitric oxide synthase (van Ruijven et al., 2005), and has additionally been shown to activate big conductance potassium channels in spiral ligament fibrocytes, which disrupts ion homeostasis and causes apoptosis (Liang et al., 2005).

Though these studies investigating cellular mechanisms of cisplatin ototoxicity have provided many glimpses into the intracellular changes occurring in specific cell types following cisplatin exposure, there are a few significant caveats limiting their interpretation. Most significantly, it must be noted that much of what is known about mechanisms of cisplatin-induced cell death in the cochlea comes from *in vitro* studies of organ explants—which do not include the spiral ganglion neurons or stria vascularis—or the HEI-OC1 or UB/OC-1 cell lines. These studies cannot of course provide any insight into cisplatin-induced changes in cochlear regions other than the organ of Corti. Additionally, it is unclear how accurately these experiments model *in vivo* conditions, especially as data are lacking on the appropriate concentration of cisplatin to use *in vitro* to approximate *in vivo* intracochlear exposure. Another caveat is that cisplatin seems to interact with many

proteins and biomolecules and so its resulting intracellular changes are expected to be similarly broad. Identification of changes in a specific pathway of interest as a result of cisplatin exposure does not prove that mechanism of toxicity to be the only or even the central mechanism involved. With this in mind, the field could likely benefit from more studies of cisplatin ototoxicity utilizing "discovery" approaches such as high-throughput proteomics and transcriptomics.

Though many studies have sought to describe the results of cisplatin exposure, very few have sought to better characterize the trafficking and distribution of cisplatin within the cochlea. Further, most studies with this intention have relied upon surrogate measures of cisplatin distribution and have not directly assayed the drug. One such approach has been to use an antibody raised against the cisplatin-DNA adduct to immunolocalize cisplatin which has bound DNA. Both a polyclonal and a monoclonal antibody have been developed and used. One group identified platinated DNA in the nuclei of outer hair cells and supporting cells of the organ of Corti, marginal cells of the stria vascularis, and cells of the basal portion of the spiral ligament (van Ruijven et al., 2005). A separate group identified platinated DNA primarily in the marginal cells of the stria vascularis (Thomas et al., 2006). The discrepancies in these findings may be explained by the specificity of the antibodies or several other differences in the experimental designs. Recently, other members of our laboratory have repeatedly attempted to use the only currently commercially available antibody for cisplatin-DNA adducts (a monoclonal) with no success. Tissues from cisplatin-treated mice repeatedly showed no specific staining of adducts anywhere within the cochlea (Aaron Rusheen, unpublished). However, given the small fraction of intracellular cisplatin known to bind DNA, the importance of DNA-independent mechanisms of cytotoxicity (Mezencev, 2015), and the low (or

absent) DNA replication activity in cochlear cell types, the immunolocalization approach has limited utility in explaining cisplatin ototoxicity.

Cisplatin pharmacokinetics have more recently been studied through two cisplatin-fluorophore conjugates which can be followed by light microscopy. One such conjugate of cisplatin and the Texas Red fluorophore has been used *in vivo* in rats. Fluorescence from the conjugate was found to be brightest in the stria vascularis in the hours following systemic administration, with minimal fluorescence detected in inner and outer hair cells (Chu et al., 2016). Another group used a conjugate of platinum and rhodamine to study cisplatin uptake into the sensory hair cells of the zebrafish lateral line, finding cisplatin uptake to require mechanotransduction (Thomas et al., 2013). These studies have provided some initial insights into how cisplatin moves throughout the cochlea and potentially into hair cells, though it must be considered that both compounds represent a very significant size increase over cisplatin (among other altered physical properties). These chemical differences may alter pharmacokinetics and have been shown to alter cytotoxicity (Chu et al., 2016, Thomas et al., 2013). As is true for immunolocalization of cisplatin-DNA adducts, this approach is a surrogate measure for cisplatin distribution within the cochlea, and so a more direct method of quantifying cisplatin in these tissues would be preferred.

Multiple methods for the direct measurement of cisplatin concentrations in tissue exist and have been used extensively to study cell lines and non-cochlear tissues. Previously used techniques include atomic absorption spectrometry (AAS), inductively coupled plasma atomic emission spectrometry (ICP-AES), and inductively coupled plasma mass spectrometry (ICP-MS). Of these techniques, ICP-MS is the most sensitive and precise (Minami et al., 1995). ICP-MS detects metals and some non-metals in the form of atomic or polyatomic species by first ionizing an

acid-digested sample with inductively coupled plasma and then detecting the produced ions on a mass spectrometer. It is commonly used for assessing metal toxicity and for industrial and biological monitoring. ICP-MS quantification of cisplatin is possible because the cisplatin molecule contains platinum metal. ICP-MS is particularly suitable for this purpose because it detects unmodified cisplatin as well as its active derivatives, primarily monoaqua- and diaquacisplatin (Berners-Price et al., 1992). Further, as platinum is not typically incorporated into biological tissues, ICP-MS quantification of cisplatin species in tissue samples can be performed with no background platinum signal contributed by the tissue itself.

To date, only a few studies have directly measured cisplatin in the cochlea. One study in guinea pigs used liquid chromatography with post-column derivatization to quantify cisplatin in the perilymph over time and ICP-MS to quantify cisplatin in total cochlear tissues at a single timepoint (Hellberg et al., 2009). Their major finding was that the less-ototoxic platinum drug oxaliplatin has a decreased level of uptake into the cochlea as compared to cisplatin. More recently, laser ablation ICP-MS has twice been used to visualize the distribution of cisplatin in cochlear tissue sections from cisplatin-treated mice. In this technique, a thin section of sample is progressively ablated by a scanning laser and concentrations of the element(s) of interest are continuously measured by an ICP-MS system, allowing for the two-dimensional mapping of the element of interest within the sample (Figure 3.4). However, only one or two time points were investigated in these prior studies, neither cisplatin regimen was demonstrated to have resulted in hearing abnormalities, and the resolution of the technique and quality of the tissue preparation greatly limited the interpretation of the images (Koppen et al., 2015, Reifschneider et al., 2013).

Overall, cisplatin is understood to damage multiple cochlear regions, with several cellular pathways proposed to mediate cisplatin-induced cell death. Emphasis has been upon describing cochlear morphology after cisplatin and identifying intracellular changes, with a very limited amount of focus falling upon describing the behavior of the drug and how its pharmacokinetics may help explain its ototoxicity. However, the severity of a drug's toxicity is driven both by the abundance of cellular targets of the drug (the inherent sensitivity of the cell or tissue) as well as the total level of drug exposure (the summed effective drug concentration over time). Those cells and tissues most susceptible to cisplatin may simply be those most exposed. Therefore, an improved understanding of cisplatin pharmacokinetics in the cochlea may help explain the susceptibility of the cochlea and specific cochlear regions to cisplatin-induced damage and provide further insight into the etiology of hearing loss. The experiments described in this chapter were designed to directly assess the distribution of cisplatin in a clinically-relevant mouse model of ototoxicity as well as in human tissue samples in order to elucidate the relationship between cisplatin pharmacokinetics and the drug's ototoxicity. ICP-MS was used to directly investigate cisplatin pharmacokinetics within the cochlea and other tissues, and a recently-developed cisplatin-fluorophore conjugate was used for high-resolution investigation of cisplatin trafficking.

3.2 METHODS

3.2.1 Cisplatin treatment

Mice underwent either a portion or the entirety of the cisplatin regimen detailed in section 2.2.1 above. In short, sub-groups of mice were euthanized and dissected at the following time points: on day 4—"Cycle 1" group, day 14—"Recovery 1", day 18—"Cycle 2" group, day 28—"Recovery 2", day 32—"Cycle 3", day 42—"Recovery 3" or "complete regimen". For analysis of cisplatin pharmacokinetics over the first 24 hours, mice received a single intraperitoneal injection of cisplatin at the standard dose of 3.5mg/kg.

3.2.2 Tissue collection for ICP-MS

A number of tissues were collected from cisplatin-treated mice and analyzed for platinum (i.e. total cisplatin species) content. Cisplatin-treated and saline-treated control mice were euthanized by CO_2 inhalation followed by rapid decapitation. To obtain serum samples, whole blood was drawn from bilateral external jugular veins, allowed to clot for at least 20 minutes at room temperature, and then spun at 2000g for 15 minutes at 4° C, with the resulting supernatant being saved. Whole organs were dissected out, rinsed in ultrapure water, and patted dry. To obtain cochleae, bony labyrinths were removed, and the vestibular organs were dissected away. Femurs were flushed of bone marrow using ultrapure water injected through a 25 gauge needle. All samples were stored at -80° C until ICP-MS analysis could be performed.

3.2.3 Cochlear microdissections

Cochleae were microdissected into separate anatomical regions in order to examine their specific platinum content. Cochleae destined for microdissection or

cryosectioning were fixed and decalcified as described in section 2.2.4 above. To isolate tissue from specific cochlear regions, decalcified cochleae were microdissected using ophthalmic straight knives (Accutome) and Dumont #55 Forceps (Fine Science Tools). The stria vascularis was peeled from the cochlear lateral wall and the organ of Corti and spiral ganglion were cut from their surrounding tissues. All three regions were then analyzed separately by ICP-MS.

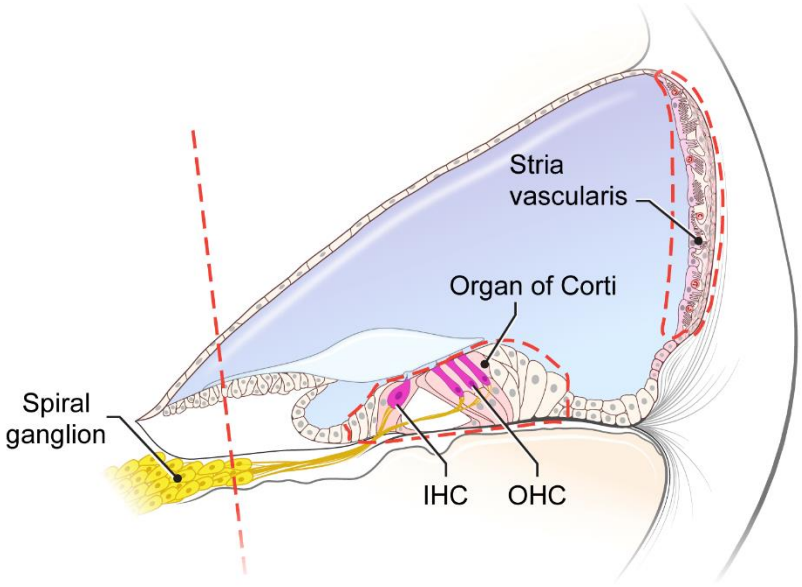


Figure 3.1: Overview of cochlear regions microdissected for ICP-MS analysis

Red dotted lines outline the stria vascularis, organ of Corti, and spiral ganglion neurons and illustrate the approximate level of precision achieved in isolating each region. The stria vascularis was peeled away with near-perfect precision. Organ of Corti microdissections included minimal portions of the inner and outer sulcus. Spiral ganglion microdissections included minimal portions of the spiral limbus. Illustration by Alan Hoofring.

3.2.4 Cochlear cryosections

Decalcified cochleae to be cryosectioned were first incubated overnight in 30% sucrose in PBS at 4° C with gentle rotation, then incubated in a 1:1 solution of 30% sucrose and Tissue-Tek OCT compound (Sakura) for 4 hours at 4° C, and finally incubated in OCT overnight at 4° C. The following day, cochleae were oriented within

OCT-containing cryomolds (Tissue-Tek, Intermediate; Sakura) and frozen on a cooling bath of absolute ethanol and dry ice. Frozen sections of 12μm thickness were cut on a cryostat (Leica CM), captured on glass slides (Superfrost Plus; Thermo Scientific), and allowed to air dry for 1 to 2 hours at room temperature.

3.2.5 Administration of BODIPY compounds

BODIPY FL-Cisplatin, a conjugate of cisplatin and the low molecular weight fluorophore BODIPY FL, as well as the free-dye (no cisplatin) compound BODIPY FL-Boc (Figure 3.2) were administered to mice *in vivo* in order to study cisplatin trafficking via confocal microscopy. Both compounds were synthesized by the Imaging Probe Development Center of the National Heart, Lung, and Blood Institute Intramural Program. The BODIPY FL-Cisplatin molecule is a validated conjugate recently shown to retain DNA damaging and cytotoxicity capacity (Jagodinsky et al., 2015, Miller et al., 2014). BODIPY FL-Cisplatin retains spectral qualities similar to those of BODIPY FL dye. The free-dye control (no cisplatin) compound BODIPY FL-Boc was used to control for any observed BODIPY FL-Cisplatin pharmacokinetics that may have been a result of the properties of the fluorophore and not of the cisplatin moiety.

Mixed gender CBA/CaJ mice at 10 weeks of age were used. Mice in the experimental group (n = 7) received a regimen of BODIPY FL-Cisplatin while control mice (n = 7) received BODIPY FL-Boc. The dosing regimen entailed three cycles, each consisting of 4 days of once-daily i.p. injections. In order to deliver the molar equivalent dose as used in the cisplatin regimen, BODIPY FL-Cisplatin injections were dosed at 7.3 mg per kg of mouse mass, and BODIPY FL-Boc injections were dosed at 5.1 mg/kg. Both compounds were delivered in a total of 1mL of saline-based solution containing 61.6mg/kg of methyl-β-cyclodextrin (Sigma-Aldrich) and 2mL/kg of dimethylformamide (Alfa Aesar). Methyl-β-cyclodextrin and

dimethylformamide were necessary to maintain BODIPY FL-Cisplatin in solution. For n = 3 mice in each experimental group, cochlea, brain, liver, and kidney tissues were collected on the day following completion of the regimen.

Cochleae were fixed and decalcified as described in section 2.2.4 above. Cochlear cryosections and microdissected organ of Corti tissue were blocked, stained, and imaged as described for hair cell counting in section 2.2.4 above. Samples from BODIPY FL-Cisplatin and BODIPY FL-Boc mice were imaged under identical acquisition settings, including laser line attenuation and detector gain. Post-acquisition processing was performed in ImageJ2 (Schindelin et al., 2015) and was applied equally and across the entire image to all images used for comparison.

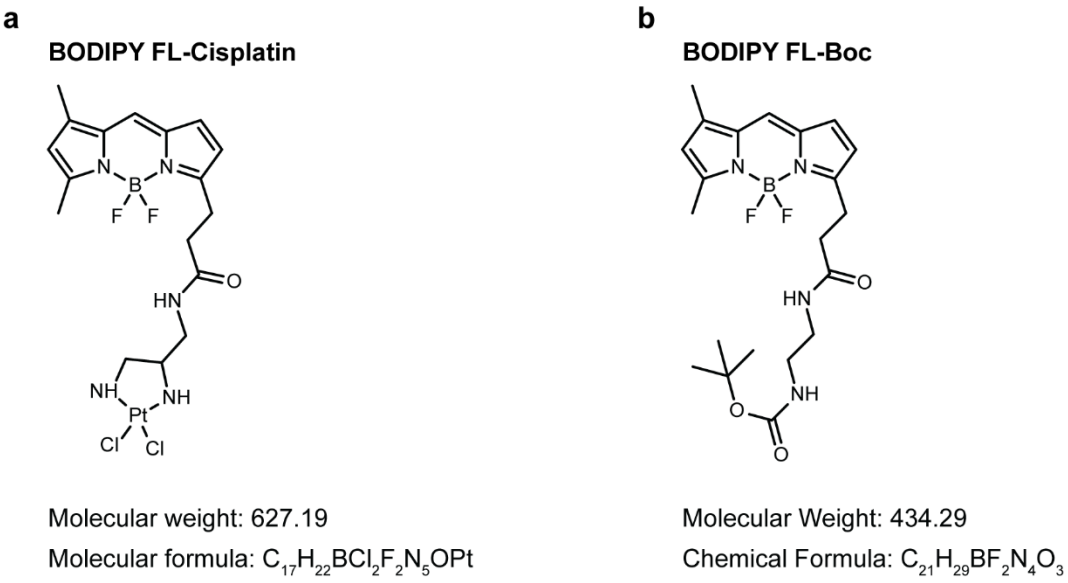


Figure 3.2: Structure of the BODIPY FL-Cisplatin conjugate and its control compound BODIPY FL-Boc

These two compounds were used to study *in vivo* cisplatin trafficking. (a) BODIPY FL-Cisplatin represents a percentage mass increase of 109% over unconjugated cisplatin, and therefore has the advantage of being much closer in size to cisplatin than previously described conjugates (Chu et al., 2016, Thomas et al., 2013). (b) The control compound BODIPY FL-Boc incorporates a tert-butyloxycarbonyl (BOC) protecting group in place of cisplatin and can be used to visualize the trafficking of the BODIPY FL dye.

3.2.6 Human patient cochlear sections

Biobanked cochlear tissue sections from patients who had received cisplatin chemotherapy were analyzed for the retention of cisplatin species following treatment. The NIH Office of Human Subjects Research Protections determined the study to be exempt from Institutional Review Board review as it utilized existing records and post-mortem pathological specimens. The National Temporal Bone Registry online database was queried to identify banked temporal bone samples from patients who had received a chemotherapy regimen including cisplatin and had sufficiently complete medical records. For inclusion, patient donors were required to have a documented and dated history of cisplatin administration and a recorded date of death. Patients with noted middle or inner ear anatomical abnormalities or tumor invasion involving or in close proximity to the cochlea were excluded. In most cases, patient ethnicity was not known. Eight cisplatin-treated patients were identified. The database was then queried to identify a sex- and age-matched control patient, who had never received cisplatin, to match each cisplatin-treated patient. Samples were obtained via a tissue transfer agreement with the NIDCD National Temporal Bone, Hearing and Balance Pathology Resource Registry at the Massachusetts Eye and Ear Infirmary. Three to four approximately mid-modiolar 20μm sections were prepared from each patient. Celloidin embedding medium was removed using sodium hydroxide and methanol according to a published protocol (O'Malley et al., 2009). The final rinse was performed in ultrapure water. Sections were manually trimmed with a fresh razor blade to only include the cochlea and immediately surrounding bone, and were then tile-scan imaged at 10x under brightfield optics (Zeiss LSM 780). Images were shading corrected and stitched in Zen 2.1 software (Carl Zeiss Microscopy) before further

processing in ImageJ2. Sections were then either digested and analyzed for total platinum content, or were analyzed via laser ablation ICP-MS.

3.2.7 Inductively coupled plasma mass spectrometry (ICP-MS)

Inductively coupled plasma mass spectrometry was used to measure total platinum concentrations in whole organs and microdissected portions of the cochlea (

Figure 3.3). ICP-MS measurements were performed by Dr. Lauren Amable. Platinum measurements were performed using a NexION 350D inductively coupled plasma-mass spectrometer (Perkin Elmer). The instrument was tuned daily for optimum performance and sensitivity. Whole organs were weighed before digestion in trace metal nitric acid (Fisher Chemical) for 20 minutes at 65˚C. An equal volume of hydrogen peroxide (Optima Grade, Fisher Chemical) was then added and the incubation was repeated. Samples were diluted 1:100 with 2% nitric acid prior to running. A quantitative analysis method in standard mode measuring the platinum 195 isotope was used to determine platinum concentrations. A platinum standard (SPEX CertiPrep) curve was generated with 0.2, 1.0, and 2.0 ppb standards. Iridium isotope 193 was used as the internal standard (10 ppb stock concentration, SPEX CertiPrep) and was added inline using the microPREP FAST SV500 injection system (Elemental Scientific, Inc.). Each sample was run in duplicate and measured platinum concentrations were normalized to organ weight.

Mouse cochlear microdissection samples were prepared by removing residual liquid by speed vacuum concentration. Samples were digested as described above, but volumes of 10 µl of nitric acid and 10 µl of hydrogen peroxide were used. Samples were resuspended to a final volume of 500 µl with 2% nitric acid. Platinum 195 and iridium 193 isotopes were measured as described above. Phosphorous and sulfur (Inorganic Ventures) were additionally measured in dynamic reaction mode (DRC) using oxygen at a 1.2 ml/min gas flow rate. The isotopes PO 47 and SO 48

were measured using a 50, 250, and 500 ppb standard curve. Beryllium isotope 7 was used as the internal standard (500 ppb stock concentration, SPEX CertiPrep) and added inline. Platinum values were normalized to sulfur values for each microdissected sample since the cochlear microdissected samples were too small to accurately use sample weight for normalization.

Human temporal bone sections were removed from the glass slide under water using a new scalpel and quantitatively transferred to a 1.5 ml tube. Each sample was digested with 50 µl nitric acid and 50 µl hydrogen peroxide for 2 hours at 65˚C. Each sample was re-suspended to a final volume of 500 µl with 2% nitric acid. Platinum, sulfur, and phosphorous were measured and normalized as described above.

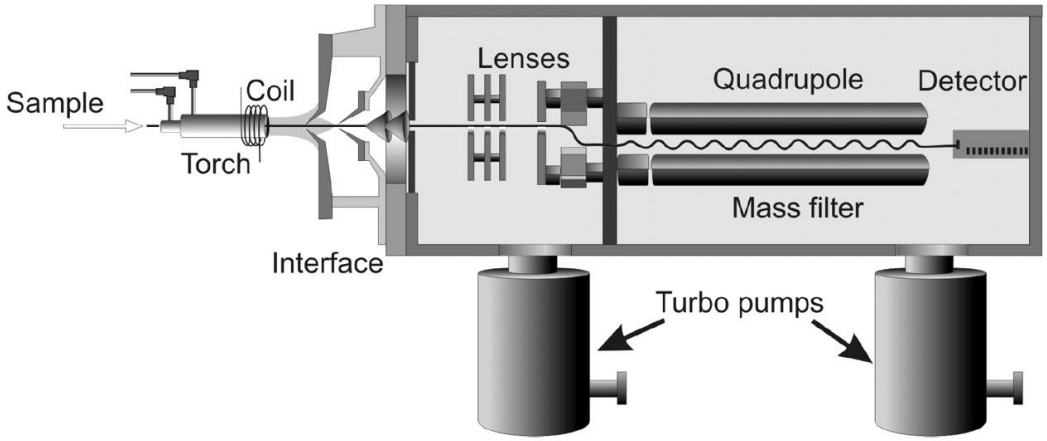


Figure 3.3: Schematic of inductively coupled plasma mass spectrometer

Inductively coupled plasma mass spectrometry can measure the concentrations of metals and several non-metals present in samples at concentrations as low as one part per quadrillion. In the standard configuration, the sample is introduced in liquid form. Solid samples are first digested and diluted in nitric acid solution to make them suitable for introduction into the machine. The liquid sample is first aerosolized and then sprayed into a plasma beam formed by inductively heating argon gas with an electromagnetic coil. The temperature of the plasma causes the sample to be both atomized (separated into individual atoms) and ionized. These ions are then extracted into the mass spectrometer portion of the instrument, which is held at high vacuum. Ions are focused by a series of ion lenses into a quadrupole mass analyzer. In the mass analyzer, ions are separated based upon their mass-to-charge ratio and detected by an electron multiplier. The intensity of the detected ion

signal is proportional to its concentration. Figure reproduced from Košler and Sylvester (2003).

3.2.8 Laser ablation ICP-MS

Laser ablation ICP-MS (Figure 3.4) was used to visualize the distribution of platinum within cochlear tissue sections. Unlike standard ICP-MS, which analyzes a fully-digested portion of tissue in liquid form, laser-ablation ICP-MS progressively ablates and analyzes a solid sample. It can thus be used to map the two-dimensional distribution of the element of interest within the sample. Laser ablation ICP-MS was performed using a NWR 213 solid state laser ablation module (Electro Scientific Industries, Inc., Portland, OR) coupled to the ICP-MS instrument. Conditions for the laser were as follows: 20 Hz repetition rate in continuous mode using 20% energy. A 25 μm X 25 μm spot size was generated using a 20 μm line spacing in Y. The scan speed was 50 μm/sec and helium gas flow was set at 650 ml/min. Platinum 195 was analyzed with calcium 43 serving as a control. Heat maps were generated using Iolite software (Paul et al., 2012) and in some instances were overlaid upon pre-ablation brightfield images. Platinum heat maps from experimental and control samples were scaled equally for intensity.

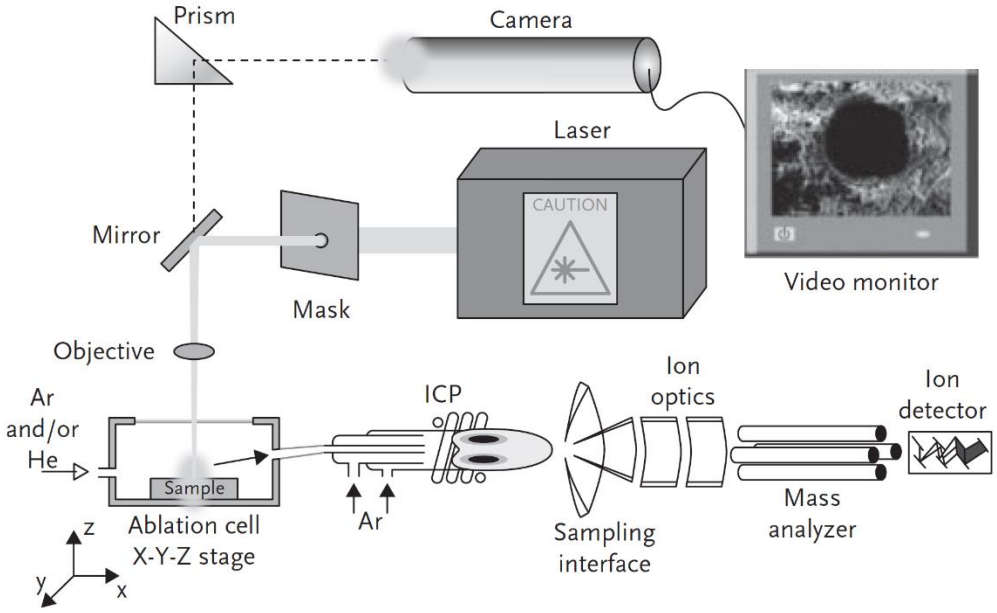


Figure 3.4: Overview of the laser ablation ICP-MS technique

Laser ablation ICP-MS allows for high resolution analysis of the physical distribution of metals (and some non-metals) in solid samples. In traditional ICP-MS, solid samples must be digested and introduced as a liquid sample, thus only a single concentration value can be obtained for a piece of tissue. Laser ablation ICP-MS modifies the manner of introduction of the sample into the ICP-MS system and allows for the two-dimensional visualization of metals within the sample. In this method, a thin section of sample is placed into an ablation cell which is purged with helium gas. A magnified image of the sample is visualized by camera and the ablation path is programmed. An ultraviolet laser is used to progressively ablate the sample along the programmed path. The resultant laser-induced aerosolized sample is continuously carried by helium gas to the ICP-MS system for continuous analysis as previously described.

3.2.9 Endocochlear potential recordings

Endocochlear potential recordings were taken in order to assess the effect of cisplatin treatment upon maintenance of the endocochlear potential in mice. These measurements were performed by Dr. Katharine Fernandez. Endocochlear potentials (EPs) were recorded from 25 total mice under deep anesthesia (Avertin, 15.1 mg/ml at 0.35 mg per kg body weight). Mice were mounted in the supine position in a secure head holder, and a midline incision in the was made in order to place a tracheal cannula between the 4th and 5th tracheal rings. Muscles underlying the thyroid were separated to expose the portion of the auditory bulla enclosing the

middle ear. An initial opening in the bulla was made using a #11 surgical blade and expanded with micro forceps to reveal the round window membrane while ensuring no contact with the stapedial artery. The darkened region near the basilar membrane where hair cells are located in the base of the cochlea was identified and used as a target for electrode placement.

A 1M KCl gel (agarose) filled glass pulled pipette reference electrode with Ag-AgCl wire (Worcester Polytechnic Institute, 1B-150F-4) was placed subcutaneously in the abdomen. Using a micromanipulator (Narishige, US-3f), the tip of a small 1M KCL filled glass pulled recording pipette with a Ag-AgCl wire electrode (Worcester Polytechnic Institute, 1B-100F-4) was advanced through the round window membrane into the scala tympani and then through the basilar membrane into the scala media, where an EP was recorded. Signals were digitally recorded (Digidata 1440A and AxoScope 10.3; Axon Instruments). An EP was confirmed as a >10mV potential that was maintained for 100 seconds and returned to 0 mV as the electrode retracted to its original position in scala tympani. At the end of the procedure, mice were euthanized without recovery from anesthesia.

3.3 RESULTS

3.3.1 Systemic cisplatin pharmacokinetics

Mice were administered a single 3.5mg/kg cisplatin injection in order to investigate cisplatin pharmacokinetics over the initial 24 hours. Peak tissue platinum levels were reached within one hour—the earliest time point examined—across all mouse tissues studied (Figure 3.5). Thus, cisplatin penetrance was broad and rapid. Platinum levels were lowest in the brain and highest in the kidney. Poor penetrance of the blood brain barrier and nephrotoxicity are both well-established characteristics of cisplatin therapy (Stewart, 1994, Stewart et al., 1982). Over the following 23 hours, platinum levels remained largely stable across all tissues, including blood. These data indicate that cisplatin rapidly enters most organs within one hour of injection. Control mice injected with saline in place of cisplatin had no detectable platinum in their tissues in all cases. ICP-MS for all saline-treated controls can be found in supplemental Figure S 1.

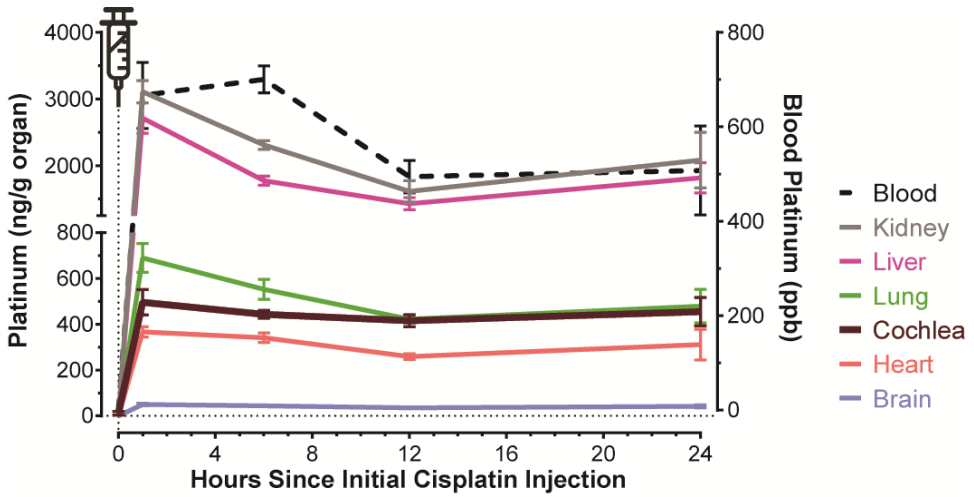


Figure 3.5: Early systemic cisplatin pharmacokinetics

Platinum concentrations in whole mouse organs isolated throughout the first 24 hours following a single i.p. injection of cisplatin. 0-hour data points represent mice prior to injection of cisplatin. Concentrations are normalized to organ mass (ng Pt/g of organ, left y-axis) or expressed as parts per billion (ppb, right y-axis) for blood.

Platinum levels peaked in most organs one hour after injection, and remained relatively stable through 24 hours. Concentrations varied significantly across organs and were highest in kidney and liver. n = 3-4 mice per time point for all organs. Mean ± s.e.m. are shown.

Cisplatin pharmacokinetics over the course of the entire ototoxicity-inducing regimen were next investigated (Figure 3.6). Tissues were harvested from subsets of mice at the end of each cisplatin cycle and each recovery (the same time points at which auditory testing was performed in Chapter 2). Cisplatin pharmacokinetics followed a similar pattern across most organs examined. Platinum levels climbed during each injection cycle and then declined over the subsequent recovery. As observed following a single dose, platinum in the brain was minimal throughout the entire regimen. The cochlea, however, exhibited unique pharmacokinetics among the organs analyzed. Platinum entered during each treatment cycle, and persisted through each recovery period. Therefore, measured platinum levels in the cochlea followed a pattern of step-wise increase when observed across the complete regimen. At the end of the regimen (day 42), platinum concentrations were highest in the liver and kidney, but had already significantly decreased from their peak (end of cycle 3) levels ($P < 0.01$ for each, two-tailed t-test). In contrast, platinum levels were next highest in the cochlea, but were similar to peak levels ($P > 0.05$, two-tailed t-test). These data suggested that cisplatin persists in the cochlea with greater efficiency than other organs.

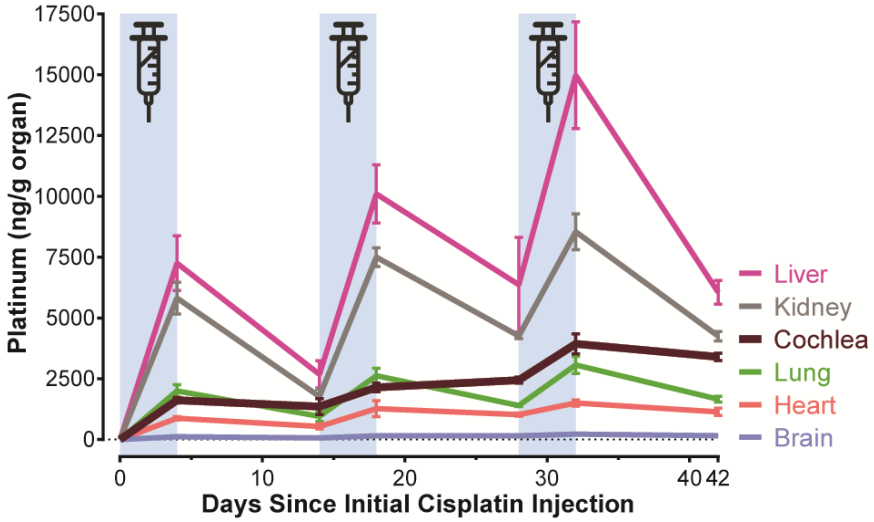


Figure 3.6: Systemic cisplatin pharmacokinetics throughout the cisplatin ototoxicity regimen

Platinum concentrations in whole mouse organs isolated throughout the cisplatin ototoxicity regimen. The three, 4-day long cycles of once-daily i.p. cisplatin are indicated by blue shading. In most organs, platinum levels increased following injection and then declined during the recovery period. In contrast, platinum levels in cochlea progressively increased with no apparent elimination during recovery periods. n = 3-4 mice at each time point for all organs. Mean ± s.e.m. are shown.

To test for long-term retention of cisplatin species in the cochlea, a subset of mice were allowed to recover for an additional 60 days following the end of the cisplatin regimen. Platinum levels in mice at the end of the regimen were compared to those in mice 60 days later (Figure 3.7). Sixty days later, platinum levels in serum had fallen by 89%, and most organs had significantly eliminated cisplatin species. The notable exceptions were cochlea and femur. These two organs showed no significant loss of platinum after 60 days. This extended retention of cisplatin species in the cochlea demonstrates that the organ is subject to a high cumulative drug exposure, which may at least partially drive ototoxicity.

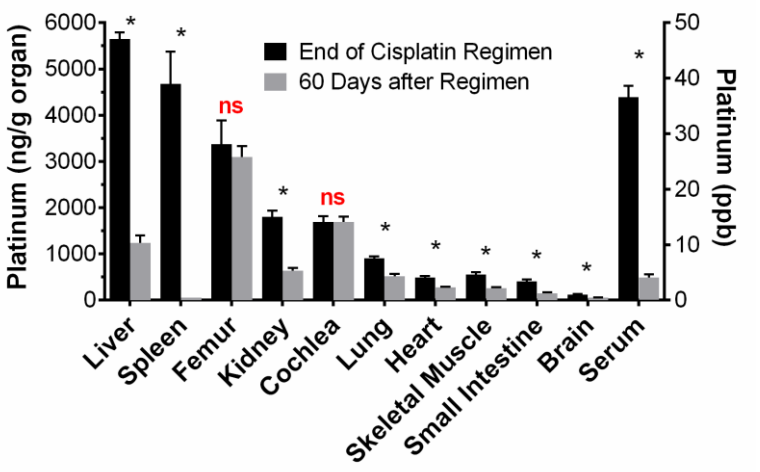


Figure 3.7: Late systemic cisplatin pharmacokinetics

Concentrations of platinum in whole organs of mice at the end of the cisplatin regimen (day 42) were compared to those following a subsequent 60-day recovery (day 102). Serum values are plotted on the right y-axis, all others on left. During this recovery period, platinum was significantly eliminated from all tested organs except the cochlea and femur. n = 3-4 mice in each group. Mean ± s.e.m. are shown. Multiple two-tailed t-tests with correction for multiple comparisons by the Holm-Šidák method were used to determine significance. ppb = parts per billion, ns = not significant, * $P < 0.05$.

3.3.2 Intracochlear cisplatin pharmacokinetics

To gain insight into the pharmacokinetics of cisplatin *within* the cochlea, cochlear regions of interest were isolated by manual microdissection and analyzed by ICP-MS. The organ of Corti, spiral ganglion, and stria vascularis have each been implicated in previous studies of cisplatin ototoxicity and were thus investigated here. As seen at the whole-organ level, peak platinum concentrations were measured in all three regions an hour after administration of a single cisplatin dose (Figure 3.8). Thus, cisplatin has fully distributed within these cochlear tissues within an hour. Though platinum concentrations in the organ of Corti and spiral ganglion neurons were similar, concentrations in the stria vascularis were significantly higher at most time points, suggesting preferential entry of cisplatin into that region.

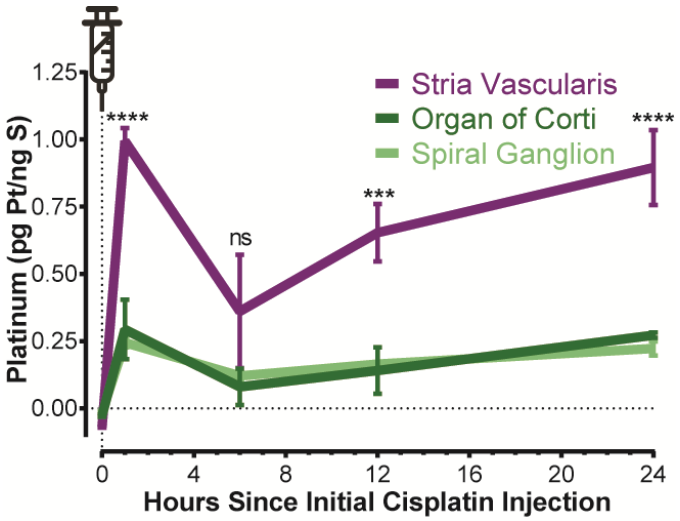


Figure 3.8: Early cisplatin pharmacokinetics within cochlear regions

Platinum concentrations in microdissected cochlear regions in the first 24 hours following a single i.p. injection of cisplatin. Platinum concentrations are normalized to sulfur content, a surrogate for total tissue quantity (Wind et al., 2003). Cisplatin readily distributed throughout these cochlear regions within the first hour, but showed increased entry into the stria vascularis as compared to either the organ of Corti or spiral ganglion. n = 3-4 mice per time point. Mean ± s.e.m. are shown. Statistical significance displayed for stria vascularis values as compared to the other two cochlear regions. Two-way ANOVA followed by the Holm-Šidák multiple comparisons test was used to determine significance. ns = not significant, *** $P < 0.001$, **** $P < 0.0001$.

Investigation of platinum concentrations in these specific cochlear regions over the course of the entire cisplatin regimen demonstrated preferential cisplatin entry into the stria vascularis over that time course as well (Figure 3.9). As observed for the whole cochlea, platinum tissue concentrations in each of these regions progressively increased over the course of the regimen.

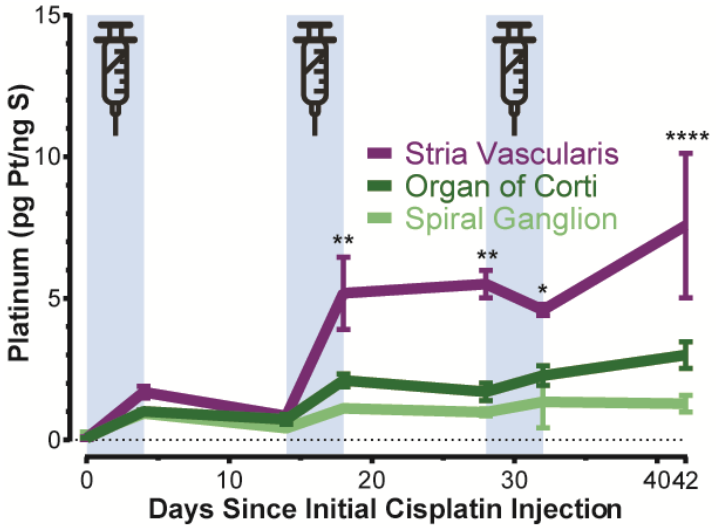


Figure 3.9: Cisplatin pharmacokinetics in cochlear regions throughout the cisplatin ototoxicity regimen

Platinum tissue concentrations progressively rose in all three cochlear regions over the course of the cisplatin regimen, but did so most significantly in the stria vascularis. Statistical significance displayed for stria vascularis values as compared to other two regions. n = 3 mice per time point. Mean ± s.e.m. are shown. Two-way ANOVA followed by the Holm-Šidák multiple comparisons test was used to determine significance. * $P < 0.05$, ** $P < 0.01$, **** $P < 0.0001$.

To examine long-term retention of cisplatin species within specific cochlear regions, tissues from mice at the end of the cisplatin regimen (protocol day 42) were again compared to those from mice allowed to recover for an additional 60 days (day 102). Sixty days later, platinum levels had decreased in all three regions of interest (Figure 3.10). Platinum levels were 52%, 39%, and 25% lower in stria vascularis, organ of Corti, and spiral ganglion, respectively. As described above, platinum levels in the entire cochlea did not measurably decline over this same time period (see Figure 3.7). There are at least two potential explanations for this apparent discrepancy. First, during this time platinum may have redistributed in such a way that it left the cochlear regions examined here, but was retained in other cochlear regions. Second, and more simply, the cochlear regions examined in this analysis constitute only a small fraction of the total cochlear mass. Therefore, the

changes observed here may be undetectable in an analysis of the whole cochlea if other portions of the cochlea—which constitute significantly more cochlear mass—retain cisplatin species more avidly. Regardless, this analysis of intracochlear cisplatin pharmacokinetics demonstrates that the stria vascularis is exposed to the highest concentrations of cisplatin and much of this cisplatin is retained long-term. This finding is fitting with previous investigations showing high levels of cisplatin-DNA adducts in the stria vascularis (Thomas et al., 2006), but represents the first time that total tissue levels of cisplatin species have been measured and reported in these cochlear regions. These results suggest against selective entry and retention of cisplatin in cochlear hair cells or organ of Corti as compare to other regions of the cochlea.

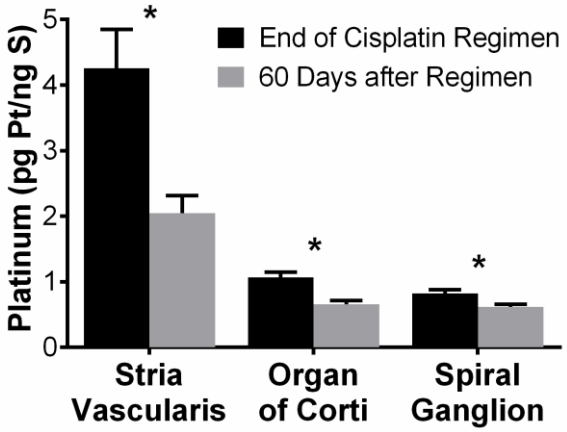


Figure 3.10: Long-term cisplatin pharmacokinetics within cochlear regions

Concentrations of platinum in cochlear regions at the end of the cisplatin regimen were compared to those following a subsequent 60-day recovery. All regions showed a decrease in platinum concentrations. n = 4 mice per group. Mean ± s.e.m. are shown. Unpaired two-tailed t-tests were used to determine significance. * $P < 0.05$.

3.3.3 Visualization of cisplatin trafficking by BODIPY FL-cisplatin

The BODIPY FL-Cisplatin conjugate was developed to permit the direct visualization by light microscopy of cisplatin movement on a cellular or subcellular

level. This compound was recently synthesized and validated by two independent groups, and has only once before been used *in vivo* (Jagodinsky et al., 2015, Miller et al., 2014). BODIPY FL-Cisplatin was used here in hopes of visualizing the localization of cisplatin in the cochlea at the cellular level, a resolution not afforded by other techniques. Following a regimen of BODIPY FL-Cisplatin that was dose-equivalent to that used for cisplatin, fluorescent signal was obvious in the stria vascularis and could also be seen in the spiral ganglion, interscalar septum, and organ of Corti (Figure 3.11a). No specific BODIPY fluorescence signal was apparent in cochlear tissue from control mice treated with the unconjugated (cisplatin-free) dye BODIPY FL-Boc.

A high-resolution examination of the stria vascularis showed BODIPY FL-Cisplatin signal throughout seemingly all strial cell types, with the highest intensity signal associated with the strial vasculature endothelium and within the vascular lumen (Figure 3.11b). Organ of Corti whole mounts were examined to assess any accumulation of BODIPY FL-Cisplatin within hair cells. No discernable fluorescent signal was present in outer or inner hair cells (punctae were proximal to, but not within inner hair cells), though punctate fluorescence was seen in the cells of the inner and outer sulci (Figure 3.11c). These results parallel those obtained by ICP-MS in suggesting that cisplatin retention within the cochlea is most pronounced in the stria vascularis and retention in hair cells and the organ of Corti is somewhat limited.

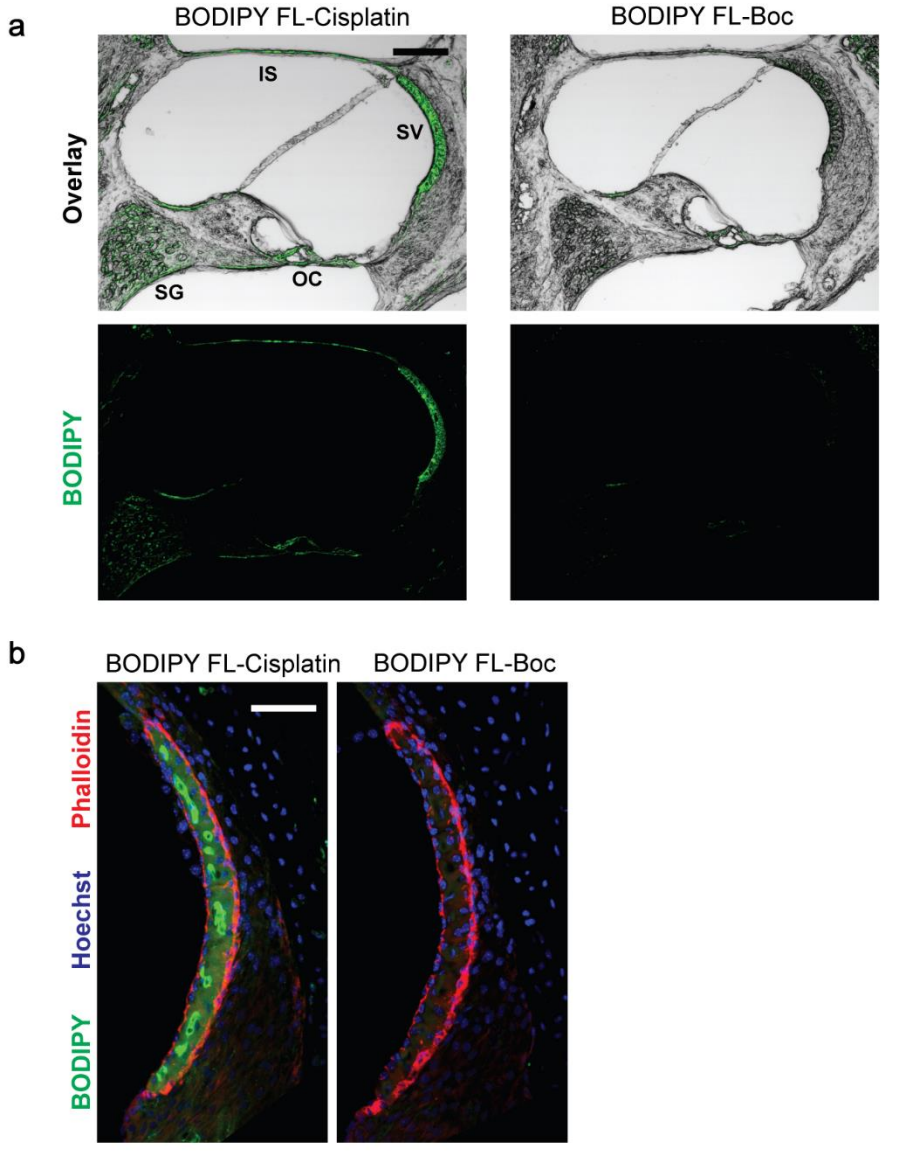

a
BODIPY FL-Cisplatin
BODIPY FL-Boc
Overlay
BODIPY
IS
SV
SG
OC
b
BODIPY FL-Cisplatin
BODIPY FL-Boc
Phalloidin
Hoechst
BODIPY
c
BODIPY FL-Cisplatin
BODIPY FL-Boc
No Injection
Outer sulcus
Outer hair cells
Inner hair cells
Inner sulcus
BODIPY
Myosin 7a
BODIPY

Figure 3.11: Cochlear accumulation of the fluorescent cisplatin conjugate BODIPY FL-Cisplatin

BODIPY FL-Cisplatin, a fluorescently tagged cisplatin conjugate, was administered to mice *in vivo* in order to visualize cisplatin trafficking within the cochlea. (a) Representative low-magnification confocal slices from cochlear cryosections of mice treated with a full regimen of BODIPY FL-Cisplatin or the control (no cisplatin) conjugate BODIPY FL-Boc. Fluorescent signal was obvious in the stria vascularis and could also be seen in the spiral ganglion (SG), interscalar septum (IS), and organ of Corti (OC). Scale bar = 100 μm. (b) Representative maximum intensity projections of thin confocal stacks of the stria vascularis only. At this higher magnification, BODIPY FL-Cisplatin in the stria vascularis appeared to fill most cells types, types but was most concentrated in the vascular endothelium and/or lumen. Scale bar = 50 μm. (c) Representative maximum intensity projections of confocal stacks of organ of Corti whole mounts. No discernable fluorescent signal was present in outer or inner hair cells (punctae in top left panel were proximal to, but not within inner hair cells). Punctate fluorescence was seen in the cells of the inner and outer sulci. Scale bar = 25 μm.

3.3.4 Cisplatin-induced changes in the endocochlear potential

Having observed high relative accumulation of cisplatin within the stria vascularis as compared to other cochlear regions, strial function was probed. Since a primary function of the stria vascularis is to maintain the endocochlear potential, direct measurement of the endocochlear potential can provide insight into strial health. Endocochlear potentials were measured both on the day following a single cycle of cisplatin as well as at the end of and sixty days after the complete cisplatin regimen, so that both early- and late-onset potential deficits could be assessed (Figure 3.12). Endocochlear potentials were decreased both on the day after a single cycle and sixty days after the entire regimen, suggesting that cisplatin can cause both rapid and persistent failure to properly maintain the composition of endolymph. Overall, these results suggest that accumulation of cisplatin in the stria vascularis is associated with loss of the endocochlear potential, which may be a direct result of strial damage. The hearing loss measured in cisplatin-treated mice is likely at least partially attributable to a reduced endocochlear potential.

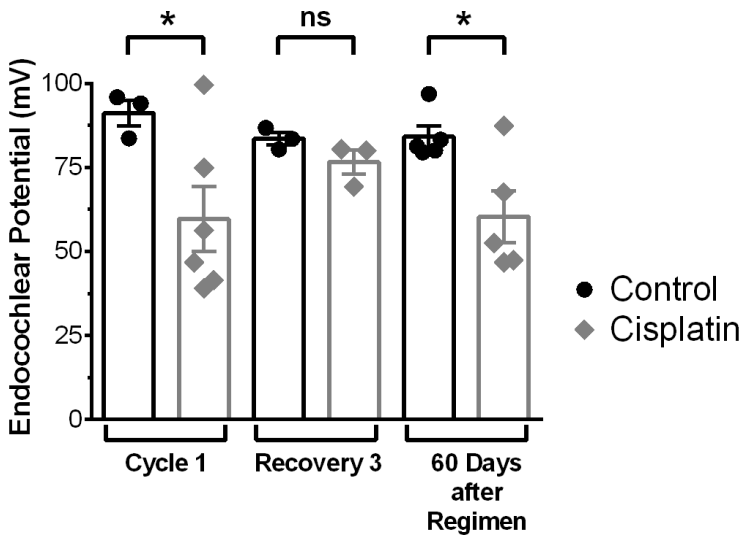


Figure 3.12: Endocochlear potentials following cisplatin treatment

Endocochlear potentials (EPs) measured in the basal endolymph following cisplatin treatment. EPs were depressed after a single cycle of cisplatin (regimen day 4), but recovered somewhat by the end of recovery 3 (day 42, end of regimen). However, 60 days later, EPs were still significantly reduced. Mean ± s.e.m. are shown. Unpaired two-tailed t-tests were used to determine significance. ns = not significant, * $P < 0.05$. Mice were 16 weeks of age at end of cycle 1, 22 weeks by the end of recovery 3, and 31 weeks at the 60 days after regimen time point.

3.3.5 Cisplatin retention in the human cochlea following chemotherapy

To investigate whether long-term cochlear retention of cisplatin species occurs in chemotherapy patients, postmortem human cochlear tissues were obtained from the NIDCD National Temporal Bone Registry. For inclusion, patient tissue donors were required to have a documented and dated history of cisplatin administration and a recorded date of death. Patients with noted middle or inner ear anatomical abnormalities or tumor invasion involving or in close proximity to the cochlea were excluded. A review of the medical and histological records identified eight patients—seven adults and one pediatric patient—who met the inclusion criteria, and eight suitable matched control patients. When analyzed for total platinum content, cochlear sections from patients who had received cisplatin

chemotherapy consistently contained significantly higher levels of platinum than sections from their matched untreated patients (Figure 3.13). Significant platinum was retained in cochleae for at least 18 months after a patient's last cisplatin infusion (the latest time point available for study). Differences in the cisplatin regimens received by these patients precluded analysis of platinum levels over time. Cochlear sections from the only pediatric patient contained significantly more platinum than any of the sections from adult patients ($P < 0.0001$), despite the pediatric patient having received a lower dose (total 180mg/m^2 BSA) than most, if not all, of the adult patients (median total dose of 245mg/m^2 BSA for all complete records). These findings demonstrate retention of cisplatin species in the human cochlea long after cisplatin chemotherapy. Though the evidence presented here is limited, this retention may be most pronounced in pediatric patients, who experience cisplatin ototoxicity at a higher rate than their adult counterparts.

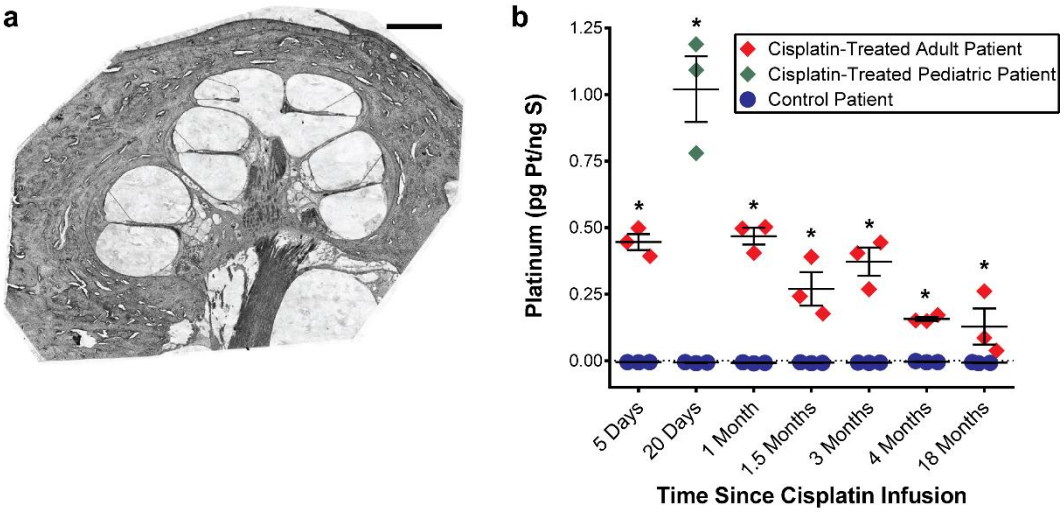


Figure 3.13: Cisplatin retention in human cochleae following chemotherapy

Overall platinum concentrations were measured in cochlear tissue sections from deceased patient donors, to examine cochlear retention of cisplatin species following chemotherapy. (a) Representative brightfield image of a cochlear section prior to ICP-MS analysis. All analyzed sections were roughly mid-modiolar, as an initial analysis showed platinum content to vary significantly with section location. Scale bar = 1mm. (b) Platinum concentrations measured in patient cochlear tissue sections. Each data point represents a single 20 μm section. Matched pairs of

patients who received cisplatin chemotherapy and control (cisplatin-naïve) patients are plotted by the time elapsed between the patient's last cisplatin infusion and their death. Mean ± s.e.m. are shown. Multiple two-tailed t-tests with correction for multiple comparisons by the Holm-Šidák method were used to determine significance. * $P < 0.05$

3.3.6 Laser ablation ICP-MS mapping of cisplatin in the cochlea

Laser ablation ICP-MS was utilized to visualize the distribution of cisplatin species within patient cochleae (Figure 3.14). With optimization of the laser ablation parameters, a resolution of 25 μm in both the x and y dimensions was achieved. Across tissue sections, platinum was detectable in all cochlear tissue, with specific regions consistently containing higher concentrations (Figure 3.14b). Platinum levels were consistently highest in the stria vascularis and in portions of the modiolus (the central axis of the cochlea), specifically at the boundary between the cochlear nerve and modiolar bone. High concentrations were also seen along the cochlear nerve fibers and along the endosteum lining the cochlear canal. Concentrations of platinum within the organ of Corti were indistinguishable from neighboring tissue, suggesting no specific retention of cisplatin within hair cells, although the resolution achieved precludes absolute determination. Ablations from untreated patients displayed no platinum signal above background (Figure 3.14c). Thus, following cisplatin chemotherapy, drug species are retained throughout the cochlea, but are most concentrated in the stria vascularis and in close proximity to the cochlear nerve. These data further point to the stria vascularis as a target of cisplatin damage.

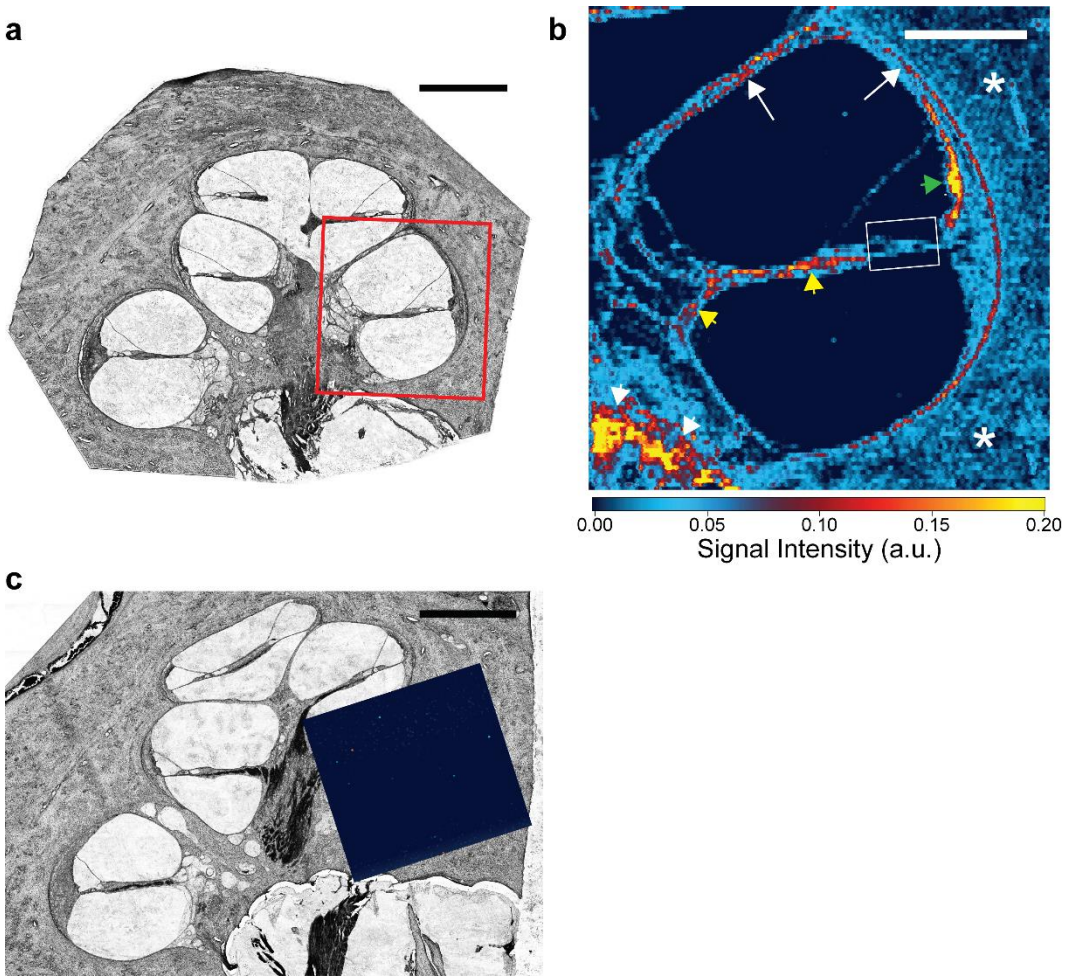


Figure 3.14: Retained cisplatin in the human cochlea visualized by laser ablation ICP-MS

Laser ablation ICP-MS was utilized to visualize the distribution of cisplatin species within human cochlear tissue sections. (a) Representative brightfield image of a cochlear section prior to ICP-MS analysis. The section was laser ablated in the region outlined in red, the results of which are presented in the following panel. Scale bar = 1mm. (b) Laser ablation ICP-MS generated heat map of platinum in cochlear tissue section. This patient died 25 days after their last cisplatin infusion. Green arrowhead marks stria vascularis, yellow arrowheads mark cochlear nerve fibers, white arrowheads mark the boundary between the cochlear nerve and the bone of the cochlear modiolus, white arrows mark the endosteum which lines the cochlear canal, asterisks mark surrounding cochlear bone, and white box frames organ of Corti. Scale bar = 500µm. Platinum signal intensity values are in arbitrary units. (c) Brightfield image of a cochlear section from a control patient with overlaid laser ablation ICP-MS results. No platinum was detected. Laser ablation results are scaled equally to those in the previous panel. a.u. = arbitrary units

3.4 DISCUSSION

The data in this chapter suggest that while largely overlooked, cisplatin pharmacokinetics may play a significant role in driving cisplatin ototoxicity. Experiments in the mouse model identified unique pharmacokinetics for cisplatin in the cochlea, and these findings were later extended to cochlear tissue from patient donors. Cisplatin species were retained in the cochleae of experimental mice and chemotherapy patients months-to-years after cisplatin chemotherapy. Though previous work has focused upon identifying the pathways responsible for cellular hypersensitivity to cisplatin within the cochlea, these results suggest that it is high exposure and not necessarily high sensitivity that may drive cisplatin ototoxicity. Cell types within the cochlea likely experience a higher total drug exposure than cell types in other tissues less susceptible to cisplatin-induced damage.

Long-term retention of active cisplatin species in the cochlea may explain the delayed progression of cisplatin-induced hearing loss which we observed in our mouse model and has been reported clinically (Kolinsky et al., 2010). These findings suggest that hearing testing should be consistently included as a component of long-term follow-up care after cisplatin chemotherapy in order to identify all patients who could benefit from hearing rehabilitation. Patients receiving only short-term audiometric testing could suffer from undiagnosed, and thus untreated, late progression of hearing loss.

Pediatric patients are most susceptible to cisplatin ototoxicity (Knight et al., 2005, Kushner et al., 2006, Li et al., 2004, Yancey et al., 2012). In this chapter, those cochlear tissue sections from the only pediatric patient donor available contained higher concentrations of platinum than those from adult counterparts, despite the patient receiving a lower total dose (per body surface area) of cisplatin. This finding suggests that differences in cisplatin pharmacokinetics between adult and pediatric

patients may explain the increased susceptibility of children to cisplatin-induced hearing loss.

The data in this chapter repeatedly point to the stria vascularis as a region of the cochlea exposed to some of the highest concentrations of cisplatin, both in experimental mice and human patients. The endocochlear potential was found to be decreased, suggestive of strial dysfunction, as has been reported previously (Klis et al., 2000, Ravi et al., 1995, Tsukasaki et al., 2000). Notably, the endocochlear potential is the first physiologic measure here found altered after cisplatin, with EPs decreased after a single cycle of cisplatin. The severity of cisplatin-induced hearing loss seems at least partially attributable to reduced endocochlear potential, and not hair cell loss alone. Consistent with this, DPOAE amplitudes were decreased even at low and middle frequencies, despite preservation of outer hair cells in those frequency regions, suggesting that the function of surviving outer hair cells was compromised. Reduced endocochlear potential would cause such an effect. When tested at the end of the cisplatin regimen (day 42), endocochlear potentials trended worse, but were not significantly depressed (Figure 3.12). There may be physiological compensation occurring at this time point (before later decompensation). Alternatively, earlier loss of endocochlear potential may be a result of a reversible pathology, while late loss is a result of a different, more permanent pathology. It should be noted that strial dysfunction is not the only possible cause of a decreased endocochlear potential, another possibility being that the scala media has become leaky, and thus allows cations to flow out (down their concentration gradient). However, this possibility seems less likely given the sealing and scarring-over of the sensory epithelium following damage that has been previously reported and described above (section 3.1).

Decreased endocochlear potential may have a more complicated relationship with cisplatin ototoxicity, being not only a result of cisplatin ototoxicity but also playing a role in propagating it. The common activated forms of cisplatin, monoaquacisplatin and diaquacisplatin, are positively charged. As the positive potential of the endolymph falls, the charge barrier for entry of these compounds into the endolymph falls. Therefore, monoaquacisplatin and diaquacisplatin may move into the endolymph more readily. Once in endolymph they have direct access to the organ of Corti, can enter hair cells via the MET channel and/or other routes, and can cause hair cell death.

Despite existing understanding that cisplatin damages multiple areas of the cochlea, experimental interventions have focused upon the hair cell alone (Kalinec et al., 2003, Karasawa and Steyger, 2015, Stawicki et al., 2015) Interestingly, minimal cisplatin was observed in the organ of Corti by ICP-MS of tissue microdissections or laser ablation ICP-MS, and no accumulation of the BODIPY FL-Cisplatin conjugate was observed there either. This finding is particularly notable when considered in comparison to the other major class of ototoxic drugs—aminoglycoside antibiotics. The aminoglycosides are preferentially retained in hair cells, which may explain why hair cells are particularly susceptible to aminoglycoside damage (Dulon et al., 1993). The data in this chapter strongly suggest against such a mechanism for cisplatin-induced hair cell loss. The loss of outer hair cells may be better explained by an inability of the outer hair cells to survive even small amounts of cisplatin. Hair cell cytotoxicity may be meditated through a DNA damage repair related pathway, a reactive oxygen species related pathway, or another not yet identified pathway. Over the long-term, some hair cell loss may result from chronic depression of the endocochlear potential, as primary deficits in the endocochlear potential have been shown to produce secondary loss of outer hair cells (Potter et al., 2016). However,

given the more acute time course here, that is unlikely to be the primary mechanism of hair cell loss in this model.

Looking beyond the auditory field, these data may have broader implications for understanding the long-term sequelae of cisplatin chemotherapy and associated toxicities. Long-term retention of high levels of platinum was observed in the long bones (femur). Long-term exposure to circulating platinum has previously been associated with a number of late toxicities of cisplatin treatment, and platinum has been detected in the blood of chemotherapy patients more than 20 years after treatment (Boer et al., 2015, Gietema et al., 2000, Hjelle et al., 2015, Sprauten et al., 2012, Tothill et al., 1992). Such long-term elevated platinum levels in the blood are likely a result of cisplatin species being re-mobilized from a tissue reservoir. Our results suggest that bone may serve as a reservoir for cisplatin species, and may thus have an important role in mediating the late toxicities of this drug in cancer survivors. In support of this idea, cisplatin has recently been demonstrated to bind extensively to type I collagen, the major protein component of bone (Chang et al., 2016).

These results point to interventions at the level of the stria vascularis as a more promising approach to preventing cisplatin ototoxicity. As the vascular tissue of the cochlea, the stria vascularis represents a likely and proposed entry point for cisplatin (Karasawa and Steyger, 2015). The analyses presented here did not have the temporal resolution to investigate the mechanism of cisplatin entry into the cochlea, but such an analysis may be possible with these same techniques and could be used to confirm the stria as the point of entry. If the cochlea avidly retains cisplatin species, the most effective and feasible methods for preventing cisplatin ototoxicity may be those which prevent the initial entry of cisplatin into cochlear tissues. The relative abundance of cisplatin-binding drugs amongst the experimental

therapies previously reported to decrease cisplatin ototoxicity further supports this. The alternative approach—therapies to improve the ability of cochlear cell types to cope with cisplatin exposure—could require those therapies to be active in the cochlea as long as cisplatin persists there, which seems challenging given the cisplatin pharmacokinetics described here.

It is unclear how cisplatin uptake into the stria and trafficking throughout the cochlea are facilitated. Transport of cisplatin species across the cell membrane is mediated by several mechanisms, both known and unknown. Two of the best characterized mechanisms are via the mammalian copper transporter 1 (CTR1) and via organic cation transporters (OCT1-3). Expression of CTR1 has been reported in hair cells, stria vascularis, and spiral ganglion, and competitive inhibition of CTR1 has been shown to reduce cisplatin ototoxicity *in vivo* (More et al., 2010). OCT2 expression has been reported in the organ of Corti and stria vascularis (Ciarimboli et al., 2010). A single nucleotide polymorphism in OCT2 confers protection against cisplatin ototoxicity to pediatric patients (Lanvers-Kaminsky et al., 2017) and OCT1/2 double knockout mice seem to have reduced ototoxicity (Ciarimboli et al., 2010). Local (cochlear) inhibition of these or other uptake mechanisms may prove an effective approach to prevention of cisplatin ototoxicity. Coupling of ICP-MS techniques to the mouse model of cisplatin ototoxicity reported in this thesis will allow for screening of such interventions.

Overall, these data provide the first direct view of cisplatin distribution in the human cochlea after cisplatin chemotherapy. They demonstrate that cochlear susceptibility to cisplatin is associated with high cumulative exposure to the drug and not simply an inherent sensitivity of cochlear cell types. Further, this work emphasizes that the field must broaden investigation beyond just hair cells if

cisplatin ototoxicity is to be successfully addressed, and it highlights techniques that should prove useful for further investigation in that vein.

3.5 OUTLOOK

The work detailed in this chapter provides a new mechanistic insight into cisplatin ototoxicity at the tissue level, but does not provide insight at the cellular level. Experiments currently in progress are designed to address this gap in current knowledge through transcriptomic approaches. Advancements in single-cell transcriptomics now allow for single-cell transcriptome analysis of dissociated cells from the adult cochlea, with some techniques capable of partitioning thousands of cells in a few minutes. Thus, comparative single-cell transcriptomics of cochlear cells from cisplatin-treated and control mice may allow for the identification of the affected cell types and the damage pathways at play.

Great potential remains for the use of ICP-MS approaches in studying cisplatin ototoxicity. Ongoing improvements in laser ablation ICP-MS in particular could allow for investigations at the single-cell or even sub-cellular level (Chang et al., 2017). These techniques may be used to investigate cisplatin trafficking within the cochlea, the mechanisms behind differing ototoxicity profiles of different platinum-based chemotherapeutics, and the increased susceptibility of the cochlear base to cisplatin, among other experimental questions.

ICP-MS also holds exciting promise as a tool for developing interventions against cisplatin ototoxicity. *In vivo* testing of candidate interventions currently requires administering a work-intensive, multi-week cisplatin regimen as detailed in Chapter 2 with auditory testing as an experimental endpoint. However, quantification of cisplatin retention in the cochlea may represent a more accessible experimental endpoint. Given the sensitivity of ICP-MS, this endpoint could be assessed after only a few doses of cisplatin, thus allowing for higher throughput screening.

The work presented in this chapter also illustrates the utility of BODIPY FL-Cisplatin, which represents an improved fluorescent cisplatin conjugate. However, this compound is not without its limitations. BODIPY FL-Cisplatin has low aqueous solubility and so its effective delivery *in vivo* requires the use of potentially toxic organic solvents and/or other vehicles. In this study, three full cycles of BODIPY FL-Cisplatin were required in order to observe obvious fluorescence signal in the cochlea, and so its utility was limited to identifying the cochlear regions with the highest accumulation of the compound and no conclusions could be made regarding the exclusion of the compound from any cell types. The most significant limitation of this compound is of course that is only a surrogate for cisplatin, and the addition of the BODIPY dye may significantly alter the behavior of the cisplatin moiety. This can only partially be controlled for by parallel use of a free BODIPY dye control. With this in mind, BODIPY FL-Cisplatin still represents an improvement over previous conjugates, as it better approximates the size and cytotoxicity of cisplatin. If the above limitations are kept in mind, its use could be very informative, especially if observations are correlated to those achieved by other approaches.

4 SENSORY HAIR CELL PROTECTION AGAINST AMINOGLYCOSIDE ANTIBIOTICS

4.1 INTRODUCTION

In contrast to cisplatin, which is known to directly damage multiple cell types in the inner ear, aminoglycoside ototoxicity is understood to be more limited in scope. The preponderance of evidence points to aminoglycoside damage primarily (though not exclusively) to hair cells of both the cochlea and vestibular organs (Xie et al., 2011). Histopathological studies of patient cochleae have demonstrated loss of hair cells progressing from base to apex and from outer hair cells to inner hair cells. Only after all hair cells are lost have degeneration of nerve fibers and supporting cells been noted (Huizing and De Groot, 1987, Johnsson et al., 1981). Similarly, hair cell loss with no loss of neurons has been observed in the vestibular organs (Tsuji et al., 2000). Studies in animal models, including the mouse, have too shown selective damage to hair cells (Wu et al., 2001).

Aminoglycosides are understood to enter hair cells by endocytic and non-endocytic pathways, in a manner that requires MET channel activity (Alharazneh et al., 2011, Hailey et al., 2017). Though aminoglycosides are rapidly cleared from the serum, they appear to persist in hair cells (Dulon et al., 1993). Once inside hair cells, aminoglycosides may negatively interact with the 12S mitochondrial ribosomal RNA subunit, interfering with mitochondrial protein translation (Qian and Guan, 2009). As aminoglycosides target the bacterial 30S ribosomal subunit (Misumi et al., 1978), cross reactivity with the mitochondrial ribosome concurs with the proposed endosymbiotic origin of mitochondria. As noted previously, mutations in mitochondrial ribosomal RNA can sensitize patients to aminoglycoside ototoxicity.

The generation of reactive oxygen species is presumed to be one of the primary mechanisms of aminoglycoside-induced hair cell death, as increased ROS and their reaction products have been observed following aminoglycoside treatment both *in vitro* and *in vivo* (Clerici et al., 1996, Jiang et al., 2005). The mechanisms of this increased ROS production remain unclear and may involve dysfunction of the mitochondrial ribosome (which translates protein complexes used in oxidative phosphorylation) and non-enzymatic formation of ROS via the Fenton reaction (Priuska and Schacht, 1995). Apart from an ROS-dependent mechanism of hair cell toxicity, aminoglycosides have also been shown to interfere with cytosolic protein synthesis and activate a signaling pathway similar to the so-called ribotoxic stress response (Francis et al., 2013). Though the exact mechanisms whereby aminoglycosides cause hair cell death are unknown, the understanding that aminoglycosides selectively damage hair cells means that investigation can appropriately focus on protective strategies for hair cells.

Prior to the start of this dissertation, work in our lab demonstrated the importance of supporting cells in determining whether hair cells live or die following exposure to aminoglycosides. On one hand, supporting cells were shown to phagocytose dying hair cells and facilitate their removal from the sensory epithelium of the adult mouse utricle following exposure to aminoglycosides (Hawkins, 1973, Bohne and Rabbitt, 1983, Forge, 1985, Leonova and Raphael, 1997, Bird et al., 2010, Monzack et al., 2015). On the other hand, supporting cells were shown able to promote hair cell survival through a heat shock protein 70-dependent mechanism (May et al., 2013). From that *in vitro* study of adult mouse utricles came several salient details. First, an *in vitro* pre-exposure to heat shock induced a stress response in the utricle which made hair cells more resistant to subsequent aminoglycoside toxicity. Second, this improvement in hair cell survival was both

dependent-upon heat shock protein 70 (HSP70) and could be replicated through overexpression of HSP70 alone. Third, HSP70 expression was induced by heat shock, but almost exclusively in supporting cells rather than hair cells. Fourth, HSP70 was released extracellularly and it was extracellular HSP70 which exerted the protective effect of heat shock, despite no evidence for its later internalization by hair cells (May et al., 2013). Further understanding of how HSP70 may act extracellularly to prevent aminoglycoside-induced hair cell death is desired, as HSP70 is central to the most fundamental cellular stress response pathway and knowledge of its action could be used to guide development of methods to prevent aminoglycoside ototoxicity and potentially hair cell loss from other forms of stress as well.

The term HSP70 is broadly used to describe what is actually a family of stress response chaperone proteins. In the mouse, the HSP70 family has at least four members, including the major constitutive form commonly referred to as HSC70 and the two most prominent inducible forms HSP70.1 and HSP70.3 (as well as inducible HSP70.2, which is restricted to spermatogenic cells). In humans, the major constitutive form is similarly referred to as HSC70, and the analogous inducible forms are HSP70-1a and HSP70-1b, respectively (Daugaard et al., 2007). However, the human HSP70 family is larger than that of the mouse, comprised of at least eight unique gene products differing from each other by amino acid sequence, expression level and sub-cellular localization (Tavaria et al., 1996). The previous work in our lab described above implicated murine inducible HSP70.1 and HSP70.3, and it is these forms which are investigated in this thesis as their expression in the utricle is much more responsive to heat shock than that of HSC70 (Nora Welsh, unpublished). However, it should be noted that amino acid sequence homology between constitutive HSC70 and inducible forms of HSP70 ranges from 84 to 87 percent and

so some techniques used, particularly antibody-based techniques, may have difficulty—at least in theory—in differentiating between constitutive and inducible.

HSP70 proteins play a central role in proteostasis under both physiologic and pathologic conditions. Their intracellular functions include folding and refolding of proteins as well as transport of proteins between cellular compartments, degradation of unstable or misfolded proteins, and uncoating of clathrin-coated vesicles (Daugaard et al., 2007). The importance of HSP70 to cellular health is underscored by the fact that it is one of the most conserved proteins in evolution (Hunt and Morimoto, 1985).

It is now well-established that HSP70 can be released from cells into the extracellular environment, however, this finding was initially met with suspicion. That is because HSP70 does not contain a consensus peptide signal for secretion via the classic ER-Golgi pathway, and inhibitors of this pathway do not block the release of HSP70 from healthy cells (Hightower and Guidon, 1989, De Maio and Vazquez, 2013). Now, secretion of HSP70 from healthy cells has been repeatedly shown to occur via incorporation of the protein into secretory vesicles, either within the lumen of the vesicles or via insertion in their membrane (Vega et al., 2008, Thery et al., 2009, Gastpar et al., 2005, Chalmin et al., 2010). The biological activity of this extracellular HSP70 is not protein chaperoning, but rather mediated through cell surface receptors, including toll-like receptors 2 and 4 (Calderwood et al., 2016, Calderwood et al., 2007). Though it should be noted that extracellular HSP70 unassociated with vesicles has also been described, it is largely understood to come from necrotic cells (Basu et al., 2000, De Maio, 2014).

We hypothesized that following heat shock of the utricle, HSP70 is released from supporting cells via exosomes—a type of extracellular vesicle (EV). Given the known capability of HSP70 to translocate into cellular membranes (Vega et al.,

2008), we hypothesized HSP70 released from supporting cells is embedded in the membrane of exosomes with the exposed portion of the protein able to then act via a cell-surface receptor on hair cells to promote their survival.

Exosomes represent a specific subset of extracellular vesicles, distinct from microvesicles and apoptotic bodies in size, content, and cellular origin. They are understood to have a unique method of biogenesis, formed initially as intraluminal vesicles (ILVs) through inward budding into an early endosome (as part of the endocytic pathway) and then later released as that resulting multivesicular body (MVB, also known as a "multivesicular endosome") fuses with the plasma membrane (Klumperman and Raposo, 2014, Johnstone et al., 1987, Raposo et al., 1996). In general, the budding of exosomes into endosomes can occur via one of two mechanisms: Endosomal Sorting Complex Required for Transport (ESCRT) machinery-dependent budding and ESCRT-independent budding (Kowal et al., 2014), though these processes may not be mutually exclusive. ESCRT-dependent budding involves four complexes. ESCRT complex-0 is responsible for cargo clustering, ESCRT-I and ESCRT-II induce bud formation, ESCRT-III drives vesicle scission, and the accessory proteins allow dissociation and recycling of the ESCRT machinery (Henne et al., 2013, Raiborg and Stenmark, 2009). ESCRT-independent budding can occur through multiple mechanisms, and can occur in cells alongside ESCRT-dependent budding (Stuffers et al., 2009). ESCRT-independent mechanisms include budding processes dependent upon ceramide (Trajkovic et al., 2008) or phospholipase D2 (Laulagnier et al., 2004). The four-transmembrane domain proteins of the tetraspanin family have also been shown to play roles in both exosomal cargo sorting and exosome secretion (van Niel et al., 2011, Perez-Hernandez et al., 2013, Andreu and Yanez-Mo, 2014). In this chapter, pharmacological inhibitors of neutral sphingomyelinase II—the enzyme which

catalyzes the production of ceramide—were used to demonstrate ceramide-dependent of exosomes from the utricle.

Following MVB formation, trafficking of the MVB to the plasma membrane and secretion of exosomes from the cell may require members of the Rab family of small GTPase proteins, including Rab27a and Rab27b (Ostrowski et al., 2010, Bobrie et al., 2012b), Rab11 (Savina et al., 2005), and Rab35 (Hsu et al., 2010). Current understanding of exosome biogenesis is schematized in Figure 4.1. It must be noted, however, that diverse and overlapping mechanisms of exosome biogenesis seem to exist across cell types and likely exist simultaneously even within a particular cell type.

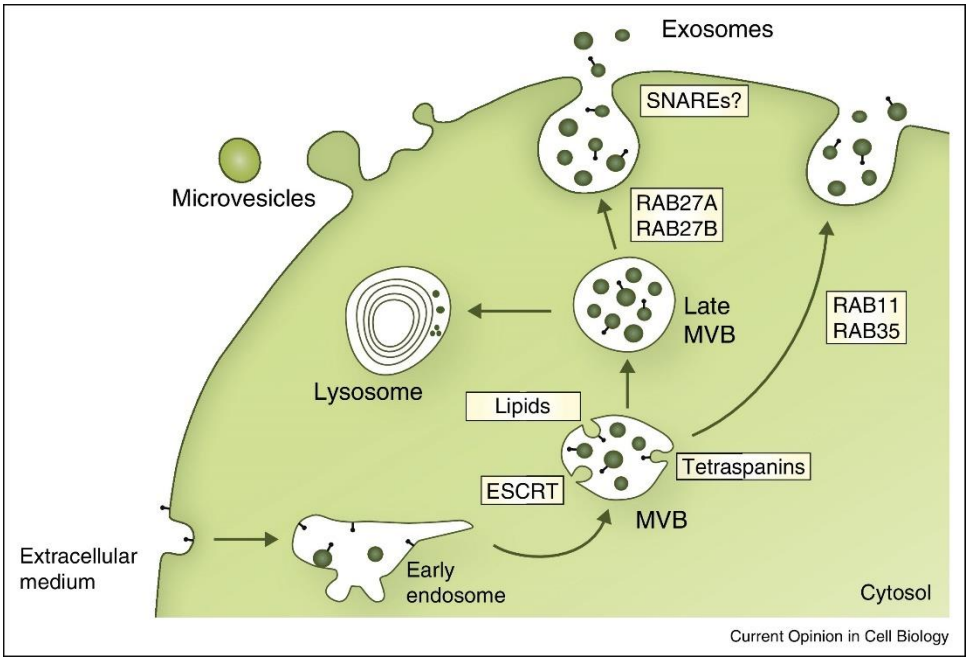


Figure 4.1: Exosome biogenesis and secretion

An overview of the current understanding of exosome biogenesis and secretion is shown. Exosomes are first formed as intraluminal vesicles by budding into early endosomes. The resulting multivesicular body (MVB) can either fuse with a lysosome and undergo degradation or fuse with the plasma membrane, releasing its intraluminal vesicles as exosomes. Molecules understood to be involved in the biogenesis of intraluminal vesicles include the ESRCT machinery, lipids such as ceramide, and tetraspanin proteins. Members of the Rab family of proteins are understood to help facilitate trafficking of MVBs to the plasma membrane and

exosome secretion. ESCRT = endosomal sorting complexes required for transport, SNARE = soluble NSF attachment protein receptor. Figure reproduced with permission from Kowal et al. (2014).

Released exosomes have a characteristic size distribution of ~40-120 nm in diameter (E. L. Andaloussi et al., 2013, Raposo and Stoorvogel, 2013). They carry a wide variety of sorted cargo, including proteins, metabolites, RNA, and lipids. In target cells, exosomal proteins can act at the surface (Chalmin et al., 2010) or intracellularly (Takeuchi et al., 2015), exosomal microRNAs can alter gene expression (Montecalvo et al., 2012, Mittelbrunn et al., 2011), and exosomal messenger RNAs can be translated into functional protein (Valadi et al., 2007).

Some of the most ubiquitous exosomal cargo proteins have been considered exosomal markers, used to classify identified vesicles as exosomes or to confirm the presence of exosomes in a sample. These include membranes of the tetraspanin protein family, primarily CD9, CD63, and CD81; tumor susceptibility gene 101 (TSG101), a member of the ESCRT-I complex, and ALG-2-interacting Protein X (ALIX), an ESCRT accessory protein; the lipid raft-associated protein flotillin-1; as well as both constitutive HSC70 and inducible HSP70 (Raposo and Stoorvogel, 2013, Kowal et al., 2016, Lee et al., 2012, Kim et al., 2013).

Indeed, HSP70 proteins are some of the most frequently identified proteins in exosomes (Kim et al., 2015), and several studies have described biological activity for exosomal HSP70. One line of investigation particularly relevant to the biology of the inner ear is examination of how exosomes from glial cell types may act upon neurons, as these interactions may be analogous to the interactions between glia-like supporting cells and the sensory receptor hair cells of the inner ear. Several reports have provided evidence for glial-derived exosomes acting upon neurons to

promote proper function under normal and stressful conditions (Lopez-Verrilli and Court, 2012, Lopez-Verrilli et al., 2013, Frohlich et al., 2014, Fruhbeis et al., 2013).

The role of glial-secreted heat shock proteins is particularly interesting because 1) glia, but not neurons, turn on stress protein synthesis following heat and other stresses (analogous to what our laboratory has seen in the utricle) and 2) the distance of neuronal axons—and thus of potential sites of axonal damage—from the neuronal cell body means that stress response proteins newly-synthesized in the cell body could take days to be transported to their site of required action, suggesting a quicker response mechanism may exist (Tytell, 2005). With this in mind, a model in which glial cells release HSP70 in exosomes in order to protect and repair neurons has been proposed (Tytell et al., 2016). In agreement with this model, astrocytes have been shown to release HSP70/HSC70 in exosomes and to upregulate this release following hyperthermia (Taylor et al., 2007) and multiple studies have shown the importance of extracellular HSP70 in promoting motor and sensory neuron survival (Robinson et al., 2005, Tidwell et al., 2004, Guzhova et al., 2001). A more recent study in *Drosophila* has shown that HSP70 can be released from one population of cells and help mediate proteostasis in a separate population of neurons (Takeuchi et al., 2015). Thus, the model of supporting cells releasing HSP70-containing exosomes which act upon hair cells to improve their stress response capability parallels current understanding in other neuronal contexts.

It should be noted that nomenclature of extracellular vesicles is an area of intense scientific discussion. Exosomes were originally defined biologically as vesicles released from the cell via MVB fusion with the plasma membrane (Johnstone et al., 1987, Raposo et al., 1996). However, more recently investigators have defined them physically as EVs whose diameter falls between 40 and 120nm or empirically as vesicles which pellet only after ultracentrifugation at 70,000-100,000

x gravity (Thery et al., 2006, Gould and Raposo, 2013). In this chapter, the term "small extracellular vesicles" or "small EVs" is used to discuss EVs which have been isolated according to protocols for the isolation of exosomes, but have not been sufficiently characterized to warrant their classification as exosomes, as per the International Society for Extracellular Vesicles recommendations (Lotvall et al., 2014). That is, the vesicles have not been characterized at the single vesicle level by multiple techniques and the presence of protein markers has not been confirmed. When small EVs have been sufficiently characterized to warrant their categorization as exosomes, they are referred to as such.

The experiments described in this chapter were designed to further our understanding of the mechanisms behind HSP70-mediated hair cell protection and how this pathway may be utilized to prevent hearing loss clinically. Evidence supporting the proposed model is presented and it is shown that exosomes purified from scalable, cell line sources can be used to prevent aminoglycoside-induced hair cell death *in vitro.* Additionally, this chapter presents technical approaches which should prove useful for the further study of exosomes/small EVs.

4.2 METHODS

4.2.1 Mice

Dissected utricles from adult mice were used as an *in vitro* model system for experiments presented in this chapter. CBA/J mice of age 4-8 weeks (Jackson Laboratory, Stock No. 000656) were used for wildtype tissue throughout. Roughly equal numbers of male and female mice were used in each individual experiment. Transgenic *ROSA26*^{mTmG} mice (Jackson Laboratory, Stock No. 007676), referred to as "mT/mG" mice from hereon, were used for visualization of extracellular vesicles. These mice carry an inserted two-color fluorescent Cre-reporter allele. tdTomato (mT) is expressed ubiquitously prior to Cre recombination, while EGFP (mG) is expressed (and tdTomato expression is discontinued) following Cre recombination. Both fluorescent proteins carry an N-terminal sequence recognized by the cellular enzyme N-myristoyltransferase, which catalyzes the covalent attachment of a myristoyl group, promoting insertion of the proteins into lipid membranes throughout the tissue. Vesicles released from mTmG mice were fluorescently labeled with tdTomato, allowing for their visualization by light microscopy techniques. For this reason, utricles from mTmG homozygous mice were used for co-culture experiments examining the transfer of vesicles between labeled and unlabeled utricles.

To differentially label vesicles derived from hair cells and supporting cells, *Gfi1*$^{Cre/+}$ mice (generated by Dr. Lin Gan, University of Rochester) were crossed to *ROSA26*$^{mTmG/mTmG}$ mice. *Gfi1*$^{Cre/+}$ mice are a knock-in strain expressing Cre recombinase in the locus for the transcriptional repressor GFI1, which is required for hair cell differentiation and survival. These mice are therefore a hair cell-specific Cre line. Resulting offspring were *Gfi1*$^{Cre/+}$; *ROSA26*$^{mTmG/+}$, and were confirmed to

express membrane localized EGFP in hair cells and membrane localized tdTomato in supporting cells by confocal microscopy (shown in Figure 4.7).

4.2.2 Utricle explant culture and aminoglycoside exposure

Explanted adult mouse utricles were used as an *in vitro* model system of inner ear hair cell and supporting cell biology. To culture utricles, mice were euthanized by CO_2 inhalation followed by decapitation. Bilateral utricles were removed and placed into culture as previously described (Cunningham, 2006, Brandon et al., 2012). In short, the complete bony labyrinth was removed by hand and placed into Medium 199 (Gibco) at 37°. Utricles were removed from the bony labyrinth under sterile conditions using micro forceps under a dissecting microscope (Carl Zeiss Microscopy, Stemi). All cultured utricles were initially transferred into complete medium consisting of DMEM/F12 basal medium with phenol red (Gibco) supplemented with 5% heat-inactivated FBS (Gibco) and 50 units/mL of Penicillin G (Sigma-Aldrich) and were cultured free-floating overnight in 1mL of this complete medium in a 24-well tissue culture plate prior to any experimental intervention. The incubator was maintained at 37°C and 5% CO_2.

As FBS is known to contain large amounts of extracellular vesicles, experiments in which EVs in the culture medium were to be isolated and/or analyzed were performed in serum-free culture medium consisting of DMEM/F12 basal medium with phenol red (Gibco) supplemented with 50 units/mL of Penicillin G (Sigma-Aldrich). For confocal imaging of EVs in solution, medium without phenol red was used.

The aminoglycoside neomycin was used as a representative ototoxic aminoglycoside throughout. Utricles were treated with neomycin *in vitro* in order to induce hair cell loss and thus model ototoxicity. For neomycin exposure, stock

neomycin sulfate in aqueous solution at a concentration of 140 mg/mL (VetOne) was added to culture medium to achieve a final concentration of 3 mM. Neomycin-containing medium was equilibrated in the incubator for at least two hours prior to use.

4.2.3 Utricle heat shock

Heat stress has previously been shown to induce hair cell protection against subsequent exposure to ototoxic drugs. Here the role of extracellular vesicles in mediating this protective effect was investigated *in vitro*. To heat shock utricles, utricles and their culture medium were transferred from the culture plate to sterile microcentrifuge tubes using a sterile Pasteur pipette. Microcentrifuge tubes containing utricles to be heat shocked were placed into a 43°C water bath for 30 minutes, while tubes containing control (no heat shock) utricles were placed in the incubator at 37°C for 30 minutes. At the end of the incubation, all utricles were immediately transferred back to the tissue culture plate and returned to the incubator under standard culture conditions. Utricles were allowed to recover in their complete medium for two hours prior to change to serum-free medium (for extracellular vesicle analyses) and/or drug-containing medium (for aminoglycoside exposure or application of inhibitors).

4.2.4 Nanoparticle tracking analysis (NTA)

Nanoparticle tracking analysis (Figure 4.2) was used to measure the concentration and size distribution of extracellular vesicles in samples derived from utricles or cells in culture. To analyze the total population of EVs released from heat-shocked and control utricles, conditioned medium was removed from utricles in culture and spun at 2,000 x gravity for 10 minutes to pellet tissue and cellular debris. The remaining supernatant was drawn off and used for analysis.

For cell lines, conditioned medium was removed and filtered through a 33mm diameter, 0.22µm pore size, hydrophilic polyvinylidene fluoride membrane syringe filter (Millipore Sigma, Millex) in order to remove cellular debris and large vesicles. This filtered, conditioned medium was either analyzed directly or further purified as described in section 4.2.8 below.

Nanoparticle tracking analysis of extracellular vesicles in aqueous solution was performed on a NanoSight NS300 running NTA software version 3.1 (Malvern Instruments). Between 500 µL and 1mL of sample was pushed through the system fluidics. Light from a 488 nm wavelength laser was scattered off vesicles undergoing Brownian motion, and particle motion was recorded at 30 frames per second. Three or five recordings of length 30 or 60 seconds each were made for each sample. The camera level was set at 15 for the video capture, and the detection threshold was set at 3 for particle detection and analysis. Samples at high starting concentrations (>10^9 vesicles per mL, as suggested by an initial NTA attempt) were diluted in additional buffer or culture medium (whichever the original sample was suspended in) to bring them into the accurately measurable range. Correction for this dilution was performed within the NTA software.

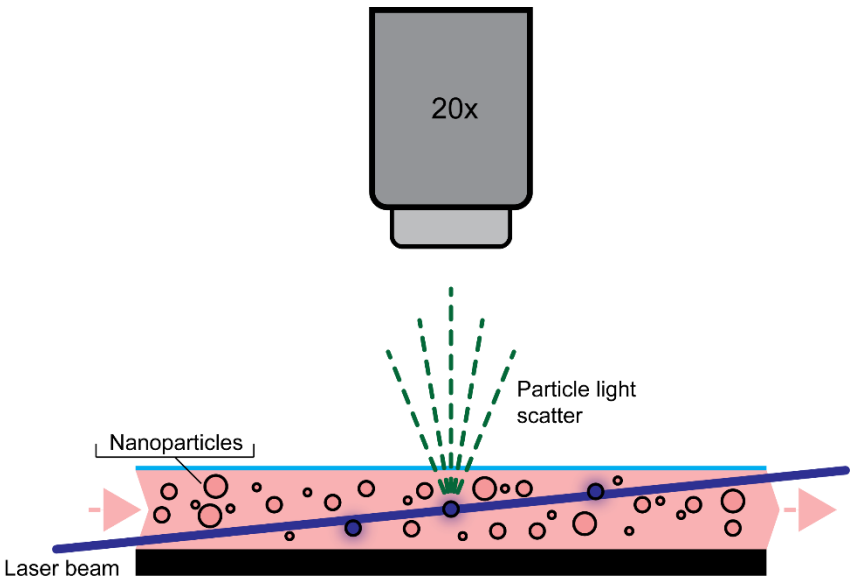


Figure 4.2: Nanoparticle tracking analysis

Nanoparticle tracking analysis (NTA) is a technique for analyzing nanoscale-sized particles—including extracellular vesicles—on the single particle level. Light scatter is used to visualize the location of vesicles smaller than the limits of light microscopy resolution. The principles of Brownian motion are used to calculate the size of each vesicle based upon the speed of its random movement. Vesicles are illuminated by an angled laser beam passed through a narrow flow channel of sample. The resulting light scatter is magnified by a 20x microscope objective and the simultaneous movement of all illuminated vesicles is recorded by a high frame rate video camera. The NTA software then is used to analyze the recorded video. The size of each visualized particle is calculated from its rate of Brownian motion using the Stokes-Einstein equation, factoring in the temperature and viscosity of the sample. The number of visualized vesicles per frame is used to calculate the concentration of vesicles in the sample.

4.2.5 Pharmacologic inhibition of exosome production

Utricles were treated with one of two drugs to inhibit the formation of exosomes, and thus probe their biological significance. Both drugs, spiroepoxide and GW4869, are inhibitors of the enzyme neutral sphingomyelinase II. Neutral sphingomyelinase II catalyzes the production of ceramide, which has been proposed to be necessary for exosome production in some systems. Spiroepoxide (Santa Cruz Biotechnology) was dissolved in dimethyl sulfoxide (DMSO) to prepare a stock solution of concentration 0.01 g/mL. This stock solution was added to culture medium via serial dilution to achieve a final concentration of 0.375 μM. GW4869 (Sigma-Aldrich) was dissolved in DMSO to prepare a stock solution of concentration 0.2 mg/mL. Stock was added to culture medium to achieve a final concentration of 0.5 μM. All drug treatments were performed for 24 hours. When utricles were exposed to both neomycin and spiroepoxide, both drugs were added to the culture medium and exposure was performed simultaneously.

4.2.6 Utricle co-culture

Populations of utricles were co-cultured such that they were physically separated but could share culture medium. This culture setup was utilized to

investigate the transfer of extracellular vesicles from one population of (labeled) utricles to another (unlabeled) population. Co-culture experiments were performed in a 24-well tissue culture plate format using basket co-culture devices with a semi-permeable polyethylene terephthalate membrane with 0.4μm pore size (Corning, Transwell). Utricles from mTmG mice (or wildtype CBA/J mice for negative controls) were cultured in the basket and utricles from CBA/J mice were cultured in the well below. Before initiation of co-culture, 600μL of medium was added to the well and 100μL of medium was added to the co-culture basket, and the two chambers were allowed to equilibrate for at least 1 hour in the culture incubator. Utricles were added to both compartments, 12 mTmG utricles in the basket and 6-12 CBA/J utricles in the well, and were co-cultured in this way for incubation times ranging from 30 minutes to 24 hours. Both Airyscan confocal microscopy (section 4.2.9) and immunoelectron microscopy (section 4.2.12) were used to look for transferred EVs in recipient co-cultured utricles.

4.2.7 Cell culture

Cell culture was employed for three separate applications in this chapter. First, HEI-OC1 cells were used to produce EV-containing conditioned medium used in the validation of the ultracentrifugation and size-exclusion chromatography methods of small EV isolation. Second, HEK 293T cells stably expressing the mTmG construct and (untransfected) Huh7 cells were used to validate the mTmG method for labeling and imaging EV transfer between cells. Finally, CT26, HEI-OC1, C8-D1A, and C8-B4 cells were used to produce small EVs, and the ability of those small EVs to protect utricle hair cells against neomycin ototoxicity was investigated.

Huh7 human hepatocellular carcinoma cells (Nakabayashi et al., 1982), HEK 293T cells (American Type Culture Collection, CRL-3216) stably expressing the mTmG transgene (a gift from Liqun Luo, Addgene plasmid # 26123), C8-D1A cells

(American Type Culture Collection, CRL-2541), and C8-B4 cells (American Type Culture Collection, CRL-2540) were cultured in DMEM basal medium (Gibco) supplemented with 10% heat inactivated FBS and antibiotic-antimycotic (Gibco; 100U/mL penicillin, 100ug/mL streptomycin, 250ng/mL amphotericin B). HEI-OC1 cells (Kalinec et al., 2003) were cultured in DMEM supplemented with 10% heat inactivated FBS, 50 U/mL interferon gamma (Sigma-Aldrich), and 100 U/mL penicillin (Sigma-Aldrich). CT26 cells were cultured in RPMI basal medium (Gibco) supplemented with 10% heat inactivated FBS and antibiotic-antimycotic. Cells were maintained at 37° and 5% CO_2 in a humidified incubator, with the exception of HEI-OC1 cells which were maintained at 33° and 10% CO_2. Passaging was performed using TrypLE™ Express (Gibco) reagent—a recombinant protease solution—at 1x concentration.

For collection of small EVs from cell lines, cells at 70-80% confluence were first rinsed with, and then changed to Opti-MEM medium (Gibco) without any serum supplementation. Cells were cultured in Opti-MEM for 24 hours in order to condition the medium, and conditioned medium was then drawn off and processed for downstream applications. Cells were kept at low passage number and were visualized at least once daily under an inverted light microscope (Carl Zeiss Microscopy) to check for any changes in cell viability or morphology.

4.2.8 Extracellular vesicle isolation

Small EVs for study were purified from conditioned medium via one of two approaches: ultracentrifugation or size-exclusion chromatography. In general, the ultracentrifugation method provided higher yield, and the size-exclusion chromatography method provided higher sample purity. The choice of either technique for a particular application was based upon these specific advantages.

Small EVs were isolated from utricle conditioned culture medium using an abbreviated version of the differential ultracentrifugation isolation protocol described by Thery et al. (2006), and traditionally considered the "gold standard" for exosome purification (Lobb et al., 2015). Conditioned medium (1 mL) was first spun at 300 x g for 10 minutes to pellet cells and other very large debris, the resulting supernatant was then spun at 10,000 x g for 30 minutes to pellet large vesicles and other cell debris. Both spins were performed in a refrigerated microcentrifuge (Eppendorf). The supernatant from that spin was then spun at 100,000 x g for 70 minutes in order to pellet small EVs. Polycarbonate sample tubes (Beckman Coulter, 3.5 mL capacity), a TLA-100.3 rotor (Beckman Coulter), and an Optima MAX-XP (Beckman Coulter) tabletop ultracentrifuge were used. All spins were performed at 4° C. Pelleted EVs were re-suspended in buffer or medium by tituration with a micropipette (~100 repetitions).

Small EVs were isolated from cell line conditioned culture media either via differential ultracentrifugation as described above (for results shown in Figure 4.15b) or via a different ultrafiltration and size-exclusion chromatography (SEC) based method (for results shown in Figure 4.15a). In the size-exclusion chromatography method, conditioned medium was first filtered through 0.22 μm pore size, hydrophilic polyvinylidene fluoride membrane syringe filter (Millipore Sigma, Millex) in order to remove cellular debris and large vesicles. Vesicles in the sample were then concentrated on a 100 kDa molecular weight cut-off (MWCO) centrifugation-based ultrafiltration device (Millipore Sigma, Amicon) via centrifugation at 3,000 x g. Concentrated sample of ~500 μL volume was then injected onto a 24 mL bed volume Superose 6 Increase (GE Healthcare Life Sciences) size-exclusion chromatography column using an ÄKTA pure 25 L liquid chromatograph system (GE Healthcare Life Sciences) kept at 4° C. The column was

equilibrated with PBS at pH 7.4, and a constant flow rate of 0.5 mL/min was maintained. UV absorbance at 280 nm was continuously recorded. Eluted sample fractions were collected every 1 mL for column volumes 0-1 and every 2 mL for column volumes 1-1.5. Small EV-containing fractions were determined via the UV chromatograph and NTA analysis of each fraction as shown in Figure 4.12. EVs in these fractions were then re-concentrated on a 3 kDa molecular weight cut-off (MWCO) centrifugation-based ultrafiltration device (Millipore Sigma, Amicon), before NTA analysis and use *in vitro*.

4.2.9 Immunohistochemistry and confocal microscopy

Utricles were imaged by confocal microscopy to assess hair cell survival, confirm fluorescent reporter expression, or visualize internalized EVs. Utricles to be imaged were fixed in 4% paraformaldehyde (PFA) in PBS for 30 minutes at room temperature. Blocking and staining were then carried out as described for cochlear tissue in section 2.2.4 above. Stained utricles were mounted in Fluoromount-G (Southern Biotech) using imaging spacers (Secure-Seal™, Grace Bio-Labs) to prevent tissue compression and flattening of the hair cell stereocilia. Mounted utricles were imaged on an LSM 780 laser scanning confocal microscope (Carl Zeiss Microscopy) additionally equipped with an Airyscan superresolution detector. For most confocal imaging, the standard confocal detector was used. In all cases, experimental and control samples were imaged under identical acquisition settings, including laser line attenuation and detector gain. Processing was applied equally and across the entire image to all images used for comparison.

To count surviving hair cells in collected z-stacks, manual cell counts were performed within five 2500μM^2 or 900μM^2 regions of interest (ROIs) within the extrastriolar region of each utricle. Individual counts were averaged to produce a single average hair cell density per utricle.

When utricles were imaged to visualize internalized EVs, imaging was performed using the Airyscan superresolution detector. In these cases, the Airyscan detector was chosen for its improved signal-to-noise and resolution capability (which come at the expense of decreased imaging and processing speed as well as challengingly large file sizes). The Airyscan detector captures the entire Airy pattern produced by focused light emitted from the sample through an extended concentric detector array. In a traditional scanning confocal microscope, the light outside the central Airy disk (the rest of the Airy pattern) is rejected at the pinhole and therefore not detected, leading to tradeoffs in sensitivity and resolution. The increased signal captured on the extended Airyscan detector array, however, can then be reassigned to its correct spatial position, achieving improved signal-to-noise ratio and a theoretical resolution improvement of up to 1.7x (Sheppard et al., 2013).

4.2.10 HSP70 ELISA

A high-sensitivity enzyme-linked immunosorbent assay (ELISA) kit (Enzo Life Sciences) was used to investigate HSP70 expression in utricles and their conditioned media (and fractions thereof). This kit (product # ADI-EKS-715) is independently reported to have high specificity for inducible HSP70 with negligible reactivity against constitutive HSC70 (Multhoff and Hightower, 2011). Four utricles were cultured under control conditions, and 40 utricles were heat-shocked. Conditioned medium from the heat-shocked utricles (1 mL) was spun at 2,000 x g for 10 minutes to pellet tissue and cellular debris. The remaining supernatant was split into two 500 µL fractions. One fraction was supplemented with Triton X-100 (Sigma-Aldrich) at a final concentration of 0.1% (v/v) and then analyzed (the "conditioned medium" sample), and the other fraction underwent differential ultracentrifugation. The supernatant of the 100,000 x g spin was similarly supplemented with Triton X-100 and analyzed (the "supernatant" sample) and the

EV pellet was resuspended in culture medium, supplemented with Triton X-100 and then analyzed (the "pellet" sample). Four utricles each from control and heat shock culture were Dounce homogenized in kit assay buffer and also analyzed. The ELISA was performed according to the manufacturer's instructions. Absorbance measurements at 450 nm with correction at 540 nm were taken on a microplate reader (Berthold Technologies Mithras, LB 940). Sample values were calculated from a recombinant HSP70 standard curve with curve fitting and interpolation performed in GraphPad Prism 6 software.

4.2.11 Confocal imaging of vesicles released from *Gfi1*$^{Cre/+}$; *ROSA26*$^{mTmG/+}$ utricles

Utricles from *Gfi1*$^{Cre/+}$; *ROSA26*$^{mTmG/+}$ mice had differentially labeled hair cells and supporting cells. As both reporters were membrane-associated, they incorporated into EVs and the cell type of origin of a particular EV could be determined by the particular reporter present on the EV. In order to determine the relative abundance of hair cell and supporting cell-produced EVs, a laser scanning confocal microscope was used to image conditioned medium from these heat-shocked *Gfi1*$^{Cre/+}$; *ROSA26*$^{mTmG/+}$ utricles.

Following heat shock and a two-hour recovery, 8-10 utricles (for each biological replicate) from *Gfi1*$^{Cre/+}$; *ROSA26*$^{mTmG/+}$ mice were transferred to 100 µL of phenol red-free, serum-free medium. Conditioned medium was collected 24 hours later and spun at 2,000 x g for 10 minutes. The supernatant was then taken forward to imaging. A 50 µL droplet of sample was placed inside a 35 mm glass coverslip-bottomed culture dish (MatTek) and covered to prevent evaporation. The liquid sample was imaged under 63x magnification on a laser scanning confocal microscope (Carl Zeiss Microscopy, LSM780). The objective was first focused at the

coverslip-sample interface and the focal point was then advanced 200 μm further into the sample. Imaging parameters were optimized to achieve sufficient signal-to-noise ratio while maintaining an imaging speed fast enough to freeze vesicle motion and were as follows: per pixel scaling of 0.26 μm x 0.26 μm at a resolution of 512 x 512, frame averaging of 2, pixel time of 1.27 μs, and frame time of 0.78 μs. 1000 frames were collected in a continuous time series, and one channel was imaged at a time. Excitation laser intensities were adjusted to produce equal count rates in blank medium. Time series were post-processed in ImageJ2 and analyzed manually to count the number of visualized vesicles in each channel.

4.2.12 Transmission electron microscopy (TEM)

Transmission electron microscopy was used to characterize the utricle following heat shock, including examination for the presence of multivesicular bodies. Transmission electron microscopy was performed according to a previously published protocol (Szarama et al., 2013, May-Simera et al., 2015). Control and heat-shocked utricles and ultracentrifugation-pelleted small EVs were fixed in 2% paraformaldehyde and 2.5% glutaraldehyde in 0.1 M phosphate buffer (pH 7.4) for 30 minutes at room temperature followed by 2 hours at 4°C. Samples were washed with phosphate buffer, and then transferred to Dr. Ronald Petralia and Dr. Ya-Xian Wang who performed subsequent steps. Samples were post-fixed with 1% osmium tetroxide, dehydrated through a graded alcohol series and stained with 1% uranyl acetate in 50% ethanol. Tissue was embedded in Poly/BED 812 resin (Polysciences Inc.). Thin sections were cut with a ultramicrotome (Leica), stained with lead citrate, and mounted on mesh grids.

Immunoelectron microscopy was used to follow labeled EVs and was performed according to methods previously published in great detail (Zhang et al., 2016). Briefly, co-cultured utricles and controls were fixed in 4% paraformaldehyde

and 0.5% glutaraldehyde in 0.1 M phosphate buffer and then cryoprotected in graded glycerol with a final concentration of 30%. Utricles were plunge-frozen in liquid propane at -184°C in a Leica EM CPC freezing instrument. Freeze substitution embedding in Lowicryl HM-20 resin was performed at low temperature using a Leica AFS freeze substitution instrument. Following freeze substitution, samples were transferred to Dr. Ronald Petralia and Dr. Ya-Xian Wang who performed subsequent steps. Thin sections (70 nm) were cut with a ultramicrotome (Leica), collected on grids, and blocked with a solution of 0.1% saponin (Sigma-Aldrich) and 2% BSA (Sigma-Aldrich). Sections were stained with a primary antibody against red fluorescent protein (Rockland Immunochemicals, rabbit polyclonal) at a dilution of 1:25 followed by a 10 nm-gold conjugated secondary antibody, before staining with uranyl acetate and lead citrate.

Images were collected using a JEM-1010 transmission electron microscope (JEOL) equipped with a Hamamatsu camera, using software from Advanced Microscopy Techniques. Post-acquisition processing was performed in ImageJ2.

4.2.13 Quantitative tandem mass spectrometry

Quantitative tandem mass spectrometry was used to investigate the protein content of small EVs released from utricles. Utricle-derived EVs destined for proteomic analysis were purified via the size-exclusion chromatography-based method described above. Samples were flash-frozen in liquid nitrogen and stored at -80° C until further processing. Frozen samples were transferred to Dr. D. Eric Anderson, who performed the sample processing and data collection steps detailed immediately below. I performed all data analysis.

Nine volumes of 1% sodium laurate (Lin et al., 2013) and an aliquot of a control protein (200 fmol of ovalbumin) was added to each sample, and the samples

were then heated to 90° C for 30 minutes. Next, 1/10th volume of 100 mM dithiothreitol (DTT) was added and the sample incubated at 50° C for 20 minutes with agitation. After cooling to room temperature, 1.5 times the DTT addition volume of 200mM chloroacetamide was added, the sample mixed, and allowed to sit in a dark drawer for one hour. The same volume of 200mM beta-mercaptoethanol was then added, the sample mixed, and allowed to sit a further 15 minutes in the dark. The samples were diluted to bring the concentration of sodium laurate to 0.1% and trypsin was added a ratio of 20:1 estimated sample:trypsin protein mass. Samples were allowed to sit at room temperature overnight. After acidification to ~pH 2 with trifluoroacetic acid, the auric acid was removed by washing 3 times with ethyl acetate. The resulting aqueous phase of each sample was transferred to a new container. 200uL of 0.5% formic acid was then added to the original container to recover residual aqueous phase and combined with the solution in the new container. These samples were then exposed to a stream of dry nitrogen while being held at 50° C to blow off residual ethyl acetate and reduce volumes.

Samples were applied to in-house manufactured reversed phase STAGE tips. The tips were washed and then a solution of formaldehyde and sodium cyanoborohydride was applied as described by Boersema et al. (2009) “protocol C”. After washing, the samples were eluted and combined and next applied to a 10 core SCX-STAGE column which was used to create a six fraction SCX separation as described by Kulak et al. (2014). Six LC/MS/MS data sets were then collected using a NanoAcquity UHPLC system (vented configuration using a 180 µm by 2 cm Symmetry C18-5 pre-column and 75 µm by 25 cm BEH130 C18 analytical column). Gradient points were 1% (start), 25% (538 minutes), 80% (558 minutes), 5 minute hold, and then down to 1% (580 minutes).

A Q Exactive instrument (Thermo Fisher) was operated in data-dependent acquisition mode with a top30 program with 3 co-added spectra used in MS1. Data were analyzed using default settings in MaxQuant software version 1.5.8.3, as described by Cox and Mann (2008) with matching to a *Mus musculus* Ensembl 87 database and to common contaminants. Gene Ontology term enrichment analysis was performed using STRING version 10.5 (Szklarczyk et al., 2015).

4.2.14 Cell line protection experiments

The ability of EVs from cell lines to protect utricular hair cells against aminoglycosides was investigated. Small EVs were purified from cells in culture as detailed in sections 4.2.7and 4.2.8 above. Purified vesicle samples were analyzed by NTA to determine the concentration of vesicles in each. The volume of sample calculated to contain 2.5 x 10^9 vesicles was used for each cell line. This sample was added to equilibrated, neomycin-containing culture media. Utricles were transferred to these media and incubated for 24 hours before fixation and quantification of surviving hair cells as detailed in section 4.2.9.

4.2.15 Statistics

As described in section 2.2.5 above.

4.3 RESULTS

4.3.1 Release of vesicles from the utricle following heat shock

Heat shock of the utricle is known to induce hair cell protection against aminoglycoside-induced death, and this protection is known to be paracrine in nature. With this in mind, the association between utricle heat shock and extracellular vesicle release was first investigated (Figure 4.3). Control utricles cultured in serum-free medium at 37° C for 24 hours released a basal population of vesicles into the surrounding culture medium, measurable by nanoparticle tracking analysis. Most vesicles were in the 50-150nm size range. When the same number of utricles was heat-shocked for 30 minutes at 43° C two hours prior to a 24-hour incubation in serum-free medium, they released ~2.5 times as many vesicles. This induction of vesicle release was largely specific to vesicles in the 50-100nm size range. Transmission electron microscopy performed on ultracentrifugation (UC) pelleted EVs from heat-shocked utricles demonstrated numerous lipid bilayer-bounded vesicles which were around 100 nm in diameter. These results demonstrate that extracellular vesicle release is a component of the utricle response to heat shock and that the released vesicles are in the size range of exosomes or other “small EVs”.

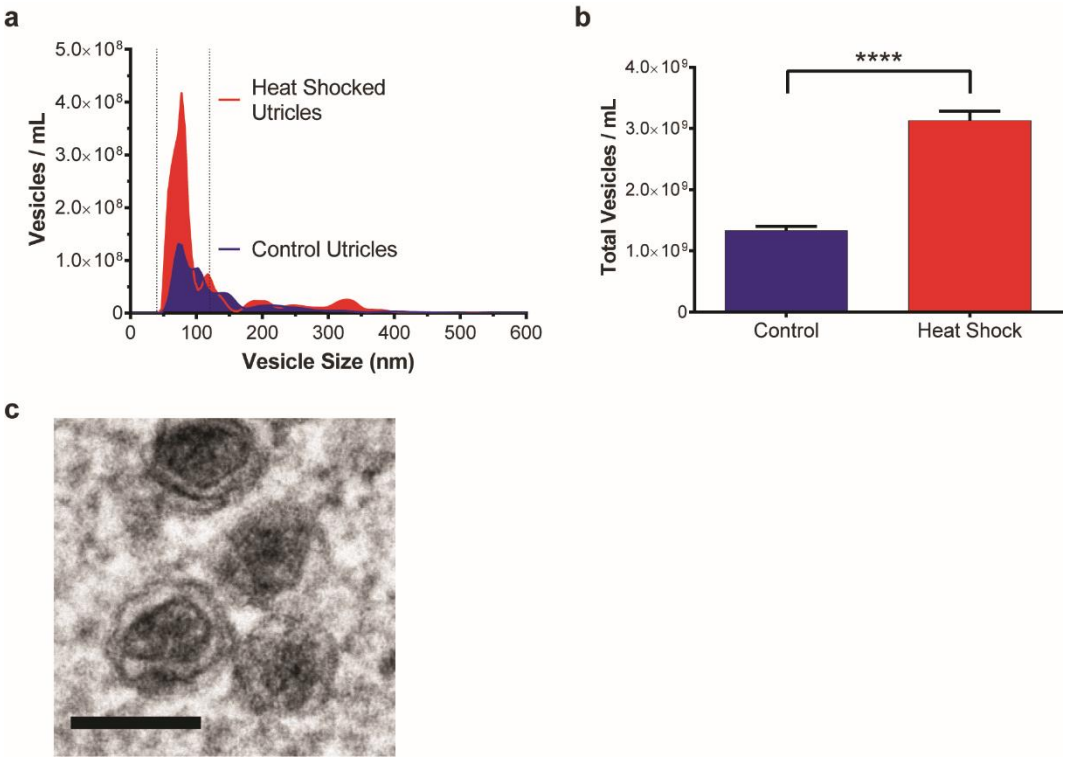


Figure 4.3: Induction of extracellular vesicle release from the utricle following heat shock

Nanoparticle tracking analysis and transmission electron microscopy were used to quantify and visualize vesicles released from control and heat-shocked utricles. (a-b) Nanoparticle tracking analysis of 24 hour conditioned culture medium from control and heat-shocked utricles. (a) In both groups, extracellular vesicles ranged in size from ~50nm to ~400nm with most vesicles falling in the 50-150nm size range. (b) In total, heat-shocked utricles released about 2.5 times as many vesicles. Both samples were centrifuged at a speed only sufficient to clear (i.e. pellet) dead cells prior to analysis, thus these measurements represent the total population of vesicles released from the utricles. Mean ± s.e.m. are shown. An unpaired two-tailed t-test was used to determine significance. ****$P < 0.0001$ (c) TEM image of vesicles pelleted via differential ultracentrifugation from the conditioned medium of heat-shocked utricles. Visualized vesicles have the characteristic size and cup-shaped morphology of previously reported exosomes. Scale bar = 100 nm.

4.3.2 Pharmacological inhibition of vesicle release

The sphingolipid ceramide has been shown to trigger the budding of some exosomes into the lumen of multivesicular bodies, and can thus be necessary for exosome biogenesis (Trajkovic et al., 2008). The role of ceramide in vesicle release from the utricle was investigated using two pharmacologic inhibitors of neutral

sphingomyelinase II (Figure 4.4). Neutral sphingomyelinase II (N-SMase II) is a hydrolase which facilitates the breakdown of sphingomyelin into phosphocholine and ceramide. It is irreversibly inhibited by spiroepoxide (Arenz and Giannis, 2000) and reversibly, non-competitively inhibited by GW4869 (Luberto et al., 2002). When heat-shocked utricles were incubated in either inhibitor, they released significantly fewer vesicles than when incubated in vehicle (DMSO) alone. These results suggest that the vesicles released from heat-shocked utricles are generated via a ceramide-dependent pathway and are thus similar to some previously-described exosomes.

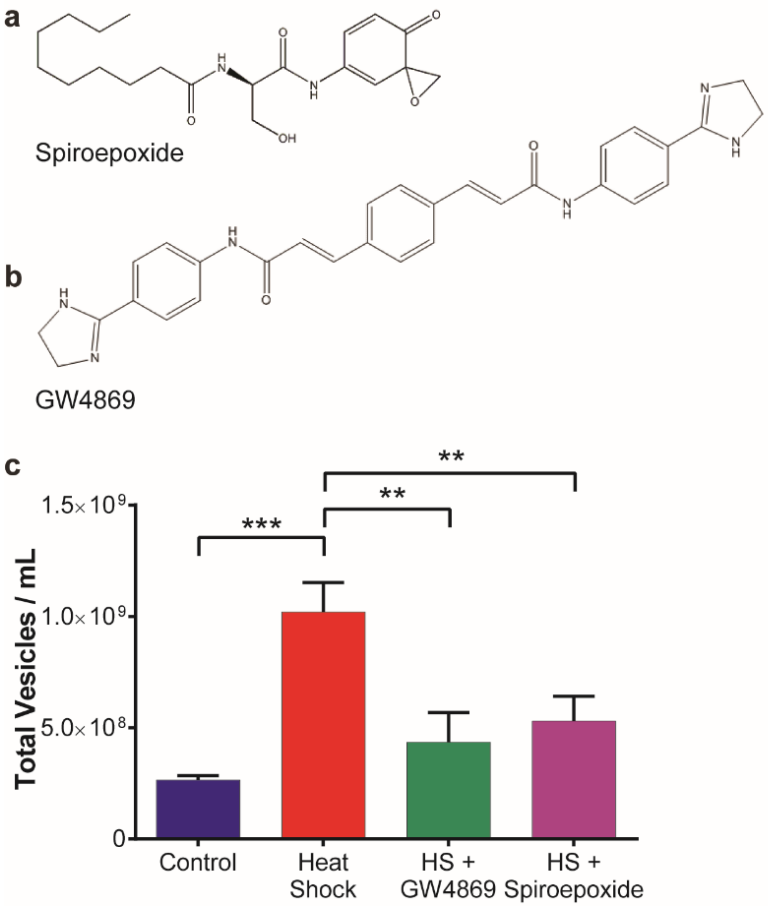


Figure 4.4: Pharmacological inhibition of exosome biogenesis

Nanoparticle tracking analysis was used to quantify total extracellular vesicles released over 24 hours from utricles in culture. Experimental utricles were heat shocked and then recovered in normal medium or medium containing one of two N-

SMase-II inhibitors. (a) Spiroepoxide is an irreversible inhibitor of neutral sphingomyelinase II. (b) GW4869 is a non-competitive, reversible inhibitor. (c) Total quantity of EVs released from control utricles, heat-shocked utricles treated with vehicle alone, and heat-shocked utricles treated with either of two N-SMase II inhibitors. Treatment of utricles with either GW4869 at a concentration of 0.375 μM or spiroepoxide at a concentration of 0.5 μM significantly blunted the increase in extracellular vesicle release induced by heat shock. HS = heat shock. Mean ± s.e.m. are shown. One-way ANOVA followed by the Holm-Šidák multiple comparisons test was used to determine significance. **P < 0.01, ***P < 0.001

4.3.3 The protective effect of heat shock requires extracellular vesicles

With an association between heat shock and vesicle release established, it was next examined whether vesicle release is necessary for heat stress to induce protection of sensory hair cells. Spiroepoxide was first demonstrated to not induce hair cell toxicity when combined with the stress of heat shock (Figure 4.5a). In a separate experiment, hair cell death was induced through culture in neomycin, an ototoxic aminoglycoside, and surviving hair cells were quantified (Figure 4.5b). After 24 hours, utricles in neomycin-containing medium had significantly fewer surviving hair cells than controls. As previously reported, this hair cell loss could be significantly prevented through pre-exposure of utricles to heat stress (30 minutes at 43° C). However, the addition of spiroepoxide to the culture medium abolished any hair cell protection otherwise mediated by heat shock, suggesting that heat shock mediates protection of hair cells via an exosome-dependent mechanism.

To test the biological activity of vesicles, a method for isolating extracellular vesicles from conditioned media was first validated. Tests of multiple ultrafiltration formats repeatedly demonstrated a high loss of vesicle yield from vesicles adherent-to or trapped-within the filtration membrane (data not shown), and so a differential ultracentrifugation-based approach was adopted. When conditioned medium was pelleted by differential ultracentrifugation, 68% of vesicles (as measured in un-processed conditioned medium) were recovered in the pellet after a 1 hour spin at

100,000 g (Figure 4.5c). Additionally, only 10% of recovered vesicles remained in the supernatant. Both the total recovery of vesicles, and relative enrichment in the pellet versus the supernatant only increased slightly with longer spin durations. Given these results, conditioned medium was then collected from heat-shocked utricles and small EVs were isolated via ultracentrifugation with a 1 hour final spin. When these isolated vesicles were added to utricles in neomycin-containing culture medium, hair cell survival was significantly improved (Figure 4.5d), an effect not seen when supernatant was added. Therefore, small EVs from heat-shocked utricles are sufficient to mediate the hair cell protection of heat shock.

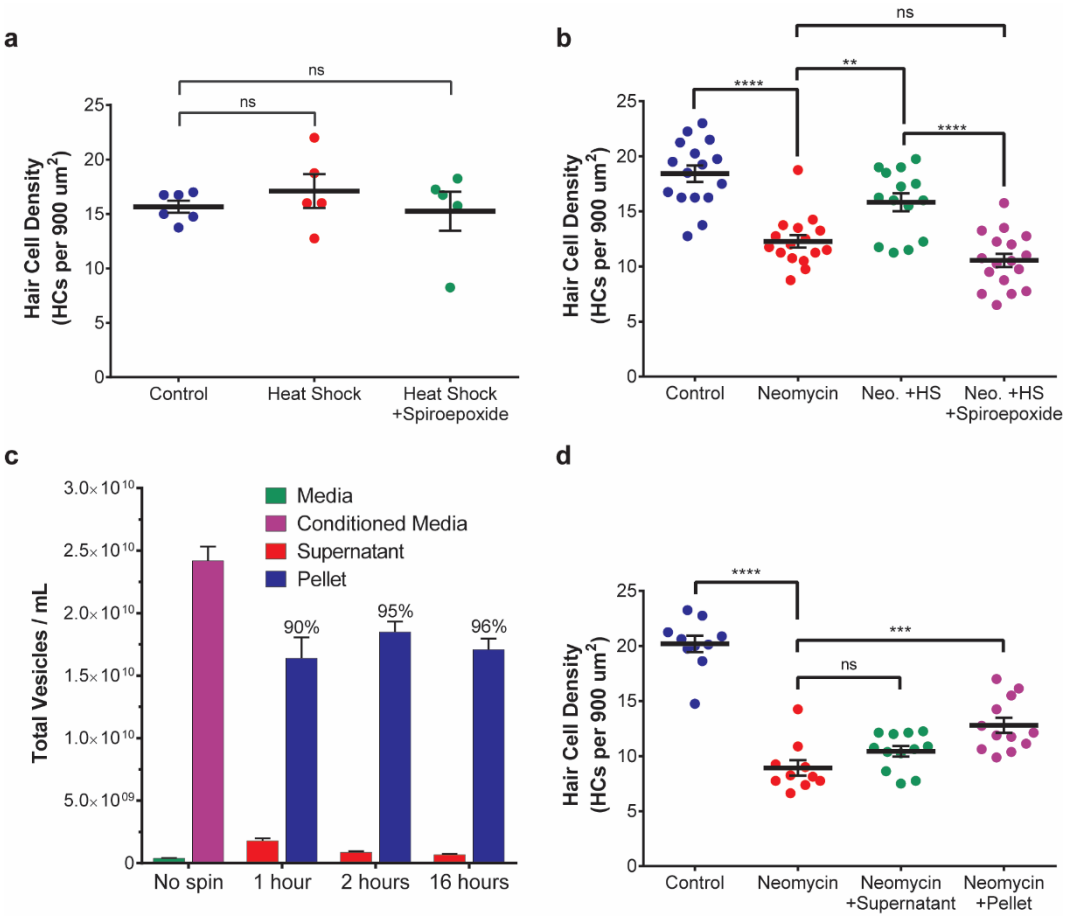


Figure 4.5: Importance of extracellular vesicles in mediating heat shock-induced protection of hair cells

Utricles were dissected from mixed gender CBA/J mice at 4-8 weeks of age. Utricle hair cell survival after *in vitro* treatment was assessed by manual quantification of remaining myosin VIIa positive cells in confocal microscopy images. (a) Utricles from mixed-gender CBA/J mice at 4-8 weeks of age were cultured under control and heat shock conditions. Addition of spiroepoxide to the culture medium did not cause hair cell death, even when given in combination with heat stress. Unpaired two-tailed t-tests were used to determine significance. (b) Utricles were cultured in neomycin for 24 hours to induce hair cell loss. If utricles were heat-shocked prior to neomycin exposure, hair cell survival was increased. However, treatment of heat-shocked utricles with 0.5 μM spiroepoxide significantly abolished any protection mediated by heat shock. One-way ANOVA followed by the Holm-Šidák multiple comparisons test was used to determine significance. (c) The pelleting efficiency of differential ultracentrifugation was examined using conditioned medium from HEI-OC1 cells. 1mL of conditioned medium (the same volume as typically derived from utricles in culture) was 0.22 μm filtered and then was either directly analyzed by NTA or spun at 100,000 g for 1, 2, or 16 hours. Resulting pellets were resuspended back into 1mL of serum-free culture medium and analyzed alongside their respective supernatant. Percentages denote the percentage of total vesicles (pellet + supernatant) measured in the pellet alone. (d) Small vesicles were pelleted from conditioned medium from one population of heat-shocked utricles. When these isolated small EVs were applied to a second population of utricles co-exposed to neomycin, hair cell survival was significantly improved. This effect was not observed with the addition of the supernatant (non-vesicle) portion of the conditioned medium. One-way ANOVA followed by the Holm-Šidák multiple comparisons test was used to determine significance. Data points represent individual utricles throughout. Mean ± s.e.m. are shown throughout. ns = not significant, **P < 0.01, ***P < 0.001, ****P < 0.0001.

4.3.4 Association of HSP70 with vesicles

The association of HSP70 with extracellular vesicles was next investigated. Differential ultracentrifugation was used to isolate vesicles from heat-shocked utricles and HSP70 content was quantified by ELISA (Figure 4.6). Heat-shocked utricles had robustly upregulated expression of HSP70 in the tissue compared to controls and released measurable HSP70 into the culture medium. HSP70 was not detected in unconditioned medium. When conditioned medium from heat-shocked utricles was processed via differential ultracentrifugation, HSP70 was reliably measured in the EV pellet, suggesting that HSP70 was associated with the pelleted vesicles. Notably, the bulk of HSP70 from conditioned medium was detected in the ultracentrifugation supernatant. Given the UC pelleting efficiency demonstrated in Figure 4.5, this HSP70 is not likely to be associated with un-pelleted vesicles. It may,

however, be from lysed hair cells, as some hair cells in the striola region of the utricle express HSP70 (Nora Welsh, unpublished) and a few striolar hair cells are known to die and lose membrane integrity during culture (Monzack et al., 2015). Alternatively, HSP70 in the supernatant could represent secreted, free HSP70. However, HSP70 secretion is currently understood to require incorporation into membrane-bounded structures. Additional attempts to directly immunolocalize HSP70 via either immunoelectron microscopy or fluorescence NTA have suffered from lack of an antibody able to detect HSP70 in freeze-substitution embedded tissue or insufficient sensitivity of the instrument, respectively. However, these ELISA results provide some evidence for the association of HSP70 with small extracellular vesicles from the heat-shocked utricle.

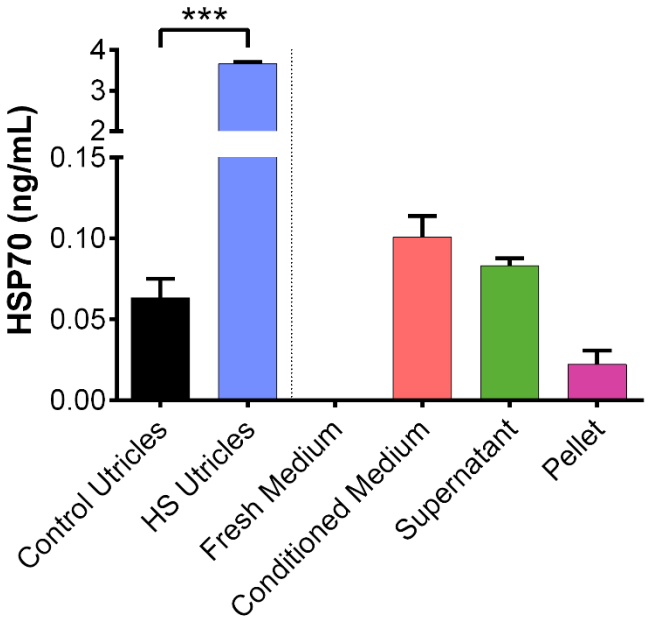


Figure 4.6: ELISA detection of HSP70 in utricles and conditioned medium fractions

An ELISA was used to quantify HSP70 content in the tissue of control and heat-shocked utricles and in the medium derived from heat-shocked utricles. Conditioned medium from the same population of utricles was split, with half being analyzed directly and the other half separated into vesicle (pellet) and non-vesicle (supernatant) fractions by ultracentrifugation. 0.1% Triton X was added to all liquid

samples in order to facilitate lysis of EVs. While serum-free medium was devoid of HSP70, significant HSP70 was detected in conditioned medium from heat-shocked utricles and the EV pellet and supernatant derived from that conditioned medium. Total HSP70 in both the vesicle and non-vesicle fractions approximated that measured in the un-processed conditioned medium. Mean ± s.e.m. of technical replicates are shown. An unpaired two-tailed t-test was used to determine significance. ***P < 0.001.

4.3.5 Cell type-specific production of extracellular vesicles

Utricles in culture represent a mixed population of cell types. The predominant cell types are hair cells and supporting cells and additionally present cell types include macrophages as well as fibroblasts and capillary endothelial cells of the stroma. An understanding of how extracellular vesicles function to protect hair cells in the utricle requires knowledge of which cell types are producing those vesicles. This question was investigated using a differential fluorescent labeling approach. The mTmG mouse expresses myristoylated-tdTomato protein in the absence of Cre-recombinase and myristoylated-EGFP protein following Cre-recombination. As both fluorophores are myristoylated (a lipidation modification), they ubiquitously associate with cellular membranes. The fluorophores are incorporated into the membranes of extracellular vesicles, thus labeling those vesicles with the fluorophore expressed in the cell of origin. As the labeling is not dependent upon the integration of a particular protein into the vesicle (as fluorophore-protein fusion approaches are, for example) the fluorophore is more likely to label all vesicles, rather than a particular subset. mTmG mice were crossed with mice expressing Cre-recombinase under control of the growth factor independent 1 (Gfi1) promoter (Figure 4.7a). In the utricle, Gfi1 is expressed only in hair cells and macrophages (Yang et al., 2010), and so the resulting offspring had differentially labeled hair cells and supporting cells (Figure 4.7b). The extracellular vesicles released from differentially labeled utricles had fluorescence intensities

which fell below the detection threshold for imaging flow cytometry (data not shown), but could be visualized in solution by continuous imaging on a laser scanning confocal microscope (Figure 4.7c), and subsequently quantified (Figure 4.7d). After heat shock, differentially labeled utricles released a mixed population of vesicles into their culture medium. Of all the vesicles visualized, 84% carried the tdTomato fluorophore expressed in supporting cells and 16% carried the EGFP fluorophore expressed in hair cells. These data suggest that the majority of vesicles released from the utricle after heat shock are derived from supporting cells.

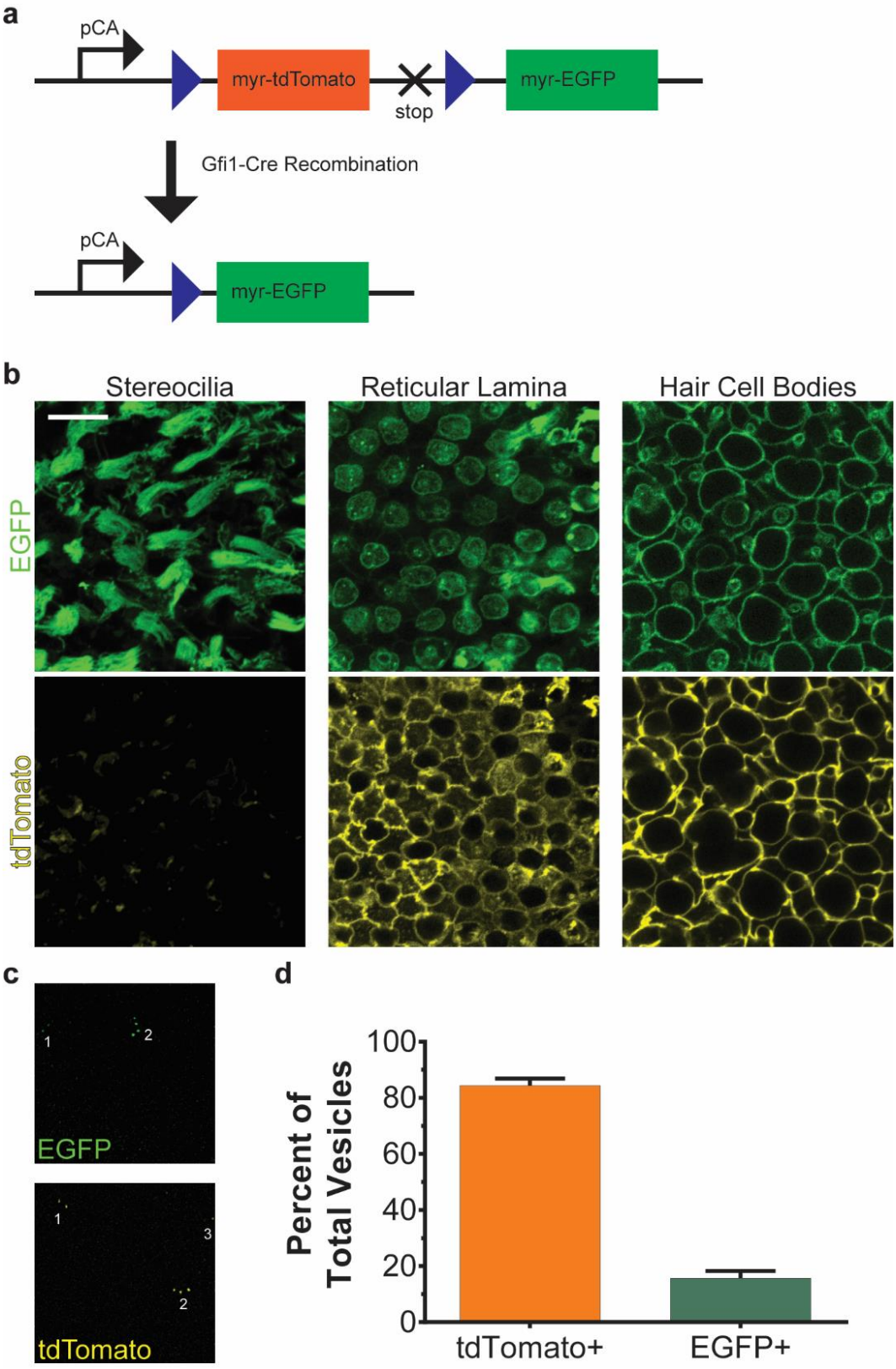


Figure 4.7: Differential labeling and quantification of vesicles derived from hair cells and supporting cells

Dual reporter utricles with differentially labeled hair cells and supporting cells were used to determine the percent contribution of EVs from each cell type to the total population of released EVs. (a) The mTmG transgenic mouse expresses membrane-targeted tdTomato prior to Cre recombination and membrane-targeted EGFP following Cre recombination. These transgenic mice were bred to Gfi1-Cre (a hair cell-specific Cre recombinase) mice in order to differentially labeled hair cells and supporting cells. pCA = CMV enhancer/chicken beta-actin core promoter. (b) Confocal z-slices from differentially labeled utricles. Images in each column represent the same z-slice. Hair cells universally express membrane-associated EGFP, while supporting cells universally express membrane-associated tdTomato. Scale bar = 10 μm. (c) A laser scanning confocal microscope was focused into conditioned medium from heat shock utricles and 1000 continuous frames (0.78 seconds in duration each) were collected. Summed intensity projections of four continuous confocal frames are shown. Vesicles and their trail of movement can be visualized. Numbers mark the location of vesicles. (d) The number of vesicles positive for each fluorophore visualized throughout the confocal collection period was manually counted and is represented as a percentage of all vesicles counted. The majority of vesicles were labeled with tdTomato, suggesting they were derived from supporting cells. Data are from n = 3 biological replicates of 8-10 utricles each.

Electron microscopy was also used to examine heat-shocked and control utricles for the presence of MVBs and other vesicle structures (Figure 4.8). TEM provided insight into vesicle morphology and location. In hair cells, vesicles were abundant around the edges of and directly below the cuticular plate (the dense actin mesh where the stereocilia insert into the hair cell). This vesicle population appeared to be mixed, with some vesicles, both small and large appearing empty, and others having the vesicle-within-a-vesicle appearance of MVBs. In some instances, vesicles appeared to be either fused with the plasma membrane or pinching off from the plasma membrane in either an exocytic or endocytic event (best seen in Figure 4.8 panel c). Though potentially more pronounced following heat shock, this hair cell morphology was also observable under control conditions, suggesting that it may represent a normal baseline physiologic process. In supporting cells, vesicles appeared generally less abundant, but more often had the appearance of MVBs. These MVBs were almost exclusively identified in one of two general regions, either near the apical membrane or near the lateral cell border in

the apical half of the cell. As with hair cells, similar vesicles could be seen in control utricles as well. No correlation between heat shock and the relative abundance of vesicles in hair cells versus supporting cells was obvious. TEM of this nature is of course not a quantitative technique and an abundance of extracellular vesicles could be associated with either increased or depleted intracellular vesicles. Regardless, these results demonstrate that MVBs are present in both hair cells and supporting cells and that there is abundant vesicle activity inside hair cells involving a morphologically mixed population of vesicles.

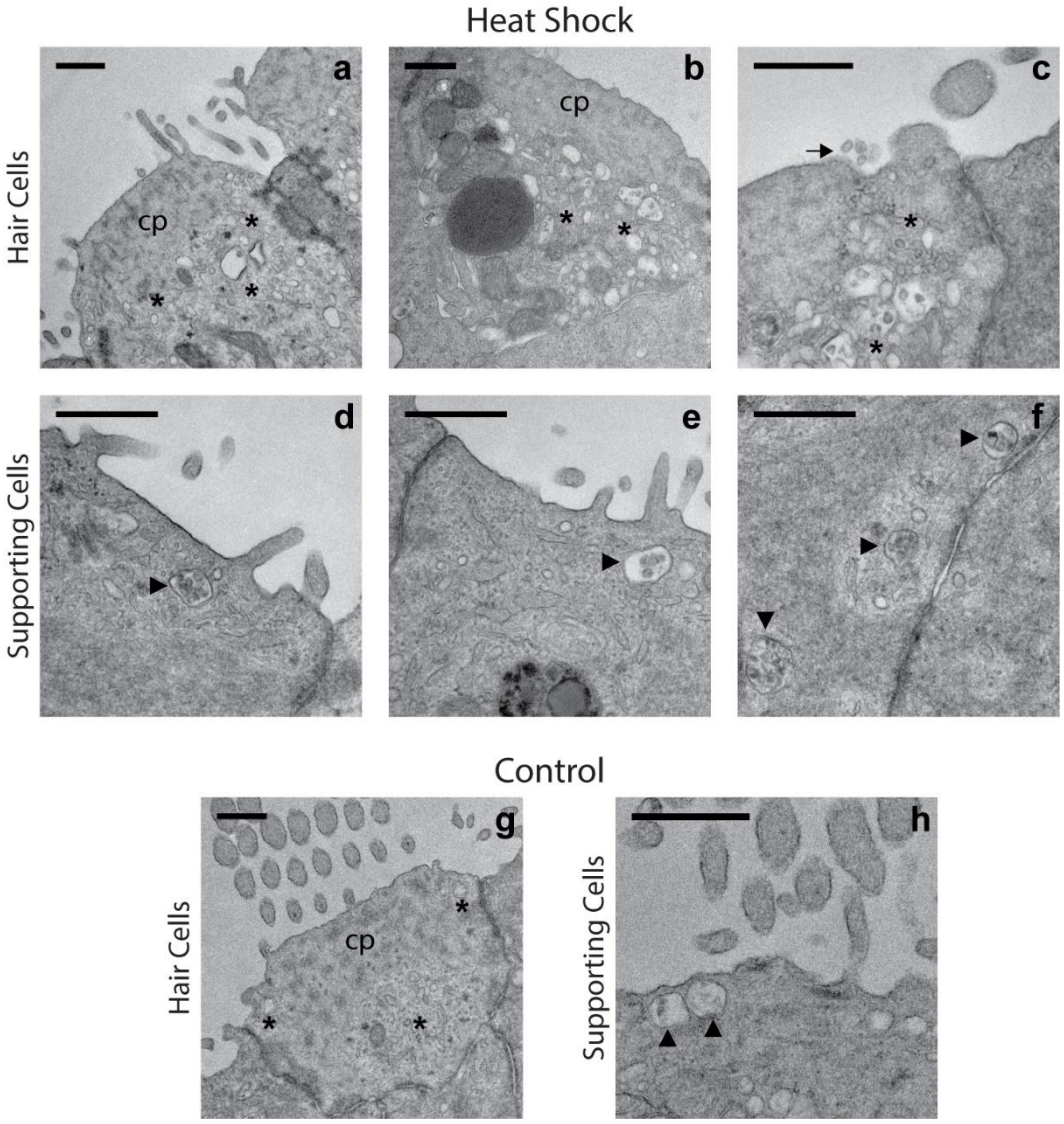


Figure 4.8: Transmission electron microscopy of heat-shocked and control utricles

TEM was used to image vesicles present in hair cells and supporting cells following *in vitro* heat shock of utricles in culture. Utricles cultured in parallel under standard culture conditions acted as controls. Hair cells can be differentiated from supporting cells by their lighter cytoplasm and large, actin-rich stereocilia, as well as the presence of abundant microvilli on supporting cells. (a-c) Hair cells from heat-shocked utricles and (g) from a control utricle. CP = cuticular plate. Asterisks mark the region of abundant vesicles observed around and below the cuticular plate. Arrow points to exocytic/endocytic event at hair cell apical surface in (c). (d-f) Supporting cells from heat-shocked utricles and (h) from control a utricle. Arrowheads identify structures which appear to be MVBs. Scale bars = 500 nm throughout.

4.3.6 The fate of vesicles released from the utricle

In many studies, small extracellular vesicles have either been demonstrated to, or are presumed to, exert a biological effect on recipient cells via their internalization and the intracellular delivery of specific cargo (Raposo and Stoorvogel, 2013, Lee et al., 2012). The fate of vesicles released from the utricle was investigated *in vitro* through further use of the mTmG transgenic mouse, following successful validation of the approach in cell lines. As discussed above, the mTmG transgene expresses myr-tdTomato prior to Cre-recombination and the fluorophore inserts into lipid membranes and is incorporated into extracellular vesicles. Using myr-tdTomato labeling in combination with superresolution confocal microscopy by the "Airyscan" method, the uptake of EVs was investigated in cell lines. Conditioned medium was collected from HEK 239T cells stably transfected with the mTmG construct, filtered, and then applied to Huh7 cells in culture. These cell types were chosen as Huh7 cells have previously been shown to avidly take up CD63 positive vesicles derived from HEK cells (Heusermann et al., 2016). Following four hours in mTmG HEK conditioned medium, many—seemingly individual—tdTomato positive vesicles could be resolved inside the Huh7 cells (Figure 4.9). No vesicles were detected in Huh7 cells exposed to conditioned medium from wildtype HEK 293T cells. This demonstrated the utility of vesicle labeling by myr-tdTomato in conjunction with vesicle imaging by Airyscan superresolution confocal microscopy in investigating the cellular uptake of EVs.

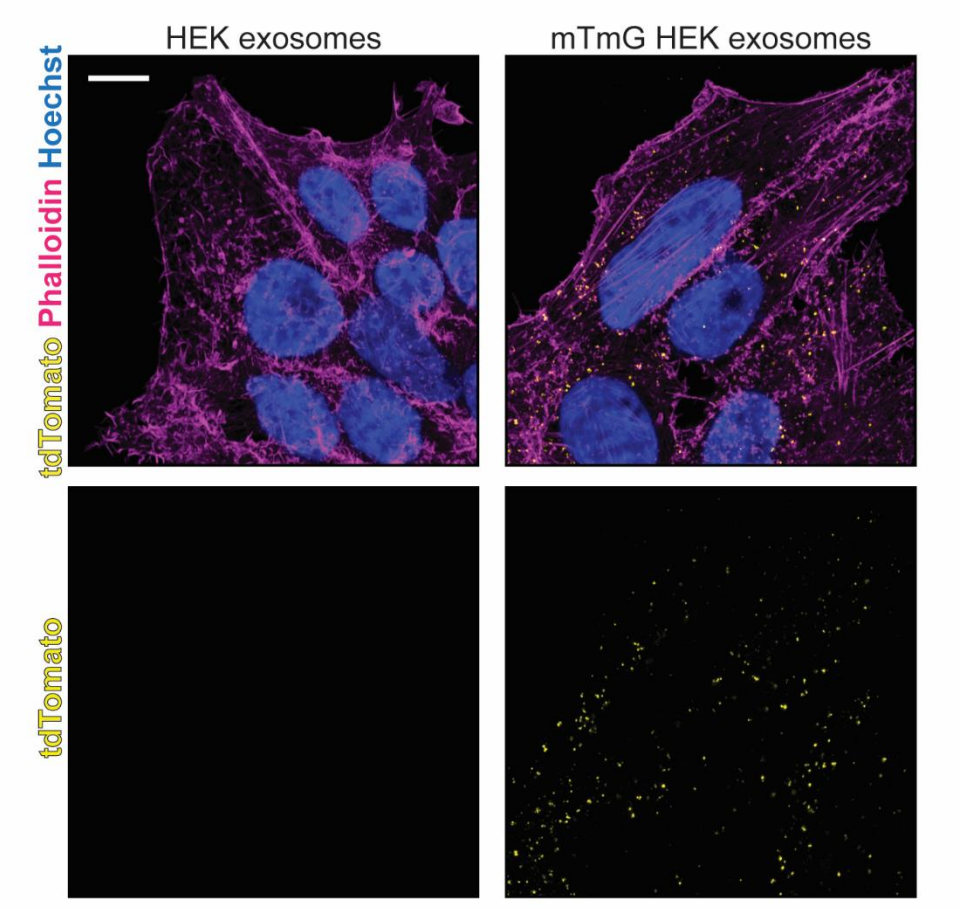


Figure 4.9: Airyscan confocal imaging of internalized myr-tdTomato labeled extracellular vesicles

Huh7 cells were treated with conditioned medium from wildtype HEK 293T cells (left column) or mTmG transgenic HEK 293T cells (right column) for 4 hours prior to fixation and staining. Maximum intensity projections of Airyscan (superresolution) confocal images are shown. Many tdTomato-labeled vesicles can be resolved in the cells exposed to mTmG HEK 293T conditioned medium; none are scene in the controls. Scale bar = 10 μm.

With the approach validated, vesicle uptake by cells in the utricle was investigated in a parallel fashion. Using a basket co-culture insert, two populations of utricles were cultured such that they were physically separated, but shared culture medium. Heat-shocked utricles from the mTmG mouse (Figure 4.10a) were cultured inside the co-culture basket (0.4 μm membrane pore size), with naïve utricles from CBA/J mice cultured in the well below. When concentrated conditioned

medium from mTmG HEK 293T cells was applied to CBA/J utricles as a positive control, labeled vesicles were visualized within the utricle, predominantly just below the reticular lamina (Figure 4.10b). However, no vesicles were ever visualized inside CBA/J utricles which had been co-cultured with mTmG utricles across a range of co-culture durations from 30 minutes to 24 hours (select timepoints shown in figure). These co-cultured utricles were indistinguishable from negative control CBA/J utricles which had been co-cultured with heat-shocked CBA/J utricles. These results provide evidence against a mechanism of EV protection whereby vesicles are released from some utricle cells and internalized by others.

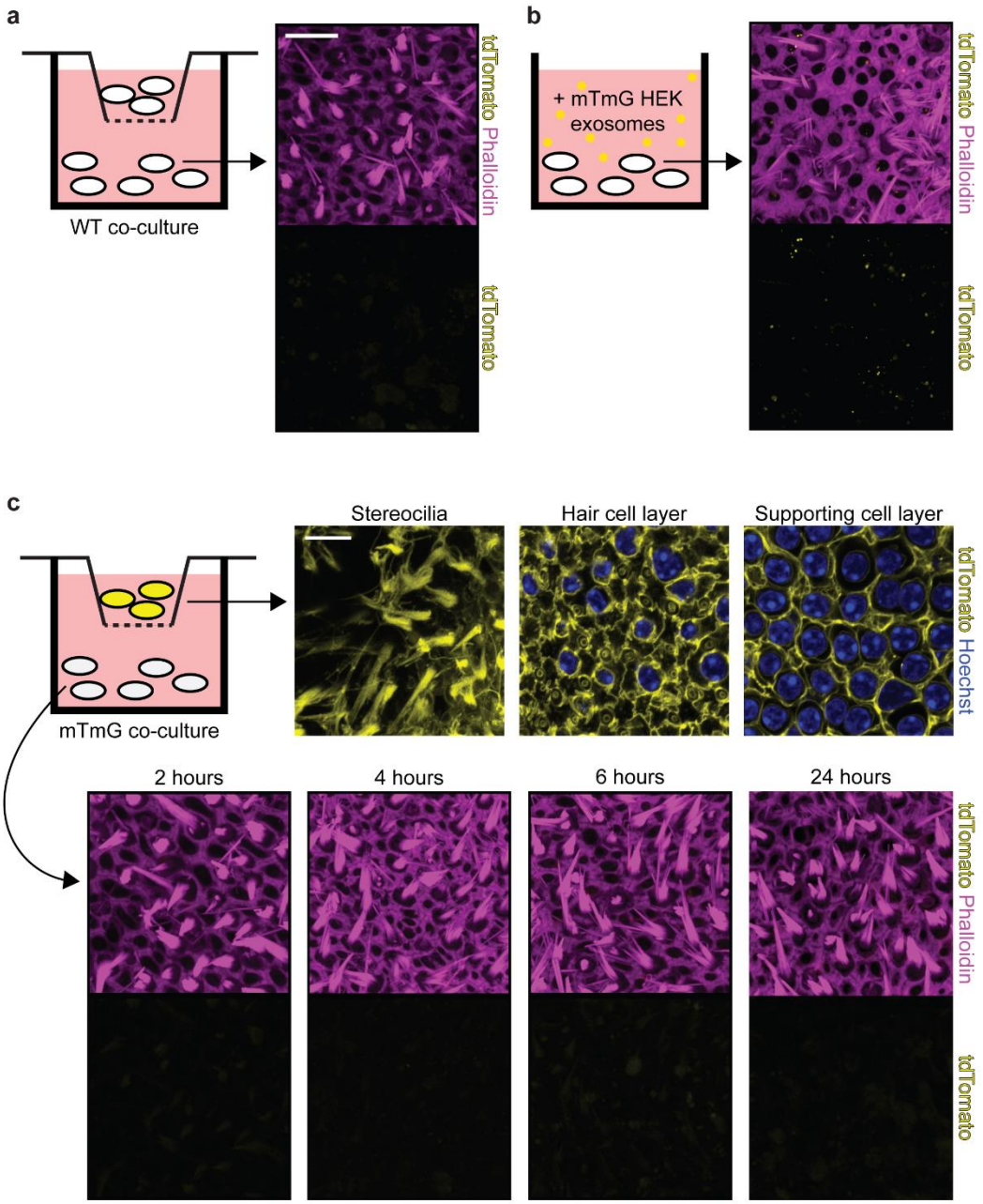


Figure 4.10: Light microscopy investigation of EV internalization by cells in the utricle

Transfer of vesicles between utricles was investigated using fluorescently labeled utricles, a co-culture setup, and Airyscan confocal microscopy. (a) For negative controls, CBA/J utricles were co-cultured with a separate population of heat-shocked CBA/J utricles for 24 hours. Heat-shocked utricles in the top basket acted as EV donors, while naïve utricles in the bottom of the culture well acted as EV recipients. No background tdTomato fluorescence signal was visible in recipient utricles. Dual channel image is shown on top, single channel (tdTomato only) on bottom (b) For positive controls, CBA/J utricles were treated with purified exosomes from HEK 293T cells expressing myristoylated tdTomato. Punctate tdTomato

fluorescence from internalized labeled EVs was visualized within the treated utricles. (c) To examine the transfer of EVs between utricles, heat-shocked mTmG utricles (donors) were co-cultured above wildtype CBA/J utricles (recipients). Upper row: mTmG utricles were imaged to confirm expression of myr-tdTomato throughout the tissue. Select confocal z-slices are shown. Lower row: CBA/J utricles were imaged to look for the presence of internalized labeled EVs at several time points. No internalized EVs were ever apparent. Maximum intensity projections of z-stacks are shown. Confocal stacks extended from the tips of stereocilia through the hair cell body. Scale bars = 10 μm.

The above approach to visualizing the uptake of utricle-derived EVs has some limitations in sensitivity which make it difficult to rule out uptake in this system. If a vesicle is to directly fuse with the plasma membrane (or later fuse with another cellular membrane) the myr-tdTomato will disperse throughout the membrane, losing local concentration, and becoming undetectable above background. Additionally, the area below the utricle reticular lamina (the apical portion of hair cells and supporting cells) appears rich in autofluorescent structures (such as mitochondria) which can elevate the background fluorescence and make the detection of small fluorescent structures, such as individual EVs, difficult. With these limitations in mind, utricle internalization of EVs was also investigated by immunoelectron (Immunogold) microscopy (Figure 4.11). When mTmG utricles were stained using an antibody raised against red fluorescent protein (detects tdTomato) moderate gold particle labeling of cell membranes was seen. This labeling was obvious at the cell surface (Figure 4.11 panel a) and included labeling of what appeared to be exosomes inside an MVB (Figure 4.11 panel b). In utricles co-cultured with heat-shocked mTmG utricles for 6 hours, a few clusters of gold particles could be seen in close association with the cell plasma membrane or inside the apical portion of hair cells and supporting cells, however, they did not appear associated with any vesicles. Further, similar clusters were observed in negative control utricles co-cultured with CBA/J utricles, suggesting that this level of staining

represented background non-specific antibody binding. With lower concentrations of antibody, the density of staining in positive controls decreased, and with higher concentrations of antibody the density of staining in negative controls increased, and so this dilution (1:25) was considered to be optimal. These data further suggest against significant internalization of EVs as a mechanism of EV-mediated protection, however, the sensitivity of this technique to detect tdTomato-positive EVs seems limited by the antibody as even the positive controls only show moderate staining for tdTomato.

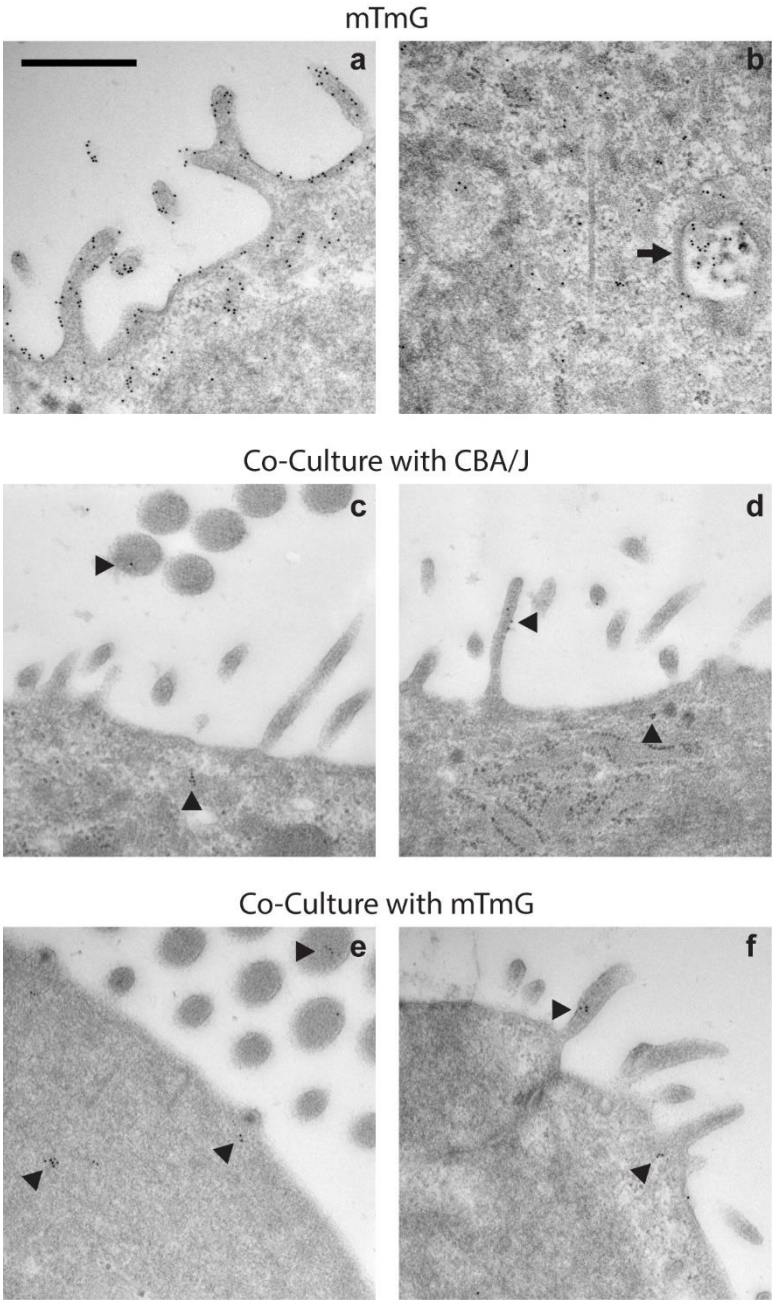


Figure 4.11: Immunoelectron microscopy of EV internalization by the utricle

Transfer of labeled EVs between utricles was investigated using anti-tdTomato Immunogold transmission electron microscopy. (a-b) tdTomato was detected in the membrane of mTmG (positive control) utricles, and also labeled what appears to be ILVs inside an MVB, denoted by an arrow in (b). (c-d) CBA/J negative control utricles show limited background labeling for tdTomato. (e-f) Utricles co-cultured with heat-shocked mTmG utricles for 6 hours have a similar labeling pattern and abundance as negative controls. Arrowheads in (c-f) point to clusters of gold particles. Scale bar = 500 nm throughout.

4.3.7 Proteomic investigation of extracellular vesicle content

Heat shock protein 70 was found to be associated with EVs from heat-shocked utricles by ELISA, however, the remaining protein complement of those EVs remained unknown. Tandem mass spectrometry was thus employed to elucidate the protein content of utricle EVs and to gain further insight into their generation and function. As differential ultracentrifugation has previously been demonstrated to co-pellet protein complexes along with small EVs, an alternative size-exclusion chromatography-based method, as recently described by Nordin et al. (2015) was used to generate a sample of utricle EVs of improved purity. In SEC separation, the EVs typically outsize the pore diameter of the resin beads, and so they can transit the column quickly by bypassing the beads, while most non-vesicle associated proteins (i.e. contaminants) are able to enter the resin beads and thus take longer to transit the column. Vesicles are eluted earlier than contaminants and can thus be isolated for downstream analysis or application.

For this study, a chromatography column with Superose 6 Increase resin (GE Healthcare) was chosen. This resin has not been previously used to purify EVs in the literature, however, it was investigated and employed here because its published characteristics suggested it well-suited for this purpose. With a fractionation range of 5,000 to 5 x 10^6 relative molecular mass, this resin has a high fractionation upper limit and thus fractionates some of the largest known proteins and allows for their removal from the EV sample. The high resolution of the resin allows for the use of a smaller column to achieve similar levels of separation as other resins. This in turn decreases the amount of dilution of the sample which occurs over the chromatography process and thus decreases the amount of re-concentration required post-chromatography, a process during which significant yield can be lost.

Due to the low yield of EVs from utricles, SEC purification of small EVs via Superose 6 Increase resin was validated using HEI-OC1 cells instead. Conditioned medium from HEI-OC1 cells was filtered and concentrated on an ultrafiltration device before application to the size-exclusion column. EVs were eluted off the column in the earliest fractions and they produced a small protein peak as measured by absorbance at 280 nm (Figure 4.12). This peak represented only 3.2% of the area under the absorbance curve. The majority of protein was eluted in the latter fractions, representing a significant amount of potential contamination that was effectively separated away by this technique. These data validated the utility of the Superose 6 Increase resin for this purpose and the location of the EV peak guided the identification of the vesicle-containing fractions in subsequent experiments.

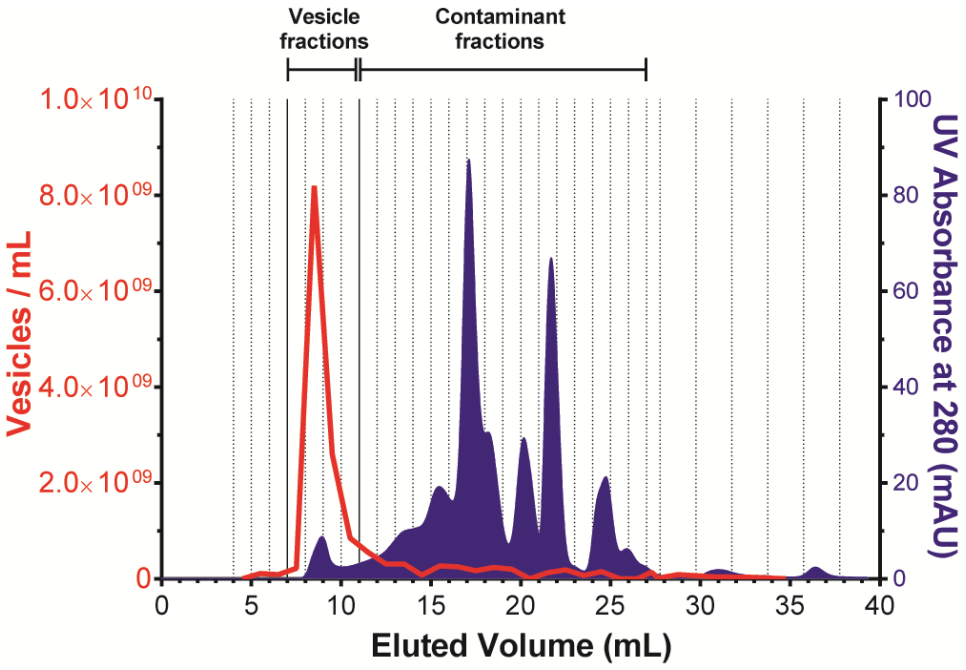


Figure 4.12: Size-exclusion chromatography purification of HEI-OC1 extracellular vesicles

HPLC chromatograph generated during SEC fractionation of concentrated HEI-OC1 conditioned medium. The sample was run through a 24 mL bed volume Superose 6 Increase resin column. As the sample was eluted off the column, UV absorbance at 280 nm was continuously measured (plotted in blue, right y-axis) and 1 mL fractions were collected (indicated by dotted vertical lines). The concentration of vesicles in

each fraction was then analyzed by NTA and is plotted in red. For this and following SEC purifications, vesicle fractions were identified as those comprising and immediately surrounding the initial absorbance peak (at ~9 mL eluted volume in this plot), with contaminant (non-vesicle) fractions being the remaining fractions up to ~27 mL of eluted volume.

The effective separation of vesicles from contaminants via this SEC method (comparable to that in the literature) suggested it to be suitable for sample preparation for proteomic analysis by tandem mass spectrometry, as has been previously achieved with other SEC-purified vesicle samples (Nordin et al., 2015). EV samples analyzed by mass spectrometry are typically derived from at least several large flasks of cells at near confluence, and so the low yield available from utricles in cultures was recognized as a significant challenge from the outset. To help overcome this challenge, a total of 298 utricles were cultured, with 65 utricles undergoing heat shock and 233 acting as controls. This ~3:1 ratio of control to heat shocked utricles was used in order to compensate for the ~3 times greater production of exosomes observed from heat shocked utricles. SEC was used to purify EVs from the conditioned media of both populations of utricles and quantitative mass spectrometry was performed via dimethyl labeling. The non-vesicle fractions were also pooled and analyzed as they presumably contained directly-secreted proteins potentially important to understanding the utricle biology. In total, 105 proteins were identified with 51 uniquely identified in the vesicle fractions (Figure 4.13a). The total list of identified mouse proteins in each sample type can be found in supplementary Figure S 2 and Figure S 3. Measured protein abundance ratios were adjusted for the number of utricles present in each condition. Proteins identified in the vesicle fractions were universally more abundant from heat-shocked utricles than control utricles (Figure 4.13b), while proteins in the non-vesicle fractions could be more abundant in either the heat shock or control medium

(Figure 4.13c). Individual proteins identified included extracellular matrix and structural proteins such as laminins, heparin sulfate proteoglycan, and aggrecan; inner ear-specific structural proteins such as otoancorin, otogelin, and tectorin alpha and beta; histones; and the exosomal marker CD9 (Figure 4.13d). Notably, HSP70 was not detected in either sample type, in contrast to the results obtained by HSP70 ELISA.

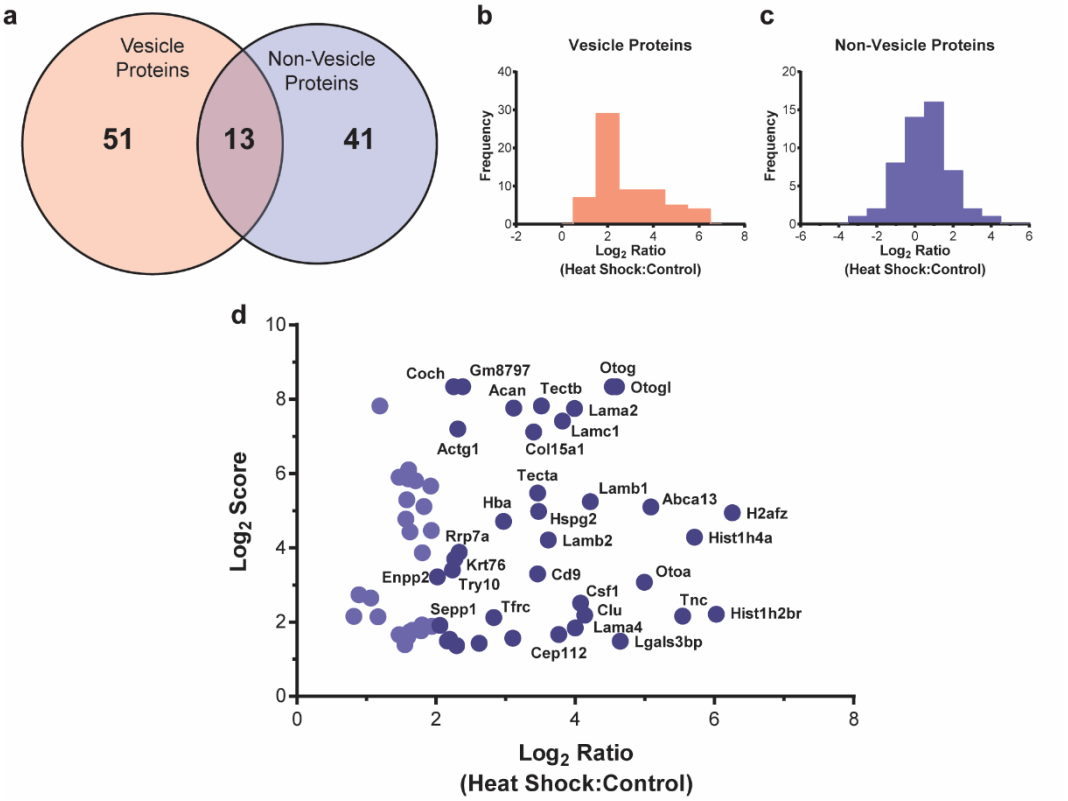


Figure 4.13: Tandem mass spectrometry analysis of utricle conditioned medium fractions

Quantitative tandem mass spectrometry analysis of vesicle-associated and vesicle-unassociated proteins in the conditioned medium of heat-shocked and control utricles. Vesicle and non-vesicle proteins were separated by size-exclusion chromatography as described above. Heat shock samples were run with their respective control samples, with quantitative comparison performed via dimethyl labeled of the two sample types. (a) Venn diagram of identified proteins. 105 proteins were identified in total. (b) Distribution of adjusted protein ratios (abundance from heat-shocked utricles: abundance from control utricles) of those proteins identified in the vesicle fractions from SEC. Identified proteins are universally more abundant from heat-shocked utricles than controls. (c) Distribution of adjusted protein ratios of those proteins identified in the non-vesicle

fractions. (d) Identification scores (a measure of the confidence of the protein identification) and abundance ratios for proteins identified in the vesicle fractions. Most of the 38 proteins with an abundance ratio greater than four are labeled with their gene name.

Gene ontology enrichment analysis was performed on those proteins identified in the vesicle fractions using the STRING database. Analysis by cellular component ontology identified significant enrichment of proteins associated with extracellular exosomes and membrane-bounded vesicles as well as those associated with multiples types of extracellular structures such as the extracellular matrix and basal lamina (Figure 4.14a). Analysis by biological process ontology identified significant enrichment of proteins associated with sensory perception of sound; glia cell generation, differentiation, and development; cell and cell-substrate adhesion; and receptor-mediated endocytosis, among others (Figure 4.14b). Altogether, the gene ontology analysis was consistent with a sample of extracellular proteins derived from inner ear tissue. The collection of identified proteins suggested that the sample contained both extracellular vesicles as well as co-isolated extracellular matrix and other structures. The identification of CD9, a well-characterized protein marker for exosomes, in the vesicle fractions provides further evidence that the vesicles released from heat-shocked utricles may be best categorized as exosomes.

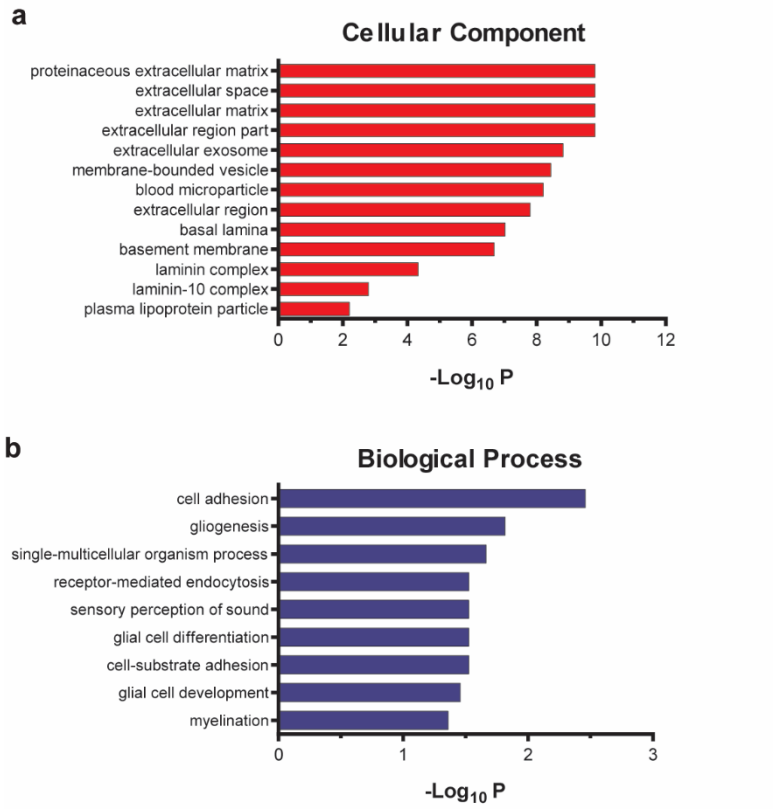


Figure 4.14: Gene ontology term enrichment analysis of vesicle proteins

Significantly enriched gene ontology terms of proteins identified in vesicles were determined using the STRING database, which compares the distribution of observed proteins to that expected for a random set of proteins of similar size, drawn from the same genome (a) Significantly enriched "cellular component" ontologies. (b) Significantly enriched "biological process" ontologies.

4.3.8 Hair cell protection *in vitro* using cell line-derived small EVs

The results detailed thus far in this chapter provided evidence that exosomes released from the utricle play an important role in mediating the protection from aminoglycosides granted by heat shock. This knowledge in combination with published data demonstrating HSP70 protein to be common to small EVs from a wide-range of cell types (Kim et al., 2015) suggested that small EVs purified from other cellular sources may be able to recreate the protective effect of heat shock. Conditioned media were collected from CT26 mouse colon carcinoma, HEI-OC1

mouse inner ear, C8-B4 mouse microglial, and C8-D1A mouse astrocyte cells in culture. Small EVs were isolated and applied to utricles cultured in neomycin. EVs derived from CT26 cells significantly improved the survival of hair cells, an effect not seen with EVs derived from the other cell types (Figure 4.15a). The protective capacity of CT26 extracellular vesicles was further confirmed when improved utricle hair cell survival was again observed following the application of small EVs isolated in a different manner—via ultracentrifugation (Figure 4.15b). These data demonstrate that EVs purified from an exogenous source can effectively protect hair cells from aminoglycoside-induced death *in vitro*, and imply that these vesicles may represent an effective vehicle for delivery of other therapeutics. The differential protection seen across EVs from different cell sources suggests the increased presence of either pro-survival proteins or proteins necessary for interaction with the utricle in CT26 EVs as compared to the other types examined.

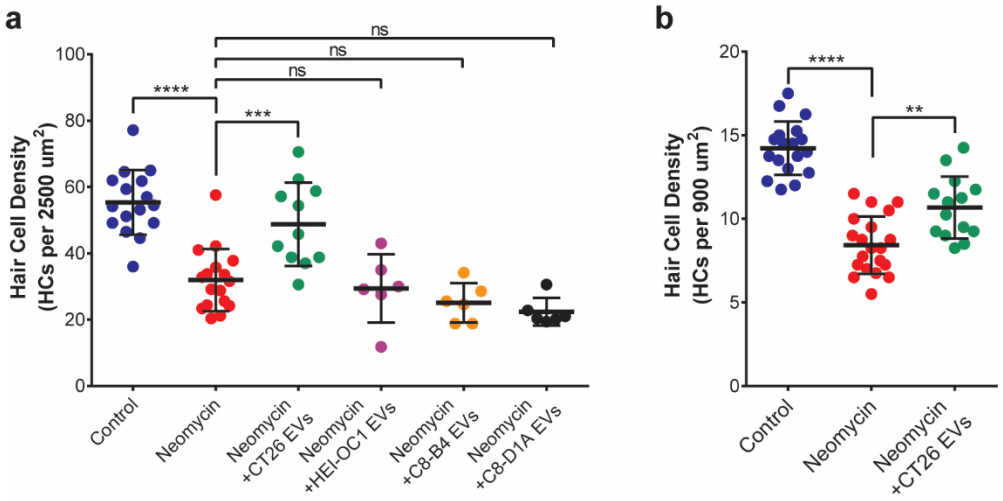


Figure 4.15: Protection of utricle hair cells *in vitro* via exogenous exosomes

Surviving hair cells were quantified in utricles that had been cultured in neomycin-containing media with or without the addition of cell line-derived small extracellular vesicles. (a) Small EVs were purified from four different cell lines using filtration and SEC. 2.5 x 10^9 exosomes from each cell line were added to utricles in neomycin-containing culture medium. Only CT26 cell-derived EVs were able to significantly

prevent the loss of hair cells from utricles. One-way ANOVA followed by the Holm-Šidák multiple comparisons test was used to determine significance. (b) CT26 cell-derived EVs purified via a different method, namely differential ultracentrifugation, again prevented the loss of hair cells otherwise caused by exposure to neomycin. Data points represent individual utricles. Mean ± s.e.m. are shown. One-way ANOVA followed by the Holm-Šidák multiple comparisons test was used to determine significance. ns = not significant, ** $P < 0.01$, *** $P < 0.001$, **** $P < 0.0001$.

4.4 DISCUSSION

The data presented in this chapter support, but do not prove, a model in which exosomes carrying HSP70 are released from supporting cells of heat-shocked utricles and act via an external interaction to protect hair cells. Extracellular vesicles released from heat-shocked utricles appeared to be both necessary and sufficient to improve hair cell survival in utricles exposed to the aminoglycoside neomycin. The majority of EVs released from the utricle seem to be derived from supporting cells, and no direct evidence for their downstream internalization was found in either hair cells or supporting cells.

Supporting cell-derived exosomes carrying HSP70 may confer hair cell protection by binding toll-like receptor 4 (TLR4), leading to downstream activation of heat shock protein 27 (HSP27), a true heat shock protein which is well-known to have antiapoptotic and antioxidant properties (Arrigo, 2017). This proposed model, schematized in Figure 4.16, would parallel a role recently described for exosomes in protecting against ischemia-reperfusion injury in the heart. In that study, plasma-derived exosomes carrying HSP70 on their surface were found to interact with TLR4 on cardiomyocytes, ultimately leading to activation of HSP27 and cardioprotection against ischemia-reperfusion (Vicencio et al., 2015). Work by another member of our laboratory has recently shown that either conditional knockout of TLR4 in

utricle hair cells or application of a TLR4 signaling inhibitor abolishes the hair cell protection typically mediated by heat shock (Shimon Francis, unpublished).

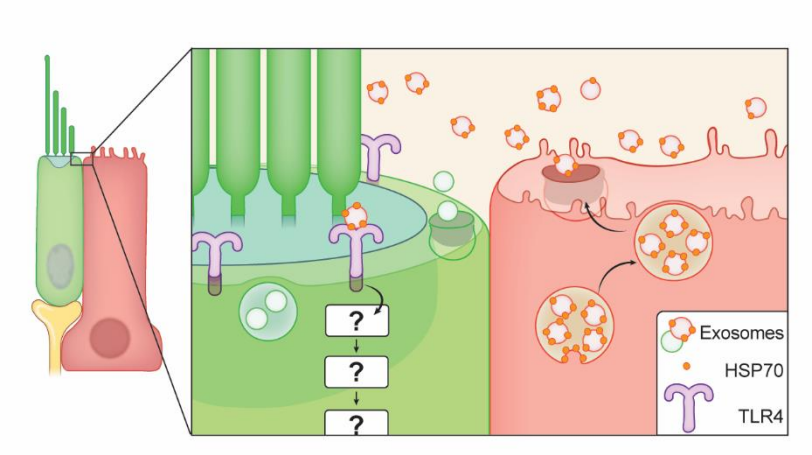


Figure 4.16: Proposed model for the role of exosomes in hair cell protection

In the proposed model, heat shock selectively induces HSP70 expression in supporting cells and some of this HSP70 is released from supporting cells incorporated into the membrane of exosomes. These exosomes then act via a cell surface receptor to stimulate protective pathways in hair cells, ultimately improving the capacity of hair cells to handle ototoxic stress. Hair cells also contribute a small proportion of vesicles to the total extracellular population, the significance of which remains unclear. Hair cells often have large numbers of intracellular vesicles located beneath and around the cuticular plate. These vesicles have been previously reported (the so-called "pericuticular necklace") and have been demonstrated to, at least in part, be endocytic (Kachar et al., 1997, Richardson et al., 1997, Hasson et al., 1997). Illustration by Erina He.

The predominant population of vesicles released from the utricle may be best categorized as exosomes. Their size distribution of largely 50 to 100 nm is most consistent with exosomes, as opposed to other types of EVs such as microvesicles and apoptotic bodies, which are typically larger and/or of a broader size distribution (Raposo and Stoorvogel, 2013, Zaborowski et al., 2015). The release of EVs from the utricle following heat shock also seemed to require the sphingolipid ceramide as inhibition of neutral sphingomyelinase II prevented their release. Ceramide is understood to trigger the budding of some exosomes into MVBs (Trajkovic et al., 2008). Additionally, the work in this chapter associates two known protein markers

of exosomes with the EVs released from heat-shocked utricles: HSP70 by ELISA, and CD9 by tandem mass spectrometry (Colombo et al., 2014). Finally, electron microscopic images of pelleted vesicles show exosome morphology while TEM images of utricles show what appear to be MVBs within the utricle and often near the apical cell surfaces. It should be noted that EV nomenclature is still evolving. The field continues to develop new methods of separating and subsequently describing sub-populations of EVs with populations of vesicles previously assumed to be homogenous (Kowal et al., 2016). However, as the EVs described here share characteristics with vesicles previously categorized as exosomes, the existing exosome literature may help guide further investigation of these vesicles.

Analysis of the conditioned culture medium from utricles revealed a somewhat mixed population of extracellular vesicles. Small EVs, between 50 and 100 nm were predominant in both control or heat shock conditions, however, larger particles/vesicles ranging in size up to ~350 nm in diameter were also detected. These may represent apoptotic bodies from the small population of hair cells known to die in culture or perhaps microvesicles released from any cell type present. For the NTA analyses of EVs from utricles presented in this chapter, conditioned medium was analyzed without any steps taken to specifically enrich a certain EV population. This approach was taken to provide an unbiased view of the total population of vesicles released from the utricle under both control and experimental conditions. Though the entire vesicle population was always quantified, it was largely the small EVs which showed a significant increase in release following heat shock and a significantly blunted release in the presence of either N-SMase inhibitor.

The finding that inhibition of vesicle release with spiroepoxide abolishes the hair cell protection typically mediated by heat shock suggests that release of small EVs is required to mediate this protection. Likewise, the ability of small EVs purified

from one population of heat-shocked utricles to mediate hair cell protection in a second population of utricles suggests that EVs are sufficient to mediate protection. Both these results demonstrate the importance of extracellular factors in mediating hair cell protection in the utricle, and the former result further suggests lack of a redundant non-extracellular pathway of protection. In the spiroepoxide experiment, the same utricles which were heat-shocked were then treated with spiroepoxide and neomycin and analyzed for surviving hair cells. The fact that spiroepoxide decreased the number of surviving hair cells in these utricles suggests that they rely upon paracrine signaling via EVs for mediating protection and that protection is not significantly mediated via direct cell-to-cell signaling or transfer via gap junctions or another conduit. This agrees with a previous result in our laboratory in which addition of a function-blocking antibody against HSP70 to the utricle culture medium was seen to abolish the protection of heat shock (May et al., 2013). Both results demonstrate that the protection mediated by heat shock requires extracellular factors.

HSP70 was detected in exosomes released from utricles by performing an ELISA on exosomes pelleted from utricles via ultracentrifugation. However, it should be noted that HSP70 was not identified in the tandem mass spectrometry analysis. The most likely explanation for this discrepancy is that HSP70 was present at a level insufficient for its detection by tandem mass spectrometry. Given the very limited input quantity of protein, the small number of proteins identified is more likely a result of this limited input than a true reflection of compositional simplicity of the sample. Previous proteomic analyses of EVs performed by our laboratory and others typically have identified several hundred or more proteins. With this in mind, conclusions from the proteomic analysis reported here should only be drawn from the proteins identified, and not from those not identified. An alternative explanation

to the discrepancy in the HSP70 ELISA and mass spectrometry data may be that the ELISA kit is not specific for HSP70. Observed activity of the kit against recombinant HSP70 demonstrate that it detects HSP70, but additional cross reactivity with other targets cannot be entirely ruled out at this time. However, the low level of detection in control utricles suggests against significant background cross reactivity.

A more direct method of visualizing the association between exosomes and HSP70 is still desired. Though commonly-accepted practice, the detection of proteins in the ultracentrifugation pellet does not prove the presence of those proteins in the vesicles, as it is possible that they have simply been co-pelleted (Webber and Clayton, 2013). One such method of more direct visualization could be via fluorescent nanoparticle tracking. While typical NTA localizes and follows vesicles by continuous imaging of their light scatter, fluorescent NTA uses the filtered fluorescence produced by laser-excited labeled vesicles (Dragovic et al., 2011). In this way, the presence of epitopes on an intact vesicle can be detected with fluorescent antibodies. Unfortunately, this technique requires a high initial yield of EVs for analysis. The sensitivity of the NTA is an order of magnitude lower in fluorescence detection mode than light scatter detection mode (~13x in pilot experiments, data not shown), requiring a much more concentrated sample for analysis. Compounding this low sensitivity is the additional loss of sample during the staining process, during which unbound labeled antibody in the solution must be separated from vesicles with bound antibody. Because of this yield challenge, the technique was found to be unsuitable for studying utricle-derived exosomes. Another method of direct visualization of HSP70 associated with exosomes could be via immunoelectron microscopy. Successful application of this technique will require the identification of an HSP70 antibody with sufficient sensitivity in tissue prepared for electron microscopy, attempts at which have thus far been

unsuccessful. However, if such an antibody is identified or produced, immunoelectron microscopy has the additional advantage of potentially resolving whether HSP70 is associated with the exosome membrane or is encapsulated within the vesicle. The identification of HSP70 in utricle-derived exosomes is not surprising given the numerous reports of its presence in exosomes derived from many different cell types (Lancaster and Febbraio, 2005, Takeuchi et al., 2015, De Maio, 2014, Yanez-Mo et al., 2015, Kim et al., 2015).

Quantification of fluorescent vesicles labeled in a cell type-specific manner suggested that the majority of EVs released from heat-shocked utricles were derived from supporting cells. One caveat of this analysis is the presence of multiple cell types in the dissected utricle. Though hair cells and supporting cells are predominant, some stromal cells and macrophages are also present. In the utricles from the *Gfi1*$^{Cre/+}$; *ROSA26*$^{mTmG/+}$ mice used in this study, hair cells and macrophages expressed myr-EGFP while supporting cells and stromal fibrocytes expressed myr-tdTomato. Therefore, both vesicle populations are from a mixed population of cells. However, ongoing experiments should help overcome this caveat. *GLAST-CreER* mice (Jackson Laboratory, Stock No. 012586) are being crossed to *ROSA26*$^{mTmG/mTmG}$ mice. *GLAST-CreER* mice are a transgenic line expressing tamoxifen-inducible Cre recombinase under the control of the glial high affinity glutamate transporter (GLAST) promoter. Resulting *GLAST-CreER*; *ROSA26*$^{mTmG/+}$ offspring are expected to express myr-EGFP in supporting cells and limited macrophages, and myr-tdTomato in hair cells and stromal fibrocytes. Therefore, hair cells and supporting cells will have an inverted labeling scheme while stromal fibrocytes and macrophages will have unchanged labeling. This should allow for further clarification of the exact contribution of each cell type to the total vesicle population. Though automated high-throughput analysis of the labeled vesicle populations by flow cytometry was

attempted without success in this study, continued improvements in sensitivity and nanoscale flow capabilities may allow for high-throughput, automated analyses of this type in the near future.

No direct evidence for subsequent internalization of released exosomes was observed, suggesting that their protective effect is mediated via an external interaction and not necessarily through uptake and delivery of cargo into recipient cells. To investigate this trafficking, a light microscopy-based approach was first developed and validated. Vesicles were labelled via membrane-targeted myristoylated-tdTomato and imaged via Airyscan superresolution microscopy. This approach has advantages over previous, more-common approaches. A common method, EV labeling by conjugation of fluorophores to specific EV marker proteins, may lead to biased labeling of only a subset of vesicles. Another approach, use of fluorescent dyes for EV labeling, may introduce artifacts from carry-over of unbound dye and the half-life of the dye may exceed that of the vesicle, leading to misleading spatiotemporal conclusions (Lai et al., 2015, Lai et al., 2014). The labeling technique used here largely avoids the limitations of both these other approaches, and Airyscan confocal microscopy allows for imaging of these vesicles with resolution as small as 140 nm without the need for specialized fluorophores or high labeling density, as required by other superresolution techniques (Sivaguru et al., 2016, Maglione and Sigrist, 2013). This approach should prove useful for future studies of vesicle trafficking. Additionally, selective Cre-recombination in the mTmG mouse or of mTmG expressing cells could allow for the simultaneous study of trafficking of vesicles derived from different cell types.

This light microscopy approach to visualization of vesicle trafficking is not without limitations however. Dispersion of myr-tdTomato throughout membranes following exosome fusion may leave no detectable trace of once-internalized

exosomes. However, in the co-culture setup, exosomes are continuously being released by the donor utricles and so any uptake would likely be continuously occurring as well. Therefore, one would expect to be able to identify exosomes that have been internalized, but have not yet undergone fusion or disassembly, if such a process is occurring. Direct fusion of exosomes with the plasma membrane, however, may be undetectable by this approach or the other approaches mentioned without the use of live imaging.

By Immunogold TEM, no internalized exosomes or accumulated tdTomato were identified, though the ability to detect tdTomato appeared less-than-optimal. Together then, these results suggest against substantial uptake of exosomes into co-cultured utricles, but such uptake cannot be ruled out. These results agree with another previous study in our laboratory. In that study, expression of fluorescently tagged HSP70 was driven in supporting cells of the utricle (May et al., 2013). Though this HSP70-mCherry expression conferred protection against neomycin to both the expressing utricles and co-cultured utricles, no mCherry signal was ever detected in co-cultured utricles. It is worth noting that although many studies have shown uptake of applied exosomes or other vesicles into cells, often vesicles are applied in an extreme overabundance, that is, the vesicle sample prep is derived *from* orders of magnitude more cells than it is applied *to*, and so the vesicle concentration used *in vitro* is almost certainly supraphysiologic. Further, most studies have used cell lines and primary cell cultures, which of course may not accurately represent the biology of the organ of derivation. In the utricle, under the conditions studied here, exosomes appear to act via an extracellular interaction, which may be a receptor-mediated event.

With a size-exclusion chromatography method for purification of EVs validated with cell line small EVs, further understanding of utricle exosome biology

was sought through quantitative proteomic analysis of control and heat shock-induced exosomes. The isotope dimethyl labeling approach was applied to provide more robust quantitation than a label-free approach (Boersema et al., 2009). Acquisition of sufficient material for analysis required the culture of many utricles (298 in total). Even so, only 64 total proteins were identified in the purified exosomes. Because of the number of animals required for this analysis, only one biological replicate was performed. This caveat must be considered when drawing conclusions from the data acquired. Of the upregulated proteins identified in exosomes from heat-shocked utricles, the majority either help form extracellular structures or are known to be associated with them. This suggests that extracellular structures of the utricle were co-isolated with exosomes, a complication not apparent when exosomes were isolated and analyzed from a cell line in culture (data not shown). This co-isolation is conceivable given that these proteins are of course extracellular and exist in large complexes which, if intact, could behave like vesicles in the size-exclusion medium by exceeding the resin pore size and traveling quickly through the column. Additionally, some histones were highly upregulated in the vesicle fraction. Though histones have previously been reported in exosomes, current understanding is that they are more likely to represent contamination with apoptotic bodies or intracellular material (Kowal et al., 2016, Thery et al., 2001). Despite this apparent contamination of the sample, a few discovered proteins may be worthy of further follow-up, the most notable of which is CD9.

CD9 is a tetraspanin protein very commonly identified in exosomes, and considered by many to be a robust protein marker of exosomes. As with other classical protein markers of exosomes, the understanding of CD9 association with EVs is becoming increasingly complex. CD9 expression does not necessarily correlate with other tetraspanin markers and it has also been identified in larger

vesicles (Bobrie et al., 2012a). Additionally, while Rab27a was found to modulate exosome and CD63 secretion in one study, it did not affect CD9 secretion (Ostrowski et al., 2010). In other studies, exosome secretion from dendritic cells has been shown to require CD9, and it has been demonstrated to promote the incorporation of certain proteins into exosomes, including MHC II and metalloprotease CD10 (Buschow et al., 2009, Mazurov et al., 2013, Chairoungdua et al., 2010). In general, evolving understanding is that tetraspanin markers of exosomes are not as universal as once thought and that their expression and role in EV biology may differ significantly across cell types (Andreu and Yanez-Mo, 2014). Further exploration of the role of CD9 in the utricle may be informative. Investigating the effect of CD9 knockdown or knockout upon vesicle release from the utricle and/or upon heat shock mediated protection of the utricle should be considered.

Another identified protein worthy of further consideration is clusterin. This protein was highly upregulated (~18 fold) in the vesicle fraction following heat shock. Clusterin is understood to be a component of the heat shock response, and is regulated by the central heat shock factor 1 (HSF1) transcription factor (Loison et al., 2006). It exists in both secreted and cytoplasmic forms, and the secreted form is known to have a wide range of pro-survival effects ranging from chaperone activity and inhibition of protein aggregation to cell surface receptor based inhibition of pro-apoptotic signaling (Zoubeidi et al., 2010, Yerbury et al., 2007, Carver et al., 2003). Expression of clusterin in supporting cells of the cochlea has recently been described (Lee et al., 2017), and although it can be directly secreted, it has also been described incorporated into exosomes and exosomal clusterin has been shown to help reduce cardiomyocyte apoptosis following infarction (Foglio et al., 2015). A pro-survival role for extracellular clusterin in the inner ear seems plausible.

As made obvious by this proteomics analysis, the single greatest challenge confounding investigation of the role of EVs in the inner ear is the limited EV yield achievable from culture of inner ear tissue like the utricle. Without physiologically relevant cell culture models there appears to be no immediate way around this challenge. Most obviously, low EV yield limits proteomics, transcriptomics, and other discovery approaches to only being able to detect the most abundant species, and it prevents the detection of proteins by standard benchtop techniques such as Western blotting. Less obviously, low yield places significant limitations upon the use of certain purification strategies and techniques which depend on them. For example, the loss of EVs on centrifugal ultrafiltration devices largely prevented their use for purification of EVs from utricles in this study. Additionally, low yield of vesicles prevents the use of several techniques which require high vesicle concentration in solution, including fluorescent nanoparticle tracking analysis and fluorescence correlation spectroscopy.

As alluded to above, the use of cell lines as a source of EVs makes possible the use of a wide range of techniques for their study and manipulation. With this in mind, exosomes from multiple cell lines were tested for their innate ability to protect utricle hair cells against aminoglycoside-induced death. Most cell types investigated were identified as somewhat analogous to supporting cells: HEI-OC1 inner ear progenitor cells, C8-B4 microglia, and C8-D1A astrocytes. The CT26 cell line was investigated as it had previously been reported to produce exosomes expressing HSP70 on their surface, and this exosome-associated HSP70 was additionally shown to bind cell surface receptors, specifically toll-like receptor 2 (Chalmin et al., 2010). Of these cell lines, the CT26 cells were the only ones to produce small EVs which could improve the survival of hair cells exposed to neomycin. That this result was repeatable across two purification methods helps

rule out confounding effects of a sample contaminant/co-isolate. It is tempting to ascribe the innate protective ability of CT26 small EVs to the activity of surface HSP70, but further work needs to be done to prove this mechanism. Further use of the HSP70 function-blocking antibody and/or manipulation of HSP70 expression in the CT26 cells should help test this hypothesis.

The different biological activity of small EVs from different cell sources presents an opportunity to identify proteins critical to EV-mediated protection of hair cells. Small EVs isolated from CT26 cells were found to promote the survival of hair cells *in vitro*, and this activity was not observed with small EVs from the three other cell lines investigated. Differential proteomics between CT26-derived EVs and EVs from at least one other non-protective cell line should allow for the identification of those proteins which are either unique to or significantly more abundant in CT26 exosomes. This group of proteins would be expected to include those proteins which play a role in the unique ability of CT26 EVs to protect hair cells. Such proteins could either be critical pro-survival proteins or proteins critical to the ability of small EVs to interact with the hair cell.

Regardless of the exact mechanism of protection, the results of this experiment demonstrate that small EVs from cell lines can interact with and exert biological activity on cells of intact inner ear tissue. These cell line sources are scalable and could thus be used to produce small EVs designed for future therapeutic applications. Beyond any innate protective properties, small EVs may hold potential as a method of delivery of a wide range of therapeutic moieties to the inner ear, including proteins, genetic material, and small molecules as EVs properties may be modified by genetic modification of their producing cells or through *ex vivo* physical methods (Fais et al., 2016, E. L. Andaloussi et al., 2013, Gyorgy et al., 2015). These applications are an area of intense investigation in other

fields, but represent a currently unexplored area of research in the auditory field. Understanding the compositional differences between the protective and non-protective vesicles observed in this study may help guide the development of small EVs which are able to interact with and act upon inner ear cells. The EV purification and labeling strategies detailed in this chapter should also prove useful for the development of such therapies.

4.5 OUTLOOK

Two lines of continuing investigation follow from the work presented in this chapter: further investigation of the mechanism whereby exosomes help mediate hair cell protection in the inner ear, and initial steps to develop small-EV based therapeutics for the inner ear. A number of ongoing and proposed experiments designed to further describe the role of exosomes in mediating hair cell protection have been described in the previous section and include: knockdown of proteins which may be required for exosome release such as neutral sphingomyelinase, CD9, or Rab27 proteins; direct visualization of proteins of interest (HSP70, CD9, clusterin) via immunoelectron microscopy of isolated exosomes; and further clarification of the cell type-specific contributions of vesicles via an inverse mTmG labeling strategy.

Additionally, the downstream effects induced by exosomes remain unclear. It is unknown which cell types are affected and in what ways. One approach to answer these questions is through single-cell RNA sequencing of utricles which have been exposed to exosomes from heat-shocked utricles—either via co-culture or application of purified exosomes. Our laboratory has developed a set of techniques for performing single-cell RNA-sequencing on the utricle, and is therefore positioned to perform such a study. A similar proteomics-based approach could also be utilized. More targeted investigations of downstream changes based upon the proposed model are already underway by other members of the laboratory.

In regard to development of small-EV based therapeutics for the inner ear, an initial hurdle is successful targeting of the cell type of interest. This may require screening of EVs from many different sources, as has been the approach for identifying appropriate viral vectors for inner ear application (Shu et al., 2016). The integrin profile of EVs may be an important consideration as the integrin profile of exosomes from tumor cells has been shown to determine their tissue tropism

(Hoshino et al., 2015). HEK 239T cell EVs may be a promising candidate as their association with adeno-associated virus has been shown to improve viral infection rates in the inner ear (Gyorgy et al., 2017). Though the use of exosomes as a drug delivery platform in the inner ear remains entirely unexplored, they may hold several advantages over existing delivery methods. Exosomes appear minimally immunogenic, can have a long half-life *in vivo*, and can be modified to target specific tissues following systemic administration (Vader et al., 2016, Luan et al., 2017, Alvarez-Erviti et al., 2011).

5 SUMMARY OF FINDINGS

The results presented in this thesis together help advance current understanding of how clinical ototoxicity occurs and how it may be overcome. The major findings of each chapter are as follows:

2 Modeling Cisplatin Ototoxicity in the Mouse

- A multi-cycle mouse model of cisplatin ototoxicity accurately recreates the nature of hearing loss and pathological changes experienced by cisplatin chemotherapy patients
- Mice have improved survival rates and more consistent hearing loss than in previous models

3 The Role of Cisplatin Pharmacokinetics in Cisplatin Ototoxicity

- Cisplatin accumulates and is selectively retained in the cochlea as compared to most other organs, and this may drive ototoxicity
- The stria vascularis is the cochlear region which experiences the highest tissue levels of cisplatin and it represents both a site of damage as well as a potentially key site of intervention
- ICP-MS-based techniques will continue to provide new insights into mechanisms of cisplatin ototoxicity and can be leveraged in the development of preventive therapies

4 Sensory Hair Cell Protection Against Aminoglycoside Antibiotics

- Supporting cells seem to confer protection against aminoglycoside ototoxicity to hair cells via exosomes carrying HSP70
- Hair cell protection can be achieved through application of exogenous small extracellular vesicles derived from cell lines, suggesting the potential utility of extracellular vesicles for delivery of inner ear therapeutics

Significant further investigation is required if clinical ototoxicity is to be fully addressed, however, the use of ototoxic drugs is likely to persist. Clinical ototoxicity has existed in plain sight for several decades and continues to affect the lives of millions of new patients yearly.

6 SUPPLEMENTAL DATA

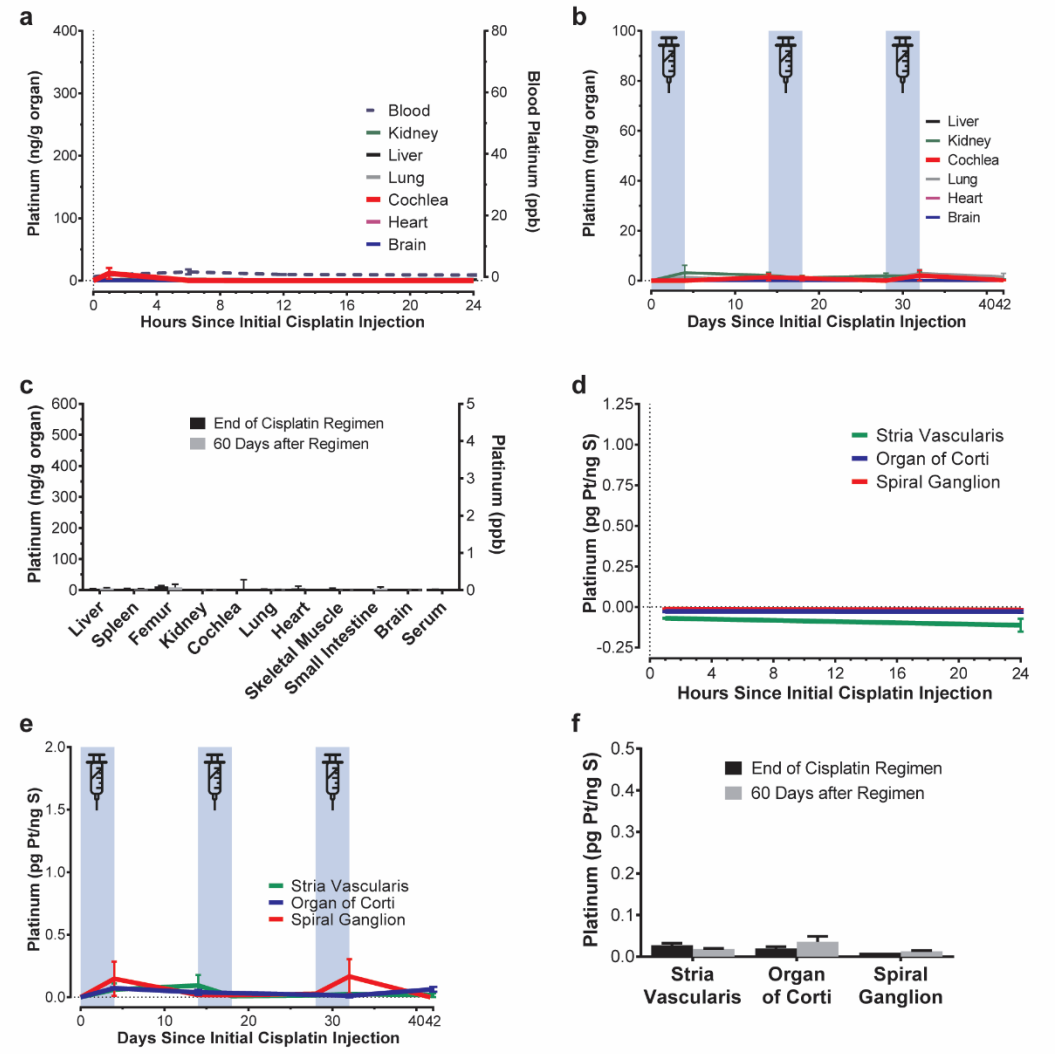


Figure S 1: Platinum levels measured in saline-treated control mice

Background concentrations of platinum are exceedingly low in all samples from saline-treated control mice. (a) Concentrations of platinum in isolated whole organs from the first 24 hours following a single i.p. injection of saline. Compare to Figure 3.5. n = 3 mice per time point. (b) Measured concentrations of platinum in whole mouse organs throughout the complete saline control regimen. Compare to Figure 3.6. n = 3 mice per time point. (c) Concentrations of platinum in whole mouse organs at the end of the saline regimen and following a subsequent 60-day recovery. Compare to Figure 3.7. n = 3-4 mice in each group. (d) Platinum measured in microdissected regions of the mouse cochlea during the first 24 hours following a single i.p. injection of saline. Compare to Figure 3.8. n = 3 mice at each time point. (e) Concentrations of platinum in microdissected regions of the mouse cochlea throughout the complete saline control regimen. Compare to Figure 3.9. n = 3 mice at each time point. (f) Concentrations of platinum in cochlear regions at the end of the saline regimen and following a subsequent 60-day recovery. Compare to Figure 3.10. n = 4-7 mice. Mean ± s.e.m. are shown.

Gene Name	Ratio (Heat Shock:Control)	Log2 Ratio	Score	Majority protein IDs
H2afz;Hist1h2al;Hist1h2aa;Hist1h2ah;H2afv;H2afj;Hist2h2ac;Hist1h2ak;Hist1h2af;Hist3h2a;Hist2h2aa1;Hist2h2ab;Hist1h2ab;H2afx	76.57132769	6.258732368	30.756	G3UWL7;Q3UA95;F8WIX8;A0A0N4SV66;Q8CGP4;Q8CGP6;Q3THW5;P0C0S6;Q8R1M2;Q64523;Q8CGP7;Q8CGP5;Q8BFU2;Q6GSS7;Q64522;P22752;P27661
Hist1h2br;Hist3h2ba;Hist1h2bp;Hist1h2bk;Hist3h2bb;Hist1h2bc;Hist2h2bb;Hist2h2be;Hist1h2bh;Hist1h2bb;Hist1h2bm;Hist1h2bf;Hist1h2ba	65.30058	6.029023901	4.6356	Q8CBB6;Q9D2U9;Q8CGP2;Q8CGP1;Q8CGP0;Q6ZWY9;Q64525;Q64524;Q64478;Q64475;P10854;P10853;P70696;Q8CGP2-2
Hist1h4a	52.49633385	5.714144769	19.49	P62806
Tnc	46.65448615	5.543943908	4.4675	Q80YX1-5;Q80YX1-4;Q80YX1-3;Q80YX1-2;Q80YX1
Abca13	33.96129138	5.085819414	34.277	Q5SSE9-2;Q5SSE9
Otoa	31.86608369	4.993949819	8.4159	Q8K561;E9PVT3
Lgals3bp	25.05846892	4.647226363	2.7984	Q07797
Otogl	24.13396077	4.592992799	323.31	F7A4A7-2;F7A4A7
Otog	23.18339246	4.535019788	323.31	G3UWC8;O55225
Lamb1	18.61365308	4.218289318	37.96	E9QN70;P02469
Clu	17.59666185	4.137229865	4.555	Q06890
Csf1	16.89024169	4.078118068	5.6933	D3YTW1;D3Z090;F6RNW8;P07141-2;P07141
Lama4	15.99559338	3.999602608	3.5801	P97927
Lama2	15.87938015	3.989082693	215.7	Q60675
Lamc1	14.09381154	3.816989923	170.88	F8VQJ3;P02468
Cep112	13.56318092	3.761623663	3.1688	I7HPW3;A2ABQ5;S4R1I4;J3JS86;Q5PR68
Lamb2	12.23586954	3.613044725	18.522	Q61292
Tectb	11.40760831	3.511924446	225.66	D3Z3Y6;O08524;F6Z818
Hspg2	11.10922492	3.47368626	31.527	B1B0C7;E9PZ16;Q05793
Cd9	10.99509077	3.458787609	9.8402	P40240
Tecta	10.99236646	3.458430101	44.552	O08523-2;O08523
Col15a1	10.57658692	3.402802238	139.1	A2AJY2;O35206;A2AJY7;A2AJY5
Acan	8.662868308	3.114844786	217.75	Q61282
Mfn2	8.595800154	3.103631942	2.9617	Q80U63-2;Q80U63
Hba	7.836937077	2.970289914	26.269	Q91VB8;P01942
Tfrc	7.106535846	2.829146475	4.3527	Q8C872;Q62351
Ppl	6.145715538	2.619580992	2.6971	G5E898
Gm8797;Uba52;Kxd1;Ubc;Ubb;Rps27a;Gm5239	5.218088769	2.383521487	323.31	A0A0A6YW67;E9Q9J0;E9Q4P0;E9Q5F6;E9QNP0;Q5SX22;P62984;P62983;P0CG49;P0CG50;D3YYZ2
Rrp7a	5.034914923	2.331967401	14.739	F6VVA3;Q9D1C9
Actg1;Actb;Actg2;Acta1;Actc1;Acta2	4.972470923	2.313962935	147.44	P63260;P60710;E9Q5F4;G3UZ07;E9Q1F2;P63268;P68134;P68033;P62737;G3UYG0;E9Q606;D3Z2K3;D3YZY0
Cyp2c70	4.915224615	2.297257346	2.5736	Q91W64
Krt76	4.819766308	2.268963197	12.972	Q3UV17
Coch	4.764061385	2.252192002	323.31	Q62507
Try10	4.705954769	2.234487454	10.576	Q792Z1
Fhdc1	4.583504308	2.196451029	2.9044	Q3ULZ2
Slc17a5	4.476503538	2.162372327	2.8087	Q8BN82-2;Q8BN82
Sepp1	4.159587692	2.056440532	3.7587	E0CX80;E0CZC5;P70274
Enpp2	4.054450923	2.01950655	9.3169	Q9R1E6;Q9R1E6-3;G3UXY9;Q9R1E6-2
Igkv6-29;Igkv7-33	3.834068769	1.938876214	3.7026	A0A075B5N2;A0A140T8P2;A0A0G2JEI6;A0A075B5N1;A0A0G2JDJ8;P01657;P01632;P01634
Vcl	3.816790923	1.93236016	22.111	Q64727
Hpx	3.792164615	1.923021592	50.613	Q91X72
Hp	3.544213185	1.825465385	34.649	Q61646
Prss1	3.492074954	1.804084525	14.581	Q9Z1R9
Igkv8-28	3.482912677	1.800294302	3.7993	A0A075B5N3;A0A0G2JE47;A0A140T8P5
Plg	3.474811446	1.796934695	3.6483	P20918
Eps15	3.444428246	1.784264524	3.4081	F6W2Q5;Q5JC28;H3BK65;P42567;A0A0R4J0A0;P42567-2
Cfi	3.263785138	1.706546085	55.873	Q61129;A0A0G2JF07
Gal3st1	3.162430138	1.661033609	3.4372	Q9JHE4
Ppip5k1	3.085131492	1.62533198	3.3438	A2ARP1-3;A2ARP1-2;A2ARP1
Igkv1-110;Igkv1-35;Igkv1-99;Igkv1-115	3.0830094	1.624339288	21.614	A0A140T8M9;A0A140T8M0;A0A0B4J1I0;A0A075B5N0;A0A075B5K8;F6XWB2;A0A140T8N1;A0A0G2JDE5;P01631
	3.045033985	1.60645833	68.707	P18528
Aldoa;Aldoart2	3.037810985	1.603032107	57.94	D3Z510;A0A0U1RPN8;D3YV98;A0A0U1RPT5;D3YWI1;A6ZI47;A6ZI44;P05064
Serpina1f	3.0249924	1.596931518	3.0566	E9PUC6;G3X9Z5;Q9DCQ7-2;Q9DCQ7
Cpb2	2.986185354	1.578303717	39.152	Q9JHH6
Igkv8-27	2.958092723	1.564667275	27.422	A0A075B5N4;A0A140T8P7;A0A0G2JF28;A0A140T8M3;A0A140T8M4;A0A140T8N7;A0A140T8N5;A0A0G2JFN8
Smtn	2.933401892	1.552574742	2.6267	D3YVS1;D3Z3Q3;Q921U8-4;Q921U8-3;Q921U8-2;Q921U8
Ttn	2.769326877	1.469535352	3.1641	E9Q8N1;E9Q8K5;A2ASS6-2;A2ASS6
Cfb;Gm20547	2.768685231	1.469201044	59.663	H3BK95;B8JJM5;F6VQX8;B8JJN0;P04186;B8JJM3;F6W2T4;F6XQ00;B8JJM6
S100b	2.282468	1.190594634	225.91	P50114
Apc2	2.244732754	1.166543695	4.4134	D3YYQ9;G5E832;Q9Z1K7;D3Z3K9;D3Z344;D3YTR0
Apoc1	2.089422123	1.063103988	6.2605	P34928
Gm20425;Tf;Trf	1.857314692	0.893218278	6.6531	E9Q035;Q921I1;F7CJN9;F7BAE9
2210010C04Rik	1.763128923	0.818137971	4.4478	Q9CPN9

Figure S 2: Proteins identified in utricle EVs via mass spectrometry

Gene Name	Ratio (Heat Shock:Control)	Log2 Ratio	Score	Majority protein IDs
Igkv8-27	17.46037477	4.12601262	27.422	A0A075B5N4;A0A140T8P7;A0A0G2JF28;A0A140T8M3;A0A140T8M4;A0A140T8N7;A0A140T8N5;A0A0G2JFN8
Smtn	10.38778523	3.376816186	2.6267	D3YVS1;D3Z3Q3;Q921U8-4;Q921U8-3;Q921U8-2;Q921U8
2210010C04Rik	6.727749538	2.750123998	4.4478	Q9CPN9
Hpx	5.240743538	2.389771511	50.613	Q91X72
Cfi	3.819802	1.933497858	55.873	Q61129;A0A0G2JF07
Ttn	3.750726462	1.907170052	3.1641	E9Q8N1;E9Q8K5;A2ASS6-2;A2ASS6
S100a1	3.638958154	1.863525461	4.0147	Q91V77;P56565
Apc2	3.451722938	1.787316667	4.4134	D3YYQ9;G5E832;Q9Z1K7;D3Z3K9;D3Z344;D3YTR0
Ralbp1	3.269144138	1.708912988	3.0939	Q62172
Igkv1-110;Igkv1-35;Igkv1-99;Igkv1-115	3.2611146	1.70536514	21.614	A0A140T8M9;A0A140T8M0;A0A0B4J1I0;A0A075B5N0;A0A075B5K8;F6XWB2;A0A140T8N1;A0A0G2JDE5;P01631
1300017J02Rik;Ica	2.506022538	1.32539939	11.258	D3YY36;Q9DBD0;D3Z4X8
Park7	2.444833154	1.289736013	16.887	A2A817;A2A816;A2A815;A2A813;Q99LX0
Ywhaz	2.410474615	1.269317237	50.719	P63101
Ywhae	2.386242615	1.254740733	14.787	P62259;F6WA09
Sod1	2.250937723	1.170526142	11.788	P08228
Ca3	2.197534123	1.135885568	108.24	P16015
Prdx6	2.188411277	1.129883895	3.0303	D3Z0Y2;Q6GT24;O08709
Prdx1	1.9614872	0.971947921	8.2582	B1AXW5;B1AXW6;P35700
Ldhb	1.926383062	0.945894612	84.141	P16125;A0A0N4SVV8;D3Z7F0
Pgam1	1.905391554	0.930087499	7.4527	Q9DBJ1
Gsta4	1.901351692	0.927025411	6.7434	P24472
Glo1	1.712259646	0.775901488	3.1938	Q9CPU0
Pebp1	1.668426969	0.738488538	140.24	P70296;D6RHS6;D3Z1V4
S100b	1.536351815	0.619508622	225.91	P50114
Calm1	1.475391846	0.561098168	68.472	P62204;Q3UKW2
Skp1	1.446517769	0.532584046	9.7248	Q9WTX5
Ckb	1.399200846	0.484603067	323.31	Q04447
Dbi	1.3950642	0.480331516	56.783	P31786;M0QWU8;Q4VWZ5
Fbxo2	1.358067385	0.441555065	3.6419	Q80UW2
Ldha	1.347905	0.430718819	4.8844	A0A1B0GSR9;Q564E2;A0A1B0GSX0;P06151
Mdh1	1.204144	0.26800793	10.262	P14152
Slc12a2	1.076008338	0.105689258	44.712	E9QM38;P55012
Gm8797;Uba52;Kxd1;Ubc;Ubb;Rps27a;Gm5239	0.962856369	-0.05460749	323.31	UBIQUITIN;A0A0A6YW67;E9Q9J0;E9Q4P0;E9Q5F6;E9QNP0;Q5SX22;P62984;P62983;P0CG49;P0CG50;D3YYZ2
Actg1;Actb;Actg2;Acta1;Actc1;Acta2	0.884346123	-0.17731696	147.44	P63260;P60710;E9Q5F4;G3UZ07;E9Q1F2;P63268;P68134;P68033;P62737;G3UYG0;E9Q606;D3Z2K3;D3YZY0
Sptbn1	0.859124769	-0.21906043	3.5399	A0A0A0MQG2;Q62261-2;Q62261
Got2	0.826938508	-0.27414804	72.89	P05202
Gsn	0.763171785	-0.38992026	117.95	P13020-2;P13020;A0A0J9YUQ8
Cst6	0.761289862	-0.39348223	8.7681	Q9D1B1
C3	0.726440231	-0.46108399	2.97	P01027
Mdh2	0.718475215	-0.4769897	89.166	P08249
Sparc	0.683331646	-0.54934215	31.3	Q5NCU4;A0A1L1SSH9;P07214
Lcn2	0.661089108	-0.59708335	12.633	A0A0A6YW77;P11672
Coch	0.657149615	-0.60570622	323.31	Q62507
Ptgds	0.610345292	-0.71230244	192.53	O09114-2;O09114
Orm3;Orm1;Orm2	0.544277246	-0.87758637	2.8779	J3JRU4;Q63805;Q60590;P07361
Spp1	0.474355738	-1.07595869	37.773	D3Z4N2;F8WIP8;P10923;D3Z513
Ctsb	0.471509554	-1.08464109	56.488	P10605
Cst3	0.450112985	-1.15164091	65.834	A2APX3;P21460
Serpina3n	0.218774095	-2.19248617	3.8281	G3X8T9;Q91WP6
Hspe1	0.210192168	-2.25021918	8.8256	Q64433
Gm20425;Tf;Trf	0.149496026	-2.74182096	6.6531	E9Q035;Q921I1;F7CJN9;F7BAE9

Figure S 3: Proteins identified in non-vesicle fractions of utricle conditioned medium via mass spectrometry

7 REFERENCES

AL-KHATIB, T., COHEN, N., CARRET, A. S. & DANIEL, S. 2010. Cisplatinum ototoxicity in children, long-term follow up. *Int J Pediatr Otorhinolaryngol,* 74**,** 913-9.

ALAM, S. A., IKEDA, K., OSHIMA, T., SUZUKI, M., KAWASE, T., KIKUCHI, T. & TAKASAKA, T. 2000. Cisplatin-induced apoptotic cell death in Mongolian gerbil cochlea. *Hear Res,* 141**,** 28-38.

ALHARAZNEH, A., LUK, L., HUTH, M., MONFARED, A., STEYGER, P. S., CHENG, A. G. & RICCI, A. J. 2011. Functional hair cell mechanotransducer channels are required for aminoglycoside ototoxicity. *PLoS One,* 6**,** e22347.

ALVAREZ-ERVITI, L., SEOW, Y., YIN, H., BETTS, C., LAKHAL, S. & WOOD, M. J. 2011. Delivery of siRNA to the mouse brain by systemic injection of targeted exosomes. *Nat Biotechnol,* 29**,** 341-5.

ANDREU, Z. & YANEZ-MO, M. 2014. Tetraspanins in extracellular vesicle formation and function. *Front Immunol,* 5**,** 442.

ARAYA-SECCHI, R., NEEL, B. L. & SOTOMAYOR, M. 2016. An elastic element in the protocadherin-15 tip link of the inner ear. *Nature communications,* 7**,** 13458.

ARENZ, C. & GIANNIS, A. 2000. Synthesis of the First Selective Irreversible Inhibitor of Neutral Sphingomyelinase. *Angew Chem Int Ed Engl,* 39**,** 1440-1442.

ARLINGER, S. 2003. Negative consequences of uncorrected hearing loss--a review. *Int J Audiol,* 42 Suppl 2**,** 2S17-20.

ARNESANO, F., SCINTILLA, S. & NATILE, G. 2007. Interaction between platinum complexes and a methionine motif found in copper transport proteins. *Angewandte Chemie,* 119**,** 9220-9222.

ARRIGO, A. P. 2017. Mammalian HspB1 (Hsp27) is a molecular sensor linked to the physiology and environment of the cell. *Cell Stress Chaperones,* 22**,** 517-529.

ASHMORE, J. F. 1987. A fast motile response in guinea-pig outer hair cells: the cellular basis of the cochlear amplifier. *J Physiol,* 388**,** 323-47.

ASSAD, J. A., SHEPHERD, G. M. & COREY, D. P. 1991. Tip-link integrity and mechanical transduction in vertebrate hair cells. *Neuron,* 7**,** 985-994.

BAIRD, R., STEYGER, P. & SCHUFF, N. 1996. Mitotic and nonmitotic hair cell regeneration in the bullfrog vestibular otolith organs. *Annals of the New York Academy of Sciences,* 781**,** 59-70.

BAJORIN, D. F., SAROSDY, M. F., PFISTER, D. G., MAZUMDAR, M., MOTZER, R. J., SCHER, H. I., GELLER, N. L., FAIR, W. R., HERR, H., SOGANI, P. & ET AL. 1993. Randomized trial of etoposide and cisplatin versus etoposide and carboplatin in patients with good-risk germ cell tumors: a multiinstitutional study. *J Clin Oncol,* 11**,** 598-606.

BASU, S., BINDER, R. J., SUTO, R., ANDERSON, K. M. & SRIVASTAVA, P. K. 2000. Necrotic but not apoptotic cell death releases heat shock proteins, which deliver a partial maturation signal to dendritic cells and activate the NF-kappa B pathway. *Int Immunol,* 12**,** 1539-46.

BENEDETTI PANICI, P., GREGGI, S., SCAMBIA, G., BAIOCCHI, G., LOMONACO, M., CONTI, G. & MANCUSO, S. 1993. Efficacy and toxicity of very high-dose cisplatin in advanced ovarian carcinoma: 4-year survival analysis and neurological follow-up. *Int J Gynecol Cancer,* 3**,** 44-53.

BERGLUND, A. & RYUGO, D. 1987. Hair cell innervation by spiral ganglion neurons in the mouse. *Journal of Comparative Neurology,* 255**,** 560-570.

BERNERS-PRICE, S. J., FRENKIEL, T. A., FREY, U., RANFORD, J. D. & SADLER, P. J. 1992. Hydrolysis products of cisplatin: pKa determinations via[1H, 15N] NMR spectroscopy. *Journal of the Chemical Society, Chemical Communications***,** 789-791.

BERTOLINI, P., LASSALLE, M., MERCIER, G., RAQUIN, M. A., IZZI, G., CORRADINI, N. & HARTMANN, O. 2004. Platinum Compound-Related Ototoxicity in Children: Long-Term Follow-Up Reveals Continuous Worsening of Hearing Loss. *J Pediatr Hematol Oncol,* 26**,** 649-655.

BETTS, J. G., COLLEGE, O., DESAIX, P., JOHNSON, J. E., JOHNSON, E. W., KOROL, O., KRUSE, D., POE, B., WISE, J. & WOMBLE, M. D. 2013. *Anatomy and Physiology*, OpenStax College.

BIRD, J. E., DAUDET, N., WARCHOL, M. E. & GALE, J. E. 2010. Supporting cells eliminate dying sensory hair cells to maintain epithelial integrity in the avian inner ear. *J Neurosci,* 30**,** 12545-56.

BOBRIE, A., COLOMBO, M., KRUMEICH, S., RAPOSO, G. & THERY, C. 2012a. Diverse subpopulations of vesicles secreted by different intracellular mechanisms are present in exosome preparations obtained by differential ultracentrifugation. *J Extracell Vesicles,* 1.

BOBRIE, A., KRUMEICH, S., REYAL, F., RECCHI, C., MOITA, L. F., SEABRA, M. C., OSTROWSKI, M. & THERY, C. 2012b. Rab27a supports exosome-dependent and -independent mechanisms that modify the tumor microenvironment and can promote tumor progression. *Cancer Res,* 72**,** 4920-30.

BOER, H., PROOST, J. H., NUVER, J., BUNSKOEK, S., GIETEMA, J. Q., GEUBELS, B. M., ALTENA, R., ZWART, N., OOSTING, S. F., VONK, J. M., LEFRANDT, J. D., UGES,

D. R., MEIJER, C., DE VRIES, E. G. & GIETEMA, J. A. 2015. Long-term exposure to circulating platinum is associated with late effects of treatment in testicular cancer survivors. *Ann Oncol,* 26**,** 2305-10.

BOERSEMA, P. J., RAIJMAKERS, R., LEMEER, S., MOHAMMED, S. & HECK, A. J. 2009. Multiplex peptide stable isotope dimethyl labeling for quantitative proteomics. *Nat Protoc,* 4**,** 484-94.

BOHNE, B. A. & RABBITT, K. D. 1983. Holes in the reticular lamina after noise exposure: implication for continuing damage in the organ of Corti. *Hearing research,* 11**,** 41-53.

BOKEMEYER, C., BERGER, C. C., HARTMANN, J. T., KOLLMANNSBERGER, C., SCHMOLL, H. J., KUCZYK, M. A. & KANZ, L. 1998. Analysis of risk factors for cisplatin-induced ototoxicity in patients with testicular cancer. *Br J Cancer,* 77**,** 1355-62.

BOKEMEYER, C., KOHRMANN, O., TISCHLER, J., WEISSBACH, L., RATH, U., HAUPT, A., SCHOFFSKI, P., HARSTRICK, A. & SCHMOLL, H. J. 1996. A randomized trial of cisplatin, etoposide and bleomycin (PEB) versus carboplatin, etoposide and bleomycin (CEB) for patients with 'good-risk' metastatic non-seminomatous germ cell tumors. *Ann Oncol,* 7**,** 1015-21.

BRANDON, C. S., VOELKEL-JOHNSON, C., MAY, L. A. & CUNNINGHAM, L. L. 2012. Dissection of adult mouse utricle and adenovirus-mediated supporting-cell infection. *J Vis Exp*.

BROWNELL, W. E., BADER, C. R., BERTRAND, D. & DE RIBAUPIERRE, Y. 1985. Evoked mechanical responses of isolated cochlear outer hair cells. *Science,* 227**,** 194-6.

BURNS, J. C., KELLY, M. C., HOA, M., MORELL, R. J. & KELLEY, M. W. 2015. Single-cell RNA-Seq resolves cellular complexity in sensory organs from the neonatal inner ear. *Nat Commun,* 6**,** 8557.

BURNS, J. C., ON, D., BAKER, W., COLLADO, M. S. & CORWIN, J. T. 2012. Over half the hair cells in the mouse utricle first appear after birth, with significant numbers originating from early postnatal mitotic production in peripheral and striolar growth zones. *J Assoc Res Otolaryngol,* 13**,** 609-27.

BUSCHOW, S. I., NOLTE-'T HOEN, E. N., VAN NIEL, G., POLS, M. S., TEN BROEKE, T., LAUWEN, M., OSSENDORP, F., MELIEF, C. J., RAPOSO, G., WUBBOLTS, R., WAUBEN, M. H. & STOORVOGEL, W. 2009. MHC II in dendritic cells is targeted to lysosomes or T cell-induced exosomes via distinct multivesicular body pathways. *Traffic,* 10**,** 1528-42.

CALDERWOOD, S. K., GONG, J. & MURSHID, A. 2016. Extracellular HSPs: The Complicated Roles of Extracellular HSPs in Immunity. *Front Immunol,* 7**,** 159.

CALDERWOOD, S. K., THERIAULT, J., GRAY, P. J. & GONG, J. 2007. Cell surface receptors for molecular chaperones. *Methods,* 43**,** 199-206.

CAMPBELL, K., MEECH, R. P., RYBAK, L. P. & HUGHES, L. F. 2003. The effect of D-methionine on cochlear oxidative state with and without cisplatin administration: mechanisms of otoprotection. *Journal of the American Academy of Audiology,* 14**,** 144-156.

CARDINAAL, R. M., DE GROOT, J. C., HUIZING, E. H., VELDMAN, J. E. & SMOORENBURG, G. F. 2000. Cisplatin-induced ototoxicity: morphological evidence of spontaneous outer hair cell recovery in albino guinea pigs? *Hear Res,* 144**,** 147-56.

CARVER, J. A., REKAS, A., THORN, D. C. & WILSON, M. R. 2003. Small heat-shock proteins and clusterin: intra- and extracellular molecular chaperones with a common mechanism of action and function? *IUBMB Life,* 55**,** 661-8.

CASANO, R. A., JOHNSON, D. F., BYKHOVSKAYA, Y., TORRICELLI, F., BIGOZZI, M. & FISCHEL-GHODSIAN, N. 1999. Inherited susceptibility to aminoglycoside ototoxicity: genetic heterogeneity and clinical implications. *Am J Otolaryngol,* 20**,** 151-6.

CASIMIRO, M. C., KNOLLMANN, B. C., EBERT, S. N., VARY, J. C., JR., GREENE, A. E., FRANZ, M. R., GRINBERG, A., HUANG, S. P. & PFEIFER, K. 2001. Targeted disruption of the Kcnq1 gene produces a mouse model of Jervell and Lange-Nielsen Syndrome. *Proc Natl Acad Sci U S A,* 98**,** 2526-31.

CEDERROTH, C. R. 2012. Loss of aminoglycoside sensitivity in HEI-OC1 cells? *Hear Res,* 292**,** 83-5; author response pg 86.

CHAIROUNGDUA, A., SMITH, D. L., POCHARD, P., HULL, M. & CAPLAN, M. J. 2010. Exosome release of beta-catenin: a novel mechanism that antagonizes Wnt signaling. *J Cell Biol,* 190**,** 1079-91.

CHALMIN, F., LADOIRE, S., MIGNOT, G., VINCENT, J., BRUCHARD, M., REMY-MARTIN, J. P., BOIREAU, W., ROULEAU, A., SIMON, B., LANNEAU, D., DE THONEL, A., MULTHOFF, G., HAMMAN, A., MARTIN, F., CHAUFFERT, B., SOLARY, E., ZITVOGEL, L., GARRIDO, C., RYFFEL, B., BORG, C., APETOH, L., REBE, C. & GHIRINGHELLI, F. 2010. Membrane-associated Hsp72 from tumor-derived exosomes mediates STAT3-dependent immunosuppressive function of mouse and human myeloid-derived suppressor cells. *J Clin Invest,* 120**,** 457-71.

CHANG, Q., ORNATSKY, O. I., SIDDIQUI, I., LOBODA, A., BARANOV, V. I. & HEDLEY, D. W. 2017. Imaging Mass Cytometry. *Cytometry A,* 91**,** 160-169.

CHANG, Q., ORNATSKY, O. I., SIDDIQUI, I., STRAUS, R., BARANOV, V. I. & HEDLEY, D. W. 2016. Biodistribution of cisplatin revealed by imaging mass cytometry identifies extensive collagen binding in tumor and normal tissues. *Sci Rep,* 6**,** 36641.

CHEN, F. Q., HILL, K., GUAN, Y. J., SCHACHT, J. & SHA, S. H. 2012. Activation of apoptotic pathways in the absence of cell death in an inner-ear immortomouse cell line. *Hear Res,* 284**,** 33-41.

CHOE, W.-T., CHINOSORNVATANA, N. & CHANG, K. W. 2004. Prevention of cisplatin ototoxicity using transtympanic N-acetylcysteine and lactate. *Otology & Neurotology,* 25**,** 910-915.

CHU, Y. H., SIBRIAN-VAZQUEZ, M., ESCOBEDO, J. O., PHILLIPS, A. R., DICKEY, D. T., WANG, Q., RALLE, M., STEYGER, P. S. & STRONGIN, R. M. 2016. Systemic Delivery and Biodistribution of Cisplatin in Vivo. *Mol Pharm,* 13**,** 2677-82.

CIANFRONE, G., PENTANGELO, D., CIANFRONE, F., MAZZEI, F., TURCHETTA, R., ORLANDO, M. P. & ALTISSIMI, G. 2011. Pharmacological drugs inducing ototoxicity, vestibular symptoms and tinnitus: a reasoned and updated guide. *Eur Rev Med Pharmacol Sci,* 15**,** 601-36.

CIARIMBOLI, G., DEUSTER, D., KNIEF, A., SPERLING, M., HOLTKAMP, M., EDEMIR, B., PAVENSTADT, H., LANVERS-KAMINSKY, C., AM ZEHNHOFF-DINNESEN, A., SCHINKEL, A. H., KOEPSELL, H., JURGENS, H. & SCHLATTER, E. 2010. Organic cation transporter 2 mediates cisplatin-induced oto- and nephrotoxicity and is a target for protective interventions. *Am J Pathol,* 176**,** 1169-80.

CLERICI, W. J., HENSLEY, K., DIMARTINO, D. L. & BUTTERFIELD, D. A. 1996. Direct detection of ototoxicant-induced reactive oxygen species generation in cochlear explants. *Hear Res,* 98**,** 116-24.

COLOMBO, M., RAPOSO, G. & THERY, C. 2014. Biogenesis, secretion, and intercellular interactions of exosomes and other extracellular vesicles. *Annu Rev Cell Dev Biol,* 30**,** 255-89.

COREY, D. & HUDSPETH, A. 1979. Ionic basis of the receptor potential in a vertebrate hair cell. *Nature,* 281**,** 675-677.

COREY, D. & HUDSPETH, A. 1983. Kinetics of the receptor current in bullfrog saccular hair cells. *Journal of Neuroscience,* 3**,** 962-976.

CORTI, A. 1851. *Recherches sur l'organe de l'ouie des mammiferes*.

COX, B. C., CHAI, R., LENOIR, A., LIU, Z., ZHANG, L., NGUYEN, D. H., CHALASANI, K., STEIGELMAN, K. A., FANG, J., RUBEL, E. W., CHENG, A. G. & ZUO, J. 2014. Spontaneous hair cell regeneration in the neonatal mouse cochlea in vivo. *Development,* 141**,** 816-29.

COX, J. & MANN, M. 2008. MaxQuant enables high peptide identification rates, individualized p.p.b.-range mass accuracies and proteome-wide protein quantification. *Nat Biotechnol,* 26**,** 1367-72.

CRIDER, S. E., HOLBROOK, R. J. & FRANZ, K. J. 2010. Coordination of platinum therapeutic agents to met-rich motifs of human copper transport protein1. *Metallomics,* 2**,** 74-83.

CROUCH, J. J., SAKAGUCHI, N., LYTLE, C. & SCHULTE, B. A. 1997. Immunohistochemical localization of the Na-K-Cl co-transporter (NKCC1) in the gerbil inner ear. *J Histochem Cytochem,* 45**,** 773-8.

CUNNINGHAM, L. L. 2006. The adult mouse utricle as an in vitro preparation for studies of ototoxic-drug-induced sensory hair cell death. *Brain Res,* 1091**,** 277-81.

CURHAN, S. G., EAVEY, R., SHARGORODSKY, J. & CURHAN, G. C. 2010. Analgesic use and the risk of hearing loss in men. *Am J Med,* 123**,** 231-7.

DALLOS, P. & FAY, R. R. 2012. *The Cochlea*, Springer New York.

DANNHOF, B. J. & BRUNS, V. 1993. The innervation of the organ of Corti in the rat. *Hearing research,* 66**,** 8-22.

DAUGAARD, M., ROHDE, M. & JAATTELA, M. 2007. The heat shock protein 70 family: Highly homologous proteins with overlapping and distinct functions. *FEBS Lett,* 581**,** 3702-10.

DAVIES, H. R., CADAR, D., HERBERT, A., ORRELL, M. & STEPTOE, A. 2017. Hearing Impairment and Incident Dementia: Findings from the English Longitudinal Study of Ageing. *J Am Geriatr Soc*.

DAVIS, H. 1953. Energy into nerve impulses: the inner ear. *Adv. Sci,* 9**,** 420-425.

DE BOER, E. 1991. Auditory physics. Physical principles in hearing theory. III. *Physics Reports,* 203**,** 125-231.

DE MAIO, A. 2014. Extracellular Hsp70: export and function. *Curr Protein Pept Sci,* 15**,** 225-31.

DE MAIO, A. & VAZQUEZ, D. 2013. Extracellular heat shock proteins: a new location, a new function. *Shock,* 40**,** 239-46.

DENMAN-JOHNSON, K. & FORGE, A. 1999. Establishment of hair bundle polarity and orientation in the developing vestibular system of the mouse. *Journal of neurocytology,* 28**,** 821-835.

DESAI, S. S., ZEH, C. & LYSAKOWSKI, A. 2005. Comparative morphology of rodent vestibular periphery. I. Saccular and utricular maculae. *Journal of Neurophysiology,* 93**,** 251-266.

DESANTIS, C. E., LIN, C. C., MARIOTTO, A. B., SIEGEL, R. L., STEIN, K. D., KRAMER, J. L., ALTERI, R., ROBBINS, A. S. & JEMAL, A. 2014. Cancer treatment and survivorship statistics, 2014. *CA Cancer J Clin,* 64**,** 252-71.

DEVARAJAN, P., SAVOCA, M., CASTANEDA, M. P., PARK, M. S., ESTEBAN-CRUCIANI, N., KALINEC, G. & KALINEC, F. 2002. Cisplatin-induced apoptosis in auditory cells: role of death receptor and mitochondrial pathways. *Hear Res,* 174**,** 45-54.

DIJKGRAAF, S. 1963. The functioning and significance of the lateral-line organs. *Biological Reviews,* 38**,** 51-105.

DRAGOVIC, R. A., GARDINER, C., BROOKS, A. S., TANNETTA, D. S., FERGUSON, D. J., HOLE, P., CARR, B., REDMAN, C. W., HARRIS, A. L., DOBSON, P. J., HARRISON, P. & SARGENT, I. L. 2011. Sizing and phenotyping of cellular vesicles using Nanoparticle Tracking Analysis. *Nanomedicine,* 7**,** 780-8.

DULON, D., HIEL, H., AUROUSSEAU, C., ERRE, J. & ARAN, J. 1993. Pharmacokinetics of gentamicin in the sensory hair cells of the organ of Corti: rapid uptake and long term persistence. *Comptes rendus de l'Academie des sciences. Serie III, Sciences de la vie,* 316**,** 682-687.

DURRANT, J. D., CAMPBELL, K., FAUSTI, S., GUTHRIE, O. N., JACOBSON, G., LONSBURY-MARTIN, B. L. & POLING, G. 2009. Position Statement and Clinical Practice Guidelines. American Academy of Audiology.

E. L. ANDALOUSSI, S., MAGER, I., BREAKEFIELD, X. O. & WOOD, M. J. 2013. Extracellular vesicles: biology and emerging therapeutic opportunities. *Nat Rev Drug Discov,* 12**,** 347-57.

EATOCK, R. A., FAY, R. R. & POPPER, A. N. 2006. *Vertebrate hair cells*, Springer.

EATOCK, R. A., XUE, J. & KALLURI, R. 2008. Ion channels in mammalian vestibular afferents may set regularity of firing. *Journal of Experimental Biology,* 211**,** 1764-1774.

ECHANDIA, E. L. R. & BURGOS, M. H. 1965. The fine structure of the stria vascularis of the guinea-pig inner ear. *Zeitschrift für Zellforschung und Mikroskopische Anatomie,* 67**,** 600-619.

ECHTELER, S. M. 1992. Developmental segregation in the afferent projections to mammalian auditory hair cells. *Proceedings of the National Academy of Sciences,* 89**,** 6324-6327.

EKBORN, A., HANSSON, J., EHRSSON, H., EKSBORG, S., WALLIN, I., WAGENIUS, G. & LAURELL, G. 2004. High-Dose Cisplatin With Amifostine: Ototoxicity and Pharmacokinetics. *The Laryngoscope,* 114**,** 1660-1667.

EL KECHAI, N., AGNELY, F., MAMELLE, E., NGUYEN, Y., FERRARY, E. & BOCHOT, A. 2015. Recent advances in local drug delivery to the inner ear. *Int J Pharm,* 494**,** 83-101.

ELFERINK, F., VAN DER VIJGH, W. J., KLEIN, I. & PINEDO, H. M. 1986. Interaction of cisplatin and carboplatin with sodium thiosulfate: reaction rates and protein binding. *Clin Chem,* 32**,** 641-5.

ESTREM, S. A., BABIN, R. W., RYU, J. H. & MOORE, K. C. 1981. Cis-diamminedichloroplatinum (II) ototoxicity in the guinea pig. *Otolaryngol Head Neck Surg,* 89**,** 638-45.

FAIS, S., O'DRISCOLL, L., BORRAS, F. E., BUZAS, E., CAMUSSI, G., CAPPELLO, F., CARVALHO, J., CORDEIRO DA SILVA, A., DEL PORTILLO, H., EL ANDALOUSSI, S., FICKO TRCEK, T., FURLAN, R., HENDRIX, A., GURSEL, I., KRALJ-IGLIC, V.,

KAEFFER, B., KOSANOVIC, M., LEKKA, M. E., LIPPS, G., LOGOZZI, M., MARCILLA, A., SAMMAR, M., LLORENTE, A., NAZARENKO, I., OLIVEIRA, C., POCSFALVI, G., RAJENDRAN, L., RAPOSO, G., ROHDE, E., SILJANDER, P., VAN NIEL, G., VASCONCELOS, M. H., YANEZ-MO, M., YLIPERTTULA, M. L., ZAROVNI, N., ZAVEC, A. B. & GIEBEL, B. 2016. Evidence-Based Clinical Use of Nanoscale Extracellular Vesicles in Nanomedicine. *ACS Nano,* 10**,** 3886-99.

FAUSTI, S. A., FREY, R. H., HENRY, J. A., OLSON, D. J. & SCHAFFER, H. I. 1992. Early detection of ototoxicity using high-frequency, tone-burst-evoked auditory brainstem responses. *J Am Acad Audiol,* 3**,** 397-404.

FEE, W. E., JR. 1980. Aminoglycoside ototoxicity in the human. *Laryngoscope,* 90**,** 1-19.

FELDMAN, L., EFRATI, S., EVIATAR, E., ABRAMSOHN, R., YAROVOY, I., GERSCH, E., AVERBUKH, Z. & WEISSGARTEN, J. 2007. Gentamicin-induced ototoxicity in hemodialysis patients is ameliorated by N-acetylcysteine. *Kidney international,* 72**,** 359-363.

FERNANDEZ, C., GOLDBERG, J. & BAIRD, R. A. 1990. The vestibular nerve of the chinchilla. III. Peripheral innervation patterns in the utricular macula. *Journal of Neurophysiology,* 63**,** 767-780.

FETTIPLACE, R. & HACKNEY, C. M. 2006. The sensory and motor roles of auditory hair cells. *Nat Rev Neurosci,* 7**,** 19-29.

FISCHER, F. P. 1992. Quantitative analysis of the innervation of the chicken basilar papilla. *Hearing research,* 61**,** 167-178.

FISHER, M. J., LANGE, B. J., NEEDLE, M. N., JANSS, A. J., SHU, H. K. G., ADAMSON, P. C. & PHILLIPS, P. C. 2004. Amifostine for children with medulloblastoma treated with cisplatin-based chemotherapy. *Pediatric blood & cancer,* 43**,** 780-784.

FLINT, P. W., HAUGHEY, B. H., NIPARKO, J. K., RICHARDSON, M. A., LUND, V. J., ROBBINS, K. T., LESPERANCE, M. M. & THOMAS, J. R. 2010. *Cummings Otolaryngology - Head and Neck Surgery E-Book: Head and Neck Surgery, 3-Volume Set*, Elsevier Health Sciences.

FOGLIO, E., PUDDIGHINU, G., FASANARO, P., D'ARCANGELO, D., PERRONE, G. A., MOCINI, D., CAMPANELLA, C., COPPOLA, L., LOGOZZI, M., AZZARITO, T., MARZOLI, F., FAIS, S., PIERONI, L., MARZANO, V., GERMANI, A., CAPOGROSSI, M. C., RUSSO, M. A. & LIMANA, F. 2015. Exosomal clusterin, identified in the pericardial fluid, improves myocardial performance following MI through epicardial activation, enhanced arteriogenesis and reduced apoptosis. *Int J Cardiol,* 197**,** 333-47.

FORGE, A. 1985. Outer hair cell loss and supporting cell expansion following chronic gentamicin treatment. *Hearing research,* 19**,** 171-182.

FORGE, A., LI, L., CORWIN, J. T. & NEVILL, G. 1993. Ultrastructural evidence for hair cell regeneration in the mammalian inner ear. *Ratio,* 340**,** 380.

FORGE, A., LI, L. & NEVILL, G. 1998. Hair cell recovery in the vestibular sensory epithelia of mature guinea pigs. *Journal of Comparative Neurology,* 397**,** 69-88.

FOULADI, M., CHINTAGUMPALA, M., ASHLEY, D., KELLIE, S., GURURANGAN, S., HASSALL, T., GRONEWOLD, L., STEWART, C. F., WALLACE, D. & BRONISCER, A. 2008. Amifostine protects against cisplatin-induced ototoxicity in children with average-risk medulloblastoma. *Journal of Clinical Oncology,* 26**,** 3749-3755.

FRANCIS, S. P., KATZ, J., FANNING, K. D., HARRIS, K. A., NICHOLAS, B. D., LACY, M., PAGANA, J., AGRIS, P. F. & SHIN, J. B. 2013. A novel role of cytosolic protein synthesis inhibition in aminoglycoside ototoxicity. *J Neurosci,* 33**,** 3079-93.

FREYER, D. R., CHEN, L., KRAILO, M. D., KNIGHT, K., VILLALUNA, D., BLISS, B., POLLOCK, B. H., RAMDAS, J., LANGE, B., VAN HOFF, D., VANSOELEN, M. L., WIERNIKOWSKI, J., NEUWELT, E. A. & SUNG, L. 2017. Effects of sodium thiosulfate versus observation on development of cisplatin-induced hearing loss in children with cancer (ACCL0431): a multicentre, randomised, controlled, open-label, phase 3 trial. *Lancet Oncol,* 18**,** 63-74.

FRISINA, R. D., WHEELER, H. E., FOSSA, S. D., KERNS, S. L., FUNG, C., SESSO, H. D., MONAHAN, P. O., FELDMAN, D. R., HAMILTON, R., VAUGHN, D. J., BEARD, C. J., BUDNICK, A., JOHNSON, E. M., ARDESHIR-ROUHANI-FARD, S., EINHORN, L. H., LIPSHULTZ, S. E., DOLAN, M. E. & TRAVIS, L. B. 2016. Comprehensive Audiometric Analysis of Hearing Impairment and Tinnitus After Cisplatin-Based Chemotherapy in Survivors of Adult-Onset Cancer. *J Clin Oncol,* 34**,** 2712-20.

FROHLICH, D., KUO, W. P., FRUHBEIS, C., SUN, J. J., ZEHENDNER, C. M., LUHMANN, H. J., PINTO, S., TOEDLING, J., TROTTER, J. & KRAMER-ALBERS, E. M. 2014. Multifaceted effects of oligodendroglial exosomes on neurons: impact on neuronal firing rate, signal transduction and gene regulation. *Philos Trans R Soc Lond B Biol Sci,* 369.

FRUHBEIS, C., FROHLICH, D., KUO, W. P., AMPHORNRAT, J., THILEMANN, S., SAAB, A. S., KIRCHHOFF, F., MOBIUS, W., GOEBBELS, S., NAVE, K. A., SCHNEIDER, A., SIMONS, M., KLUGMANN, M., TROTTER, J. & KRAMER-ALBERS, E. M. 2013. Neurotransmitter-triggered transfer of exosomes mediates oligodendrocyte-neuron communication. *PLoS Biol,* 11**,** e1001604.

FUCHS, P., EVANS, M. & MURROW, B. 1990. Calcium currents in hair cells isolated from the cochlea of the chick. *The Journal of Physiology,* 429**,** 553-568.

FUERTES, M. A., ALONSO, C. & PEREZ, J. M. 2003. Biochemical modulation of Cisplatin mechanisms of action: enhancement of antitumor activity and circumvention of drug resistance. *Chem Rev,* 103**,** 645-62.

FURMAN, J. M. & LEMPERT, T. 2016. *Neuro-Otology*, Elsevier Science.

FURNESS, D., KATORI, Y., KUMAR, B. N. & HACKNEY, C. 2008. The dimensions and structural attachments of tip links in mammalian cochlear hair cells and the effects of exposure to different levels of extracellular calcium. *Neuroscience,* 154**,** 10-21.

GASTPAR, R., GEHRMANN, M., BAUSERO, M. A., ASEA, A., GROSS, C., SCHROEDER, J. A. & MULTHOFF, G. 2005. Heat shock protein 70 surface-positive tumor exosomes stimulate migratory and cytolytic activity of natural killer cells. *Cancer Res,* 65**,** 5238-47.

GATELL, J. M., FERRAN, F., ARAUJO, V., BONET, M., SORIANO, E., TRASERRA, J. & SANMIGUEL, J. G. 1987. Univariate and multivariate analyses of risk factors predisposing to auditory toxicity in patients receiving aminoglycosides. *Antimicrob Agents Chemother,* 31**,** 1383-7.

GATES, G. A., ANDERSON, M. L., MCCURRY, S. M., FEENEY, M. P. & LARSON, E. B. 2011. Central auditory dysfunction as a harbinger of Alzheimer dementia. *Arch Otolaryngol Head Neck Surg,* 137**,** 390-5.

GAVRIELI, Y., SHERMAN, Y. & BEN-SASSON, S. A. 1992. Identification of programmed cell death in situ via specific labeling of nuclear DNA fragmentation. *The Journal of cell biology,* 119**,** 493-501.

GÉLÉOC, G., LENNAN, G., RICHARDSON, G. & KROS, C. 1997. A quantitative comparison of mechanoelectrical transduction in vestibular and auditory hair cells of neonatal mice. *Proceedings of the Royal Society of London B: Biological Sciences,* 264**,** 611-621.

GERMILLER, J. A., SMILEY, E. C., ELLIS, A. D., HOFF, J. S., DESHMUKH, I., ALLEN, S. J. & BARALD, K. F. 2004. Molecular characterization of conditionally

immortalized cell lines derived from mouse early embryonic inner ear. *Dev Dyn,* 231**,** 815-27.

GIETEMA, J. A., MEINARDI, M. T., MESSERSCHMIDT, J., GELEVERT, T., ALT, F., UGES, D. R. & SLEIJFER, D. T. 2000. Circulating plasma platinum more than 10 years after cisplatin treatment for testicular cancer. *Lancet,* 355**,** 1075-6.

GINZBERG, R. D. & MEREST, D. K. 1983. A study of cochlear innervation in the young cat with the Golgi method. *Hearing research,* 10**,** 227-246.

GINZBERG, R. D. & MOREST, D. K. 1984. Fine structure of cochlear innervation in the cat. *Hearing research,* 14**,** 109-127.

GIRARD, S. A., PICARD, M., DAVIS, A. C., SIMARD, M., LAROCQUE, R., LEROUX, T. & TURCOTTE, F. 2009. Multiple work-related accidents: tracing the role of hearing status and noise exposure. *Occup Environ Med,* 66**,** 319-24.

GOLDSTEIN, J. 1967. Auditory nonlinearity. *The Journal of the Acoustical Society of America,* 41**,** 676-699.

GOLUB, J. S., TONG, L., NGYUEN, T. B., HUME, C. R., PALMITER, R. D., RUBEL, E. W. & STONE, J. S. 2012. Hair cell replacement in adult mouse utricles after targeted ablation of hair cells with diphtheria toxin. *J Neurosci,* 32**,** 15093-105.

GONZALEZ, V. M., FUERTES, M. A., ALONSO, C. & PEREZ, J. M. 2001. Is cisplatin-induced cell death always produced by apoptosis? *Mol Pharmacol,* 59**,** 657-63.

GOULD, S. J. & RAPOSO, G. 2013. As we wait: coping with an imperfect nomenclature for extracellular vesicles. *J Extracell Vesicles,* 2.

GRAHAM, J., GREENWOOD, R. & LECKY, B. 1980. Cortical deafness: a case report and review of the literature. *Journal of the neurological sciences,* 48**,** 35-49.

GREWAL, S., MERCHANT, T., REYMOND, R., MCINERNEY, M., HODGE, C. & SHEARER, P. 2010. Auditory late effects of childhood cancer therapy: a report from the Children's Oncology Group. *Pediatrics,* 125**,** e938-50.

GROSSMAN, G. E., LEIGH, R. J., ABEL, L., LANSKA, D. J. & THURSTON, S. 1988. Frequency and velocity of rotational head perturbations during locomotion. *Experimental brain research,* 70**,** 470-476.

GROVES, A. K. 2010. The challenge of hair cell regeneration. *Experimental Biology and Medicine,* 235**,** 434-446.

GULLEY, R. L. & REESE, T. S. 1976. Intercellular junctions in the reticular lamina of the organ of Corti. *J Neurocytol,* 5**,** 479-507.

GURNEY, J. G., TERSAK, J. M., NESS, K. K., LANDIER, W., MATTHAY, K. K., SCHMIDT, M. L. & CHILDREN'S ONCOLOGY, G. 2007. Hearing loss, quality of life, and academic problems in long-term neuroblastoma survivors: a report from the Children's Oncology Group. *Pediatrics,* 120**,** e1229-36.

GUTHRIE, O. W., LI-KOROTKY, H. S., DURRANT, J. D. & BALABAN, C. 2008. Cisplatin induces cytoplasmic to nuclear translocation of nucleotide excision repair factors among spiral ganglion neurons. *Hear Res,* 239**,** 79-91.

GUZHOVA, I., KISLYAKOVA, K., MOSKALIOVA, O., FRIDLANSKAYA, I., TYTELL, M., CHEETHAM, M. & MARGULIS, B. 2001. In vitro studies show that Hsp70 can be released by glia and that exogenous Hsp70 can enhance neuronal stress tolerance. *Brain Res,* 914**,** 66-73.

GYORGY, B., HUNG, M. E., BREAKEFIELD, X. O. & LEONARD, J. N. 2015. Therapeutic applications of extracellular vesicles: clinical promise and open questions. *Annu Rev Pharmacol Toxicol,* 55**,** 439-464.

GYORGY, B., SAGE, C., INDZHYKULIAN, A. A., SCHEFFER, D. I., BRISSON, A. R., TAN, S., WU, X., VOLAK, A., MU, D., TAMVAKOLOGOS, P. I., LI, Y., FITZPATRICK, Z., ERICSSON, M., BREAKEFIELD, X. O., COREY, D. P. & MAGUIRE, C. A. 2017. Rescue of Hearing by Gene Delivery to Inner-Ear Hair Cells Using Exosome-Associated AAV. *Mol Ther,* 25**,** 379-391.

HAILEY, D. W., ESTERBERG, R., LINBO, T. H., RUBEL, E. W. & RAIBLE, D. W. 2017. Fluorescent aminoglycosides reveal intracellular trafficking routes in mechanosensory hair cells. *J Clin Invest,* 127**,** 472-486.

HAMASAKI, K. & RANDO, R. R. 1997. Specific binding of aminoglycosides to a human rRNA construct based on a DNA polymorphism which causes aminoglycoside-induced deafness. *Biochemistry,* 36**,** 12323-8.

HAMERS, F. P., WIJBENGA, J., WOLTERS, F. L., KLIS, S. F., SLUYTER, S. & SMOORENBURG, G. F. 2003. Cisplatin ototoxicity involves organ of Corti, stria vascularis and spiral ganglion: modulation by alphaMSH and ORG 2766. *Audiol Neurootol,* 8**,** 305-15.

HARRIS, M. S., GILBERT, J. L., LORMORE, K. A., MUSUNURU, S. A. & FRITSCH, M. H. 2011. Cisplatin ototoxicity affecting cochlear implant benefit. *Otol Neurotol,* 32**,** 969-72.

HARRISON, R. T., SEILER, B. M. & BIELEFELD, E. C. 2016. Ototoxicity of 12 mg/kg cisplatin in the Fischer 344/NHsd rat using multiple dosing strategies. *Anticancer Drugs,* 27**,** 780-6.

HASSON, T., GILLESPIE, P. G., GARCIA, J. A., MACDONALD, R. B., ZHAO, Y., YEE, A. G., MOOSEKER, M. S. & COREY, D. P. 1997. Unconventional myosins in inner-ear sensory epithelia. *J Cell Biol,* 137**,** 1287-307.

HAWKINS, J. 1973. Comparative otopathology: aging, noise, and ototoxic drugs. *Otophysiology.* Karger Publishers.

HE, J., YIN, S., WANG, J., DING, D. & JIANG, H. 2009. Effectiveness of different approaches for establishing cisplatin-induced cochlear lesions in mice. *Acta Otolaryngol,* 129**,** 1359-67.

HELLBERG, V., WALLIN, I., ERIKSSON, S., HERNLUND, E., JERREMALM, E., BERNDTSSON, M., EKSBORG, S., ARNER, E. S., SHOSHAN, M., EHRSSON, H. & LAURELL, G. 2009. Cisplatin and oxaliplatin toxicity: importance of cochlear kinetics as a determinant for ototoxicity. *J Natl Cancer Inst,* 101**,** 37-47.

HENNE, W. M., STENMARK, H. & EMR, S. D. 2013. Molecular mechanisms of the membrane sculpting ESCRT pathway. *Cold Spring Harb Perspect Biol,* 5.

HENRY, K. R. 2004. Males lose hearing earlier in mouse models of late-onset age-related hearing loss; females lose hearing earlier in mouse models of early-onset hearing loss. *Hearing research,* 190**,** 141-148.

HENRY, K. R. & CHOLE, R. A. 1980. Genotypic differences in behavioral, physiological and anatomical expressions of age-related hearing loss in the laboratory mouse: original papers travaux originaux. *Audiology,* 19**,** 369-383.

HEUSERMANN, W., HEAN, J., TROJER, D., STEIB, E., VON BUEREN, S., GRAFF-MEYER, A., GENOUD, C., MARTIN, K., PIZZATO, N., VOSHOL, J., MORRISSEY, D. V., ANDALOUSSI, S. E., WOOD, M. J. & MEISNER-KOBER, N. C. 2016. Exosomes surf on filopodia to enter cells at endocytic hot spots, traffic within endosomes, and are targeted to the ER. *J Cell Biol,* 213**,** 173-84.

HIGHTOWER, L. E. & GUIDON, P. T., JR. 1989. Selective release from cultured mammalian cells of heat-shock (stress) proteins that resemble glia-axon transfer proteins. *J Cell Physiol,* 138**,** 257-66.

HILL, G. W., MOREST, D. K. & PARHAM, K. 2008. Cisplatin-induced ototoxicity: effect of intratympanic dexamethasone injections. *Otol Neurotol,* 29**,** 1005-11.

HIROKAWA, N. 1978. The ultrastructure of the basilar papilla of the chick. *Journal of Comparative Neurology,* 181**,** 361-374.

HITCHCOCK, Y. J., TWARD, J. D., SZABO, A., BENTZ, B. G. & SHRIEVE, D. C. 2009. Relative contributions of radiation and cisplatin-based chemotherapy to sensorineural hearing loss in head-and-neck cancer patients. *Int J Radiat Oncol Biol Phys,* 73**,** 779-88.

HJELLE, L. V., GUNDERSEN, P. O., OLDENBURG, J., BRYDOY, M., TANDSTAD, T., WILSGAARD, T., FOSSA, S. D., BREMNES, R. M. & HAUGNES, H. S. 2015. Long-term platinum retention after platinum-based chemotherapy in testicular cancer survivors: a 20-year follow-up study. *Anticancer Res,* 35**,** 1619-25.

HOISTAD, D. L., ONDREY, F. G., MUTLU, C., SCHACHERN, P. A., PAPARELLA, M. M. & ADAMS, G. L. 1998. Histopathology of human temporal bone after cis-platinum, radiation, or both. *Otolaryngol Head Neck Surg,* 118**,** 825-32.

HOLLEY, M., NISHIDA, Y. & GRIX, N. 1997. Conditional immortalization of hair cells from the inner ear. *International journal of developmental neuroscience,* 15**,** 541-552.

HOLLEY, M. C. & LAWLOR, P. W. 1997. Production of conditionally immortalised cell lines from a transgenic mouse. *Audiol Neurootol,* 2**,** 25-35.

HOSHINO, A., COSTA-SILVA, B., SHEN, T. L., RODRIGUES, G., HASHIMOTO, A., TESIC MARK, M., MOLINA, H., KOHSAKA, S., DI GIANNATALE, A., CEDER, S., SINGH,

S., WILLIAMS, C., SOPLOP, N., URYU, K., PHARMER, L., KING, T., BOJMAR, L., DAVIES, A. E., ARARSO, Y., ZHANG, T., ZHANG, H., HERNANDEZ, J., WEISS, J. M., DUMONT-COLE, V. D., KRAMER, K., WEXLER, L. H., NARENDRAN, A., SCHWARTZ, G. K., HEALEY, J. H., SANDSTROM, P., LABORI, K. J., KURE, E. H., GRANDGENETT, P. M., HOLLINGSWORTH, M. A., DE SOUSA, M., KAUR, S., JAIN, M., MALLYA, K., BATRA, S. K., JARNAGIN, W. R., BRADY, M. S., FODSTAD, O., MULLER, V., PANTEL, K., MINN, A. J., BISSELL, M. J., GARCIA, B. A., KANG, Y., RAJASEKHAR, V. K., GHAJAR, C. M., MATEI, I., PEINADO, H., BROMBERG, J. & LYDEN, D. 2015. Tumour exosome integrins determine organotropic metastasis. *Nature,* 527**,** 329-35.

HSU, C., MOROHASHI, Y., YOSHIMURA, S., MANRIQUE-HOYOS, N., JUNG, S., LAUTERBACH, M. A., BAKHTI, M., GRONBORG, M., MOBIUS, W., RHEE, J., BARR, F. A. & SIMONS, M. 2010. Regulation of exosome secretion by Rab35 and its GTPase-activating proteins TBC1D10A-C. *J Cell Biol,* 189**,** 223-32.

HUANG, E., TEH, B. S., STROTHER, D. R., DAVIS, Q. G., CHIU, J. K., LU, H. H., CARPENTER, L. S., MAI, W. Y., CHINTAGUMPALA, M. M., SOUTH, M., GRANT, W. H., 3RD, BUTLER, E. B. & WOO, S. Y. 2002. Intensity-modulated radiation therapy for pediatric medulloblastoma: early report on the reduction of ototoxicity. *Int J Radiat Oncol Biol Phys,* 52**,** 599-605.

HUDSPETH, A. 2014. Integrating the active process of hair cells with cochlear function. *Nature Reviews Neuroscience,* 15**,** 600-615.

HUDSPETH, A. & COREY, D. 1977. Sensitivity, polarity, and conductance change in the response of vertebrate hair cells to controlled mechanical stimuli. *Proceedings of the National Academy of Sciences,* 74**,** 2407-2411.

HUDSPETH, A. J. 2008. Making an effort to listen: mechanical amplification in the ear. *Neuron,* 59**,** 530-45.

HUIZING, E. & DE GROOT, J. 1987. Human cochlear pathology in aminoglycoside ototoxicity—a review. *Acta Oto-Laryngologica,* 104**,** 117-125.

HUNT, C. & MORIMOTO, R. I. 1985. Conserved features of eukaryotic hsp70 genes revealed by comparison with the nucleotide sequence of human hsp70. *Proc Natl Acad Sci U S A,* 82**,** 6455-9.

HUTH, M. E., HAN, K. H., SOTOUDEH, K., HSIEH, Y. J., EFFERTZ, T., VU, A. A., VERHOEVEN, S., HSIEH, M. H., GREENHOUSE, R., CHENG, A. G. & RICCI, A. J. 2015. Designer aminoglycosides prevent cochlear hair cell loss and hearing loss. *J Clin Invest,* 125**,** 583-92.

HYPPOLITO, M. Â., DE OLIVEIRA, J. A. A. & ROSSATO, M. 2006. Cisplatin ototoxicity and otoprotection with sodium salicylate. *European Archives of Oto-Rhino-Laryngology and Head & Neck,* 263**,** 798-803.

IKEDA, K. & MORIZONO, T. 1989. Electrochemical profiles for monovalent ions in the stria vascularis: cellular model of ion transport mechanisms. *Hear Res,* 39**,** 279-86.

ISHIKAWA, T. & ALI-OSMAN, F. 1993. Glutathione-associated cis-diamminedichloroplatinum (II) metabolism and ATP-dependent efflux from leukemia cells. Molecular characterization of glutathione-platinum complex and its biological significance. *Journal of Biological Chemistry,* 268**,** 20116-20125.

IURATO, S. 1960. Submicroscopic structure of the membranous labyrinth. *Zeitschrift für Zellforschung und Mikroskopische Anatomie,* 52**,** 105-128.

JAGGER, D. J., HOLLEY, M. C. & ASHMORE, J. F. 1999. Ionic currents expressed in a cell line derived from the organ of Corti of the Immortomouse. *Pflugers Arch,* 438**,** 8-14.

JAGODINSKY, J. C., SULIMA, A., CAO, Y., POPRAWSKI, J. E., BLACKMAN, B. N., LLOYD, J. R., SWENSON, R. E., GOTTESMAN, M. M. & HALL, M. D. 2015. Evaluation of fluorophore-tethered platinum complexes to monitor the fate of cisplatin analogs. *J Biol Inorg Chem,* 20**,** 1081-95.

JAHNKE, K. 1975. [Intercellular junctions in the guinea pig stria vascularis as shown by freeze-etching (author's transl)]. *Anat Embryol (Berl),* 147**,** 189-201.

JAT, P. S., NOBLE, M. D., ATALIOTIS, P., TANAKA, Y., YANNOUTSOS, N., LARSEN, L. & KIOUSSIS, D. 1991. Direct derivation of conditionally immortal cell lines from an H-2Kb-tsA58 transgenic mouse. *Proceedings of the National Academy of Sciences,* 88**,** 5096-5100.

JIANG, H., SHA, S. H. & SCHACHT, J. 2005. NF-kappaB pathway protects cochlear hair cells from aminoglycoside-induced ototoxicity. *J Neurosci Res,* 79**,** 644-51.

JIANG, T., KINDT, K. & WU, D. K. 2017. Transcription factor Emx2 controls stereociliary bundle orientation of sensory hair cells. *eLife,* 6**,** e23661.

JOHNSSON, L.-G. & HAWKINS, J. E. 1967. Otolithic membranes of the saccule and utricle in man. *Science,* 157**,** 1454-1456.

JOHNSSON, L.-G., HAWKINS JR, J. E., KINGSLEY, T. C., BLACK, F. O. & MATZ, G. J. 1981. Aminoglycoside-induced inner ear pathology in man, as seen by microdissection. *Aminoglycoside Ototoxicity, Little, Brown and Co., Boston***,** 389-408.

JOHNSTONE, R. M., ADAM, M., HAMMOND, J. R., ORR, L. & TURBIDE, C. 1987. Vesicle formation during reticulocyte maturation. Association of plasma membrane activities with released vesicles (exosomes). *J Biol Chem,* 262**,** 9412-20.

JUHN, S. K. 1988. Barrier systems in the inner ear. *Acta Otolaryngol Suppl,* 458**,** 79-83.

KACHAR, B., BATTAGLIA, A. & FEX, J. 1997. Compartmentalized vesicular traffic around the hair cell cuticular plate. *Hear Res,* 107**,** 102-12.

KACHAR, B., BROWNELL, W. E., ALTSCHULER, R. & FEX, J. 1986. Electrokinetic shape changes of cochlear outer hair cells. *Nature,* 322**,** 365-8.

KACHAR, B., PARAKKAL, M., KURC, M., ZHAO, Y.-D. & GILLESPIE, P. G. 2000. High-resolution structure of hair-cell tip links. *Proceedings of the National Academy of Sciences,* 97**,** 13336-13341.

KALINEC, G., THEIN, P., PARK, C. & KALINEC, F. 2016. HEI-OC1 cells as a model for investigating drug cytotoxicity. *Hear Res,* 335**,** 105-117.

KALINEC, G. M., WEBSTER, P., LIM, D. J. & KALINEC, F. 2003. A cochlear cell line as an in vitro system for drug ototoxicity screening. *Audiol Neurootol,* 8**,** 177-89.

KARASAWA, T., SIBRIAN-VAZQUEZ, M., STRONGIN, R. M. & STEYGER, P. S. 2013. Identification of cisplatin-binding proteins using agarose conjugates of platinum compounds. *PLoS One,* 8**,** e66220.

KARASAWA, T. & STEYGER, P. S. 2015. An integrated view of cisplatin-induced nephrotoxicity and ototoxicity. *Toxicol Lett,* 237**,** 219-27.

KAZMIERCZAK, P., SAKAGUCHI, H., TOKITA, J., WILSON-KUBALEK, E. M., MILLIGAN, R. A., MÜLLER, U. & KACHAR, B. 2007. Cadherin 23 and protocadherin 15 interact to form tip-link filaments in sensory hair cells. *Nature,* 449**,** 87-91.

KEMP, D. T. 1978. Stimulated acoustic emissions from within the human auditory system. *The Journal of the Acoustical Society of America,* 64**,** 1386-1391.

KHYNRIAM, D. & PRASAD, S. B. 2002. Changes in glutathione-related enzymes in tumor-bearing mice after cisplatin treatment. *Cell Biol Toxicol,* 18**,** 349-58.

KIKUCHI, T., ADAMS, J. C., MIYABE, Y., SO, E. & KOBAYASHI, T. 2000. Potassium ion recycling pathway via gap junction systems in the mammalian cochlea and its interruption in hereditary nonsyndromic deafness. *Med Electron Microsc,* 33**,** 51-6.

KIM, D. K., KANG, B., KIM, O. Y., CHOI, D. S., LEE, J., KIM, S. R., GO, G., YOON, Y. J., KIM, J. H., JANG, S. C., PARK, K. S., CHOI, E. J., KIM, K. P., DESIDERIO, D. M., KIM, Y. K., LOTVALL, J., HWANG, D. & GHO, Y. S. 2013. EVpedia: an integrated database of high-throughput data for systemic analyses of extracellular vesicles. *J Extracell Vesicles,* 2.

KIM, D. K., LEE, J., KIM, S. R., CHOI, D. S., YOON, Y. J., KIM, J. H., GO, G., NHUNG, D., HONG, K., JANG, S. C., KIM, S. H., PARK, K. S., KIM, O. Y., PARK, H. T., SEO, J. H., AIKAWA, E., BAJ-KRZYWORZEKA, M., VAN BALKOM, B. W., BELTING, M., BLANC, L., BOND, V., BONGIOVANNI, A., BORRAS, F. E., BUEE, L., BUZAS, E. I., CHENG, L., CLAYTON, A., COCUCCI, E., DELA CRUZ, C. S., DESIDERIO, D. M., DI VIZIO, D., EKSTROM, K., FALCON-PEREZ, J. M., GARDINER, C., GIEBEL, B., GREENING, D. W., GROSS, J. C., GUPTA, D., HENDRIX, A., HILL, A. F., HILL, M. M., NOLTE-'T HOEN, E., HWANG, D. W., INAL, J., JAGANNADHAM, M. V., JAYACHANDRAN, M., JEE, Y. K., JORGENSEN, M., KIM, K. P., KIM, Y. K., KISLINGER, T., LASSER, C., LEE, D. S., LEE, H., VAN LEEUWEN, J., LENER, T., LIU, M. L., LOTVALL, J., MARCILLA, A., MATHIVANAN, S., MOLLER, A., MORHAYIM, J., MULLIER, F., NAZARENKO, I., NIEUWLAND, R., NUNES, D. N., PANG, K., PARK, J., PATEL, T., POCSFALVI, G., DEL PORTILLO, H., PUTZ, U., RAMIREZ, M. I., RODRIGUES, M. L., ROH, T. Y., ROYO, F., SAHOO, S., SCHIFFELERS, R., SHARMA, S., SILJANDER, P., SIMPSON, R. J., SOEKMADJI, C., STAHL, P., STENSBALLE, A., STEPIEN, E., TAHARA, H., TRUMMER, A., VALADI, H., VELLA, L. J., WAI, S. N., WITWER, K., YANEZ-MO, M., YOUN, H., ZEIDLER, R. & GHO, Y. S. 2015. EVpedia: a community web portal for extracellular vesicles research. *Bioinformatics,* 31**,** 933-9.

KIMURA, R. S. 1966. Hairs of the cochlear sensory cells and their attachment to the tectorial membrane. *Acta oto-laryngologica,* 61**,** 55-72.

KIRKEGAARD, M. & NYENGAARD, J. R. 2005. Stereological study of postnatal development in the mouse utricular macula. *J Comp Neurol,* 492**,** 132-44.

KLIS, S. F., O'LEARY, S. J., HAMERS, F. P., DE GROOT, J. C. & SMOORENBURG, G. F. 2000. Reversible cisplatin ototoxicity in the albino guinea pig. *Neuroreport,* 11**,** 623-6.

KLUMPERMAN, J. & RAPOSO, G. 2014. The complex ultrastructure of the endolysosomal system. *Cold Spring Harb Perspect Biol,* 6**,** a016857.

KNIGHT, K. R., CHEN, L., FREYER, D., APLENC, R., BANCROFT, M., BLISS, B., DANG, H., GILLMEISTER, B., HENDERSHOT, E., KRAEMER, D. F., LINDENFELD, L., MEZA, J., NEUWELT, E. A., POLLOCK, B. H. & SUNG, L. 2017. Group-Wide, Prospective Study of Ototoxicity Assessment in Children Receiving Cisplatin Chemotherapy (ACCL05C1): A Report From the Children's Oncology Group. *J Clin Oncol,* 35**,** 440-445.

KNIGHT, K. R., KRAEMER, D. F. & NEUWELT, E. A. 2005. Ototoxicity in children receiving platinum chemotherapy: underestimating a commonly occurring toxicity that may influence academic and social development. *J Clin Oncol,* 23**,** 8588-96.

KNOWLTON, V. Y. 1967. Correlation of the development of membranous and bony labyrinths, acoustic ganglia, nerves, and brain centers of the chick embryo. *Journal of Morphology,* 121**,** 179-207.

KOCYIGIT, I., VURAL, A., UNAL, A., SIPAHIOGLU, M. H., YUCEL, H. E., AYDEMIR, S., YAZICI, C., SAHIN, M. I., OYMAK, O. & TOKGOZ, B. 2015. Preventing amikacin related ototoxicity with N-acetylcysteine in patients undergoing peritoneal dialysis. *European Archives of Oto-Rhino-Laryngology,* 272**,** 2611-2620.

KOEHLER, K. R., MIKOSZ, A. M., MOLOSH, A. I., PATEL, D. & HASHINO, E. 2013. Generation of inner ear sensory epithelia from pluripotent stem cells in 3D culture. *Nature,* 500**,** 217-21.

KOEHLER, K. R., NIE, J., LONGWORTH-MILLS, E., LIU, X. P., LEE, J., HOLT, J. R. & HASHINO, E. 2017. Generation of inner ear organoids containing functional hair cells from human pluripotent stem cells. *Nat Biotechnol,* 35**,** 583-589.

KOLINSKY, D. C., HAYASHI, S. S., KARZON, R., MAO, J. & HAYASHI, R. J. 2010. Late onset hearing loss: a significant complication of cancer survivors treated with Cisplatin containing chemotherapy regimens. *J Pediatr Hematol Oncol,* 32**,** 119-23.

KOPELMAN, J., BUDNICK, A. S., SESSIONS, R. B., KRAMER, M. B. & WONG, G. Y. 1988. Ototoxicity of high-dose cisplatin by bolus administration in patients with advanced cancers and normal hearing. *Laryngoscope,* 98**,** 858-64.

KOPPEN, C., REIFSCHNEIDER, O., CASTANHEIRA, I., SPERLING, M., KARST, U. & CIARIMBOLI, G. 2015. Quantitative imaging of platinum based on laser ablation-inductively coupled plasma-mass spectrometry to investigate toxic side effects of cisplatin. *Metallomics,* 7**,** 1595-603.

KORVER, K. D., RYBAK, L. P., WHITWORTH, C. & CAMPBELL, K. M. 2002. Round window application of D-methionine provides complete cisplatin otoprotection. *Otolaryngology—Head and Neck Surgery,* 126**,** 683-689.

KOŠLER, J. & SYLVESTER, P. J. 2003. Present trends and the future of zircon in geochronology: laser ablation ICPMS. *Reviews in mineralogy and geochemistry,* 53**,** 243-275.

KOWAL, J., ARRAS, G., COLOMBO, M., JOUVE, M., MORATH, J. P., PRIMDAL-BENGTSON, B., DINGLI, F., LOEW, D., TKACH, M. & THERY, C. 2016. Proteomic comparison defines novel markers to characterize heterogeneous

populations of extracellular vesicle subtypes. *Proc Natl Acad Sci U S A,* 113**,** E968-77.

KOWAL, J., TKACH, M. & THERY, C. 2014. Biogenesis and secretion of exosomes. *Curr Opin Cell Biol,* 29**,** 116-25.

KULAK, N. A., PICHLER, G., PARON, I., NAGARAJ, N. & MANN, M. 2014. Minimal, encapsulated proteomic-sample processing applied to copy-number estimation in eukaryotic cells. *Nat Methods,* 11**,** 319-24.

KURIMA, K., EBRAHIM, S., PAN, B., SEDLACEK, M., SENGUPTA, P., MILLIS, B. A., CUI, R., NAKANISHI, H., FUJIKAWA, T. & KAWASHIMA, Y. 2015. TMC1 and TMC2 localize at the site of mechanotransduction in mammalian inner ear hair cell stereocilia. *Cell reports,* 12**,** 1606-1617.

KUSHNER, B. H., BUDNICK, A., KRAMER, K., MODAK, S. & CHEUNG, N. K. 2006. Ototoxicity from high-dose use of platinum compounds in patients with neuroblastoma. *Cancer,* 107**,** 417-22.

LAI, C. P., KIM, E. Y., BADR, C. E., WEISSLEDER, R., MEMPEL, T. R., TANNOUS, B. A. & BREAKEFIELD, X. O. 2015. Visualization and tracking of tumour extracellular vesicle delivery and RNA translation using multiplexed reporters. *Nat Commun,* 6**,** 7029.

LAI, C. P., MARDINI, O., ERICSSON, M., PRABHAKAR, S., MAGUIRE, C., CHEN, J. W., TANNOUS, B. A. & BREAKEFIELD, X. O. 2014. Dynamic biodistribution of extracellular vesicles in vivo using a multimodal imaging reporter. *ACS Nano,* 8**,** 483-494.

LANCASTER, G. I. & FEBBRAIO, M. A. 2005. Exosome-dependent trafficking of HSP70: a novel secretory pathway for cellular stress proteins. *J Biol Chem,* 280**,** 23349-55.

LANGER, T., AM ZEHNHOFF-DINNESEN, A., RADTKE, S., MEITERT, J. & ZOLK, O. 2013. Understanding platinum-induced ototoxicity. *Trends Pharmacol Sci,* 34**,** 458-69.

LANVERS-KAMINSKY, C., ZEHNHOFF-DINNESEN, A. A., PARFITT, R. & CIARIMBOLI, G. 2017. Drug-induced ototoxicity: Mechanisms, Pharmacogenetics, and protective strategies. *Clin Pharmacol Ther,* 101**,** 491-500.

LAULAGNIER, K., GRAND, D., DUJARDIN, A., HAMDI, S., VINCENT-SCHNEIDER, H., LANKAR, D., SALLES, J. P., BONNEROT, C., PERRET, B. & RECORD, M. 2004. PLD2 is enriched on exosomes and its activity is correlated to the release of exosomes. *FEBS Lett,* 572**,** 11-4.

LAURELL, G. & BAGGER-SJOBACK, D. 1991. Dose-dependent inner ear changes after i.v. administration of cisplatin. *J Otolaryngol,* 20**,** 158-67.

LEE, J. E., NAKAGAWA, T., KIM, T. S., ENDO, T., SHIGA, A., IGUCHI, F., LEE, S. H. & ITO, J. 2004a. Role of reactive radicals in degeneration of the auditory system of mice following cisplatin treatment. *Acta Otolaryngol,* 124**,** 1131-5.

LEE, J. E., NAKAGAWA, T., KITA, T., KIM, T. S., IGUCHI, F., ENDO, T., SHIGA, A., LEE, S. H. & ITO, J. 2004b. Mechanisms of apoptosis induced by cisplatin in marginal cells in mouse stria vascularis. *ORL J Otorhinolaryngol Relat Spec,* 66**,** 111-8.

LEE, S., SHIN, J. O., SAGONG, B., KIM, U. K. & BOK, J. 2017. Spatiotemporal expression patterns of clusterin in the mouse inner ear. *Cell Tissue Res*.

LEE, Y., EL ANDALOUSSI, S. & WOOD, M. J. 2012. Exosomes and microvesicles: extracellular vesicles for genetic information transfer and gene therapy. *Hum Mol Genet,* 21**,** R125-34.

LEONOVA, E. V. & RAPHAEL, Y. 1997. Organization of cell junctions and cytoskeleton in the reticular lamina in normal and ototoxically damaged organ of Corti. *Hear Res,* 113**,** 14-28.

LERNER, S. A., SCHMITT, B. A., SELIGSOHN, R. & MATZ, G. J. 1986. Comparative study of ototoxicity and nephrotoxicity in patients randomly assigned to treatment with amikacin or gentamicin. *Am J Med,* 80**,** 98-104.

LEWIS, E. R., BAIRD, R. A., LEVERENZ, E. L. & KOYAMA, H. 1982a. Inner ear: dye injection reveals peripheral origins of specific sensitivities. *Science,* 215**,** 1641-1643.

LEWIS, E. R., LEVERENZ, E. L. & KOYAMA, H. 1982b. The tonotopic organization of the bullfrog amphibian papilla, an auditory organ lacking a basilar membrane. *Journal of Comparative Physiology A: Neuroethology, Sensory, Neural, and Behavioral Physiology,* 145**,** 437-445.

LI, A., XUE, J. & PETERSON, E. H. 2008. Architecture of the mouse utricle: macular organization and hair bundle heights. *Journal of Neurophysiology,* 99**,** 718-733.

LI, G., LIU, W. & FRENZ, D. 2006. Cisplatin ototoxicity to the rat inner ear: a role for HMG1 and iNOS. *Neurotoxicology,* 27**,** 22-30.

LI, G., SHA, S.-H., ZOTOVA, E., AREZZO, J., VAN DE WATER, T. & SCHACHT, J. 2002. Salicylate protects hearing and kidney function from cisplatin toxicity without compromising its oncolytic action. *Laboratory investigation,* 82**,** 585-596.

LI, L. & FORGE, A. 1997. Morphological evidence for supporting cell to hair cell conversion in the mammalian utricular macula. *International journal of developmental neuroscience,* 15**,** 433-446.

LI, Y., DING, D., JIANG, H., FU, Y. & SALVI, R. 2011. Co-administration of cisplatin and furosemide causes rapid and massive loss of cochlear hair cells in mice. *Neurotox Res,* 20**,** 307-19.

LI, Y., WOMER, R. B. & SILBER, J. H. 2004. Predicting cisplatin ototoxicity in children: the influence of age and the cumulative dose. *Eur J Cancer,* 40**,** 2445-51.

LIANG, F., SCHULTE, B. A., QU, C., HU, W. & SHEN, Z. 2005. Inhibition of the calcium- and voltage-dependent big conductance potassium channel ameliorates cisplatin-induced apoptosis in spiral ligament fibrocytes of the cochlea. *Neuroscience,* 135**,** 263-71.

LIGHTHILL, J. 1981. Energy flow in the cochlea. *Journal of Fluid Mechanics,* 106**,** 149-213.

LIN, F. R., METTER, E. J., O'BRIEN, R. J., RESNICK, S. M., ZONDERMAN, A. B. & FERRUCCI, L. 2011. Hearing loss and incident dementia. *Arch Neurol,* 68**,** 214-20.

LIN, Y., HUO, L., LIU, Z., LI, J., LIU, Y., HE, Q., WANG, X. & LIANG, S. 2013. Sodium laurate, a novel protease- and mass spectrometry-compatible detergent for mass spectrometry-based membrane proteomics. *PLoS One,* 8**,** e59779.

LINDEMAN, H. 1973. Anatomy of the otolith organs. *Otophysiology.* Karger Publishers.

LINDEMAN, H. H. 1969. Studies on the morphology of the sensory regions of the vestibular apparatus with 45 figures. *Ergeb Anat Entwicklungsgesch,* 42**,** 1-113.

LOBB, R. J., BECKER, M., WEN, S. W., WONG, C. S., WIEGMANS, A. P., LEIMGRUBER, A. & MOLLER, A. 2015. Optimized exosome isolation protocol for cell culture supernatant and human plasma. *J Extracell Vesicles,* 4**,** 27031.

LOISON, F., DEBURE, L., NIZARD, P., LE GOFF, P., MICHEL, D. & LE DREAN, Y. 2006. Up-regulation of the clusterin gene after proteotoxic stress: implication of HSF1-HSF2 heterocomplexes. *Biochem J,* 395**,** 223-31.

LOPEZ-VERRILLI, M. A. & COURT, F. A. 2012. Transfer of vesicles from schwann cells to axons: a novel mechanism of communication in the peripheral nervous system. *Front Physiol,* 3**,** 205.

LOPEZ-VERRILLI, M. A., PICOU, F. & COURT, F. A. 2013. Schwann cell-derived exosomes enhance axonal regeneration in the peripheral nervous system. *Glia,* 61**,** 1795-806.

LOTVALL, J., HILL, A. F., HOCHBERG, F., BUZAS, E. I., DI VIZIO, D., GARDINER, C., GHO, Y. S., KUROCHKIN, I. V., MATHIVANAN, S., QUESENBERRY, P., SAHOO, S., TAHARA, H., WAUBEN, M. H., WITWER, K. W. & THERY, C. 2014. Minimal experimental requirements for definition of extracellular vesicles and their functions: a position statement from the International Society for Extracellular Vesicles. *J Extracell Vesicles,* 3**,** 26913.

LUAN, X., SANSANAPHONGPRICHA, K., MYERS, I., CHEN, H., YUAN, H. & SUN, D. 2017. Engineering exosomes as refined biological nanoplatforms for drug delivery. *Acta Pharmacol Sin,* 38**,** 754-763.

LUBERTO, C., HASSLER, D. F., SIGNORELLI, P., OKAMOTO, Y., SAWAI, H., BOROS, E., HAZEN-MARTIN, D. J., OBEID, L. M., HANNUN, Y. A. & SMITH, G. K. 2002. Inhibition of tumor necrosis factor-induced cell death in MCF7 by a novel inhibitor of neutral sphingomyelinase. *J Biol Chem,* 277**,** 41128-39.

MADDOX, P. T., SAUNDERS, J. & CHANDRASEKHAR, S. S. 2009. Sudden hearing loss from PDE-5 inhibitors: A possible cellular stress etiology. *Laryngoscope,* 119**,** 1586-9.

MAGLIONE, M. & SIGRIST, S. J. 2013. Seeing the forest tree by tree: super-resolution light microscopy meets the neurosciences. *Nat Neurosci,* 16**,** 790-7.

MARCUS, D. C. & SHEN, Z. 1994. Slowly activating voltage-dependent K+ conductance is apical pathway for K+ secretion in vestibular dark cells. *American Journal of Physiology-Cell Physiology,* 267**,** C857-C864.

MARINA, N., CHANG, K. W., MALOGOLOWKIN, M., LONDON, W. B., FRAZIER, A. L., WOMER, R. B., RESCORLA, F., BILLMIRE, D. F., DAVIS, M. M. & PERLMAN, E. J. 2005. Amifostine does not protect against the ototoxicity of high-dose cisplatin combined with etoposide and bleomycin in pediatric germ-cell tumors. *Cancer,* 104**,** 841-847.

MARSHAK, T., STEINER, M., KAMINER, M., LEVY, L. & SHUPAK, A. 2014. Prevention of cisplatin-induced hearing loss by intratympanic dexamethasone: a randomized controlled study. *Otolaryngology--Head and Neck Surgery,* 150**,** 983-990.

MAY-SIMERA, H. L., PETRALIA, R. S., MONTCOUQUIOL, M., WANG, Y. X., SZARAMA, K. B., LIU, Y., LIN, W., DEANS, M. R., PAZOUR, G. J. & KELLEY, M. W. 2015. Ciliary proteins Bbs8 and Ift20 promote planar cell polarity in the cochlea. *Development,* 142**,** 555-66.

MAY, L. A., KRAMARENKO, II, BRANDON, C. S., VOELKEL-JOHNSON, C., ROY, S., TRUONG, K., FRANCIS, S. P., MONZACK, E. L., LEE, F. S. & CUNNINGHAM, L. L. 2013. Inner ear supporting cells protect hair cells by secreting HSP70. *J Clin Invest,* 123**,** 3577-87.

MAZUROV, D., BARBASHOVA, L. & FILATOV, A. 2013. Tetraspanin protein CD9 interacts with metalloprotease CD10 and enhances its release via exosomes. *FEBS J,* 280**,** 1200-13.

MCGINN, M. D., BEAN-KNUDSEN, D. & ERMEL, R. W. 1992. Incidence of otitis media in CBA/J and CBA/CaJ mice. *Hearing research,* 59**,** 1-6.

MCGWIN, G., JR. 2010. Phosphodiesterase type 5 inhibitor use and hearing impairment. *Arch Otolaryngol Head Neck Surg,* 136**,** 488-92.

MEECH, R. P., CAMPBELL, K. C., HUGHES, L. P. & RYBAK, L. P. 1998. A semiquantitative analysis of the effects of cisplatin on the rat stria vascularis. *Hear Res,* 124**,** 44-59.

METCALFE, W. K., KIMMEL, C. B. & SCHABTACH, E. 1985. Anatomy of the posterior lateral line system in young larvae of the zebrafish. *Journal of Comparative Neurology,* 233**,** 377-389.

MEZENCEV, R. 2015. Interactions of cisplatin with non-DNA targets and their influence on anticancer activity and drug toxicity: the complex world of the platinum complex. *Curr Cancer Drug Targets,* 14**,** 794-816.

MILLER, M. A., ASKEVOLD, B., YANG, K. S., KOHLER, R. H. & WEISSLEDER, R. 2014. Platinum compounds for high-resolution in vivo cancer imaging. *ChemMedChem,* 9**,** 1131-5.

MINAMI, S. B., SHA, S. H. & SCHACHT, J. 2004. Antioxidant protection in a new animal model of cisplatin-induced ototoxicity. *Hear Res,* 198**,** 137-43.

MINAMI, T., ICHII, M. & OKAZAKI, Y. 1995. Comparison of three different methods for measurement of tissue platinum level. *Biol Trace Elem Res,* 48**,** 37-44.

MINOR, L. B., LASKER, D. M., BACKOUS, D. D. & HULLAR, T. E. 1999. Horizontal vestibuloocular reflex evoked by high-acceleration rotations in the squirrel monkey. I. Normal responses. *Journal of neurophysiology,* 82**,** 1254-1270.

MISUMI, M., NISHIMURA, T., KOMAI, T. & TANAKA, N. 1978. Interaction of kanamycin and related antibiotics with the large subunit of ribosomes and the inhibition of translocation. *Biochem Biophys Res Commun,* 84**,** 358-65.

MITTELBRUNN, M., GUTIERREZ-VAZQUEZ, C., VILLARROYA-BELTRI, C., GONZALEZ, S., SANCHEZ-CABO, F., GONZALEZ, M. A., BERNAD, A. & SANCHEZ-MADRID, F. 2011. Unidirectional transfer of microRNA-loaded exosomes from T cells to antigen-presenting cells. *Nat Commun,* 2**,** 282.

MOHAN, S., SMYTH, B. J., NAMIN, A., PHILLIPS, G. & GRATTON, M. A. 2014. Targeted amelioration of cisplatin-induced ototoxicity in guinea pigs. *Otolaryngol Head Neck Surg,* 151**,** 836-9.

MONTECALVO, A., LARREGINA, A. T., SHUFESKY, W. J., STOLZ, D. B., SULLIVAN, M. L., KARLSSON, J. M., BATY, C. J., GIBSON, G. A., ERDOS, G., WANG, Z., MILOSEVIC, J., TKACHEVA, O. A., DIVITO, S. J., JORDAN, R., LYONS-WEILER, J., WATKINS, S. C. & MORELLI, A. E. 2012. Mechanism of transfer of functional microRNAs between mouse dendritic cells via exosomes. *Blood,* 119**,** 756-66.

MONZACK, E. L., MAY, L. A., ROY, S., GALE, J. E. & CUNNINGHAM, L. L. 2015. Live imaging the phagocytic activity of inner ear supporting cells in response to hair cell death. *Cell Death Differ,* 22**,** 1995-2005.

MORE, S. S., AKIL, O., IANCULESCU, A. G., GEIER, E. G., LUSTIG, L. R. & GIACOMINI, K. M. 2010. Role of the copper transporter, CTR1, in platinum-induced ototoxicity. *J Neurosci,* 30**,** 9500-9.

MORGAN, D. J., OKEKE, I. N., LAXMINARAYAN, R., PERENCEVICH, E. N. & WEISENBERG, S. 2011. Non-prescription antimicrobial use worldwide: a systematic review. *Lancet Infect Dis,* 11**,** 692-701.

MOSER, T. & BEUTNER, D. 2000. Kinetics of exocytosis and endocytosis at the cochlear inner hair cell afferent synapse of the mouse. *Proceedings of the National Academy of Sciences,* 97**,** 883-888.

MUKHERJEA, D., RYBAK, L. P., SHEEHAN, K. E., KAUR, T., RAMKUMAR, V., JAJOO, S. & SHETH, S. 2011. The design and screening of drugs to prevent acquired sensorineural hearing loss. *Expert Opin Drug Discov,* 6**,** 491-505.

MULTHOFF, G. & HIGHTOWER, L. E. 2011. Distinguishing integral and receptor-bound heat shock protein 70 (Hsp70) on the cell surface by Hsp70-specific antibodies. *Cell Stress Chaperones,* 16**,** 251-5.

MUNGUIA, R., SAHMKOW, S. I., FUNNELL, W. R. J. & DANIEL, S. J. 2010. Transtympanic Ringer's lactate application in the prevention of cisplatinum-induced ototoxicity in a chinchilla animal model. *Otolaryngology—Head and Neck Surgery,* 143**,** 134-140.

MUNNAMALAI, V. & FEKETE, D. M. 2016. Organotypic Culture of the Mouse Cochlea from Embryonic Day 12 to the Neonate. *Methods Mol Biol,* 1427**,** 293-303.

NADOL, J. B., JR. 1978. Intercellular junctions in the organ of Corti. *Ann Otol Rhinol Laryngol,* 87**,** 70-80.

NAKABAYASHI, H., TAKETA, K., MIYANO, K., YAMANE, T. & SATO, J. 1982. Growth of human hepatoma cells lines with differentiated functions in chemically defined medium. *Cancer Res,* 42**,** 3858-63.

NAKAZAWA, K., SPICER, S. S. & SCHULTE, B. A. 1995. Ultrastructural localization of Na,K-ATPase in the gerbil cochlea. *J Histochem Cytochem,* 43**,** 981-91.

NICHANI, J., BRUCE, I. A., MAWMAN, D., KHWAJA, S., RAMSDEN, R. & GREEN, K. 2013. Cochlear implantation in patients deafened by ototoxic drugs. *Cochlear Implants Int,* 14**,** 207-12.

NIN, F., HIBINO, H., DOI, K., SUZUKI, T., HISA, Y. & KURACHI, Y. 2008. The endocochlear potential depends on two K+ diffusion potentials and an electrical barrier in the stria vascularis of the inner ear. *Proc Natl Acad Sci U S A,* 105**,** 1751-6.

NORDIN, J. Z., LEE, Y., VADER, P., MAGER, I., JOHANSSON, H. J., HEUSERMANN, W., WIKLANDER, O. P., HALLBRINK, M., SEOW, Y., BULTEMA, J. J., GILTHORPE, J., DAVIES, T., FAIRCHILD, P. J., GABRIELSSON, S., MEISNER-KOBER, N. C., LEHTIO, J., SMITH, C. I., WOOD, M. J. & EL ANDALOUSSI, S. 2015. Ultrafiltration with size-exclusion liquid chromatography for high yield isolation of extracellular vesicles preserving intact biophysical and functional properties. *Nanomedicine,* 11**,** 879-83.

O'MALLEY, J. T., BURGESS, B. J., JONES, D. D., ADAMS, J. C. & MERCHANT, S. N. 2009. Techniques of celloidin removal from temporal bone sections. *Ann Otol Rhinol Laryngol,* 118**,** 435-41.

OCAN, M., OBUKU, E. A., BWANGA, F., AKENA, D., RICHARD, S., OGWAL-OKENG, J. & OBUA, C. 2015. Household antimicrobial self-medication: a systematic review and meta-analysis of the burden, risk factors and outcomes in developing countries. *BMC Public Health,* 15**,** 742.

OESTERLE, E. C., TSUE, T. T., REH, T. A. & RUBEL, E. W. 1993. Hair-cell regeneration in organ cultures of the postnatal chicken inner ear. *Hearing research,* 70**,** 85-108.

OH, S. Y., WASIF, N., GARCON, M. C., RODRIGUEZ, G. & SAIF, M. W. 2013. Ototoxicity associated with oxaliplatin in a patient with pancreatic cancer. *JOP,* 14**,** 676-9.

OHLEMILLER, K. K., DAHL, A. R. & GAGNON, P. M. 2010. Divergent aging characteristics in CBA/J and CBA/CaJ mouse cochleae. *Journal of the Association for Research in Otolaryngology,* 11**,** 605-623.

OSTROWSKI, M., CARMO, N. B., KRUMEICH, S., FANGET, I., RAPOSO, G., SAVINA, A., MOITA, C. F., SCHAUER, K., HUME, A. N., FREITAS, R. P., GOUD, B., BENAROCH, P., HACOHEN, N., FUKUDA, M., DESNOS, C., SEABRA, M. C., DARCHEN, F., AMIGORENA, S., MOITA, L. F. & THERY, C. 2010. Rab27a and Rab27b control different steps of the exosome secretion pathway. *Nat Cell Biol,* 12**,** 19-30; sup pp 1-13.

PAN, B., GÉLÉOC, G. S., ASAI, Y., HORWITZ, G. C., KURIMA, K., ISHIKAWA, K., KAWASHIMA, Y., GRIFFITH, A. J. & HOLT, J. R. 2013. TMC1 and TMC2 are components of the mechanotransduction channel in hair cells of the mammalian inner ear. *Neuron,* 79**,** 504-515.

PAUL, B., PATON, C., NORRIS, A., WOODHEAD, J., HELLSTROM, J., HERGT, J. & GREIG, A. 2012. CellSpace: A module for creating spatially registered laser ablation images within the Iolite freeware environment. *Journal of Analytical Atomic Spectrometry,* 27**,** 700-706.

PEREZ-HERNANDEZ, D., GUTIERREZ-VAZQUEZ, C., JORGE, I., LOPEZ-MARTIN, S., URSA, A., SANCHEZ-MADRID, F., VAZQUEZ, J. & YANEZ-MO, M. 2013. The intracellular interactome of tetraspanin-enriched microdomains reveals their function as sorting machineries toward exosomes. *J Biol Chem,* 288**,** 11649-61.

PEREZ, N., MARTIN, E. & GARCIA-TAPIA, R. 2003. Intratympanic gentamicin for intractable Meniere's disease. *Laryngoscope,* 113**,** 456-64.

PERKINS, R. & MOREST, D. 1975. A study of cochlear innervation patterns in cats and rats with the Golgi method and Nomarski optics. *Journal of Comparative Neurology,* 163**,** 129-158.

PETERSON, L. C. & BOGERT, B. P. 1950. A Dynamical Theory of the Cochlea. *The Journal of the Acoustical Society of America,* 22**,** 369-381.

PFANNENSTIEL, S. C., PRAETORIUS, M., PLINKERT, P. K., BROUGH, D. E. & STAECKER, H. 2009. Bcl-2 gene therapy prevents aminoglycoside-induced degeneration of auditory and vestibular hair cells. *Audiology and Neurotology,* 14**,** 254-266.

PICKLES, J., COMIS, S. & OSBORNE, M. 1984. Cross-links between stereocilia in the guinea pig organ of Corti, and their possible relation to sensory transduction. *Hearing research,* 15**,** 103-112.

POIRRIER, A. L., VAN DEN ACKERVEKEN, P., KIM, T. S., VANDENBOSCH, R., NGUYEN, L., LEFEBVRE, P. P. & MALGRANGE, B. 2010. Ototoxic drugs: difference in sensitivity between mice and guinea pigs. *Toxicol Lett,* 193**,** 41-9.

POTTER, P. K., BOWL, M. R., JEYARAJAN, P., WISBY, L., BLEASE, A., GOLDSWORTHY, M. E., SIMON, M. M., GREENAWAY, S., MICHEL, V. & BARNARD, A. 2016. Novel gene function revealed by mouse mutagenesis screens for models of age-related disease. *Nature communications,* 7.

PREZANT, T. R., AGAPIAN, J. V., BOHLMAN, M. C., BU, X., OZTAS, S., QIU, W. Q., ARNOS, K. S., CORTOPASSI, G. A., JABER, L., ROTTER, J. I. & ET AL. 1993. Mitochondrial ribosomal RNA mutation associated with both antibiotic-induced and non-syndromic deafness. *Nat Genet,* 4**,** 289-94.

PRIUSKA, E. M. & SCHACHT, J. 1995. Formation of free radicals by gentamicin and iron and evidence for an iron/gentamicin complex. *Biochem Pharmacol,* 50**,** 1749-52.

PUMPHREY, R. 1950. Upper limit of frequency for human hearing. *Nature,* 166**,** 571-571.

PURVES, D. 2012. *Neuroscience*, Oxford University Press.

QADDOUMI, I., BASS, J. K., WU, J., BILLUPS, C. A., WOZNIAK, A. W., MERCHANT, T. E., HAIK, B. G., WILSON, M. W. & RODRIGUEZ-GALINDO, C. 2012. Carboplatin-associated ototoxicity in children with retinoblastoma. *J Clin Oncol,* 30**,** 1034-41.

QIAN, Y. & GUAN, M.-X. 2009. Interaction of aminoglycosides with human mitochondrial 12S rRNA carrying the deafness-associated mutation. *Antimicrobial agents and chemotherapy,* 53**,** 4612-4618.

QURESHY, K., BLAKLEY, B., ALSALEH, S., QUDDUSI, T. & BERARD, S. 2011. End points for cisplatin ototoxicity. *J Otolaryngol Head Neck Surg,* 40 Suppl 1**,** S45-8.

RAIBORG, C. & STENMARK, H. 2009. The ESCRT machinery in endosomal sorting of ubiquitylated membrane proteins. *Nature,* 458**,** 445-52.

RAMÍREZ-CAMACHO, R., GARCÍA-BERROCAL, J. R., BUJÁN, J., MARTÍN-MARERO, A. & TRINIDAD, A. 2004. Supporting cells as a target of cisplatin-induced inner ear damage: therapeutic implications. *The Laryngoscope,* 114**,** 533-537.

RAPOSO, G., NIJMAN, H. W., STOORVOGEL, W., LIEJENDEKKER, R., HARDING, C. V., MELIEF, C. J. & GEUZE, H. J. 1996. B lymphocytes secrete antigen-presenting vesicles. *J Exp Med,* 183**,** 1161-72.

RAPOSO, G. & STOORVOGEL, W. 2013. Extracellular vesicles: exosomes, microvesicles, and friends. *J Cell Biol,* 200**,** 373-83.

RAVI, R., SOMANI, S. M. & RYBAK, L. P. 1995. Mechanism of cisplatin ototoxicity: antioxidant system. *Pharmacol Toxicol,* 76**,** 386-94.

REALE, E., LUCIANO, L., FRANKE, K., PANNESE, E., WERMBTER, G. & IURATO, S. 1975. Intercellular junctions in the vascular stria and spiral ligament. *J Ultrastruct Res,* 53**,** 284-97.

REIFSCHNEIDER, O., WEHE, C. A., RAJ, I., EHMCKE, J., CIARIMBOLI, G., SPERLING, M. & KARST, U. 2013. Quantitative bioimaging of platinum in polymer embedded mouse organs using laser ablation ICP-MS. *Metallomics,* 5**,** 1440-7.

RHODE, W. S. & GEISLER, C. D. 1967. Model of the displacement between opposing points on the tectorial membrane and reticular lamina. *The Journal of the Acoustical Society of America,* 42**,** 185-190.

RICHARDSON, G. P., FORGE, A., KROS, C. J., FLEMING, J., BROWN, S. D. & STEEL, K. P. 1997. Myosin VIIA is required for aminoglycoside accumulation in cochlear hair cells. *J Neurosci,* 17**,** 9506-19.

RIVOLTA, M. N., GRIX, N., LAWLOR, P., ASHMORE, J. F., JAGGER, D. J. & HOLLEY, M. C. 1998. Auditory hair cell precursors immortalized from the mammalian inner ear. *Proc Biol Sci,* 265**,** 1595-603.

ROBINSON, M. B., TIDWELL, J. L., GOULD, T., TAYLOR, A. R., NEWBERN, J. M., GRAVES, J., TYTELL, M. & MILLIGAN, C. E. 2005. Extracellular heat shock protein 70: a critical component for motoneuron survival. *J Neurosci,* 25**,** 9735-45.

ROCHE, R. J., SILAMUT, K., PUKRITTAYAKAMEE, S., LOOAREESUWAN, S., MOLUNTO, P., BOONAMRUNG, S. & WHITE, N. J. 1990. Quinine induces reversible high-tone hearing loss. *Br J Clin Pharmacol,* 29**,** 780-2.

ROY, S., RYALS, M. M., VAN DEN BRUELE, A. B., FITZGERALD, T. S. & CUNNINGHAM, L. L. 2013. Sound preconditioning therapy inhibits ototoxic hearing loss in mice. *J Clin Invest,* 123**,** 4945-9.

RUBEL, E. W., DEW, L. A. & ROBERSON, D. W. 1995. Mammalian vestibular hair cell regeneration. *Science,* 267**,** 701-7.

RUBIN, J. S., WADLER, S., BAITLER, J. J., HAYNES, H., ROZENBLET, A., MCGILL, F., GOLDBERG, G. & RUNOWICZ, C. 1995. Audiological findings in a Phase I protocol investigating the effect of WR 2721, high-dose cisplatin and radiation therapy in patients with locally advanced cervical carcinoma. *The Journal of Laryngology & Otology,* 109**,** 744-747.

RYBAK, L. P., HUSAIN, K., MORRIS, C., WHITWORTH, C. & SOMANI, S. 2000. Effect of protective agents against cisplatin ototoxicity. *Am J Otol,* 21**,** 513-20.

RYBAK, L. P., HUSAIN, K., WHITWORTH, C. & SOMANI, S. M. 1999. Dose dependent protection by lipoic acid against cisplatin-induced ototoxicity in rats: antioxidant defense system. *Toxicological sciences: an official journal of the Society of Toxicology,* 47**,** 195-202.

RYBAK, L. P., MUKHERJEA, D., JAJOO, S. & RAMKUMAR, V. 2009. Cisplatin ototoxicity and protection: clinical and experimental studies. *Tohoku J Exp Med,* 219**,** 177-86.

RYBAK, L. P., WHITWORTH, C. A., MUKHERJEA, D. & RAMKUMAR, V. 2007. Mechanisms of cisplatin-induced ototoxicity and prevention. *Hear Res,* 226**,** 157-67.

SAFIEDDINE, S., EL-AMRAOUI, A. & PETIT, C. 2012. The auditory hair cell ribbon synapse: from assembly to function. *Annual review of neuroscience,* 35**,** 509-528.

SAKAGAMI, K., WU, D. M. & PURO, D. G. 1999. Physiology of rat retinal pericytes: modulation of ion channel activity by serum-derived molecules. *J Physiol,* 521 Pt 3**,** 637-50.

SALT, A. N., MELICHAR, I. & THALMANN, R. 1987. Mechanisms of endocochlear potential generation by stria vascularis. *Laryngoscope,* 97**,** 984-91.

SAVINA, A., FADER, C. M., DAMIANI, M. T. & COLOMBO, M. I. 2005. Rab11 promotes docking and fusion of multivesicular bodies in a calcium-dependent manner. *Traffic,* 6**,** 131-43.

SCHINDELIN, J., RUEDEN, C. T., HINER, M. C. & ELICEIRI, K. W. 2015. The ImageJ ecosystem: An open platform for biomedical image analysis. *Mol Reprod Dev,* 82**,** 518-29.

SCHMITT, N. C. & PAGE, B. R. 2017. Chemoradiation-induced hearing loss remains a major concern for head and neck cancer patients. *Int J Audiol***,** 1-6.

SEPMEIJER, J. W. & KLIS, S. F. 2009. Distribution of platinum in blood and perilymph in relation to cisplatin induced ototoxicity in the guinea pig. *Hear Res,* 247**,** 34-9.

SETZEN, G., CACACE, A. T., EAMES, F., RIBACK, P., LAVA, N., MCFARLAND, D. J., ARTINO, L. M. & KERWOOD, J. A. 1999. Central deafness in a young child with Moyamoya disease: Paternal linkage in a Caucasian family: Two case reports and a review of the literature. *International journal of pediatric otorhinolaryngology,* 48**,** 53-76.

SHA, S.-H., QIU, J.-H. & SCHACHT, J. 2006. Aspirin to prevent gentamicin-induced hearing loss. *New England Journal of Medicine,* 354**,** 1856-1857.

SHEA, M., KOZIOL, J. A. & HOWELL, S. B. 1984. Kinetics of sodium thiosulfate, a cisplatin neutralizer. *Clinical Pharmacology & Therapeutics,* 35**,** 419-425.

SHEPPARD, C. J., MEHTA, S. B. & HEINTZMANN, R. 2013. Superresolution by image scanning microscopy using pixel reassignment. *Opt Lett,* 38**,** 2889-92.

SHI, X. 2016. Pathophysiology of the cochlear intrastrial fluid-blood barrier (review). *Hear Res,* 338**,** 52-63.

SHI, X., HAN, W., YAMAMOTO, H., TANG, W., LIN, X., XIU, R., TRUNE, D. R. & NUTTALL, A. L. 2008. The cochlear pericytes. *Microcirculation,* 15**,** 515-29.

SHOTWELL, S., JACOBS, R. & HUDSPETH, A. 1981. Directional sensitivity of individual vertebrate hair cells to controlled deflection of their hair bundles. *Annals of the New York Academy of Sciences,* 374**,** 1-10.

SHU, Y., TAO, Y., WANG, Z., TANG, Y., LI, H., DAI, P., GAO, G. & CHEN, Z. Y. 2016. Identification of Adeno-Associated Viral Vectors That Target Neonatal and Adult Mammalian Inner Ear Cell Subtypes. *Hum Gene Ther,* 27**,** 687-99.

SIE, K. C. & NORTON, S. J. 1997. Changes in otoacoustic emissions and auditory brain stem response after cis-platinum exposure in gerbils. *Otolaryngol Head Neck Surg,* 116**,** 585-92.

SIVAGURU, M., URBAN, M. A., FRIED, G., WESSELN, C. J., MANDER, L. & PUNYASENA, S. W. 2016. Comparative performance of airyscan and structured illumination superresolution microscopy in the study of the surface texture and 3D shape of pollen. *Microsc Res Tech*.

SLATTERY, E. L. & WARCHOL, M. E. 2010. Cisplatin ototoxicity blocks sensory regeneration in the avian inner ear. *J Neurosci,* 30**,** 3473-81.

SLEPECKY, N. B., HENDERSON, C. G. & SAHA, S. 1995. Post-translational modifications of tubulin suggest that dynamic microtubules are present in sensory cells and stable microtubules are present in supporting cells of the mammalian cochlea. *Hear Res,* 91**,** 136-47.

SLUYTER, S., KLIS, S. F., DE GROOT, J. C. & SMOORENBURG, G. F. 2003. Alterations in the stria vascularis in relation to cisplatin ototoxicity and recovery. *Hear Res,* 185**,** 49-56.

SMITH, C. A. & SJÖSTRAND, F. S. 1961. Structure of the nerve endings on the external hair cells of the guinea pig cochlea as studied by serial sections. *Journal of ultrastructure research,* 5**,** 523-556.

SOTOMAYOR, M., WEIHOFEN, W. A., GAUDET, R. & COREY, D. P. 2012. Structure of a force-conveying cadherin bond essential for inner-ear mechanotransduction. *Nature,* 492**,** 128-32.

SPICER, S. S. & SCHULTE, B. A. 1998. Evidence for a medial K+ recycling pathway from inner hair cells. *Hear Res,* 118**,** 1-12.

SPOENDLIN, H. 1969. Innervation patterns in the organ of Corti of the cat. *Acta oto-laryngologica,* 67**,** 239-254.

SPOENDLIN, H. & TACHTENSTEIGER, W. 1967. The sympathetic nerve supply to the inner ear. *European Archives of Oto-Rhino-Laryngology,* 189**,** 346-359.

SPOENDLIN, H. H. 1964. Organization of the sensory hairs in the gravity receptors in utricule and saccule of the squirrel monkey. *Cell and Tissue Research,* 62**,** 701-716.

SPRAUTEN, M., DARRAH, T. H., PETERSON, D. R., CAMPBELL, M. E., HANNIGAN, R. E., CVANCAROVA, M., BEARD, C., HAUGNES, H. S., FOSSA, S. D., OLDENBURG, J. & TRAVIS, L. B. 2012. Impact of long-term serum platinum concentrations on neuro- and ototoxicity in Cisplatin-treated survivors of testicular cancer. *J Clin Oncol,* 30**,** 300-7.

STAWICKI, T. M., ESTERBERG, R., HAILEY, D. W., RAIBLE, D. W. & RUBEL, E. W. 2015. Using the zebrafish lateral line to uncover novel mechanisms of action and prevention in drug-induced hair cell death. *Front Cell Neurosci,* 9**,** 46.

STELMACHOWICZ, P. G., PITTMAN, A. L., HOOVER, B. M., LEWIS, D. E. & MOELLER, M. P. 2004. The importance of high-frequency audibility in the speech and

language development of children with hearing loss. *Arch Otolaryngol Head Neck Surg,* 130**,** 556-62.

STEVENS, G., FLAXMAN, S., BRUNSKILL, E., MASCARENHAS, M., MATHERS, C. D., FINUCANE, M. & GLOBAL BURDEN OF DISEASE HEARING LOSS EXPERT, G. 2013. Global and regional hearing impairment prevalence: an analysis of 42 studies in 29 countries. *Eur J Public Health,* 23**,** 146-52.

STEWART, D. J. 1994. A critique of the role of the blood-brain barrier in the chemotherapy of human brain tumors. *J Neurooncol,* 20**,** 121-39.

STEWART, D. J., BENJAMIN, R. S., LUNA, M., FEUN, L., CAPRIOLI, R., SEIFERT, W. & LOO, T. L. 1982. Human tissue distribution of platinum after cis-diamminedichloroplatinum. *Cancer Chemother Pharmacol,* 10**,** 51-4.

STOHR, W., LANGER, T., KREMERS, A., BIELACK, S., LAMPRECHT-DINNESEN, A., FREY, E., BECK, J. D., GERMAN LATE EFFECTS WORKING GROUP IN THE GERMAN SOCIETY OF PEDIATRIC, O. & HEMATOLOGY 2005. Cisplatin-induced ototoxicity in osteosarcoma patients: a report from the late effects surveillance system. *Cancer Invest,* 23**,** 201-7.

STUFFERS, S., SEM WEGNER, C., STENMARK, H. & BRECH, A. 2009. Multivesicular endosome biogenesis in the absence of ESCRTs. *Traffic,* 10**,** 925-37.

SZARAMA, K. B., GAVARA, N., PETRALIA, R. S., CHADWICK, R. S. & KELLEY, M. W. 2013. Thyroid hormone increases fibroblast growth factor receptor expression and disrupts cell mechanics in the developing organ of corti. *BMC Dev Biol,* 13**,** 6.

SZIKLAI, I. & DALLOS, P. 1993. Acetylcholine controls the gain of the voltage-to-movement converter in isolated outer hair cells. *Acta oto-laryngologica,* 113**,** 326-329.

SZKLARCZYK, D., FRANCESCHINI, A., WYDER, S., FORSLUND, K., HELLER, D., HUERTA-CEPAS, J., SIMONOVIC, M., ROTH, A., SANTOS, A., TSAFOU, K. P., KUHN, M., BORK, P., JENSEN, L. J. & VON MERING, C. 2015. STRING v10: protein-protein interaction networks, integrated over the tree of life. *Nucleic Acids Res,* 43**,** D447-52.

TAKEUCHI, T., SUZUKI, M., FUJIKAKE, N., POPIEL, H. A., KIKUCHI, H., FUTAKI, S., WADA, K. & NAGAI, Y. 2015. Intercellular chaperone transmission via exosomes contributes to maintenance of protein homeostasis at the organismal level. *Proc Natl Acad Sci U S A,* 112**,** E2497-506.

TANAKA, K. & SMITH, C. A. 1978. Structure of the chicken's inner ear: SEM and TEM study. *Developmental Dynamics,* 153**,** 251-271.

TASAKI, I. & SPYROPOULOS, C. S. 1959. Stria vascularis as source of endocochlear potential. *J Neurophysiol,* 22**,** 149-55.

TAVARIA, M., GABRIELE, T., KOLA, I. & ANDERSON, R. L. 1996. A hitchhiker's guide to the human Hsp70 family. *Cell Stress Chaperones,* 1**,** 23-8.

TAYLOR, A. R., ROBINSON, M. B., GIFONDORWA, D. J., TYTELL, M. & MILLIGAN, C. E. 2007. Regulation of heat shock protein 70 release in astrocytes: role of signaling kinases. *Dev Neurobiol,* 67**,** 1815-29.

THARPE, A. M. 2008. Unilateral and mild bilateral hearing loss in children: past and current perspectives. *Trends Amplif,* 12**,** 7-15.

THERY, C., AMIGORENA, S., RAPOSO, G. & CLAYTON, A. 2006. Isolation and characterization of exosomes from cell culture supernatants and biological fluids. *Curr Protoc Cell Biol,* Chapter 3**,** Unit 3 22.

THERY, C., BOUSSAC, M., VERON, P., RICCIARDI-CASTAGNOLI, P., RAPOSO, G., GARIN, J. & AMIGORENA, S. 2001. Proteomic analysis of dendritic cell-derived

exosomes: a secreted subcellular compartment distinct from apoptotic vesicles. *J Immunol,* 166**,** 7309-18.

THERY, C., OSTROWSKI, M. & SEGURA, E. 2009. Membrane vesicles as conveyors of immune responses. *Nat Rev Immunol,* 9**,** 581-93.

THOMAS, A. J., HAILEY, D. W., STAWICKI, T. M., WU, P., COFFIN, A. B., RUBEL, E. W., RAIBLE, D. W., SIMON, J. A. & OU, H. C. 2013. Functional mechanotransduction is required for cisplatin-induced hair cell death in the zebrafish lateral line. *J Neurosci,* 33**,** 4405-14.

THOMAS DICKEY, D., MULDOON, L. L., KRAEMER, D. F. & NEUWELT, E. A. 2004. Protection against cisplatin-induced ototoxicity by N-acetylcysteine in a rat model. *Hear Res,* 193**,** 25-30.

THOMAS, J. P., LAUTERMANN, J., LIEDERT, B., SEILER, F. & THOMALE, J. 2006. High accumulation of platinum-DNA adducts in strial marginal cells of the cochlea is an early event in cisplatin but not carboplatin ototoxicity. *Molecular pharmacology,* 70**,** 23-29.

TIDWELL, J. L., HOUENOU, L. J. & TYTELL, M. 2004. Administration of Hsp70 in vivo inhibits motor and sensory neuron degeneration. *Cell Stress Chaperones,* 9**,** 88-98.

TOKGOZ, B., UCAR, C., KOCYIGIT, I., SOMDAS, M., UNAL, A., VURAL, A., SIPAHIOGLU, M., OYMAK, O. & UTAS, C. 2011. Protective effect of N-acetylcysteine from drug-induced ototoxicity in uraemic patients with CAPD peritonitis. *Nephrology Dialysis Transplantation,* 26**,** 4073-4078.

TOTHILL, P., KLYS, H. S., MATHESON, L. M., MCKAY, K. & SMYTH, J. F. 1992. The long-term retention of platinum in human tissues following the administration of cisplatin or carboplatin for cancer chemotherapy. *Eur J Cancer,* 28A**,** 1358-61.

TRAJKOVIC, K., HSU, C., CHIANTIA, S., RAJENDRAN, L., WENZEL, D., WIELAND, F., SCHWILLE, P., BRUGGER, B. & SIMONS, M. 2008. Ceramide triggers budding of exosome vesicles into multivesicular endosomes. *Science,* 319**,** 1244-7.

TROWE, M. O., MAIER, H., SCHWEIZER, M. & KISPERT, A. 2008. Deafness in mice lacking the T-box transcription factor Tbx18 in otic fibrocytes. *Development,* 135**,** 1725-34.

TSUJI, K., RAUCH, S. D., WALL III, C., VELÁZQUEZ-VILLASEÑOR, L., GLYNN, R. J. & MERCHANT, S. N. 2000. Temporal bone studies of the human peripheral vestibular system: 3. Aminoglycoside ototoxicity. *Annals of Otology, Rhinology & Laryngology,* 109**,** 20-25.

TSUKASAKI, N., WHITWORTH, C. A. & RYBAK, L. P. 2000. Acute changes in cochlear potentials due to cisplatin. *Hear Res,* 149**,** 189-98.

TUCCI, D. L. & RUBEL, E. W. 1990. Physiologic status of regenerated hair cells in the avian inner ear following aminoglycoside ototoxicity. *Otolaryngology—Head and Neck Surgery,* 103**,** 443-450.

TYTELL, M. 2005. Release of heat shock proteins (Hsps) and the effects of extracellular Hsps on neural cells and tissues. *Int J Hyperthermia,* 21**,** 445-55.

TYTELL, M., LASEK, R. J. & GAINER, H. 2016. Axonal maintenance, glia, exosomes, and heat shock proteins. *F1000Res,* 5.

ULLMAN-CULLERE, M. H. & FOLTZ, C. J. 1999. Body condition scoring: a rapid and accurate method for assessing health status in mice. *Lab Anim Sci,* 49**,** 319-23.

VADER, P., MOL, E. A., PASTERKAMP, G. & SCHIFFELERS, R. M. 2016. Extracellular vesicles for drug delivery. *Adv Drug Deliv Rev,* 106**,** 148-156.

VALADI, H., EKSTROM, K., BOSSIOS, A., SJOSTRAND, M., LEE, J. J. & LOTVALL, J. O. 2007. Exosome-mediated transfer of mRNAs and microRNAs is a novel mechanism of genetic exchange between cells. *Nat Cell Biol,* 9**,** 654-9.

VAN AS, J. W., VAN DEN BERG, H. & VAN DALEN, E. C. 2016. Platinum-induced hearing loss after treatment for childhood cancer. *Cochrane Database Syst Rev***,** CD010181.

VAN DIJK, P., MASON, M. J., SCHOFFELEN, R. L., NARINS, P. M. & MEENDERINK, S. W. 2011. Mechanics of the frog ear. *Hearing research,* 273**,** 46-58.

VAN NIEL, G., CHARRIN, S., SIMOES, S., ROMAO, M., ROCHIN, L., SAFTIG, P., MARKS, M. S., RUBINSTEIN, E. & RAPOSO, G. 2011. The tetraspanin CD63 regulates ESCRT-independent and -dependent endosomal sorting during melanogenesis. *Dev Cell,* 21**,** 708-21.

VAN RUIJVEN, M. W., DE GROOT, J. C., KLIS, S. F. & SMOORENBURG, G. F. 2005. The cochlear targets of cisplatin: an electrophysiological and morphological time-sequence study. *Hear Res,* 205**,** 241-8.

VEGA, V. L., RODRIGUEZ-SILVA, M., FREY, T., GEHRMANN, M., DIAZ, J. C., STEINEM, C., MULTHOFF, G., ARISPE, N. & DE MAIO, A. 2008. Hsp70 translocates into the plasma membrane after stress and is released into the extracellular environment in a membrane-associated form that activates macrophages. *J Immunol,* 180**,** 4299-307.

VETTER, D. E., MANN, J. R., WANGEMANN, P., LIU, J., MCLAUGHLIN, K. J., LESAGE, F., MARCUS, D. C., LAZDUNSKI, M., HEINEMANN, S. F. & BARHANIN, J. 1996. Inner ear defects induced by null mutation of the isk gene. *Neuron,* 17**,** 1251-64.

VICENCIO, J. M., YELLON, D. M., SIVARAMAN, V., DAS, D., BOI-DOKU, C., ARJUN, S., ZHENG, Y., RIQUELME, J. A., KEARNEY, J., SHARMA, V., MULTHOFF, G., HALL,

A. R. & DAVIDSON, S. M. 2015. Plasma exosomes protect the myocardium from ischemia-reperfusion injury. *J Am Coll Cardiol,* 65**,** 1525-36.

VON BÉKÉSY, G. 1951. DC Potentials and Energy Balance of the Cochlear Partition. *The Journal of the Acoustical Society of America,* 23**,** 576-582.

VON BÉKÉSY, G. 1960. *Experiments in Hearing*, McGraw.

WALKER, J. J., CLEVELAND, L. M., DAVIS, J. L. & SEALES, J. S. 2013. Audiometry screening and interpretation. *Am Fam Physician,* 87**,** 41-7.

WAN, G., CORFAS, G. & STONE, J. S. 2013. Inner ear supporting cells: rethinking the silent majority. *Semin Cell Dev Biol,* 24**,** 448-59.

WANG, J., LADRECH, S., PUJOL, R., BRABET, P., VAN DE WATER, T. R. & PUEL, J.-L. 2004. Caspase inhibitors, but not c-Jun NH2-terminal kinase inhibitor treatment, prevent cisplatin-induced hearing loss. *Cancer Research,* 64**,** 9217-9224.

WANG, T., CHAI, R., KIM, G. S., PHAM, N., JANSSON, L., NGUYEN, D. H., KUO, B., MAY, L. A., ZUO, J., CUNNINGHAM, L. L. & CHENG, A. G. 2015. Lgr5+ cells regenerate hair cells via proliferation and direct transdifferentiation in damaged neonatal mouse utricle. *Nat Commun,* 6**,** 6613.

WANGEMANN, P. 1995. Comparison of ion transport mechanisms between vestibular dark cells and strial marginal cells. *Hearing research,* 90**,** 149-157.

WANGEMANN, P. 2002. K+ cycling and the endocochlear potential. *Hear Res,* 165**,** 1-9.

WANGEMANN, P. 2006. Supporting sensory transduction: cochlear fluid homeostasis and the endocochlear potential. *J Physiol,* 576**,** 11-21.

WARCHOL, M. E., LAMBERT, P. R., GOLDSTEIN, B. J., FORGE, A. & CORWIN, J. T. 1993. Regenerative proliferation in inner sensory epithelia from adult guinea pigs and humans. *Science,* 259**,** 1619-1623.

WARR, W. B. & GUINAN JR, J. J. 1979. Efferent innervation of the organ of Corti: two separate systems. *Brain research,* 173**,** 152-155.

WATANABE, K., INAI, S., JINNOUCHI, K., BABA, S. & YAGI, T. 2003. Expression of caspase-activated deoxyribonuclease (CAD) and caspase 3 (CPP32) in the cochlea of cisplatin (CDDP)-treated guinea pigs. *Auris Nasus Larynx,* 30**,** 219-25.

WEBBER, J. & CLAYTON, A. 2013. How pure are your vesicles? *J Extracell Vesicles,* 2.

WEBSTER, D. B. & FAY, R. R. 1992. *The Mammalian Auditory Pathway: Neuroanatomy*, Springer New York.

WEVER, E. G. 1973. The ear and hearing in the frog, Rana pipiens. *Journal of morphology,* 141**,** 461-477.

WHITE, P. M., DOETZLHOFER, A., LEE, Y. S., GROVES, A. K. & SEGIL, N. 2006. Mammalian cochlear supporting cells can divide and trans-differentiate into hair cells. *Nature,* 441**,** 984-987.

WHITFIELD, T. T. 2002. Zebrafish as a model for hearing and deafness. *Developmental Neurobiology,* 53**,** 157-171.

WIND, M., WEGENER, A., EISENMENGER, A., KELLNER, R. & LEHMANN, W. D. 2003. Sulfur as the key element for quantitative protein analysis by capillary liquid chromatography coupled to element mass spectrometry. *Angew Chem Int Ed Engl,* 42**,** 3425-7.

WINGFIELD, A., MCCOY, S. L., PEELLE, J. E., TUN, P. A. & COX, L. C. 2006. Effects of adult aging and hearing loss on comprehension of rapid speech varying in syntactic complexity. *J Am Acad Audiol,* 17**,** 487-97.

WINGFIELD, A. & PEELLE, J. E. 2012. How does hearing loss affect the brain? *Aging health,* 8**,** 107-109.

WINGFIELD, A., TUN, P. A. & MCCOY, S. L. 2005. Hearing Loss in Older Adulthood. *Current Directions in Psychological Science,* 14**,** 144-148.

WU, D. K. & OH, S.-H. 1996. Sensory organ generation in the chick inner ear. *Journal of Neuroscience,* 16**,** 6454-6462.

WU, W. J., SHA, S. H., MCLAREN, J. D., KAWAMOTO, K., RAPHAEL, Y. & SCHACHT, J. 2001. Aminoglycoside ototoxicity in adult CBA, C57BL and BALB mice and the Sprague-Dawley rat. *Hear Res,* 158**,** 165-78.

WU, Z. & MULLER, U. 2016. Molecular Identity of the Mechanotransduction Channel in Hair Cells: Not Quiet There Yet. *J Neurosci,* 36**,** 10927-10934.

XIE, J., TALASKA, A. E. & SCHACHT, J. 2011. New developments in aminoglycoside therapy and ototoxicity. *Hear Res,* 281**,** 28-37.

XIONG, W., GRILLET, N., ELLEDGE, H. M., WAGNER, T. F., ZHAO, B., JOHNSON, K. R., KAZMIERCZAK, P. & MÜLLER, U. 2012. TMHS is an integral component of the mechanotransduction machinery of cochlear hair cells. *Cell,* 151**,** 1283-1295.

YANCEY, A., HARRIS, M. S., EGBELAKIN, A., GILBERT, J., PISONI, D. B. & RENBARGER, J. 2012. Risk factors for cisplatin-associated ototoxicity in pediatric oncology patients. *Pediatr Blood Cancer,* 59**,** 144-8.

YANEZ-MO, M., SILJANDER, P. R., ANDREU, Z., ZAVEC, A. B., BORRAS, F. E., BUZAS, E. I., BUZAS, K., CASAL, E., CAPPELLO, F., CARVALHO, J., COLAS, E., CORDEIRO-DA SILVA, A., FAIS, S., FALCON-PEREZ, J. M., GHOBRIAL, I. M., GIEBEL, B., GIMONA, M., GRANER, M., GURSEL, I., GURSEL, M., HEEGAARD, N. H., HENDRIX, A., KIERULF, P., KOKUBUN, K., KOSANOVIC, M., KRALJ-IGLIC, V., KRAMER-ALBERS, E. M., LAITINEN, S., LASSER, C., LENER, T., LIGETI, E., LINE, A., LIPPS, G., LLORENTE, A., LOTVALL, J., MANCEK-KEBER, M., MARCILLA, A., MITTELBRUNN, M., NAZARENKO, I., NOLTE-'T HOEN, E. N., NYMAN, T. A., O'DRISCOLL, L., OLIVAN, M., OLIVEIRA, C., PALLINGER, E., DEL PORTILLO, H. A., REVENTOS, J., RIGAU, M., ROHDE, E., SAMMAR, M., SANCHEZ-MADRID, F., SANTAREM, N., SCHALLMOSER, K., OSTENFELD, M. S., STOORVOGEL, W., STUKELJ, R., VAN DER GREIN, S. G., VASCONCELOS, M. H., WAUBEN, M. H. & DE WEVER, O. 2015. Biological properties of extracellular vesicles and their physiological functions. *J Extracell Vesicles,* 4**,** 27066.

YANG, H., GAN, J., XIE, X., DENG, M., FENG, L., CHEN, X., GAO, Z. & GAN, L. 2010. Gfi1-Cre knock-in mouse line: A tool for inner ear hair cell-specific gene deletion. *Genesis,* 48**,** 400-6.

YANG, Z., SCHUMAKER, L. M., EGORIN, M. J., ZUHOWSKI, E. G., GUO, Z. & CULLEN, K. J. 2006. Cisplatin preferentially binds mitochondrial DNA and voltage-dependent anion channel protein in the mitochondrial membrane of head and neck squamous cell carcinoma: possible role in apoptosis. *Clin Cancer Res,* 12**,** 5817-25.

YERBURY, J. J., POON, S., MEEHAN, S., THOMPSON, B., KUMITA, J. R., DOBSON, C. M. & WILSON, M. R. 2007. The extracellular chaperone clusterin influences amyloid formation and toxicity by interacting with prefibrillar structures. *FASEB J,* 21**,** 2312-22.

YLIKOSKI, J., XING-QUN, L., VIRKKALA, J. & PIRVOLA, U. 2002. Blockade of c-Jun N-terminal kinase pathway attenuates gentamicin-induced cochlear and vestibular hair cell death. *Hearing research,* 163**,** 71-81.

YORGASON, J. G., FAYAD, J. N. & KALINEC, F. 2006. Understanding drug ototoxicity: molecular insights for prevention and clinical management. *Expert Opin Drug Saf,* 5**,** 383-99.

YOSHIDA, N. & LIBERMAN, M. C. 2000. Sound conditioning reduces noise-induced permanent threshold shift in mice. *Hearing research,* 148**,** 213-219.

ZABOROWSKI, M. P., BALAJ, L., BREAKEFIELD, X. O. & LAI, C. P. 2015. Extracellular Vesicles: Composition, Biological Relevance, and Methods of Study. *Bioscience,* 65**,** 783-797.

ZENNER, H. P. 1986. Motile responses in outer hair cells. *Hear Res,* 22**,** 83-90.

ZHANG, J., PETRALIA, R. S., WANG, Y. X. & DIAMOND, J. S. 2016. High-Resolution Quantitative Immunogold Analysis of Membrane Receptors at Retinal Ribbon Synapses. *J Vis Exp***,** 53547.

ZHANG, M., LIU, W., DING, D. & SALVI, R. 2003. Pifithrin-alpha suppresses p53 and protects cochlear and vestibular hair cells from cisplatin-induced apoptosis. *Neuroscience,* 120**,** 191-205.

ZHAO, B., WU, Z., GRILLET, N., YAN, L., XIONG, W., HARKINS-PERRY, S. & MÜLLER, U. 2014. TMIE is an essential component of the mechanotransduction machinery of cochlear hair cells. *Neuron,* 84**,** 954-967.

ZOUBEIDI, A., CHI, K. & GLEAVE, M. 2010. Targeting the cytoprotective chaperone, clusterin, for treatment of advanced cancer. *Clin Cancer Res,* 16**,** 1088-93.